Modeling, Control and Optimization of a Plate Reactor

Haugwitz, Staffan

2007

Document Version:
Publisher's PDF, also known as Version of record

Modeling, Control and Optimization of a Plate Reactor

Modeling, Control and Optimization of a Plate Reactor

Staffan Haugwitz

Department of Automatic Control
Lund University
Lund, October 2007

To Elin

Department of Automatic Control
Lund University
Box 118
SE-221 00 LUND
Sweden

ISSN 0280–5316
ISRN LUTFD2/TFRT--1080--SE

Printed in Sweden by Media-Tryck.
Lund 2007

Abstract

A new chemical reactor, the Alfa Laval Plate Reactor, is being developed by Alfa Laval, a Swedish world-leading heat exchanger company. The plate reactor combines the high-heat-transfer capabilities of plate heat exchangers with the efficient mixing and reaction control typical of microreactors. With this new concept, highly exothermic reactions can be produced using more concentrated reactants and more accurate temperature control. This will reduce the reaction time and the need for downstream separation, thus saving energy and reducing the impact on the environment.

The focus of this thesis is to develop and apply control methods to take advantage of the full potential of the novel plate reactor concept. A nonlinear model of the reactor is derived based on first principles to conduct a system analysis and enable model-based control. The physical model allows a detailed investigation of the potential control inputs and how the process design and choice of inputs may affect the control design.

Two control concepts are examined, decentralized control using multiloop PID controllers and centralized control using Model Predictive Control. The concepts are evaluated and compared in terms of design methods, performance and practical aspects. A cooling system is designed and experimentally verified, where a mid-ranging control structure is implemented to increase the operating range of the hydraulic equipment.

The start-up control problem is challenging due to process uncertainty, highly nonlinear dynamics and input and temperature constraints. The dynamics and the constraints are easily captured by the process model in the optimization problem. The open question is how to address the process uncertainty. Here, robustness to uncertainty is achieved by introducing state-space constraints in the optimization formulation, which decrease the sensitivity of the optimal solution. The start-up control problem has been approached from two sides, a time-driven continuous approach and an event-driven hybrid approach.

Some of the results are specific for the plate reactor, but many parts may be generalized to other applications, for example the decentralized and centralized control design, the start-up/transition control design and use of mid-ranging control to handle two-input one-output systems.

Acknowledgments

In the very first month of my PhD studies, I participated in a CPDC course on patent rights. The two-day course was concluded with a visit to Alfa Laval in Lund. There Tommy Norén introduced us to a new reactor technology concept. Even though he couldn't say too much, due to the patents being filed at the time, he was incredibly enthusiastic about this project and couldn't stop himself from preaching about its promising potential. From that moment I had the pleasure to work on the Alfa Laval Plate Reactor project for three years.

Joining this international project as a fresh PhD student was very interesting and challenging. My supervisor Per Hagander has been my main support and we have had many long and rewarding discussions about the project and research in general. I am very grateful for all the time he has given me. He has very elegantly guided me from the initial months as a newbie up till now, giving me more and more freedom and responsibility along the way. Tore Hägglund, my co-supervisor, has taught me many valuable things about process control in general and PID control in particular. Krister Forsman from Perstorp AB was the opponent for my Licenciate Thesis and after the interesting disccusions there, he joined Per and Tore as co-supervisor. His comments and opinions, based on his long experience of process control in industry, have been most helpful.

My time at the department have indeed been joyful, which you can probably all see on my big smile. I am very fond of the trinity of the PhD program; the research, the courses and the teaching, which constitutes a well-balanced mixture. However, it is the people at the department that elevates this job from good to great, with the coffee breaks, Christmas parties, Ultimate Frisbee sessions, floor hockey and last but not least, all the rewarding discussions with my colleagues, whom I can go to with any questions. Thank you all! Johan Åkesson has been a great mentor for me and his MPC knowledge and algorithms were essential for the award-winning article at IFAC in Prague, for which he deserves a credit. This past year we have been working closely together on the reactor start-up optimization and our collaboration there has been the most interesting and rewarding time as a PhD student. My roommate Tomas Olsson de-

serves a special thanks for the patience when answering all my questions on control and non-control topics. Another significant person is Anders Robertsson, who always has time for everyone and an interest to help. I have also enjoyed the numerous hikes and board game sessions with Johan Bengtsson. Peter Alriksson has been a reliable source on estimation issues. I have had many interesting discussions with Ola Slätteke about process control, mid-ranging and MPC. I appreciated the collaboration with Stéphane Velut and Maria Karlson on the mid-ranging paper. I am also grateful to Per-Ola Larsson for reading and commenting my manuscript.

Within the Plate Reactor project I had the pleasure of working with experts from many different fields outside the control area, whom I all would like to thank. The discussions have been rewarding and given me an extensive view of chemical processes, heat transfer and reaction kinetics as well as splendid dinners and project meetings. In particular I would like to acknowledge Tommy Norén, Barry Johnson, Ian Reynolds, Fabrice Chopard, Sébastien Elgue and Kasper Höglund from Alfa Laval.

One part of the project included experiments on the process in the laboratory at Alfa Laval in Lund and in Tumba. There I appreciated the help of Bengt Göland and Michel Granath in Lund and Robert Geiding in Tumba.

My very first steps towards a PhD career was taken at University of California in Santa Barbara (UCSB), where I took graduate classes in control engineering during my undergraduate exchange year. It would not have been possible without the influential help from Karl Johan Åström and Petar Kokotovic to overcome the bureaucratic obstacles. I also want to thank Anders Åberg, who inspired and supported me to pursue a PhD, while supervising my master's thesis.

This project has been partially funded by the Centre of Process Control and Design, CPDC, the Swedish Foundation for Strategic Research, SSF and by Alfa Laval AB. The workshops and meetings of CPDC has been interesting and my gratitude goes to Bernt Nilsson, the coordinator of CPDC. For the experimental part, there was a generous equipment grant from National Instruments.

For the last two years I have been involved in the European network of excellence HYCON and their funding is gratefully acknowledged. Within this network, I would especially like to thank Olaf Stursberg, Sebastian Engell, Cesar de Prada and Christian Sonntag for interesting meetings.

Finally I would like to thank my non-controlled friends and family, for all the fun we have in terms of sailing, skiing, hikes and parties. A special thanks to my sunshine Elin for her love and support during this time.

Contents

1

Introduction

1.1 Background and Motivation

Chemical Reactions

Chemical reactions occur everywhere in our everyday life, for example, in the human body, in cell phone batteries, in a rocket engine and in the pharmaceutical and chemical industry. The reactions, see e.g. [Levenspiel, 1999], can be divided into homogeneous and heterogeneous reactions, where the homogeneous reaction takes place in a single phase, whereas the heterogeneous reaction involves at least two phases, such as oil and water.

The reaction rate does often depend on the concentrations of the reactants and the temperature. In many cases, the temperature dependency is exponentially, as described by the Arrhenius law. Furthermore, some reactions absorb or release heat during operation, and are then called endothermic and exothermic reactions, respectively. To maintain an endothermic reaction, heat must be supplied into the reactor system, whereas for the exothermic reaction, heat must be removed to avoid excessive reactor temperatures. This characteristic of the reaction will have an important implication on the reaction dynamics, as an exothermic reaction may lead to a self-accelerating reaction rate. From linear systems theory, a self-accelerating reaction corresponds to the system having unstable poles.

Chemical Reactors

There are several different types of chemical reactors, see e.g. [Denbigh and Turner, 1971]. They are usually divided into batch and continuous reactors, see Figure 1.1. In batch reactors, the reactants are added all

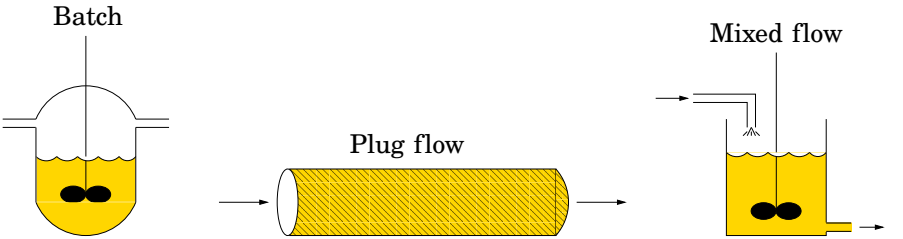

Figure 1.1 Ideal reactor types from [Levenspiel, 1999]. The plug flow and mixed flow reactor have, after an initial start-up, a steady-state flow during operation, whereas the batch reactor has no in- or outflows during operation, only filling and emptying at the end of each production cycle.

at once and after a certain time the entire reactor is emptied and the product goes to downstream processing. The key concept is the production cycle of repeated filling and emptying operations with a production time from minutes to days. The batch reactor has uniform composition everywhere in the reactor, but the composition changes with time. In a semi-batch reactor, one or many reactants are added continuously during the production cycle, instead of being added all at once initially. This small continuous feeding improves the conditions for control of temperature or quality, as the small feed has a limited impact on the entire batch, but increases the production time. One specific application for semi-batch reactors is production of exothermic reactions. The heat release from the reaction may be overwhelming, unless one of the reactants is added in a small continuous feed, to enable the heat transfer to be controlled more accurately.

In continuous reactors, such as the plug flow and mixed flow reactor, there is a continuous flow of reactants and products at the inlet and outlet of the reactor. The key concept is the continuous operation, which may be maintained for several weeks or months between each stop. This means that the flow through this type of reactors is in steady-state most of the time. In the plug flow reactor, the fluid passes through the reactor with no mixing of earlier and later entering fluid. The composition changes along the plug flow reactor, creating a composition profile along the reactor. The mixed flow reactor has the same composition everywhere within the reactor and at the exit.

Batch reactors are typically used for small to medium scale production, due to their flexibility and low capital cost. For medium to large scale production, continuous reactors are preferred, due to lower operating cost, improved conditions for automatic control and greater consistency of the operating conditions and quality [Denbigh and Turner, 1971].

Chemical reactors can also be classified using two other categories, tank reactors and tubular reactors. The batch, semi-batch and mixed flow reactors are considered tank reactors, as ideally their composition and temperature is regarded to be the same throughout the reactor. The plug flow reactor belongs to the type of tubular reactors as its composition varies along the reactor length.

Figure 1.1 shows the ideal version of each reactor type. Industrial reactors can be far more complex, with non-ideal mixing, heat transfer, or reaction.

The Plate Reactor Concept

The synthesis of fine chemicals or pharmaceuticals, widely carried out in batch or semi-batch reactors, are often strongly limited by constraints related to the dissipation of heat generated by the reactions. A common solution is to dilute the chemicals, that is, to reduce the concentrations, thus ensuring that the reaction rate and the heat release is within the heat transfer capacity of the reactor. After the reaction stage, the solvent is removed in a separation stage to provide a high-concentrated product with good quality. This separation process is both time and energy consuming, thus very expensive. The dilution also increases the reaction time, since the reaction is operated at lower concentrations, which limits the production rate.

To reduce these problems, the Plate Reactor project was initiated by Alfa Laval AB in 2002. Its objective is to design new types of reactors through process intensification (PI), where new methods and equipment are developed with the goal of allowing cleaner and more energy-efficient production in smaller reactors. The reduction in size also leads to increased safety with smaller amounts of hazardous chemicals being in use at each time. The field of PI has been an active research area since the 1980's, see for example [Ramshaw, 1995], [Green *et al.*, 1999] and [Stankiewicz and Moulin, 2000]. One example of PI innovation is the compact heat exchanger, which has been widely successful in many applications. However, attempts to use heat exchangers as chemical reactors, to utilize their high heat transfer capacity, have had limited success due to the poor micro-mixing conditions. In the 1990's, research on heat exchanger reactors, to overcome these problems, was started at the BHR Group Limited [Phillips *et al.*, 1997] and also at Alfa Laval AB [Nilsson and Sveider, 2000].

A new concept of heat exchange reactors, the Alfa Laval Plate Reactor is being developed by Alfa Laval AB, [Alfa Laval AB, 2006], [Bouaifi *et al.*, 2004], [Andersson *et al.*, 2004] and [Prat *et al.*, 2005]. The plate reactor combines the high-heat-transfer capabilities of the plate heat exchanger with the efficient mixing and reaction control typical of microreactors into

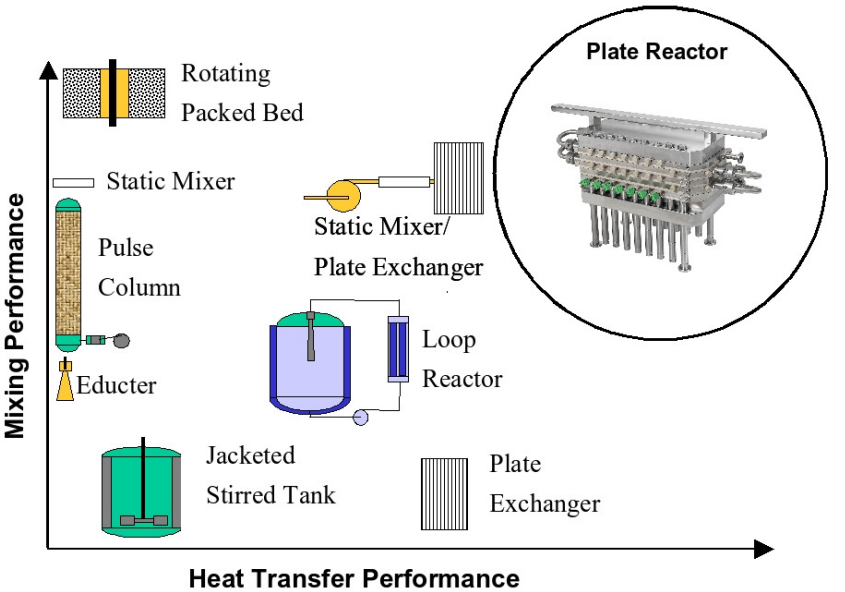

Figure 1.2 Heat transfer performance and mixing performance for the plate reactor and other kinds of chemical reactors. Courtesy of Alfa Laval AB.

a single unit. This allows complex chemical reactions to be performed with a very accurate thermal control. Therefore the plate reactor appears particularly well suited for process intensification, as it allows at the same time an increase of reactant concentration and a reduction of and solvent consumption. This leads to reduced need of down-stream separation, resulting in large savings in time, energy and money. The high heat transfer capacity enables the reaction to be operated at higher temperatures than before, which may reduce the time to reach complete reaction from hours to minutes. This leads to improved productivity, but may also improve quality as there is less time for by-product formation. The intensified production, due to the improved heat transfer and micro-mixing means that the plate reactor can replace larger conventional reactors, thus reducing plant size and investment costs. Figure 1.2 shows the heat transfer and micro-mixing capacities of different type of reactors.

Of the ideal reactor types in Figure 1.1, the plate reactor can be roughly approximated with the plug flow reactor, but with a more complex geometry.

Aim of this Thesis

The aim of this thesis is to develop and investigate control methods to achieve safe, efficient and robust production, and to be able to exploit the full potential of the plate reactor.

This research was initiated in a very early phase of the Plate Reactor project to allow for process and control design in parallel. This work has been carried out within the framework of the Center for Process Control and Design[1] (CPDC).

1.2 Outline and Contributions of the Thesis

Contributions

The main contributions presented in this thesis are:

- Design and control of a multi-purpose cooling system, with experimental verification of the efficient temperature control.
- Development of a nonlinear dynamical model of the plate reactor from first principles, to allow system analysis and model-based control and to gain deeper understanding of the physics behind the process.
- A thorough investigation of potential control inputs and how the process design and choice of control inputs may affect the control design.
- Efficient process control of the plate reactor using either decentralized control in the form of multi-loop PID controllers or centralized control in the form of Model Predictive Control. The two control structures are evaluated and compared.
- A novel approach how to achieve a safe and robust reactor start-up using dynamic optimization.
- A hybrid approach to the reactor start-up problem that transforms the problem into an event-driven sequence, which increases the robustness.

Some of the contributions are not restricted to the plate reactor application, but may be useful within the general area of process control, for example, the evaluation of decentralized and centralized control and the examples of mid-ranging control design.

[1] www.control.lth.se/cpdc

Outline of the Thesis

Chapter 2 presents the plate reactor process, its construction, concept and configurations. The process inputs and outputs are briefly described. The objectives of the production are defined and possible reactor configurations are presented.

Chapter 3 derives a nonlinear process model based on first principles. The model is used for a thorough process analysis, which facilitates the selection of the process inputs for feedback control.

Chapter 4 presents different methods for feedback control of the plate reactor at nominal operation. Decentralized multi-loop PID controllers and centralized control using MPC are designed.

Chapter 5 describes the start-up control problem and presents the special dynamics associated with the start-up. A few motivating examples indicate the need for robust start-up methods.

Chapter 6 describes a start-up method based on dynamic optimization, where robustness is achieved by introducing constraints on the reactant concentrations.

Chapter 7 describes a hybrid approach to the start-up control problem. The start-up sequence is divided into several modes, where each transition between these modes is coupled to a condition on the process state, thus rendering the start-up event-driven.

Chapter 8 presents the utility system that provides the reactor with cooling water at a desired flow rate with a desired inlet temperature. The process design and control of the utility system are described and experimental results are reported.

Chapter 9 discusses constraint handling in mid-ranging control. Potential problems are highlighted and a modified control structure is proposed, which may improve the performance when operating close to the constraints. The method is verified in experiments.

Chapter 10 concludes the thesis with a brief summary of the results and some suggestions for future work.

Awards

At the 16th IFAC World Congress in Prague, [Haugwitz and Hagander, 2005] received the IFAC Congress Applications Paper Prize.

Publications

The thesis is based on the following publications.

Haugwitz, S., J. Åkesson, and P. Hagander (2007): "Dynamic start-up optimization of a plate reactor with uncertainties." Submitted to *Journal of Process Control*.

Haugwitz, S. and P. Hagander (2007): "Analysis and design of startup control of a chemical plate reactor with uncertainties; a hybrid approach." In *Proceedings of the 16th IEEE Conference on Control Applications (CCA)*. Singapore.

Haugwitz, S., J. Åkesson, and P. Hagander (2007): "Dynamic optimization of a plate reactor start-up supported by modelica-based code generation software." In *Proceedings of 8th International Symposium on Dynamics and Control of Process Systems*. Cancun, Mexico.

Haugwitz, S., P. Hagander, and T. Norén (2007): "Modeling and control of a novel heat exchange reactor, the Open Plate Reactor." *Control Engineering Practice*, **15:7**, pp. 779–792.

Haugwitz, S. and P. Hagander (2006a): "Analysis and selection of control variables and structures for the Open Plate Reactor." In *Proceedings of Nordic Process Control Workshop*. Copenhagen, Denmark.

Haugwitz, S. and P. Hagander (2006b): "Challenges in start-up control of a heat exchange reactor with exothermic reactions; a hybrid approach." In *Proceedings of the 2nd IFAC Conference on Analysis and Design of Hybrid Systems*. Alghero, Italy.

Haugwitz, S., P. Hagander, and T. Norén (2006): "Process and control design for a novel chemical heat exchange reactor." In *Proceedings of Reglermötet*. Stockholm, Sweden.

Haugwitz, S. and P. Hagander (2005): "Process control of an Open Plate Reactor." In *Proceedings of the 16th IFAC World Congress*. Prague, Czech Republic.

Haugwitz, S., M. Karlsson, S. Velut, and P. Hagander (2005): "Anti-windup in mid-ranging control." In *Proceedings of the 44th IEEE Conference on Decision and Control and European Control Conference ECC 2005*. Seville, Spain.

Haugwitz, S. (2005a): "Modeling and Control of the Open Plate Reactor." Licentiate Thesis ISRN LUTFD2/TFRT--3237--SE. Department of Automatic Control, Lund University, Sweden.

Haugwitz, S. (2005b): "Plattreaktorn öppnar nya vägar för kemiindustrin." Popular science paper, published March 3, 2005, at the web page of the National Encyclopedia, www.ne.se, now available at www.control.lth.se (in Swedish).

Haugwitz, S. and P. Hagander (2004a): "Mid-ranging control of the cooling temperature for an Open Plate Reactor." In *Proceedings of the 12th Nordic Process Control Workshop*. Gothenburg, Sweden.

Haugwitz, S. and P. Hagander (2004b): "Temperature control of a utility system for an Open Plate Reactor." In *Proceedings of Reglermöte*. Gothenburg, Sweden.

Other Publications

Haugwitz, S. (2003): "Modelling of microturbine systems." In *Proceedings of European Control Conference*. Cambridge, Great Britain.

Haugwitz, S. (2002): "Modelling of microturbine systems." Master's Thesis ISRN LUTFD2/TFRT--5687--SE. Department of Automatic Control, Lund University, Sweden.

2

The Process

2.1 Process Description

In this thesis, the following reaction is considered,

$$A + B \rightarrow C + D. \tag{2.1}$$

The substance A is the primary reactant and the substance B is the secondary reactant, which is injected into the main flow of reactant A at multiple injection points along the reactor. The desired product is substance C. Substance D is another product, with a constant stoichiometric relationship to C.

The plate reactor is based on a modified plate heat exchanger design. It consists of reactor plates, inside which the reactants mix and react, and utility plates, inside which a cooling or heating fluid flows. There is one utility plate on top and one below each reactor plate. The utility fluid is often water, but may be replaced depending on the reaction. In this thesis, exothermic reactions are studied, thus the utility fluid often cools the reactor, even though it may in some rare cases be used for heating. In the sequel, the utility plates and the utility flow will also be referred to as cooling plates and cooling flows, respectively.

In Figure 2.1 the plate reactor is shown from two different angles. The left figure illustrates the first rows of the reactor plate. The primary reactant A flows into the reactor from the upper left inlet. Between the inlet and the outlet, the reactants are forced by inserts to flow in horizontal channels of changing directions. The flow inserts are specifically designed to enhance the micro-mixing and guarantee good heat transfer capacity, see Figure 2.2, and are patented in [Alfa Laval patent, 2001] and [Alfa Laval patent, 2002]. The dashed vertical lines of Figure 2.1 illustrate how

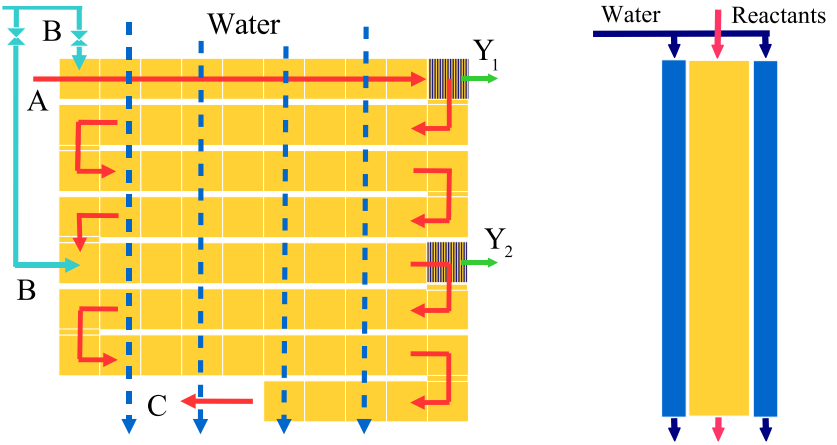

Figure 2.1 Left: A schematic of a few rows of a reactor plate. Reactant A is injected at top left and reactant B is injected at multiple sites along the reactor. Y_1 and Y_2 are internal temperature measurements used for process control and supervision. The cooling water flows from top to bottom in separate cooling plates. Right: The plate reactor seen from the side, with the reactor part in the middle and cooling plates on each side.

the cooling water flows on each side to the reactor plate. The right figure in Figure 2.1 shows the plate reactor from the side with cooling plates on each side of the reactor plate. Reactant B can be injected in arbitrary places along the reactor, typically at the beginning and middle of the reactor. Temperature, pressure or conductivity sensors can be mounted inside the reactor, for example after each injection point, for process monitoring and control.

The design concept for the reactor allows for great flexibility in adapting the process for new reaction schemes. The type of inserts and the number of plates in the reactor plate can be adjusted to provide the residence time appropriate for the chosen reaction. In Figure 2.3 a configuration with three reactor plates is shown. The process fluid enters from the top and flows through three reactor plates. The cooling water enters at lower left and exits at upper left. If the reaction needs a catalyst, it can be mounted on the flow inserts.

A pilot-scale prototype of the plate reactor is seen in Figure 2.4. The simulations and experiments carried out in this thesis are based on the size and properties of this prototype unit, however, all methods developed here are generic for a reactor of any size. With three reactor plates (the grey-white plates), the residence time is around 90 seconds at a nominal flow rate of 50 L/h. In this thesis, we primarily consider one single reactor

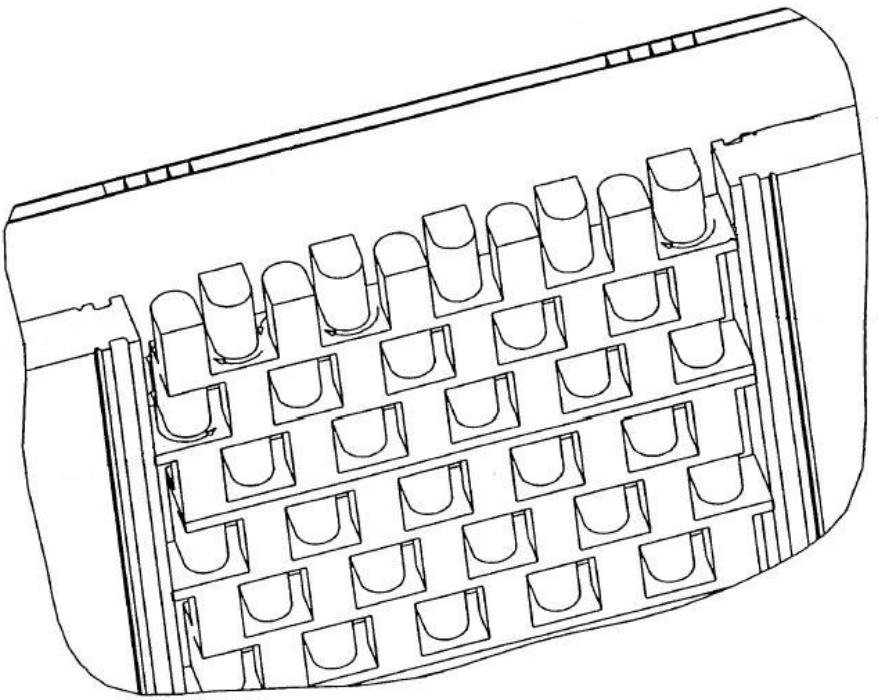

Figure 2.2 A drawing of the flow inserts and the flow channels shown in Figure 2.1. Here the fluid enters from top right and the small arrows indicate the flow direction. From [Alfa Laval patent, 2002]

plate, thus a reactor with a residence time of 30 s.

To more easily investigate the applicability of new reaction schemes to the plate reactor concept, a lab-scale version of the reactor has also been developed at Alfa Laval, see Figure 2.5. There are currently several companies running test experiments on the lab-scale reactor such as the international pharmaceutical company AstraZeneca and the Swedish specialty chemicals company Perstorp AB. Alfa Laval are also collaborating with the french chemical company Arkema within the LIFE-project[1] of the European Union to demonstrate and evaluate the continuous plate reactor technology. The tests are still in an early stage and further tests on the larger pilot-scale reactor are scheduled for end of 2007 and 2008.

[1]http://ec.europa.eu/environment/life/index.htm

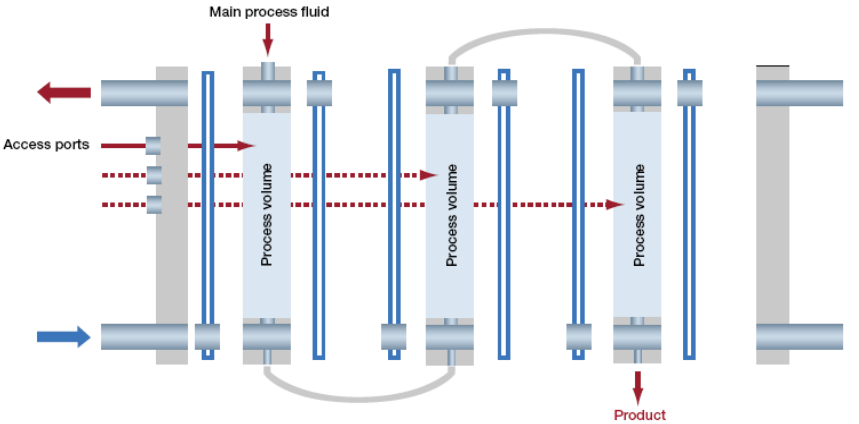

Figure 2.3 A flow scheme of the plate reactor system. The process fluid enters from above into the first reactor plate. The cooling water enters from lower left and exits at the upper left. Courtesy of Alfa Laval AB.

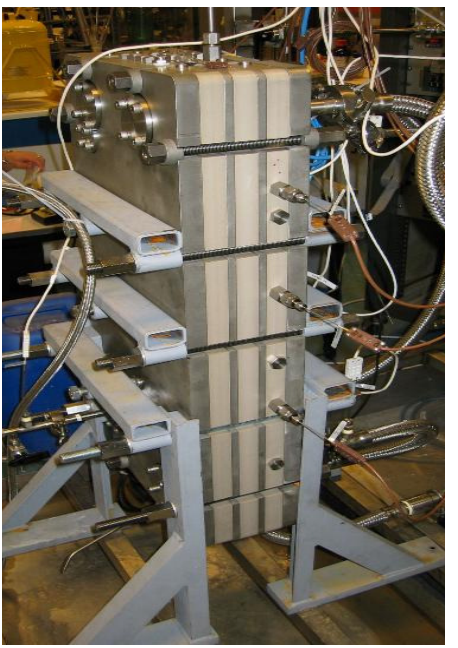

Figure 2.4 A test unit of the plate reactor with three reactor plates connected in series as in Figure 2.3. Note the temperature sensors along the side of one of the reactor plates. The thin cooling plates are mounted onto the reactor plates and are not visible in the photo. There are support plates between each cooling plate - reactor plate - cooling plate combination. Courtesy of Alfa Laval AB.

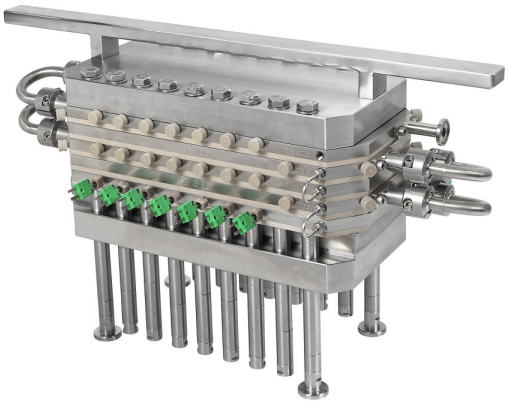

Figure 2.5 One version of a Plate Reactor, PR37, used for initial testing of new reactions, or as a production unit for small flow production, mainly pharmaceuticals. Courtesy of Alfa Laval AB.

Reactions

Several different types of chemical reactions have been tested in the plate reactor, such as liquid-phase exothermic irreversible reactions, liquid-phase exothermic reversible reactions and liquid/liquid exothermic reactions for immiscible flows (cf. oil and water). There have also been tests on liquid/gas reactions. The reaction kinetics can differ many orders of magnitude from one reaction to another. The operation of the plate reactor is generally aimed at fast reactions. Slower reactions may require a very long reactor length to achieve acceptable conversion, which would make a semi-batch reactor more suitable. Furthermore, the operation of the plate reactor is aimed at exothermic or endothermic reactions, to take advantage of the improved heat transfer capacity. The standard reaction used in this thesis is the oxidation of sodium thiosulfate $Na_2S_2O_3$ by hydrogen peroxide H_2O_2, which is a fast, exothermic, second-order[2] and liquid-phase reaction,

$$2Na_2S_2O_3 + 4H_2O_2 \rightarrow Na_2S_3O_6 + Na_2SO_4 + 4H_2O. \tag{2.2}$$

The reaction rate can be described by the Arrhenius law [Prat *et al.*, 2005],

$$r = k_0 e^{\frac{E_a}{RT_r}} c_A c_B, \tag{2.3}$$

[2]Second order, since the reaction rate depends on the concentrations of A and B.

where T_r is the reactor temperature, R is the universal gas constant, c_A is the concentration of sodium thiosulfate, c_B is the concentration of hydrogen peroxide, $k_0 = 2 \cdot 10^7$ m^3/(mol s) is the pre-exponential factor, $E_a = 68200$ J/mol is the activation energy and $\Delta H = -1.172 \cdot 10^6$ J/(mol $Na_2S_3O_6$) is the heat of reaction.

Cooling/Heating

To further increase the flexibility of operation, it is possible to have separate utility flows - with different temperatures - to cool or heat selected parts of the reactor. The utility plates are then divided into several compartments, each having an individual inlet temperature. These compartments will in the sequel be referred to as cooling zones. For some reactions it may be beneficial to cool most of the reactor, but reduce cooling in the last section to improve the conversion.

Figure 2.1 shows that the cooling water flow is vertical and the reactor flow is horizontal, which creates a cross-flow heat exchange pattern. However, the temperature of the cooling water is almost constant for each horizontal reactor row, which allows the heat exchange pattern to be approximated as concurrent in the process model.

To ensure that the utility flow (usually water) entering the reactor has the desired temperature and flow rate, a utility system has been designed and tested experimentally, see Chapter 8 for further details.

2.2 Inputs and Outputs

The aim of this section is to briefly present the input and output variables of the plate reactor, to provide an overview of how the inputs affect and the outputs reflect the properties inside the reactor. This will be used when selecting control variables in Chapter 3. A complete list of symbols is given in the Appendix.

Figure 2.6 shows the input and output variables for a plate reactor configuration with two injection points and one cooling flow. The reactant flows are often called feeds, such as feed concentration, to distinguish between the temperatures and concentrations of the inlet flows and those inside the reactor. In most cases, the feed flows of B come from the same storage tank, thus they have the same feed temperature $T_{B,\text{feed}}$ and feed concentration $c_{B,\text{feed}}$. Each additional injection point adds one degree of freedom, the flow rate of B added through this injection point. Each additional cooling zone adds in theory two degrees of freedom, the flow rate and the inlet temperature, however, usually only one of these is used for control and the other one is fixed.

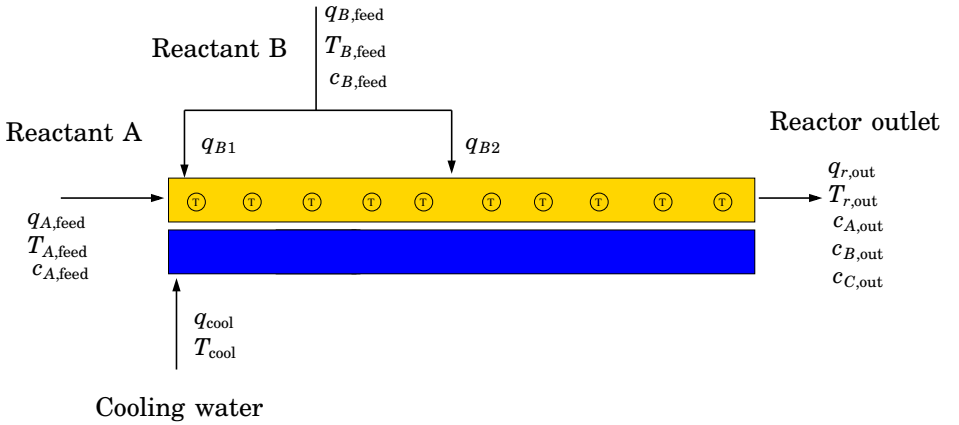

Figure 2.6 The plate reactor as a schematic tubular reactor with four inflows and one outflow. The inputs and outputs are the temperatures, flow rates and concentrations of these flows. The circles with T represents internal temperature sensors.

Figure 2.6 shows ten independent input variables. When the stoichiometric relation between A and B is considered, one degree of freedom is removed, since the total number of moles of B is fixed by the added amount of A,

$$q_{A,\text{feed}}c_{A,\text{feed}} = q_{B,\text{feed}}c_{B,\text{feed}} = (q_{B1} + q_{B2})c_{B,\text{feed}}, \tag{2.4}$$

where the sum of the injection flows $q_{B1} + q_{B2}$ defines the total feed flow $q_{B,\text{feed}}$.

Short Description of the Input Variables

- Feed flow rate of reactant A, $q_{A,\text{feed}}$, constitutes 80% of the total flow rate through the plate reactor. It therefore often serves as the main control variable for varying the production rate, i.e., the amount of product C exiting the reactor per unit time.
- Feed temperature of reactant A, $T_{A,\text{feed}}$, mainly influences the temperature at the inlet of the reactor. Especially useful during the start-up phase.
- Feed concentration of reactant A, $c_{A,\text{feed}}$, determines together with $q_{A,\text{feed}}$ the amount of A added into the reactor.
- Feed flow rate of reactant B, $q_{B,\text{feed}}$, is the total flow rate of B added to the reactor. This flow rate constitutes 20% of the total flow rate through the reactor. $q_{B,\text{feed}}$ should have a constant relationship with

$q_{A,\text{feed}}$ to maintain stoichiometric conditions. This may for example be achieved with ratio control with $q_{A,\text{feed}}$ as the master.

- Feed injection flow rates, q_{B1} and q_{B2}, are the injection flow rates of B at the two injection points. The sum $q_{B1} + q_{B2} = q_{B,\text{feed}}$ is often fixed to guarantee stoichiometric conditions. However, the flow distribution between the injection points remains as a degree of freedom. In the sequel, we will use the scaled control variables $u_{B1} = q_{B1}/q_{B,\text{feed}}$ and $u_{B2} = q_{B2}/q_{B,\text{feed}}$, with $q_{B,\text{feed}}$ as the scaling factor. Thus when $u_{B1} + u_{B2} = 1$, stoichiometric amounts of A and B are being fed into the reactor. The values of u_{B1} and u_{B2} can also be seen as an *injection distribution*. For example $u_{B1} = 0.45$ and $u_{B2} = 0.55$, mean that 45% of the stoichiometric flow of B is injected at the first point and the remaining 55% is added in the second point.
- Feed temperature of reactant B, $T_{B,\text{feed}}$, has only a minor influence on the reactor temperature as the reactant B flow only constitutes 20% of the total flow.
- Feed concentration of reactant B, $c_{B,\text{feed}}$, determines together with $q_{B,\text{feed}}$ the amount of B added into the reactor.
- Cooling flow rate, q_{cool}, has fast and simple dynamics to the reactor temperature, but suffers from highly nonlinear gain, and affects the heat transfer coefficient h.
- Inlet temperature of cooling water, T_{cool}, has more linear behavior than q_{cool}, but suffers from slower actuator dynamics.

Short Description of the Output Variables

- The production rate is defined as the product of the flow rate at reactor outlet, $q_{r,\text{out}}$, and the outlet concentration of C, $c_{C,\text{out}}$. This gives the number of moles of substance C produced per unit time.
- The outlet temperature, $T_{r,\text{out}}$, is often important for downstream processing. Sometimes $T_{r,\text{out}}$ should be high to maximize the conversion of the reactants. Sometimes it should be low to inhibit further reaction of by-products. One may then introduce a temperature constraint on $T_{r,\text{out}}$ to emphasize that no reaction should occur after the reactor outlet, for example if the flow enters a storage tank without any cooling capacity.
- The outlet concentrations of A and B, $c_{A,\text{out}}$ and $c_{B,\text{out}}$, should often be minimized in order to avoid excessive use of either reactant, thus reducing the need for downstream separation.

Disturbances

During production there may be disturbances in any of the four feed flows, see Figure 2.6, entering the plate reactor. All feed flow rates and feed temperatures as well as cooling flow rates and cooling temperatures are measured on-line, thus enabling feed forward disturbance compensation. In addition, the flow rates and some inlet temperatures will be individually controlled with low-level feedback control, thus reducing the risk of any disturbances entering the plate reactor. Online measurements of the feed concentrations are, however, only available in special cases. Disturbances in $c_{A,\text{feed}}$ and/or $c_{B,\text{feed}}$ may disrupt the stoichiometric relations between A and B and lead to loss in productivity and conversion. The most dangerous situation is when both $c_{A,\text{feed}}$ and $c_{B,\text{feed}}$ increase, thus leading to more heat being released. The temperature sensors will detect this event and with a model-based observer the disturbance may be estimated.

It may sometimes be difficult to find a clear distinction between a disturbance and a process uncertainty. An example is fouling inside the reactor, which will affect the heat transfer capacity and may be seen as a slowly varying disturbance. Uncertainties in the heat transfer coefficient may have a similar affect on the heat transfer capacity, especially if the coefficient is varying with the flow rates. The process uncertainties are further discussed in connection with the start-up control problem in Section 5.2.

2.3 Objectives for Process Operation

Before discussing how to improve the design and control of the plate reactor, we have to define the performance variables of the process. In general, there are three main objectives for the process operation of the plate reactor, see e.g. [Edgar and Himmelblau, 1989].

OBJECTIVE 2.1—SAFE PRODUCTION $T_r < T_{\max}$
In many applications, a constraint on the reactor temperature $T_r < T_{\max}$ can be derived from material limitations, possible by-product formation or the boiling point for the given reactor pressure. Too high temperatures may lead to mechanical failures, reduced product quality, or even a thermal runaway situation. It is therefore of the utmost importance to fulfill the temperature constraints. □

OBJECTIVE 2.2—MAXIMIZE CONVERSION AT OUTLET, γ
It is desired to have complete conversion of the reactants A and B to the desired product C. The focus is to maximize the outlet concentration of

C, but without having too much excess of either reactant at the outlet. The reactant conversions, γ_A and γ_B, can be defined as the ratio between how much product that was formed and how much that could have been formed at complete conversion,

$$\gamma_A = \frac{c_{C,\text{out}}}{c_{C,\text{out}} + c_{A,\text{out}}} \qquad \gamma_B = \frac{c_{C,\text{out}}}{c_{C,\text{out}} + c_{B,\text{out}}}. \tag{2.5}$$

□

Note that the conversion is a nonlinear function of the concentrations. If all reactant has been converted into product, that is, $c_{A,\text{out}} = 0$ and $c_{B,\text{out}} = 0$, then $\gamma_A = \gamma_B = 1$, which corresponds to 100% conversion. This is only possible in a reactor of infinite length. Another limitation for industrial reactors, is the temperature constraint mentioned above. This introduces the balance between high reactor temperatures to improve the conversion and low temperatures to avoid reactor failure.

Objective 2.3—Maximize production rate, $q_r \cdot c_C$
High conversion is not always a sufficient criteria to find an economically optimal operating point. A simple way to increase the conversion is to decrease the flow rate, thus increasing the residence time. However, this increase of the conversion comes at the price of reduced productivity. Therefore, the objectives for optimal operation should include maximizing the production rate, that is, the product of the flow rate and the outlet concentration of the desired substance C. □

Objective 2.4—$T_{\min} \leq T_{r,\text{out}} \leq T_{\max}$
In some applications it may be desirable to have a minimum and/or maximum outlet temperature of the reactor flow to improve conditions for downstream processing. □

These four objectives will now be considered when discussing how the process design can be optimized and what properties the process model should capture to allow process analysis.

Characteristics of the Nominal Operating Point

Figure 2.7 plots the steady-state temperature and conversion profiles at the nominal operating point. The process parameters are given in the Appendix. The x-axis is the normalized reactor length, where 0 defines the reactor inlet and 1 the reactor outlet. The two vertical lines indicate the positions and injection flow rates of reactant B, here $u_{B1} = 0.496$, i.e., 49.6% of the total feed flow rate of B is injected in the first injection point

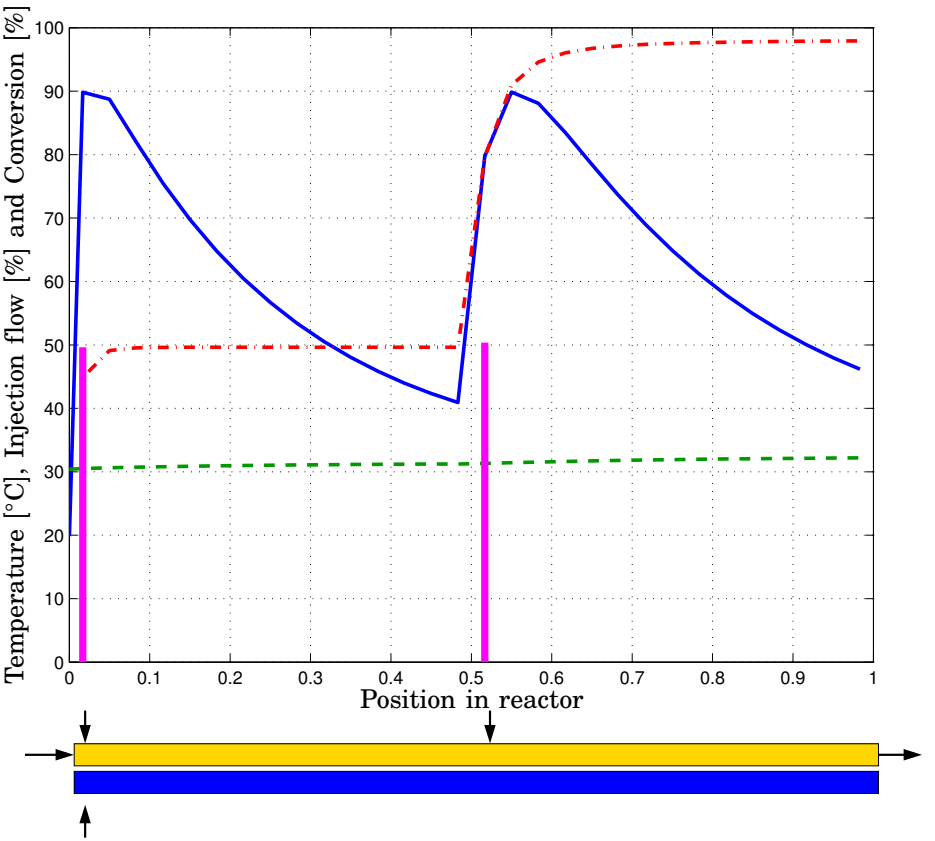

Figure 2.7 The steady-state reactor temperature profile (solid), the cooling water temperature profile (dashed), the conversion profile (dash-dot) and the injection flow rates (vertical lines at their location). The schematic figure above illustrates the spatial coordinates of the profiles.

and the remainder 50.4% ($u_{B2} = 0.504$) enters through the second injection point. The two injection flows create a typical temperature profile, where a temperature maximum is formed after each injection point, due to the heat release from the exothermic reaction. When most of the injected B has been consumed, the heat from the reaction decreases and the temperature drops due to the efficient cooling. The purpose of the cooling is two-fold, firstly to cool so that the maximum temperatures remain below the safety limit. Secondly, to cool the reactor flow between the injection points to allow more reactant B to be injected downstream. The conversion profile shows how much of reactant A that has been consumed along the reactor. After the first injection point, 49.6% of the initial amount of

A has been consumed and at the reactor outlet 97.9% has been consumed. The temperature profile of the cooling water is almost horizontal, since the the heat released from the reaction is absorbed by a very large cooling flow rate.

The objectives of the process operation can now be visualized in Figure 2.7. The first objective $T_r \leq T_{\max}$ is straight forward to inspect, the temperature profile should be below a certain constant limit. The second objective is that the conversion profile at the reactor outlet should be maximized or at least larger than some limit. The third objective involves the reactor flow rate, which is not captured by this figure. However, if the flow rate is increased, this will change these profiles and affect the first two objectives. The fourth and final objective is the temperature at the reactor outlet, which corresponds to the end point of the x-axis.

2.4 Process Design

The design of chemical processes is an enormous field of research itself. The first step is design of the reaction, where the actual chemistry needs to be understood, i.e., chemical reaction theory. Secondly, the temperature, the pressure and the concentration, at which the reaction should take place, should be determined. Thirdly, the process equipment, such as pumps, valves and heat exchangers, needed to achieve these properties are designed. Fourthly, additional process equipment is designed that will improve the quality or economy of the production, such as distillation columns or energy integration cycles. Examples of literature in this area may be [Levenspiel, 1999], [Froment and Bischoff, 1990] and [Fogler, 1992]. Traditionally, the process design and the control design has been done sequentially. In the recent decades, simultaneous approaches to design and control have been developed, see e.g. [Kookos and Perkins, 2001] or [Seferlis and Georgiadis, 2004] and the references therein.

Reactor Configurations

Reactor design and choice of operating point is outside the scope of this thesis. Nevertheless, it is very important to consider the interplay between process design, choice of operating point and control design, to avoid designs or operating points that may lead to unnecessarily hard control problems. On the other hand, with efficient process control, it is possible to choose designs and operating points that otherwise would be dangerous or inefficient.

The optimal number of the injection points and cooling zones and their locations along the reactor will vary depending on the given reaction and

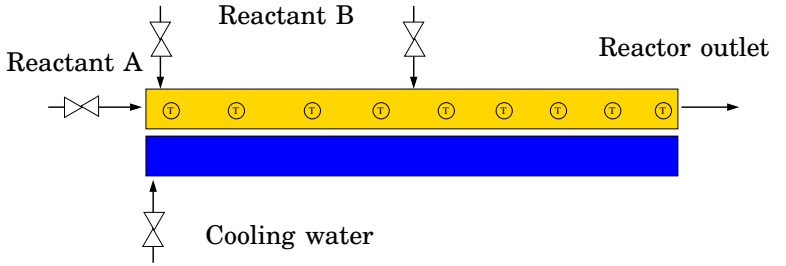

Figure 2.8 A reactor configuration with two injection points and one cooling zone.

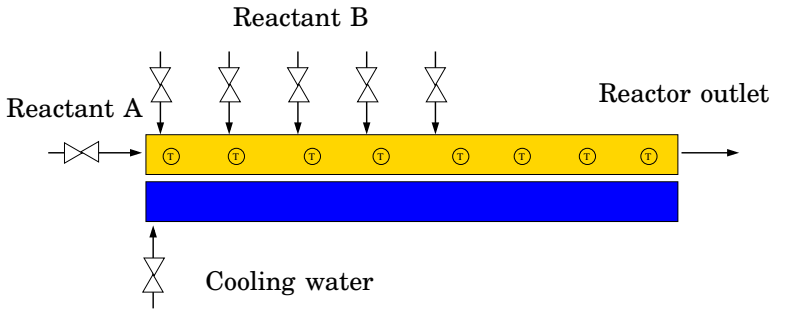

Figure 2.9 A reactor configuration with five injection points and one cooling zone. Additional injection points may improve the the production rate.

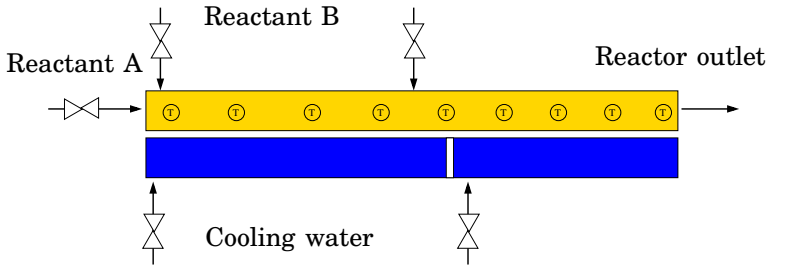

Figure 2.10 A reactor configuration with two injection points and two cooling zones. Additional cooling zones may improve the conversion.

the temperature constraints. Figures 2.8 – 2.10 illustrate three of many possible process configurations. There are predominantly advantages with additional injection points and cooling zones, but there are some practical aspects that set a limit.

Throughout the thesis, the configuration in Figure 2.8 will be used as

the standard configuration, unless stated otherwise. However, the results in this thesis can easily be extended to any type of configuration in terms of injection points and cooling zones.

Multiple Injection Points

There are two main reasons for having multiple injections, improve productivity, while respecting temperature constraints, and avoiding by-product formation.

Improve productivity in presence of constraints It is often not feasible to inject all reactant B at a single injection point, due to temperature constraints. By distributing the injections, the heat from the exothermic reaction will also be distributed, thus the cooling capacity can be better utilized. This enables higher productivity as the production rate often is limited by the available heat transfer. Figure 2.7 shows the temperature and conversion profiles along the reactor with two injection points. The second injection point allows an increase in the production rate with 80% compared to the single injection case. Figure 2.11 shows the situation with five injection points. The extra three injection points enable a further increase in production rate by additional 25%. The additional gain for each extra injection point becomes smaller and smaller. The disadvantages with many injection points are the cost associated with more pumps and sensors and the increased sensitivity for hardware failure. In addition, to uphold sufficient micro-mixing, there may be a lower limit on how small flow rate each injection can have.

Improve selectivity despite by-product formation Multiple injections may also be useful when there are parallel reactions leading to by-product formation. Assume that the following two reactions occur in the reactor,

$$A + B \rightarrow C + D \tag{2.6}$$
$$B + C \rightarrow E, \tag{2.7}$$

where as before C is the desired product and E is the unwanted by-product. With this reaction scheme, maximum selectivity of C is reached when the concentration of B is as low as possible, see e.g. [Levenspiel, 1999]. This is achieved by distributing the feed of B among multiple injection points. An extreme case of this is a tubular reactor with membrane walls, to allow continuous feed along the entire reactor, see [Cougnon *et al.*, 2006].

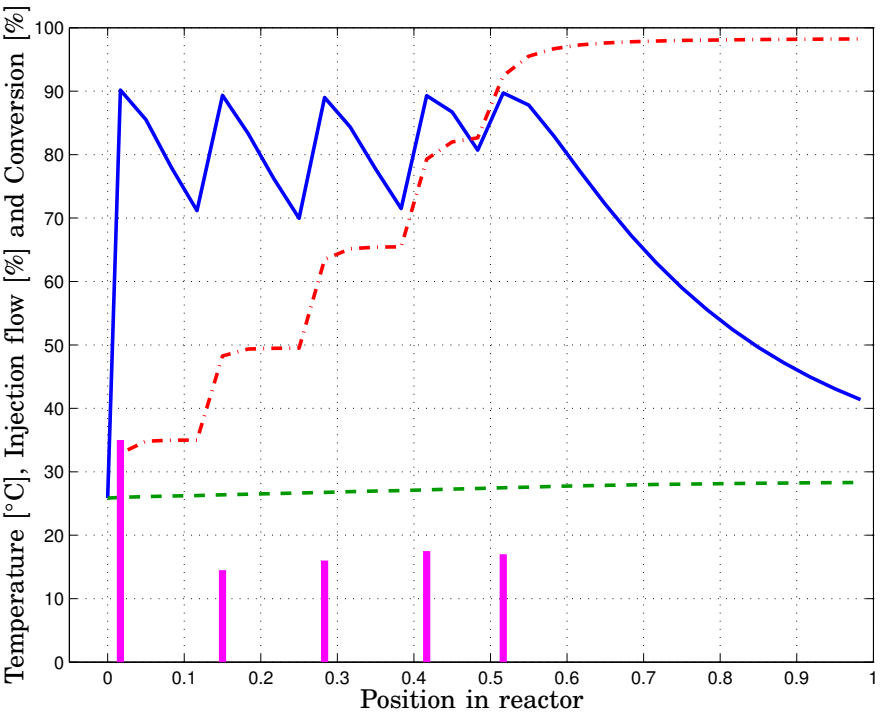

Figure 2.11 Steady-state profiles for the reactor configuration from Figure 2.9. The reactor temperature profile (solid), the cooling water temperature profile (dashed), the conversion profile (dash-dot) and the injection flow rates (vertical lines at their location).

Multiple Cooling Zones

With multiple cooling zones, it is possible to have separate cooling flows – with different temperatures – to cool different parts of the reactor. The concept is used for example in polystyrene plants [Vecchio and Petit, 2005], but the flexible construction of the plate reactor simplifies the use of these extra degrees of freedom.

With multiple cooling zones it is possible to adapt the cooling to the current temperature profile along the reactor, thus improving conversion or productivity, see e.g. [Smets *et al.*, 2002; Logist *et al.*, 2007], where optimal steady-state temperature profiles for the reactor and the cooling water are calculated. One example of the impact of two cooling zones is illustrated in Figure 2.12, where the water temperature in the second cooling zone is increased to reduce the cooling power to almost zero. This action leads to higher reactor temperatures, which improves the conver-

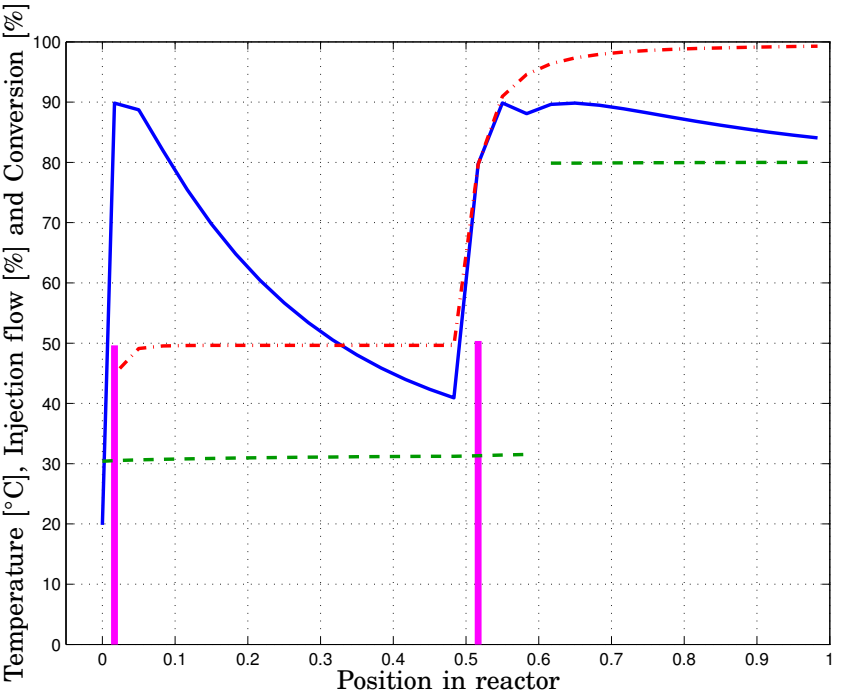

Figure 2.12 Steady-state profiles for the reactor configuration from Figure 2.10. The reactor temperature profile (solid), the cooling water temperature profile (dashed), the conversion profile (dash-dot) and the injection flow rates (vertical lines at their location). Note that the two cooling zones have separate inlet temperatures.

sion from 97.9% to 99.2%. The decrease in cooling power can alternatively be achieved by reducing the cooling flow rate.

2.5 Operating Modes

The plate reactor is a continuous reactor developed for manufacturing fine chemicals and pharmaceuticals, where the reactions are mixing and temperature sensitive, either exothermic or endothermic. The focus is on small to medium scale production. The process will spend most of its time in nominal operation, but there are also a few discrete operational modes associated to the start-up and shutdown procedures. Traditional continuous reactors are often tuned and designed for non-stop operation. The new reactor concept may allow the plate reactor to replace batch and semi-batch reactors for some reactions and the operation at higher

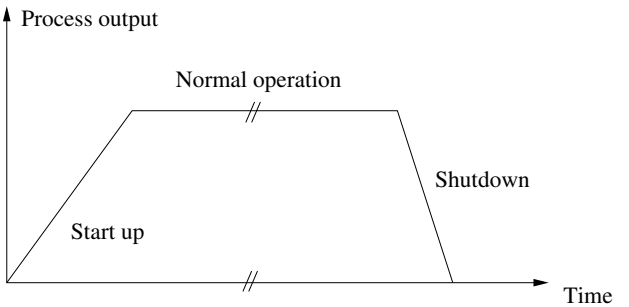

Figure 2.13 A schematic figure of a typical sequence of operation.

temperatures may lead to reduced reaction times. A single reactor unit may then be used for many different reactions, which may increase the number of start-ups and shutdowns compared to traditional operation of continuous reactors.

Furthermore, the start-up and shutdown procedures may be critical for a successful operation, especially the start-up. In this section, the three different operation modes of the plate reactor will be briefly described and the type of control needed in each operating mode, see Figure 2.13. The control at nominal operation is developed in Chapter 4 and the start-up control is presented in Chapter 5.

Start-up Control Mode

The start-up phase has to be individually adapted to each chemical reaction. In some cases it will be straightforward, but in many cases it may probably be the most difficult part of operation for the plate reactor. The aim is to safely bring the process from initial conditions to the desired steady-state of nominal operation. The main challenge is that some reactions are difficult to start, i.e., the reactor temperature needs to be raised to reach the ignition point, but after ignition the exothermic reaction needs quickly to be cooled to prevent thermal runaways. During the start-up, there will be transients in temperature, flow rates and concentrations that the control system has to deal with. The process will during this period have a strongly nonlinear behavior, which any model-based control has to consider.

The main control objective during start-up is to keep safe reactor temperatures. Second and third in priority are the conversion during start-up and the time to reach the nominal operating point.

Nominal Control Mode

In the nominal control mode, the main objectives of the control system are to ensure safe production by keeping the reactor temperature below some given safety limit and to achieve optimal conditions inside the plate reactor, which lead to maximum conversion. The operating point at which this is achieved may not exactly be known in advance. Off-line calculations can give initial suggestions, but process uncertainties may result in sub-optimal conditions or lead to reactor temperatures that are dangerously high and cause unnecessary process shutdowns. Instead of trial-and-error open loop control, feedback control can adjust the input variables to compensate for these uncertainties in for example valves and pumps characteristics, heat transfer coefficients or reaction kinetics. Since the plate reactor will operate most of if its time in this mode, it is crucial that the resulting operating point gives good performance. Even a small increase in conversion or productivity will over time give large effects on the economy of the process.

The control system should also prevent any disturbances outside the plate reactor to affect the input flows to the plate reactor, for example by feed forward control or integral action through disturbance estimation.

Shutdown Control Mode

The shutdown mode is activated when the production should be halted. It should be an orderly and safe shutdown, so that production can be restarted easily. Emergency shutdown is a different procedure that is outside the scope of this work. The shutdown control sequence will have to be designed specifically for each reaction and reactants. Normally for an exothermic reaction it would start by closing all the inlet valves of the secondary reactant and then after some time also close the inlet valve of the primary reactant. When the flow rate of the secondary reactant is stopped, a magnetic valve should be switched so that the remaining product in the plate reactor flows into a buffer tank instead of further down the production line. Depending on the reactants used, the system may need to be rinsed before restart.

In many cases, it may be wise to increase cooling during shutdown operation, to further inhibit the reaction. However, for some reactions the solubility is highly temperature sensitive. Increased cooling may then lead to particle formation and clogging inside the reactor. This underlines the importance of carefully studying the reaction and the properties of the chemicals when designing the process operations.

2.6 An Outline of Control System Design

In this chapter, the concept of the novel plate reactor has been presented and some aspects of its operation discussed. In the remainder of the thesis, the focus will be on control design for the plate reactor. The methods presented are developed for the plate reactor, but are straight-forward applicable to general tubular reactor systems. A proper control system design is much more than just finding the right controller parameters or choosing the tuning method. In [Skogestad and Postlethwaite, 2005], they present a list on suitable steps in control system design.

1. Study the system (process, plant) to be controlled and obtain initial information about the control objectives.
2. Model the system and simplify the model, if necessary.
3. Scale the variables and analyse the resulting model; determine its properties.
4. Decide which variables are to be controlled (controlled outputs).
5. Decide on the measurement and manipulated variables; what sensors and actuators will be used and where will they be placed?
6. Select the control configuration.
7. Decide on the type of controller to be used.
8. Decide on performance specification, based on the overall objectives.
9. Design a controller.
10. Analyze the resulting controlled system to see if the specifications are satisfied; and if they are not satisfied modify the specifications or the type of controller.
11. Simulate the resulting controlled system, on either a computer or a pilot plant.
12. Repeat from step 2, if necessary.
13. Choose hardware and software and implement the controller.
14. Test and validate the control system, and tune the controller on-line, if necessary.

The authors of [Skogestad and Postlethwaite, 2005] argue that textbooks on control usually focus on steps 9 and 10, whereas many real control systems are designed based on steps 1, 4, 5, 6, 7, 13 and 14 only. They also mention that the list should perhaps include a step 0, involving the

design of the process equipment itself. This emphasizes that collaboration between process engineers and control engineers are essential to develop a reliable and efficient control system.

The aim of this thesis is to approach the control design for the plate reactor from a realistic and practical point of view, inspired by the list above. In this chapter, the process concept and objectives have been presented (step 1). In Chapter 3, a nonlinear process model is developed from first principles. The model is analyzed to find the process inputs most suitable for feedback control (steps 2-5). Chapter 4 presents decentralized and centralized control methods within the general control structure. Different controllers are designed and evaluated in simulations (steps 6-11). Chapter 5 repeats these steps, but now applied to the more difficult start-up control problem.

3

Modeling and Analysis

There is a wide range of uses for dynamic models, for example, process design, control design, operator training, process analysis, and hardware-in-the-loop tests. In this chapter, a process model of the plate reactor is developed primarily for analysis. The purpose is to understand the physics of the process and how the process inputs relate to the different operational objectives defined in Section 2.3. In the list on suitable steps in control design from Section 2.6, this chapter will deal with steps 2-5. Models for control design will be discussed in Chapter 4.6.

3.1 Modeling and Simulation

A model of the plate reactor can be derived from first principles, with equations for heat transfer, reaction kinetics, mass, energy, and chemical balances, see e.g. [Froment and Bischoff, 1990].

The multiple consecutive horizontal channels inside the plate reactor in Figure 2.1 have a very small cross-section area compared to the channel length, and the cross-sectional temperature and concentration gradients can be neglected. Thus, the reactor may, from a modeling point of view, be approximated as a 1-dimensional continuous tubular reactor with injections of reactant B along the reactor and a cooling jacket around the tube.

Partial Differential Equations

The balance equations and the distributed nature of the process lead to five partial differential equations (PDEs) for the reactor temperature T_r, the cooling water temperature T_w and the concentrations for the reactants

and products, c_A, c_B, and c_C, see e.g. [Hangos and Cameron, 2001],

$$\begin{aligned}
\frac{\partial T_r}{\partial t} &= \mathcal{D}_e \frac{\partial^2 T}{\partial z^2} - v_r \frac{\partial T_r}{\partial z} - \frac{4h}{d_r \rho c_p}(T_r - T_w) + \frac{\Delta H}{\rho_r c_p} r \\
\frac{\partial T_w}{\partial t} &= - v_w \frac{\partial T_w}{\partial z} + \frac{4h}{d_w \rho c_p}(T_r - T_w) \\
\frac{\partial c_A}{\partial t} &= \mathcal{D}_m \frac{\partial^2 c_A}{\partial z^2} - v_r \frac{\partial c_A}{\partial z} - r \\
\frac{\partial c_B}{\partial t} &= \mathcal{D}_m \frac{\partial^2 c_B}{\partial z^2} - v_r \frac{\partial c_B}{\partial z} - r \\
\frac{\partial c_C}{\partial t} &= \mathcal{D}_m \frac{\partial^2 c_C}{\partial z^2} - v_r \frac{\partial c_C}{\partial z} + r
\end{aligned} \tag{3.1}$$

where the reaction rate r is defined by the Arrhenius law, see (2.3). The variable z is the position along the reactor flow channel, d_r is the reactor tube diameter, d_w is the cooling jacket tube diameter and h is the heat transfer coefficient between reactor fluid and water. The variables v_r and v_w represent the fluid velocity through the reactor and the cooling jacket, respectively. ΔH is the reaction energy term. The density and the specific heat capacity are denoted by ρ and c_p. $\mathcal{D}_e$ and $\mathcal{D}_m$ are the energy and mass dispersion coefficients, respectively. The very high flow rate of the cooling water means that the diffusion term for T_w can be neglected. A complete list of symbols is given in the Appendix.

Model approximations Several approximations have been made to obtain the model in (3.1). Experiments performed at Chalmers Institute of Technology, [Bouaifi *et al.*, 2004] and [Andersson *et al.*, 2004], have shown that perfect mixing conditions are achieved already a very short distance after injection. This implies that the inhomogeneous micro-mixing can be disregarded and that the Arrhenius law (2.3) is a valid approximation of the reaction kinetics.

The pressure dynamics are in this application neglected, i.e., the changes in mass flow rate are assumed to be instantaneous. The reason is that the flow rate of reactant A is assumed to be constant at all times and this flow constitutes roughly 80% of the total reactor flow. The thermal inertia of the metal between the reactor fluid and the water is neglected as well as the thermal conductivity in the metal in the z-direction. The heat transfer effect between neighboring reactor flow channels are neglected. Constant values of the density, specific heat capacities and heat transfer coefficients have been assumed. The density and heat capacity of the reactor fluid is approximated to the values of the cooling water.

Experiments performed at Alfa Laval have shown that the flow inside the reactor can be viewed as close to plug flow [Prat *et al.*, 2005].

The deviation from a perfect plug flow may be approximated as an axial dispersion along the reactor. The dispersion depends on the flow channel geometry, back mixing, stagnant zones, fluid properties such as viscosity, the flow rate and the molecular diffusion. In [Levenspiel, 1999], two model approximations for axial dispersion are presented, the dispersion model and the tanks-in-series model. In the dispersion model, all contributions to intermixing of the fluid may be described by the axial dispersion coefficient $\mathcal{D}$. This coefficient is fitted based on residence time distribution (RTD) analysis. However, the estimated value of $\mathcal{D}$ from the RTD analysis may be affected by the number of discretization points and the choice of discretization method.

In the tanks-in-series model, the reactor is approximated with N equal well-stirred tanks in series. The number of tanks N to be used is fitted from RTD analysis. According to [Levenspiel, 1999], the dispersion model has the advantage that it can be used for all kind of flow correlations of real reactors. On the other hand the tanks-in-series model is simple and can be extended to any arrangement of compartments. A drawback is that the number of tanks N is fixed by the RTD analysis, which may limit the flexibility of the model in simulations.

Simulation of the PDE Model

One part of the model analysis is to learn and understand the dynamics of the process through simulations. To simulate the PDEs, the infinite dimensional system is approximated to a finite dimensional system. There are many different methods, see e.g. [Hangos and Cameron, 2001], such as the Finite Difference Method or the Finite Volume Method, where both time t and space z is discretized into an set of algebraic equations. A version of this is the Method-of-Lines, [Schiesser, 1991], where only the spatial coordinate z is discretized and the time derivative remains continuous, thus leading to a set of ordinary differential equations (ODEs). Other alternatives are the methods of weighted residuals, which includes orthogonal collocation and the Galerkin method. These methods are also known as Finite Elements Methods.

In this thesis, the PDEs are discretized with the Finite Volume Method, using the Method-of-Lines, see Figure 3.1. The spatial derivatives are approximated with the backward difference method, yielding a system of ODEs. Each PDE is approximated with $N = 30$ control volumes, which is a compromise between accuracy and computational complexity. In addition, the RTD analysis of the simulated model when $N = 30$ indicates that the axial dispersion may in this case be approximated with the tanks-in-series model. However, if further accuracy of the model is required, using higher values of N, the dispersion model should be used. The model equations

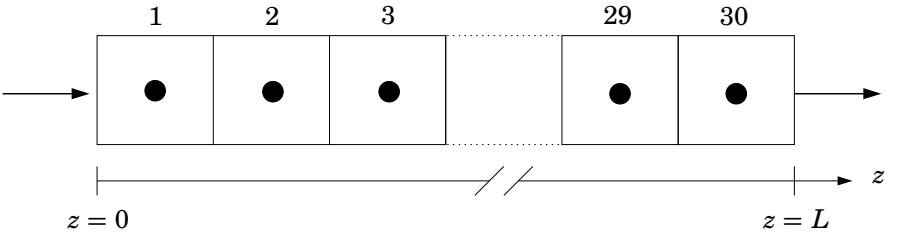

Figure 3.1 In the Finite Volume Method, the reactor is divided into several control volumes. Here, $N = 30$ control volumes are used. The PDE is integrated over each control volume, which results in a series of ODEs. The temperature and concentration of each grid point is the average value of the entire control volume.

for the first control volume can be written as

$$\begin{aligned}
\frac{dT_{r,1}}{dt} &= \frac{q_{A,\text{feed}}}{V_r}T_{A,\text{feed}} + \frac{q_{B1}}{V_r}T_{B,\text{feed}} - \frac{q_{r,1}}{V_r}T_{r,1} \\
&\quad + \frac{hA_{\text{heat}}}{\rho c_p V_r}(T_{w,1} - T_{r,1}) + \frac{\Delta H}{\rho c_p}k_0 e^{\frac{E_a}{RT_{r,1}}}c_{A,1}c_{B,1} \\
\frac{dT_{w,1}}{dt} &= \frac{q_{\text{cool}}}{V_w}T_{\text{cool}} - \frac{q_{\text{cool}}}{V_w}T_{w,1} - \frac{hA_{\text{heat}}}{\rho c_p V_w}(T_{w,1} - T_{r,1}) \\
\frac{dc_{A,1}}{dt} &= \frac{q_A}{V_r}c_{A,\text{feed}} - \frac{q_{r,1}}{V_r}c_{A,1} - k_0 e^{\frac{E_a}{RT_{r,1}}}c_{A,1}c_{B,1} \\
\frac{dc_{B,1}}{dt} &= \frac{q_{B1}}{V_r}c_{B,\text{feed}} - \frac{q_{r,1}}{V_r}c_{B,1} - k_0 e^{\frac{E_a}{RT_{r,1}}}c_{A,1}c_{B,1} \\
\frac{dc_{C,1}}{dt} &= -\frac{q_{r,1}}{V_r}c_{C,1} + k_0 e^{\frac{E_a}{RT_{r,1}}}c_{A,1}c_{B,1}.
\end{aligned} \tag{3.2}$$

where the subscript '1' represents the variables in control volume 1. In addition to the variables and parameters defined earlier in the PDEs (3.1), there are some new variables and parameters associated with the ODEs. A complete list of symbols is given in the Appendix. V_r is the volume of one reactor control volume, V_w is the volume of one cooling water control volume, q_r is the reactor flow rate, q_{cool} is the cooling flow rate, $q_{A,\text{feed}}$ is the feed flow rate of reactant A, q_{B1} is the flow rate of B into the first injection point. The inlet temperature of the cooling water is denoted T_{cool}. As the PDE is approximated with N control volumes, $\mathbf{T_r}, \mathbf{T_w}, \mathbf{c_A}, \mathbf{c_B}$ and $\mathbf{c_C}$ are all vectors of size N. The full state vector is defined as $\mathbf{x} = [\mathbf{T_r}^T \quad \mathbf{T_w}^T \quad \mathbf{c_A}^T \quad \mathbf{c_B}^T \quad \mathbf{c_C}^T]^T$ of size $5N$.

Implementation

The reactor model (3.2) has been implemented both in Matlab/Simulink [Mathworks, 2007a] and in the Modelica language, [Modelica Association,

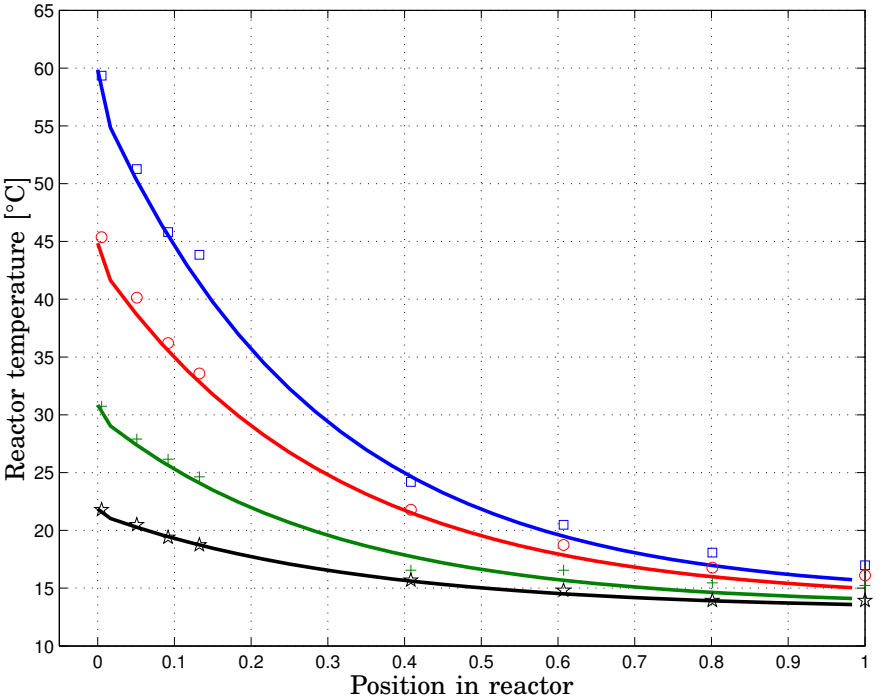

Figure 3.2 Model validation of steady-state temperature profile with water test. The simulated temperature profiles are from top: $T_{A,\text{feed}} = 60°\text{C}$, $T_{A,\text{feed}} = 45°\text{C}$, $T_{A,\text{feed}} = 31°\text{C}$ and the bottom line is when $T_{A,\text{feed}} = 22°\text{C}$. The experimental results are marked with □, ◯, + and ⋆, respectively.

2005] and simulated in Dymola, [Dynasim, 2001].

Model Validation

Data for the validation is taken from initial experiments in Toulouse with the test unit shown in Figure 2.4, [Prat *et al.*, 2005].

Steady-state validation with hot/cold water To investigate the heat transfer capabilities, hot water was used as the process fluid A. There were no injections along the reactor, that is, $q_{B,\text{feed}} = 0$. Figure 3.2 shows four steady-state temperature profiles for four different feed temperatures $T_{A,\text{feed}}$. In this experiment, the plate reactor can be seen as a simple heat exchanger. The cooling inlet temperature T_{cool} is 13°C and $q_{\text{cool}} = 0.50\ \text{m}^3/\text{h}$. The simulated profiles from the model have a very good agreement with the experimental data.

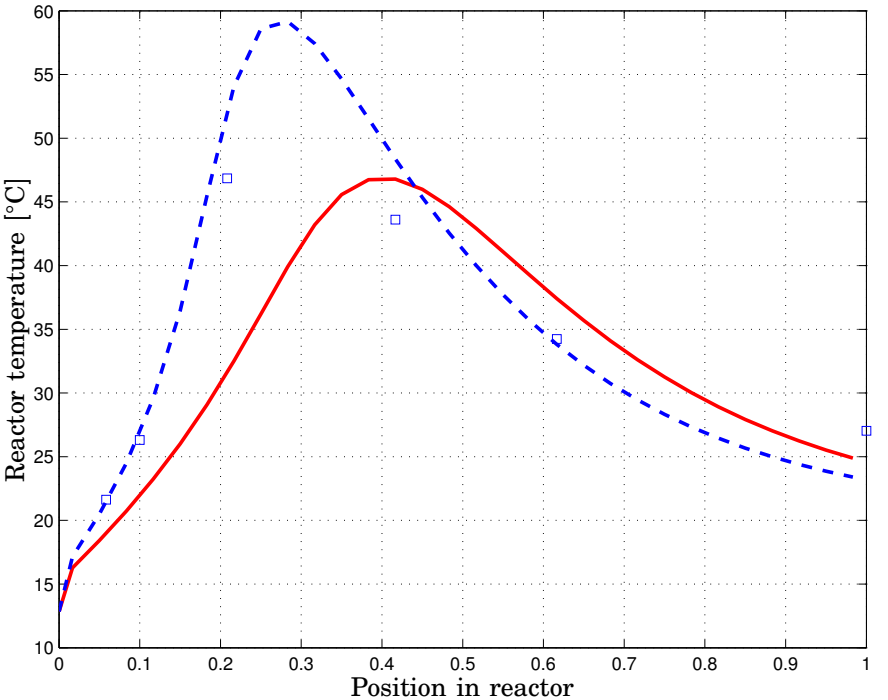

Figure 3.3 Model validation of steady-state temperature profile with the sodium thiosulfate reaction. The squares represent the temperatures from the experiment. The solid line represents the nominal model. The dashed line represents the model with a parameter deviation of 1% in E_a and ΔH.

Steady-state validation with the sodium thiosulfate reaction

When the heat transfer capacity has been verified, the next step is to validate the model with the sodium thiosulfate reaction. In the experiment reported in [Prat *et al.*, 2005], only the first injection point was used. The feed concentrations were $c_{A,\text{feed}} = 855$ mol/m^3 and $c_{B,\text{feed}} = 6920$ mol/m^3. Note that the feed concentrations in this experiment are much lower than the nominal values used in this thesis, see Appendix, which will lower the temperature maximum and shift the location of the maximum further downstream of the injection point compared to the plots in Chapter 2. The feed temperature and the cooling inlet temperature were both 13°C, and the cooling flow rate q_{cool} was 0.59 m^3/h.

The simulated temperature profile is shown in Figure 3.3. There are some differences between the simulated profile and the temperatures from the experiment, especially in the first half of the reactor. By decreasing the

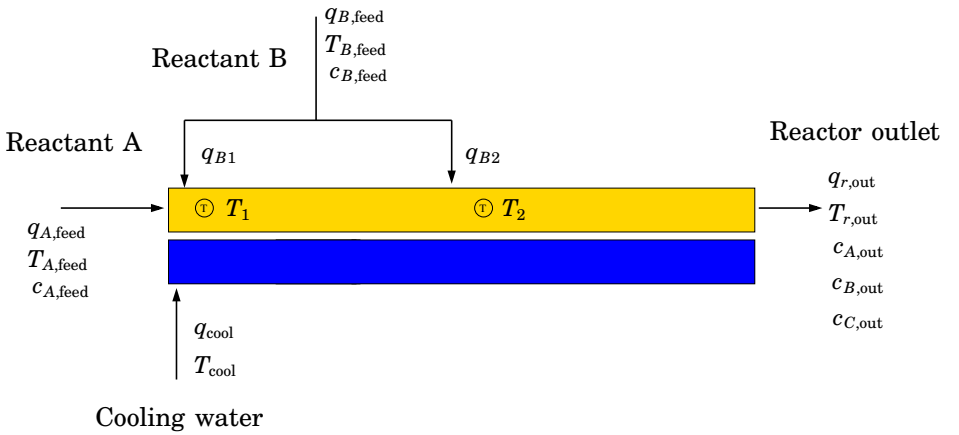

Figure 3.4 The plate reactor as a schematic tubular reactor with four inflows and one outflow. The inputs and outputs are the temperatures, flow rates and concentrations of these flows. The circles with T represent internal temperature sensors. T_1 and T_2 represent the peaks of the temperature profile.

values of the model parameters E_a and ΔH with 1%, the simulation model yielded another temperature profile, this time in better agreement with the experiment measurements. The conclusion here is that the developed model can in general represent the behavior of a plate reactor, but strong nonlinearities may yield significant plant/model mismatch. It is therefore essential that the designed controller has very good robustness towards model uncertainty. This will be investigated in Chapters 5 – 7, where the start-up control problem is solved despite large model uncertainty.

3.2 Model Analysis

In this section, we will analyze the process to gain physical insights and process knowledge that will be valuable for the control system design. An intermediate step in the analysis is to obtain information to select the best input variables for process control.

In the following analysis, we consider a plate reactor configuration with two injection points and one cooling zone, and the sodium thiosulfate reaction.

Steady-State Analysis

The process inputs were briefly described in Section 2.2. The main priority of operation is safety, thus temperature control is very important

Table 3.1 Scaled steady state gains of the linearized plate reactor model. Each entry in the table reflects the temperature deviation [°C] from a 1% or 1°C change in the input variable.

	u_{B1}	u_{B2}	$T_{A,\text{feed}}$	$T_{B,\text{feed}}$	T_{cool}	q_{cool}	$q_{A,\text{feed}}$	$c_{A,\text{feed}}$	$c_{B,\text{feed}}$
T_1	1.81	0	1.25	0.16	0.21	-2e-4	-0.87	0.18	1.03
T_2	-0.95	0.83	0.15	0.18	1.58	-0.01	0.38	1.09	0.17

and especially control of the maximum temperatures, which often occur after the injection points. To understand the impact of the process inputs on the reactor temperatures, the steady-state gains from each input to the maximum temperatures T_1 and T_2 after the two injection points were computed, see Figure 3.4. The process was linearized around the nominal operating point plotted in Figure 2.7. All gains, except from the temperature inputs, were scaled with 1% of the steady-state input value. Table 3.1 lists the scaled steady-state gains, that is, each entry in the table reflects the temperature deviation from a 1% or 1°C change in the input variable.

First of all it can be noted that some input signals has a predominant effect on either the first or the second temperature, i.e., there is a spatial variation of the gain. For example $T_{A,\text{feed}}$ and $c_{B,\text{feed}}$ mainly affect T_1, whereas u_{B2}, T_{cool}, q_{cool} and $c_{A,\text{feed}}$ mainly affect T_2. Figure 3.5 illustrates the spatial dependency of some input gains. The extra high gains at the second injection point depend on the temperature sensitive reaction there, thus each change of the input will have a larger effect on the reactor temperature there. The gain of u_{B1} is positive at the first, but negative at the second injection point. This follows from the stoichiometric relation at this specific operating point. If more B is injected at the reactor inlet, the temperature will increase locally, but this will leave less A unreacted flowing down to the second injection point, thus decreasing the reaction rate and heat release there. If there had been an excess of A, u_{B1} would not have a negative gain there.

Secondly, note that the table data reflects the linearized gains at a specific operating point. The gains will vary due to the severe nonlinearities of the process, e.g. the stoichiometric relations or the exponentially temperature dependence of the reaction rate. The nonlinear effects may cause even the slightest change of any input variable to have significant impact on the reactor temperature. The gain of the cooling flow rate is very small for this specific choice of operating point. If a much lower cooling flow rate had been used, the gain of this process input would have been larger, see also Figure 3.8.

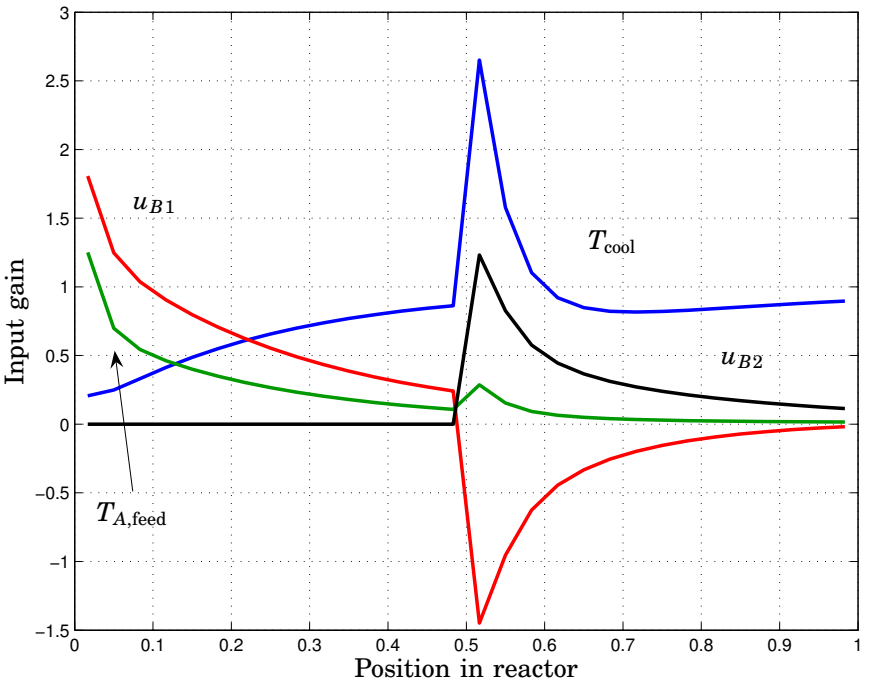

Figure 3.5 The steady state gain of u_{B1}, u_{B2}, $T_{A,\text{feed}}$ and T_{cool} at various positions along the reactor.

To further illustrate the spatial effect of the different control inputs, the steady state profiles along the reactor are studied for a wide range of input changes. Compare with the nominal operating point from Figure 2.7.

Changes in the reactant injection distribution. Figure 3.6 shows two different feed distributions of the reactant B. The first case is the steady-state point when $u_{B1} = 0.40$ and $u_{B2} = 0.60$, that is, 40 % is injected in the first injection point and 60% of the total flow of B is injected in the second injection point. In the second case the feed distribution is changed to 60/40, that is, 60% of the feed is injected at the first injection point. The figure shows the close relationship between the injection distribution and heat release distribution, causing a significant difference in the temperature profiles. When more reactant B is injected at the reactor inlet, the maximum steady-state temperature increases from 75 to 108°C. Note also that the position of the temperature maximum moves slightly upstream. The higher concentration of B leads to faster reaction rate, thus also higher temperature gradients.

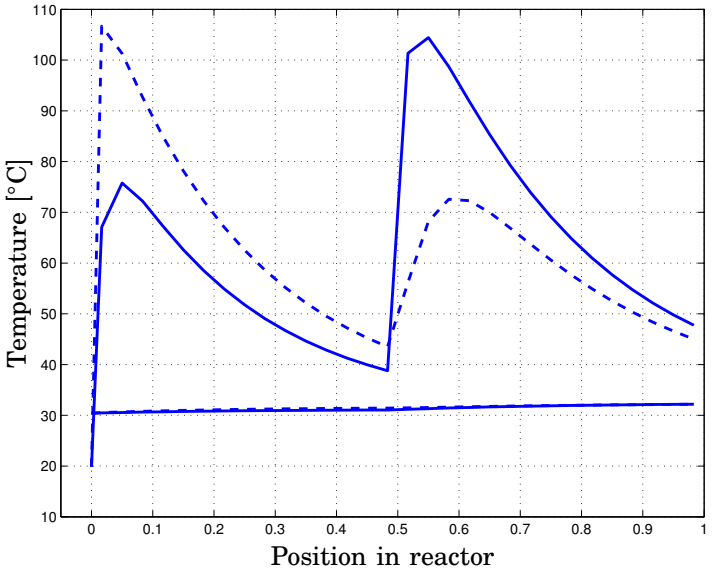

Figure 3.6 Steady-state temperature profiles along the reactor. The solid line represents the case when the injection distribution of reactant B is $[u_{B1}\ u_{B2}] = [0.40\ 0.60]$, i.e., 40% in the first injection point and 60% in the second injection point compared to the opposite case 60/40 (dashed). Compare with Figure 2.7.

Changes in the cooling temperature. In Figure 3.7, the cooling inlet temperature has been changed from 20°C to 40°C. Here we can see that the change in T_{cool} has a limited influence on the first temperature maximum compared to the second injection point. With more cooling, the reaction rate is slower in the second part of the reactor, thus leading to smaller temperature gradients and a lower conversion. Note that the cooling power, the transferred power out from the reactor, is a linear function of the temperature difference $(T_r - T_{\text{cool}})$, see Eq. 3.2, so by manipulating the cooling temperature, it is easy to control the reactor temperature around the second temperature maximum.

Changes in the cooling flow rate. In Figure 3.8, three different cooling flow rates has been used, from the nominal flow rate q_{cool} down to $0.05 \cdot q_{\text{cool}}$. The heat transfer from the reactor is proportional to the temperature difference between the reactor fluid and the water. If a very low cooling flow rate is used, $0.05 \cdot q_{\text{cool}}$, the cooling water is significantly heated by the heat release and the temperature difference, thus also the heat transfer, decreases. To increase cooling, a higher cooling flow rate is used, $0.2 \cdot q_{\text{cool}}$. The higher flow rate can absorb more heat from the

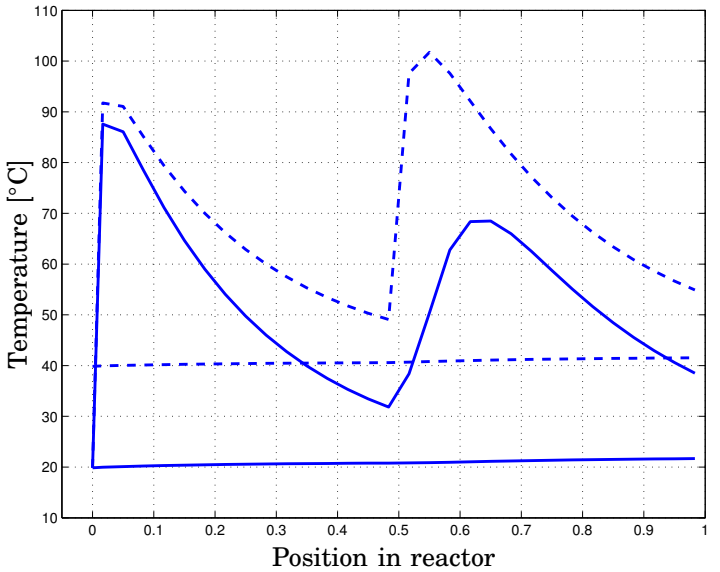

Figure 3.7 Steady-state temperature profile along the reactor when the inlet temperature of the cooling water T_{cool} is 20°C (solid) compared to 40°C (dashed). Compare with Figure 2.7. Note the shift in position of the temperature maximum.

reaction, which increases the heat transfer. The third case is the nominal flow rate q_{cool}. The flow rate is so high that the temperature of the cooling water remains almost constant. There would be no use to further increase the flow rate, since the temperature difference, thus also the heat transfer, would remain constant. This means that the process gain of the cooling flow rate goes to zero when the flow rate is so large that the cooling water temperature remains almost constant. In addition, the heat transfer coefficient h varies with the cooling flow rate, which introduces more nonlinearities, e.g. when decreasing the cooling flow rate from 1.5 m^3/h to 0.2 m^3/h, the heat transfer coefficient decreases with 50% [Prat *et al.*, 2005]. These nonlinearities may introduce difficulties when choosing the flow rate as control input.

Changes in the feed temperature. In Figure 3.9, the feed temperature of the primary reactant A is 10°C and 30°C, respectively. The change in T_{feed} has a major impact on the first temperature maximum and almost zero impact on the second maximum. The feed temperature can therefore be useful to control the temperature in the first section of the plate reactor, while not affecting the remainder of the reactor.

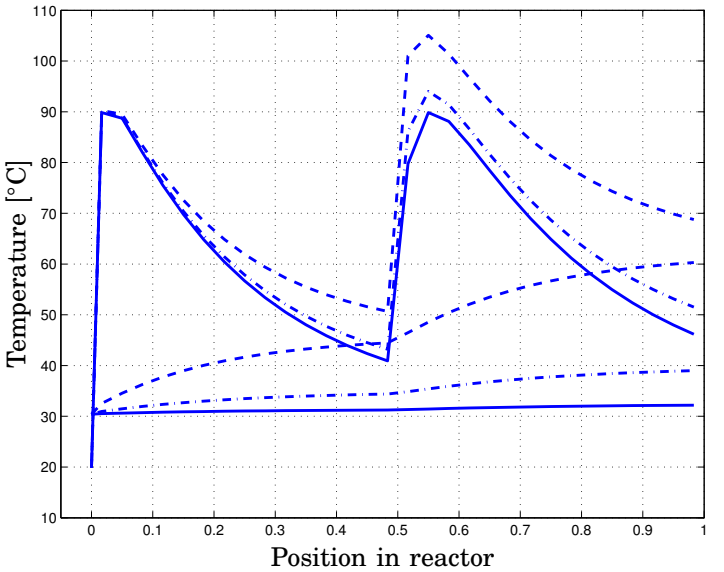

Figure 3.8 Steady-state temperature profiles along the reactor when the cooling flow rate varies from the nominal value q_{cool} (solid), to $0.2 \cdot q_{\text{cool}}$ (dash-dot) and to $0.05 \cdot q_{\text{cool}}$ (dashed).

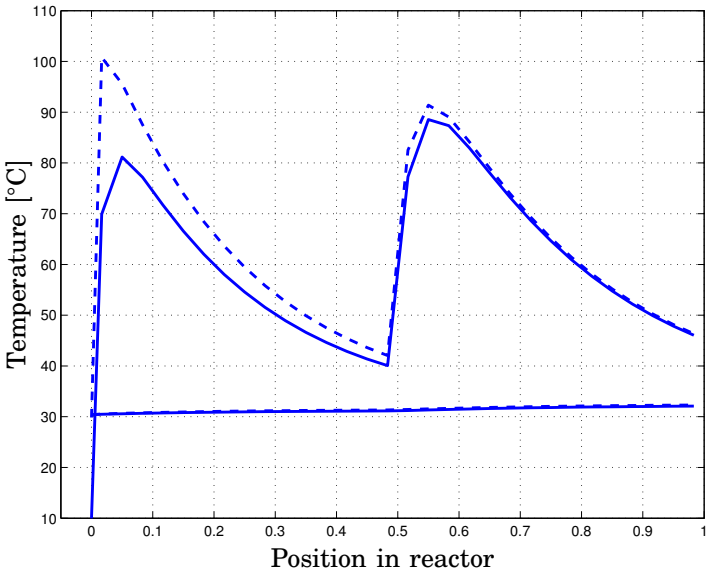

Figure 3.9 Steady-state temperature profiles along the reactor when the feed temperature $T_{A,\text{feed}}$ is 10°C (solid) compared to 30°C (dashed). Compare with Figure 2.7.

Dynamic Analysis

For control purposes it is essential to have a thorough knowledge of the process dynamics. The steady state information from the previous section is simply not sufficient, especially for exothermic reactions that may lead to unstable dynamics. It is then vital to choose control variables with fast dynamics to allow stabilizing control actions, see for example [Stein, 2003].

The plate reactor can be approximated as a tubular reactor, which is a distributed parameter system described by partial differential equations. In [Winkin *et al.*, 2000] a dynamical analysis of tubular reactors is presented within a infinite-dimensional framework. Conditions for observability, controllability and stability are derived. The nonlinear dynamics of a non-isothermal tubular reactor with perfect plug flow has one and only one solution, whereas with axial dispersion the system may have a single or multiple equilibrium profiles for a given set of control signals, [Laabissi *et al.*, 2004]. When there exists multiple equilibrium profiles, one equilibrium profile corresponds to the situation when no reaction occurs, due to too low reactor temperature. Another equilibrium profile reflects the situation when almost all reactants have converted at high reactor temperature, which is the desired operating point for the plate reactor. Finally, in between these profiles, there is an equilibrium profile, which is unstable due to the exothermic reaction.

The main dynamics of the plate reactor are the fast chemical reaction kinetics and the slower heat transfer dynamics, which leads to a potentially *stiff* system. The residence time of 30 seconds, i.e., the flow time from inlet to outlet, contributes significantly to the reactor dynamics, especially if an outlet variable is to be controlled with an inlet variable of the reactor. The flow time for the cooling water is much shorter, $1 - 2$ seconds due to a higher flow rate. This implies that a change in the outlet temperature is more easily carried out by varying an inlet variable of the cooling flow than an inlet variable of the reactor flow.

At the nominal operating point, the poles of the linearized model are all well inside the left half plane, located predominantly along the negative real axis. The poles and the zeros of the model depend on the discretization method for the PDEs, here first order backward difference is used.

The data in Table 3.1 indicates what input signals to study further for use in feedback control, for example, the low gains eliminate $T_{B,\text{feed}}$ and q_{cool}. The inputs of q_A, $c_{A,\text{feed}}$ and $c_{B,\text{feed}}$ are often fixed for a certain production rate. Figure 3.10 shows the Bode diagrams of the four most dominant open loop transfer functions from the control inputs, including actuator dynamics, to the reactor temperatures T_1 and T_2 at nominal operating point. The inputs are scaled using the same factors as in Ta-

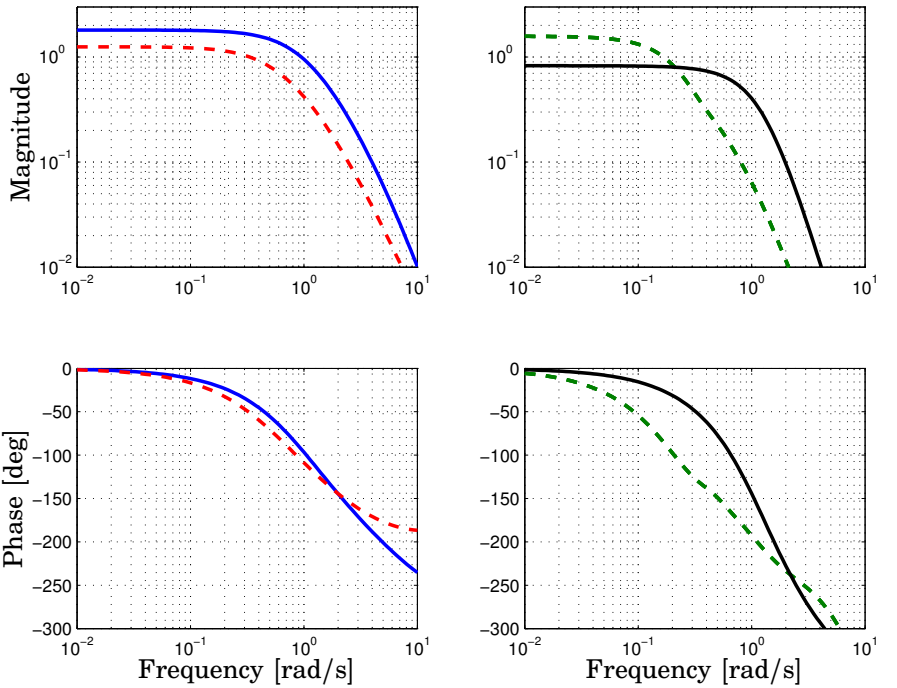

Figure 3.10 Bode diagrams Left: $u_{B1} \to T_1$ (solid), $T_{A,\text{feed}} \to T_1$ (dashed). Right: $u_{B2} \to T_2$ (solid) and $T_{\text{cool}} \to T_2$ (dashed).

ble 3.1. The four control inputs have a bandwidth[1] of 0.7, 0.7, 0.4 and 0.1 rad/s for $u_{B1}, u_{B2}, T_{A,\text{feed}}$ and T_{cool}, respectively. Nonlinear gain and input limitations may limit the available bandwidth for feedback control. The injection flow rates have slightly higher bandwidth, partly due to faster actuator dynamics.

To further investigate the dynamics of the plate reactor, step responses are plotted in Figure 3.11. The upper plots show the responses to steps in u_{B1} and $T_{A,\text{feed}}$ and the lower plots show the responses to steps in u_{B2} and T_{cool}. Three different responses are plotted, T_1, T_2 and $c_{C,\text{out}}$, which is the outlet concentration of product C. Note that these three variables have different spatial location along the reactor, representing the inlet, the middle and the outlet, respectively. The flow delays between these locations are clearly visible in the plots, 15 seconds between the two injection points and 30 seconds from inlet to outlet.

The simulations in Figure 3.11 show only the linear dynamics around

[1]Here bandwidth is defined as the frequency at which the gain has dropped to $1/\sqrt{2}$ of the steady-state gain.

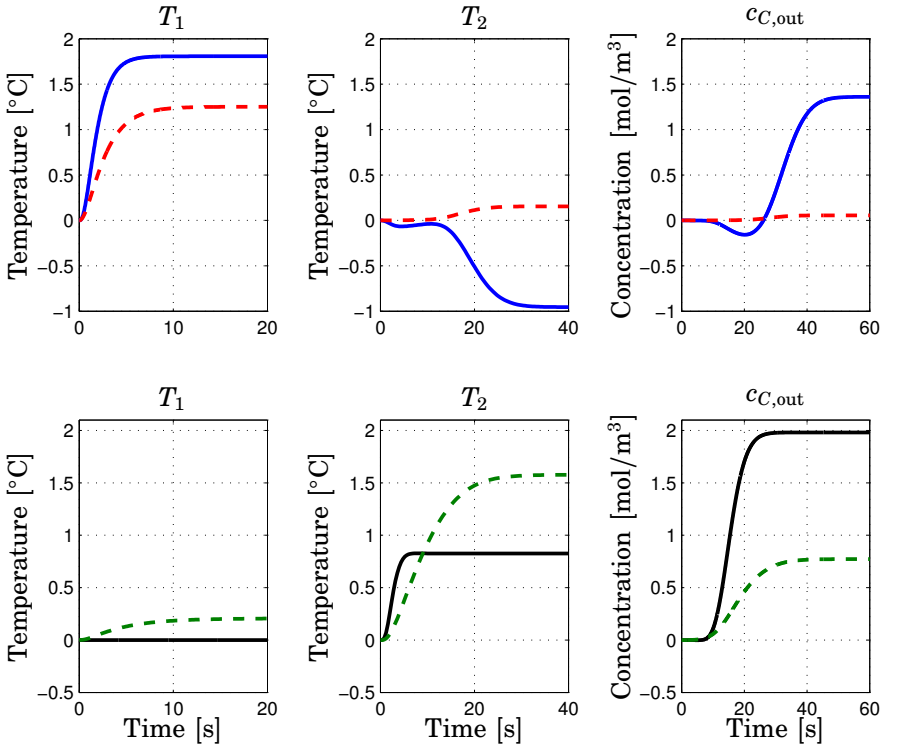

Figure 3.11 Typical step responses. Upper plots: The step responses from u_{B1} (solid) and $T_{A,\text{feed}}$ (dashed) to T_1, T_2 and $c_{C,\text{out}}$, respectively. Lower plots: The step responses from u_{B2} (solid) and T_{cool} (dashed) to T_1, T_2 and $c_{C,\text{out}}$, respectively. Note the different scales on the x-axis and the y-axis.

the nominal operating point. For larger transitions, the dynamics can show highly nonlinear behavior. One example is the dynamics during a start-up transition, see e.g. Figure 5.3 in Chapter 5.

3.3 Control Variable Selection

The previous section on the steady-state and dynamic analysis has shown how the different control input candidates affect the states inside the reactor. In this section, we will briefly summarize the control input candidates, their actuator dynamics and in what context they should be used. For example, different control objectives, such as start-up or production optimization, may require different sets of control inputs. Each control in-

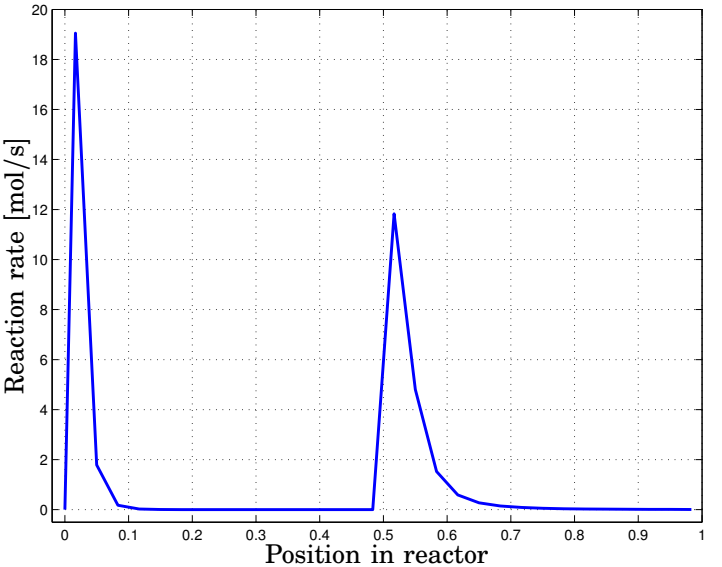

Figure 3.12 The reaction rate [mol/s] at steady-state along the reactor length. Note the very small regions where the fast reaction actually take place.

put is associated with one of the four inflows to the reactor, see Figure 3.4.

The injection flow rates u_{B1} ***and*** u_{B2} The feed injection flow rates, q_{B1} and q_{B2}, are the injection flow rates of B at the two injection points. The sum $q_{B1} + q_{B2} = q_{B,\text{feed}}$ is often fixed to guarantee stoichiometric conditions. However, the flow distribution between the injection points remains as a degree of freedom. In the sequel, we will use the scaled control variables $u_{B1} = q_{B1}/q_{B,\text{feed}}$ and $u_{B2} = q_{B2}/q_{B,\text{feed}}$, with $q_{B,\text{feed}}$ as the scaling factor. Thus when $u_{B1} + u_{B2} = 1$, stoichiometric amounts of A and B are being fed into the reactor.

The analysis shows that these injection flow rates have fast and high-gain effect on the concentration of B, thus also on the reactor temperature. The impact is spatially limited to the regions inside the reactor where the reaction occurs, see Figure 3.12. The exponentially temperature dependence of the reaction rate may also severely limit the gain from the injection flow rates to the reactor temperature. For low temperatures, the reaction rate, thus also the input gain, is almost zero, but the gain increases with temperature. Figure 3.13 plots the nonlinear relation between u_{B1} and T_1, when there is repeated steps of u_{B1} from 0 to 1% of the total flow at different temperatures. At low temperatures, almost no part of the injected B reacts, whereas at higher temperatures, almost

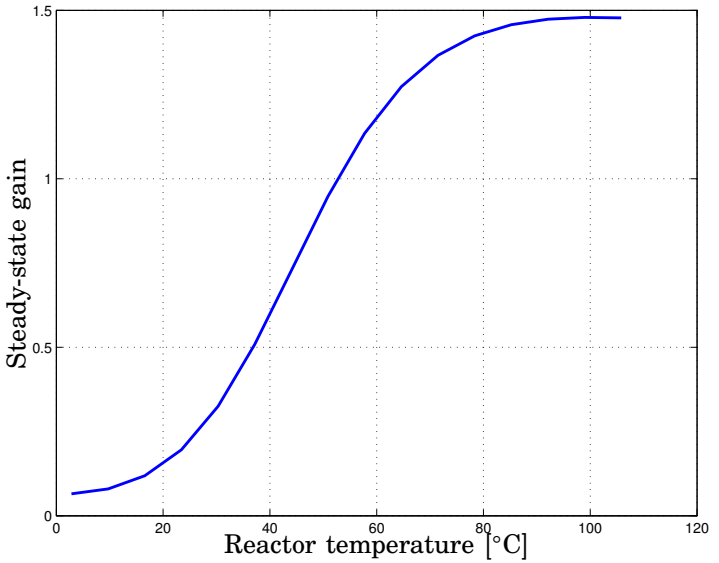

Figure 3.13 Plot of the nonlinear steady-state gain from u_{B1} to T_1 as a function of the reactor temperature T_1. The gain is computed by performing repeated step between $u_{B1} = 0$ and $u_{B1} = 0.01$ at increasing temperatures.

everything is consumed. The steady-state gain increases roughly 700% from 20°C to 60°C. This nonlinear characteristic will be very important to consider during reactor start-up, see Chapter 5.

An advantage with the injection flow rates is the fast actuator dynamics. The actuator system, which includes a control valve, a flow sensor and a low-level feedback controller, may be approximated with a first order system with a time constant of roughly 1 second.

The stoichiometric relation may introduce very sharp nonlinear effects. For example, as long as there is a shortage of B, $u_{B1}+u_{B2} < 1$, the control input u_{B2} will have a nominal impact on the reactor temperature, but when conditions change so that there is an excess of B, i.e., $u_{B1}+u_{B2} > 1$, the gain to temperature drops quickly to zero.

In addition to improve the conversion and avoid shortages of any reactant, it is essential to operate at stoichiometric ideal conditions, that is, $u_{B1} + u_{B2} = 1$. The easiest way to achieve this is to introduce an explicit constraint in the control system that $u_{B1} + u_{B2} = 1$. To implement this constraint, a new control input is defined, *the injection feed distribution* u_B. Numerically $u_B = u_{B1}$, while u_{B2} is replaced by $1-u_{B1}$. For example, $u_B = 0.45$ represents 45% of the total injection flow being fed into the first injection point and the remainder 55% is fed into the second injection flow.

An increase in u_B gives an increase in u_{B1} and a similar decrease of u_{B2}. The steady-state gain of u_B can be viewed as the following: a 1% increase in u_B leads to an increase of T_1 with 1.8° and a similar 1.8° decrease of T_2, compare with from Table 3.1. However, if there are some disturbances in either the feed concentrations or feed flow rates, the sum of u_{B1} and u_{B2} should be adjusted to regain stoichiometric relations.

The constraint $u_{B1}+u_{B2} = 1$ will preserve stoichiometric conditions at steady-state. Dynamically, however, the flow time of 15 seconds between the injection points introduces complications. A change in the flow rate at the first injection point should be followed by a corresponding change at the second injection point first after 15 seconds, to account for the flow delay. Otherwise the stoichiometric condition will experience a short transient. This leads to non-causal effects if u_{B2} should be used in feedback control, for example, 15 seconds before any change in u_{B2} is made, a corresponding change in u_{B1} should be made to achieve ideal stoichiometric conditions at all time. The injection flow rates u_{B1} and u_{B2} should be used with care in feedback control, due to these circumstances. An alternative is to use model-based multivariable control to penalize operation at non-ideal stoichiometric conditions, see Section 4.6.

To conclude, the injection flow rates u_{B1} and u_{B2} have in general a fast, high-gain effect on the concentrations and temperatures in the reactor. Its fast dynamic response shows that u_{B1} and u_{B2} may be used to quickly control the reactor temperature, which will be used during the start-up, see Chapter 5. However, any changes in the injection flow rates may upset the stoichiometric conditions, so they should be used with care. With model-based multivariable control, it is easier to consider the stoichiometric conditions.

The feed temperature $T_{A,\text{feed}}$ of the primary reactant A Feed temperature of reactant A, $T_{A,\text{feed}}$, mainly influences the temperature at the inlet of the reactor, see Figure 3.5. The spatial dependence in this figure may actually be an advantage, since its low gain and flow delay to the temperatures at the mid-section decreases potential cross-coupling effects of the multivariable system.

Depending on the operating region of the process, the feed flow may need to be heated, cooled or both, compared to the ambient temperature. In this thesis, only heating of the feed is considered. Control of the feed temperature may be realized with an actuator system, which includes a small heat exchanger, a control valve, a temperature sensor and a low-level feedback controller. The feed flow may be heated by either hot water or steam. The dynamics of the actuator system depend on the heat exchanger and the temperature of the heating medium and may be approximated by first order system with a time constant of 2 seconds. However, for large

setpoint transients, the thermal inertia may cause the control valve to saturate, which introduces dynamics similar to a rate limit.

The inlet cooling temperature T_{cool} ***and flow rate*** q_{cool} These two inputs may be manipulated to control the removal of the heat from the reaction. The response from q_{cool} to the reactor temperature has much larger nonlinearities than the response from T_{cool}. The disadvantages with T_{cool} is the slower actuator dynamics and the additional process equipment needed compared to q_{cool}. In this thesis, T_{cool} will be used as one of the main control inputs, and q_{cool} will be fixed to a constant value.

A more generic approach would be to use the enthalpy of the cooling water as a control input and then use a nonlinear combination of T_{cool} and q_{cool} to achieve the desired enthalpy.

The cooling water comes from a utility system, where a number of control valves, pumps and a heat exchanger enable accurate temperature and flow rate control of the cooling water. The utility system, its control system and experiments are presented in Chapter 8. The actuator system, which includes the utility system, sensors and low-level feedback controllers, may for small set-point changes be approximated by a first order system with a time constant of 4 seconds. However, for medium and large set-point changes the control valve may saturate, which introduces dynamics similar to a rate limit. A mid-ranging control structure is designed to extend the operating range of the utility system and to improve the control for large set-point transitions, see Chapters 8–9.

The other feed variables, $q_{A,\text{feed}}$***,*** $q_{B,\text{feed}}$***,*** $c_{A,\text{feed}}$ ***and*** $c_{B,\text{feed}}$ These variables are in general fixed given a desired production rate of the process. To maintain stoichiometric conditions, the following relation is often fixed:

$$q_{A,\text{feed}} c_{A,\text{feed}} = q_{B,\text{feed}} c_{B,\text{feed}} \tag{3.3}$$

This stoichiometric constraint and the flow delay introduce unfavorable dynamics for these inputs to be used for feedback control of the reactor temperature. On the other hand, they may easily be manipulated to increase/decrease the overall production rate of the reactor. The feed flow rates are realized with an actuator system, which includes a control valve, a flow sensor and a low-level feedback controller. The feed concentrations are often fixed to the concentrations of the storage tanks, but in some cases it may beneficial to install additional equipment to allow the feed concentration to be manipulated on-line.

Conclusion

The main control variable of the plate reactor is the inlet temperature of the cooling water. This variable can effectively control the heat transfer

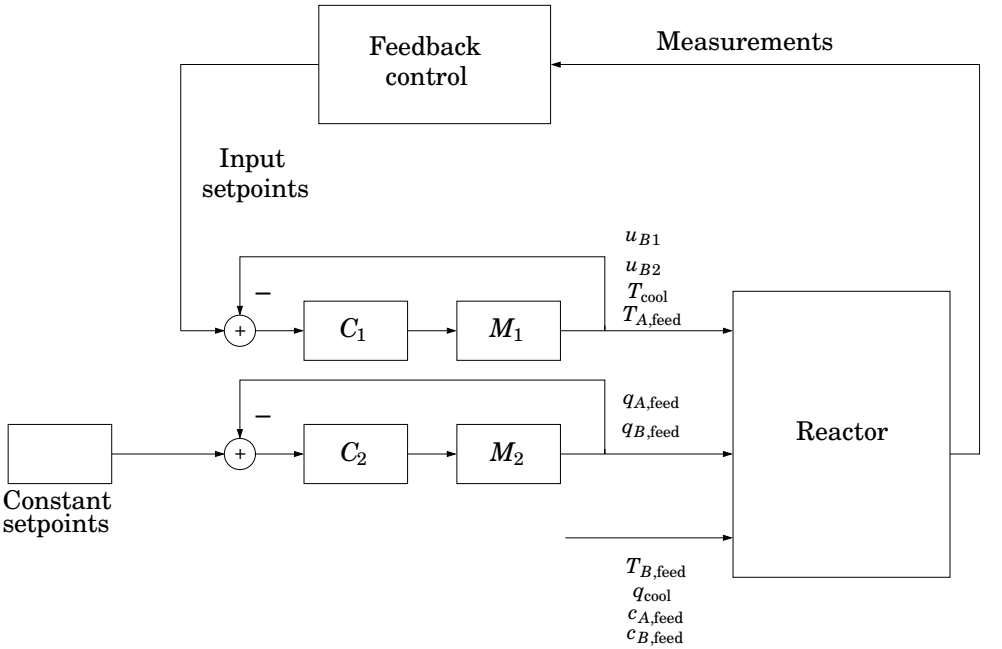

Figure 3.14 Block diagram of the feedback control structure. M_1 and M_2 represent the actuator dynamics of the control inputs and C_1 and C_2 represent the local controllers for each control input. The input signals $T_{B,\text{feed}}, q_{\text{cool}}, c_{A,\text{feed}}$ and $c_{B,\text{feed}}$ may be seen as disturbances.

out from the reactor, thus enabling accurate temperature control. However, it has limited effect in the first part of the reactor, therefore at least one additional control input is needed. The feed temperature of the reactant is a very suitable control input and is a very good complement to the cooling temperature, as we will see in Section 4.5. In addition, the injection flow rates may, if necessary, be used to increase the speed and flexibility of the control system.

To summarize, the process inputs can be used for feedback control, controlled to a constant set-point using feedback, open-loop controlled or not controlled at all, see Figure 3.14. A cascade control structure is used, where the temperatures and/or concentrations of the plate reactor are controlled by manipulating set-points to local feedback control loops.

- The feed concentrations $c_{A,\text{feed}}$ and $c_{B,\text{feed}}$ are given by the concentrations in the storage tanks or they may be controlled to constant set-points with open loop control, since in general no on-line measurements are available. In rare cases, the set-points may be manip-

ulated to vary the production rate.

- The feed flow rates $q_{A,\text{feed}}$ and $q_{B,\text{feed}}$ are controlled to constant set-points with local feedback control. The set-points may be manipulated to vary the production rate.
- The feed temperature of the secondary reactant $T_{B,\text{feed}}$ is the ambient temperature from the storage tank. Its low impact on the reactor temperature implies that it is of minor interest from control point of view.
- The cooling water flow rate q_{cool} is assumed to be constant, which is achieved by balance valves of the utility system. Since the flow rate is very large, small variations will have a very small impact.
- The remaining four control inputs, $u_{B1}, u_{B2}, T_{\text{cool}}$ and $T_{A,\text{feed}}$, have local feedback control loops. The set-point to each of these four controllers are used as manipulating variables for the control system of the plate reactor in a cascade control structure.

4

Process control

4.1 Introduction

The previous chapters have presented the concept, the model and the input/output variables of the plate reactor. In this chapter, different controllers are designed based on that knowledge.

For multivariable processes like the plate reactor, there are two main control design approaches; *decentralized* control and *centralized* control. In decentralized control, the feedback control is implemented with several single control loops, cascade control loops or mid-ranging control loops in parallel. In general, each control loop is designed independently or sequentially, leaving the completed loops in the automatic mode. There may be decoupling matrices to consider the possible cross-coupling effects of the multivariable process. PID controllers are the most common control components when constructing decentralized control structures.

In centralized control, the feedback control is often based on a multivariable process model. The controller utilizes all measurements and computes all control inputs simultaneously. With the multivariable process model, all cross-coupling effects can be handled implicitly. Examples of centralized controllers are H_∞-controllers, LQR/LQG-controllers and MPC-controllers.

According to [Skogestad and Postlethwaite, 2005], the most important reason to apply decentralized control is to save on the modeling effort. Accurate process models are a prerequisite for applying multivariable control, whereas in decentralized control the controllers are often tuned one at a time with a minimum of modeling effort. The tuning of a decentralized controller is often easier and may even be carried out online. Other advantages may be improved integrity and easier commissioning and maintenance routines, for example after sensor or actuator failures,

as the decentralized approach allows individual loops to be put in manual. Finally, a decentralized control structure may often appear transparent and is likely to receive acceptance from the operator. However, as the number of objectives and cross-couplings grow, the decentralized control structure may loose its transparency.

Centralized control may in most cases improve the control performance, due to its ability to consider the cross-couplings between the different control inputs. It may also increase the flexibility in the constraint handling, when there are limits on control inputs or outputs. These improvements should be compared with the cost of developing the process model. A process model may serve many more purposes than control design alone, such as operator training, control hardware testing, soft sensor development, process/control monitoring, process knowledge database and economic optimization. On the other hand, there is a large difference in the model complexity needed for the different purposes, for example, a simple model for control design and a more detailed model for operator training.

4.2 Related Work

An extensive review on nonlinear control of chemical processes is given in [Bequette, 1991]. Numerous design methods, such as internal model approach, feedback linearization, parameter-scheduling, differential geometry, reference system synthesis, predictive control and nonlinear optimization are discussed. [Shinskey, 1996] provides a good background on general process control and decentralized control of multivariable systems.

In [Luyben, 2001] the effect of design and kinetic parameters on the controllability of a tubular reactor is studied. To control the maximum temperature inside the reactor, several internal sensors are used and their data is sent to a selector, which singles out the maximum temperature for feedback to a PI-controller. The main advantage is the simplicity of the feedback controller, however it is not always trivial to find a suitable reference temperature for the reactor that gives optimal conversion. In addition, the system dynamics may change when there is switching between different measurements for feedback control.

The paper of [Vecchio and Petit, 2005] presents control strategies for an industrial tubular reactor for polystyrene production. A set of PI controllers are implemented in a decentralized control structure and each loop is designed one at a time. To improve the performance, the gains of the PI controllers are determined with multivariable LQR optimization. This approach may be seen as a weighting of the inputs of the PI controllers based on the process model. Finally, a full multivariable con-

troller is designed, where nonlinear reference trajectories are generated by solving off-line a nonlinear dynamic optimization problem. The tubular reactor has multiple cooling zones, similar to the plate reactor, and the most suitable sensor location in each cooling zone for feedback control is discussed.

In [Karafyllis and Daoutidis, 2002] a nonlinear control law based on feedback linearization for a distributed parameter system is derived. The aim is to have the maximum temperature inside the reactor follow a given reference temperature. The manipulating variable is the cooling temperature. The result is verified for both model and measurement errors. Also here, the choice of reference temperature is not discussed.

In [Bošković and Krstić, 2002], backstepping control is applied to a class of tubular reactors, described by nonlinear PDEs. The original PDE model is discretized with the finite difference method to a system of high order ODEs. The reactor is controlled around an unstable steady state profile by manipulating the feed temperature and feed concentration. However, this stabilization may require very large control actions that will prove difficult to implement in a real application.

In [Hoo and Zheng, 2001], low order models for nonlinear distributed parameter systems are developed for control design by the Karhunen-Loève (KL) expansion[1], the Eigenfunction (EF) method and the Singular Value Decomposition (SVD) method. In [Zheng and Hoo, 2004], a data-driven identification method is presented that yields a low-order model for control design using KL expansion and the SVD method. Based on the low-order model, a quadratic dynamic model-based controller is designed for a tubular reactor system.

In the book of Christofides, [Christofides, 2001], nonlinear and robust control design for distributed parameter systems is presented, based on geometric and Lyapunov control methods. In [Dubljevic *et al.*, 2006], predictive control is applied to a system described by linear parabolic PDEs. A low-order model is derived from a combination of the Galerkin method and the concept of inertial manifolds. A model predictive controller is then designed for the reduced order model.

In [Shang *et al.*, 2004] a novel MPC scheme is presented for control of a quasi-linear distributed parameter system based on the method of characteristics. The aim is to control the outlet concentration in a plug-flow reactor along a given reference by manipulating the cooling flow rate. The main benefit of the characteristics-based MPC is the reduced computational load compared to MPC based on finite difference approximations of the PDEs. However, since an endothermic reaction is studied, the issue of temperature constraints is not considered. The method is extended in

[1]Also known as Proper Orthogonal Decomposition

[Shang *et al.*, 2007] to parabolic systems, where convection dominates over diffusion.

In [Hudon *et al.*, 2005], an adaptive extremum seeking control law is presented for a class of nonlinear distributed parameter systems. The control law is tested on a tubular (plug-flow) reactor with the Williams-Otto reaction, which is a series of endothermic reactions. The main contribution is to allow for optimal control, even in the presence of uncertainties, when the actual optimal operating point is unknown. The method assumes that there are a finite number of control actuators to implement the calculated optimal cooling profile.

In [Cougnon *et al.*, 2006] an adaptive extremum seeking control scheme for an isothermal tubular (plug-flow) reactor is presented. To improve the selectivity for a series of parallel reactions, the reactant is added continuously along the reactor through membrane walls. Real-time optimization and an adaptive learning technique are applied to find the unknown optimal operating point.

4.3 Optimization of Stationary Operation

The main operational mode of the plate reactor is steady-state operation at the optimal operating point. This optimal operating point is often computed off-line as a part of the process design procedure.

In [Smets *et al.*, 2002] optimal control theory is used to derive open-loop analytical solutions for the cooling temperature to maximize the performance for a plug flow reactor. The performance criterion is defined as a combination of minimizing the outlet concentrations of the reactants and the global heat loss. One of the interesting results is the nearly optimal solution where a bang-bang cooling temperature profile is used. One cooling temperature is used for the first part of the reactor and after some switching point, another cooling temperature is used. This fits very well into the plate reactor framework, where the flexible configuration allows several different cooling flows to be used. The work has been extended to tubular reactors with varying dispersion in [Logist *et al.*, 2005a; Logist *et al.*, 2005b] and [Logist *et al.*, 2007] presents methods for deriving generic reference temperature profiles.

Note that these computations do not consider any disturbances or uncertainties. To compensate for this, a feedback controller should be added, which should track the off-line computed temperature references. Alternatively, the optimization may be periodically repeated on-line to find a new operating point in the presence of various disturbances.

Assume that the nonlinear process model from Chapter 3 is given on the form $\dot{\mathbf{x}} = \mathbf{f}(\mathbf{x}, \mathbf{u})$. The steady-state optimal operating problem may

then be formulated as

$$\begin{aligned} \min_{\mathbf{u}} J &= \min_{\mathbf{u}} c_{A,\text{out}}^2 + c_{B,\text{out}}^2 \\ &\text{subject to} \\ 0 &= \dot{\mathbf{x}} = \mathbf{f}(\mathbf{x}, \mathbf{u}) \\ \mathbf{u}_{\min} &\leq \mathbf{u} \leq \mathbf{u}_{\max} \\ \mathbf{x}_{\min} &\leq \mathbf{x} \leq \mathbf{x}_{\max}, \end{aligned} \tag{4.1}$$

where possible input and state constraints are defined by $\mathbf{u}_{\min}, \mathbf{u}_{\max}, \mathbf{x}_{\min}$ and $\mathbf{x}_{\max}$. The cost function J is here defined as the sum of the outlet concentrations of the two reactants A and B. By minimizing these outlet concentrations, we also maximize the reactant conversion (2.5), see Section 2.3. The optimization problem (4.1) is solved with the Matlab function `fmincon`, [Mathworks, 2007a]. The result was shown in Figure 2.7.

4.4 Feedback Control

Control Structure

Now we focus on the control based on feedback from measurements inside the reactor. The control is implemented by manipulating set-points $\mathbf{u}^{\text{sp}}$ to low-level control loops in a cascade control structure, see Figure 4.1. The superscript 'sp' is sometimes omitted when the meaning is clear from the context. The control signals $\mathbf{v}$ of the low-level controllers often correspond to valve positions or pump speeds. The block called "Feedback control" can represent either a decentralized or a centralized controller. In addition to the input variables $\mathbf{u}$ designated for feedback control actions, there are other inputs that are either controlled to a constant set-point or uncontrolled, compare with Figure 3.14.

Measurements and Sensor Location

The plate reactor is constructed to allow internal sensors, to improve conditions for process monitoring and control. The most frequent sensors are temperature and pressure sensors, but recent advances in the process analytical technology (PAT) will lead to more sensors being able to be mounted inside the reactor.

Sensor location is a very important part of the process design and is a research field of its own, see e.g. [Harris *et al.*, 1980]. It is important to locate the sensors around the maximum temperatures, to give adequate process information. However, the location of the maximum tem-

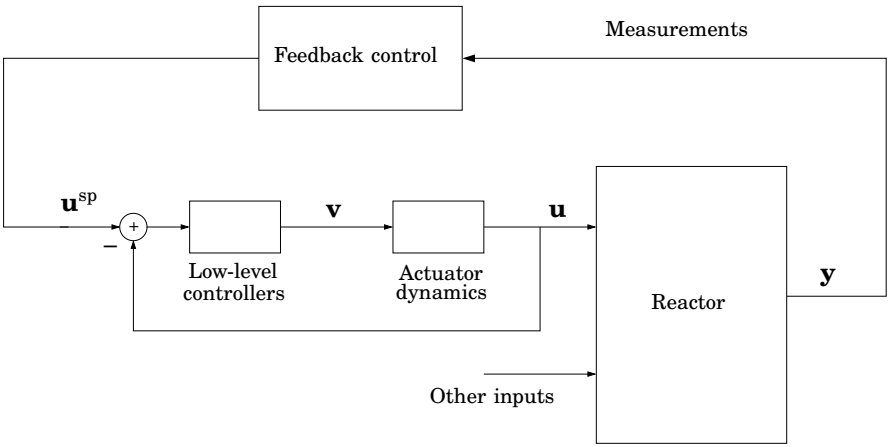

Figure 4.1 Block diagram of the feedback control structure. The other inputs, not used for feedback control, are set to constant values or may be seen as disturbances, see Figure 3.14.

peratures may change depending on the operating point, disturbances or plant/model mismatch, see e.g. Figures 3.3, 3.6-3.9.

When states within the reactor are not available on-line, a state estimator may recreate the non-measured states, for example a Kalman filter. This may also be interpreted as a soft sensor, where the value of interest is computed based on the measurements, the control inputs and a process model. With the exothermic reactions, the strong correlation between temperature and concentration allows good estimation of the concentration, based on temperature measurements. The total amount of heat released from the reaction is also a good indication of the process state. In fact, for some reactions the process operation may be optimized by seeking the combination of control inputs that within the constraints maximizes the heat release from the reaction, thus maximizing the production.

4.5 Decentralized Control

The outline for this section is as follows. The first task is to find the most suitable input/output pairing, to avoid unnecessary cross-couplings between the decentralized control loops. The second task is to design the individual SISO controllers and then analyse the resulting closed loop system. The multi-loop controller is verified in simulation for different disturbance scenarios. The design procedure is then repeated using alternative input/output pairings, to see the effect of more significant cross-couplings.

Furthermore, the section presents methods for how to extend the control structure for a general process configuration of the plate reactor and how to take advantage of additional control inputs in the control system. The section concludes with some remarks on how to deal with temperature constraints.

Introduction

Let us consider a plate reactor configuration with two injection points, one cooling zone and the sodium thiosulfate reaction. Furthermore, we assume that a steady-state optimal operating point has been computed with the temperature profiles plotted in Figure 4.2. Without online concentration measurements or a process model to develop a soft sensor (state estimator), it is difficult to control the concentrations inside the reactor. Therefore, we focus initially on temperature control and numerous temperature sensors are available for feedback control.

It is impossible for the feedback control system to achieve perfect tracking of the entire temperature profile along the reactor, due to the limited numbers of actuators and sensors along the reactor. Instead, the focus is to control T_1 and T_2, the maximum temperatures after each injection point, given the reference temperatures T_1^{ref} and T_2^{ref}. This will ensure safe operation and lead to good performance, as the conversion highly depends on the maximum temperature for this specific reaction.

It is assumed that the temperature sensors T_1 and T_2 are carefully placed, for example, after initial experiments have shown where the maximum temperatures occurred.

Input/Output Pairing for Decentralized Control

The decentralized control approach does not in general consider possible cross-coupling effects in the process. It is therefore important to wisely choose input/output pairing, so that the amount of interaction between the different control loops is reduced to a minimum. From Section 3.3, we have four possible control inputs, the injection flow rates u_{B1} and u_{B2}, the feed temperature $T_{A,\text{feed}}$ and the cooling inlet temperature T_{cool}. To emphasize the importance of maintaining stoichiometric conditions in steady-state, the sum of the injection flow rates is fixed, $u_{B1} + u_{B2} = 1$. This removes one degree of freedom and in the remainder of this section we replace the control inputs u_{B1} and u_{B2} with the injection feed distribution u_B, where $u_{B1} = u_B$ and $u_{B2} = 1 - u_B$, see Section 3.3. For the analysis in this section, a linearization of the nonlinear model from

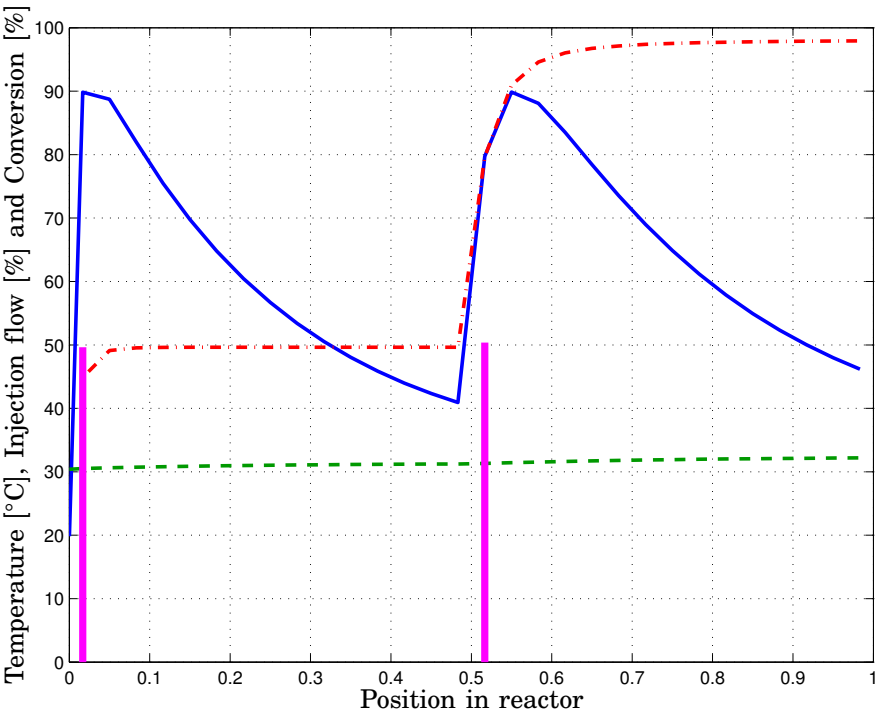

Figure 4.2 The steady-state reactor temperature profile (solid), the cooling water temperature profile (dashed), the conversion profile (dash-dot) and the injection flow rates (vertical lines at their location)

Chapter 3 yields the transfer function $\mathbf{G}(s)$,

$$\begin{bmatrix} T_1 \\ T_2 \end{bmatrix} = \mathbf{G} \begin{bmatrix} T_{A,\text{feed}}^{\text{sp}} \\ T_{\text{cool}}^{\text{sp}} \\ u_B^{\text{sp}} \end{bmatrix} = \begin{bmatrix} G_{11} & G_{12} & G_{13} \\ G_{21} & G_{22} & G_{23} \end{bmatrix} \begin{bmatrix} T_{A,\text{feed}}^{\text{sp}} \\ T_{\text{cool}}^{\text{sp}} \\ u_B^{\text{sp}} \end{bmatrix}. \tag{4.2}$$

To control T_1 and T_2 independently, it is sufficient to use two of the three control variables u_B, $T_{A,\text{feed}}$ and T_{cool}. An initial screening is made based on the steady-state gains from Table 3.1. The gains show quite clearly the impact of each process input on the reactor temperatures. To obtain further insight what variables to choose, the Relative Gain Array (RGA) number for different pairings is computed. For other methods, see for example [van de Wal and de Jager, 2001]. RGA was first presented in [Bristol, 1966] as a measure of the loop interaction in multivariable control. An overview of the properties and interpretations of RGA is given

in [Skogestad and Postlethwaite, 2005]. The RGA number is defined as the norm of the difference between the RGA matrix $\mathbf{\Lambda}$ for that pairing, and a pairing matrix. For example, the RGA matrix for the inputs $T_{A,\text{feed}}$ and T_{cool} can be expressed as

$$\mathbf{\Lambda}(i\omega) = \begin{bmatrix} G_{11} & G_{12} \\ G_{21} & G_{22} \end{bmatrix} .* \begin{bmatrix} G_{11} & G_{12} \\ G_{21} & G_{22} \end{bmatrix}^{-T} . \tag{4.3}$$

In [Skogestad and Postlethwaite, 2005], the RGA number is defined as

$$\text{RGA number}(\omega) = \left\| \Lambda(i\omega) - \begin{bmatrix} 1 & 0 \\ 0 & 1 \end{bmatrix} \right\|_{\text{sum}}, \tag{4.4}$$

where the norm is the sum norm, $||\mathbf{A}||_{\text{sum}} = \sum_{i,j} |a_{ij}|$ and the pairing matrix describes a diagonal pairing. The RGA number for each possible pairing combination is computed for varying frequencies ω. If there is no or negligible cross-coupling for this pairing, the RGA matrix will be close to the identity matrix, thus the RGA number becomes very small. A small RGA number indicates that this pairing is a good candidate for decentralized control. The RGA number for the three best input/output pairings of the six possible combinations are plotted as a function of frequency ω in Figure 4.3.

It is clear that pairing $T_{A,\text{feed}}$ with T_1 and T_{cool} with T_2 leads to the least cross-coupling for all frequencies. This is as expected as these control inputs mainly affects the reactor temperature at different spatial coordinates, see Figure 3.5. When the injection feed distribution u_B is used in any pairing, more cross-coupling is present as u_B affects both temperature maxima due to the constraint $u_{B1} + u_{B2} = 1$.The peak of the dash-dot line corresponds to large cross-coupling between u_B and $T_{A,\text{feed}}$, and the frequency of the peak is directly coupled with the flow time between the reactor inlet and the second injection point.

Control Design

For feedback control design, the following inputs and outputs are used, see Figure 4.1,

$$\mathbf{r} = \begin{bmatrix} T_1^{\text{ref}} \\ T_2^{\text{ref}} \end{bmatrix}, \quad \mathbf{y} = \begin{bmatrix} T_1 \\ T_2 \end{bmatrix}, \quad \mathbf{u}^{\text{sp}} = \begin{bmatrix} T_{A,\text{feed}}^{\text{sp}} \\ T_{\text{cool}}^{\text{sp}} \end{bmatrix}. \tag{4.5}$$

Figure 4.4 shows the process and the controller in a flow scheme. Note the cascade structure, where the primary temperature controllers K_{11} and

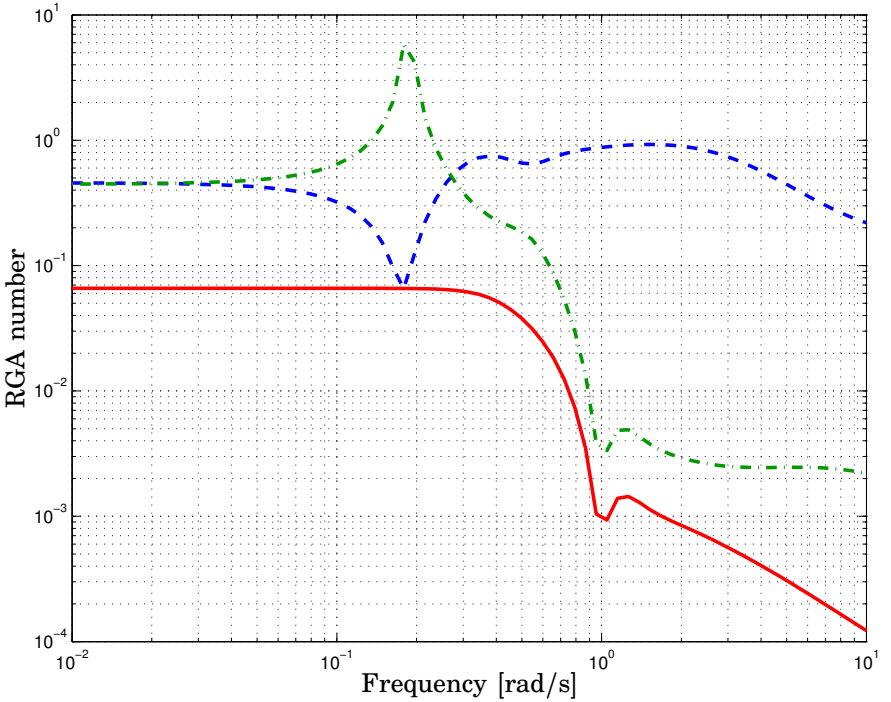

Figure 4.3 The norm of the difference between the RGA matrix $\mathbf{\Lambda}$ and suitable pairing matrix, for control variable selection. Solid line is when T_1 is controlled by $T_{A,\text{feed}}$ and T_2 by T_{cool}. Dashed line is when T_1 is controlled by u_B and T_2 by T_{cool}. Dash-dot line is when T_1 is controlled by $T_{A,\text{feed}}$ and T_2 by u_B.

K_{22} send set-points $T^{\text{sp}}_{A,\text{feed}}$ and $T^{\text{sp}}_{\text{cool}}$ to the local feedback controllers. Each local controller manipulates a control valve to ensure good tracking. The heat exchanger components (HEX) are schematic representations of the actuator systems. In the actual process, the actuator systems may often be more complex, see for example the detailed description of the cooling system in Chapter 8.

A linearized input/output representation of the process with the chosen inputs can be written as

$$\begin{bmatrix} T_1 \\ T_2 \end{bmatrix} = \begin{bmatrix} G_{11} & G_{12} \\ G_{21} & G_{22} \end{bmatrix} \begin{bmatrix} T^{\text{sp}}_{A,\text{feed}} \\ T^{\text{sp}}_{\text{cool}} \end{bmatrix}, \tag{4.6}$$

where the transfer functions G_{ii} are linearizations of the nonlinear process model from Chapter 3. For control design, low-order approximations of the transfer functions are identified individually from a series of step

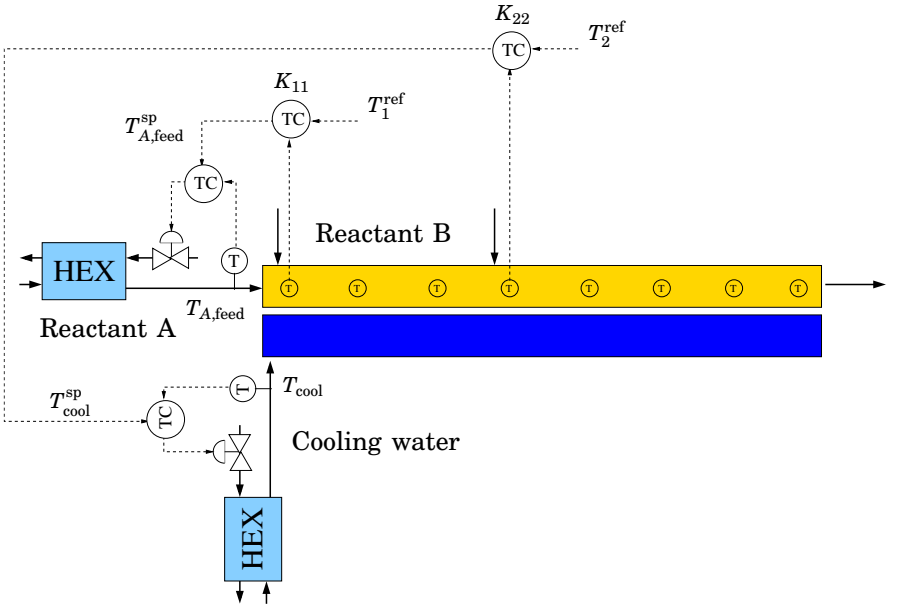

Figure 4.4 Flow scheme of the decentralized feedback control. The controllers K_{11} and K_{22} (see Equation 4.8) send set-points to the local feedback controllers in a cascade loop. The controllers are indicated with the symbol TC (temperature control).

responses on the nonlinear process model, using a least squares method from [Wallén, 2000]. The transfer functions are approximated using models of first order plus dead-time, denoted with $\hat{G}_{ii}$.

$$\begin{bmatrix} G_{11} & G_{12} \\ G_{21} & G_{22} \end{bmatrix} \approx \begin{bmatrix} \hat{G}_{11} & \hat{G}_{12} \\ \hat{G}_{21} & \hat{G}_{22} \end{bmatrix} = \begin{bmatrix} \frac{1.26}{2.39s+1}e^{-0.75s} & \frac{0.21}{4.24s+1}e^{-0.90s} \\ \frac{0.156}{5.73s+1}e^{-12.8s} & \frac{1.56}{7.73s+1}e^{-3.25s} \end{bmatrix} \tag{4.7}$$

Notice the time delays in the system, where the delays between $T_{A,\text{feed}}$ and T_{cool} to the temperature after the second injection point T_2 correspond to the flow time of the reactor fluid and the cooling fluid, respectively. The cross-coupling terms G_{12} and G_{21} are small in comparison to G_{11} and G_{22}, which emphasizes the diagonal dominance of the system matrix and supports the chosen input/output pairing from Figure 4.3.

The decentralized control is implemented as a diagonal controller $\mathbf{K}(s)$,

$$\begin{bmatrix} T_{A,\text{feed}}^{\text{sp}} \\ T_{\text{cool}}^{\text{sp}} \end{bmatrix} = \underbrace{\begin{bmatrix} K_{11} & 0 \\ 0 & K_{22} \end{bmatrix}}_{\mathbf{K}} \begin{bmatrix} T_1^{\text{ref}} - T_1 \\ T_2^{\text{ref}} - T_2 \end{bmatrix}. \tag{4.8}$$

The single-input single-output (SISO) controllers $K_{11}(s)$ and $K_{22}(s)$ are chosen to be of Proportional-Integral-Derivative (PID) type, see e.g. [Åström and Hägglund, 2005]. There are several reasons for choosing PID controllers, first they are easy to implement, second they can easily be tuned online with a minimum of modeling effort, thirdly they are easily accepted by the operators as they offer transparent control actions. Another alternative would for example be constrained LQ control [Pannocchia *et al.*, 2005], where a simplified model predictive control algorithm is developed for SISO processes to allow fast sampling time and easy tuning.

The PID controllers can easily be tuned online, for example with automatic tuning using relay feedback [Hang and Åström, 2002], but here we aim for the novel AMIGO tuning method, which involves robust loop-shaping and optimization of the integral gain, see [Åström and Hägglund, 2005]. The AMIGO method is a Ziegler-Nichols replacement, where the tuning rule gives the controller parameters as explicit functions of the identified process model parameters. Assume the process is approximated with system of first order plus dead-time

$$P(s) = \frac{K_p}{1+sT} e^{-sL}, \tag{4.9}$$

where K_p is the steady state gain, T is the approximated time constant and L is the time delay. The controller parameters for a PID controller are then

$$K_c = \frac{1}{K_p}\left(0.2 + 0.45\frac{T}{L}\right) \tag{4.10}$$

$$T_i = \frac{0.4L + 0.8T}{L + +0.1T} L \tag{4.11}$$

$$T_d = \frac{0.5LT}{0.3L + T}. \tag{4.12}$$

where K_c is the controller gain, T_i is the integral time and T_d is the derivative time. These functions have been developed as follows. First, the controller parameters for 134 different processes[2] are found by optimizing the integral gain with a robustness constraint, the so called MIGO[3] method, see [Åström and Hägglund, 2005]. Then, approximated correlations (4.10 – 4.12) are found between the optimal controller parameters and the normalized process parameters, hence the name AMIGO, which stands for approximate MIGO design. The controller parameters can now

[2]The only assumption is that the process have essentially monotone step responses, which is typically encountered in the process industry.

[3]MIGO = M-constrained integral gain optimization.

be found using these explicit functions instead of having to carry out the detailed optimization, which makes this tuning rule as easy to use as the Ziegler-Nichols methods, but also includes the robustness properties of the MIGO method.

The AMIGO tuning rule and the associated guidelines suggest the following PID controllers:

$$K_{11}(s) = 1.30\left(1 + \frac{1}{1.68s} + 0.69s\right),\ K_c = 1.30, T_i = 1.68, T_d = 0.69 \tag{4.13}$$

$$K_{22}(s) = 0.81\left(1 + \frac{1}{6.05s} + 2.89s\right),\ K_c = 0.81, T_i = 6.05, T_d = 2.89 \tag{4.14}$$

In addition, the PID controllers are implemented with an anti-windup scheme for absolute and rate constraints and a high-pass filter for the derivative part. The temperature control of the plate reactor can be realized also with pure PI controllers, but the derivative action allows a somewhat higher integral gain K_c/T_i, which gives improved performance during disturbances.

The open and closed loop system may now be analyzed in terms of stability and robustness. Figure 4.5 shows the Bode plots of the open loop compensated system. For $G_{11}(s)K_{11}(s)$, the phase margin is 70.2 degrees at 0.63 rad/s, there is an infinite amplitude margin and the delay margin is 1.9 seconds. For $G_{22}(s)K_{22}(s)$, the phase margin is 65.5 degrees at 0.23 rad/s, the amplitude margin is 10.5 at 1.77 rad/s and the delay margin is 4.9 seconds.

The sensitivity function $\mathbf{S}$ is defined as the transfer function of the closed loop system from output disturbance signals to the temperature measurement signals T_1 and T_2,

$$\mathbf{S} = [\mathbf{I} + \mathbf{GK}]^{-1}. \tag{4.15}$$

The frequency response of $\mathbf{S}$ is plotted in Figure 4.6. The figure shows the singular values of the frequency response, since the closed loop system is a MIMO system. The upper line shows the maximum singular value and the lower line shows the minimum singular value. For more details on frequency response for multivariable systems, see e.g. [Skogestad and Postlethwaite, 2005]. The integral action of the PID controllers leads to perfect attenuation of constant disturbances in steady-state. The feedback control leads to a closed loop bandwidth around $\omega_b = 0.2$ rad/s and all disturbances of lower frequencies will be attenuated, regardless of input direction. The peak of the sensitivity function is around 1.23, which indicates a fair amount of robustness.

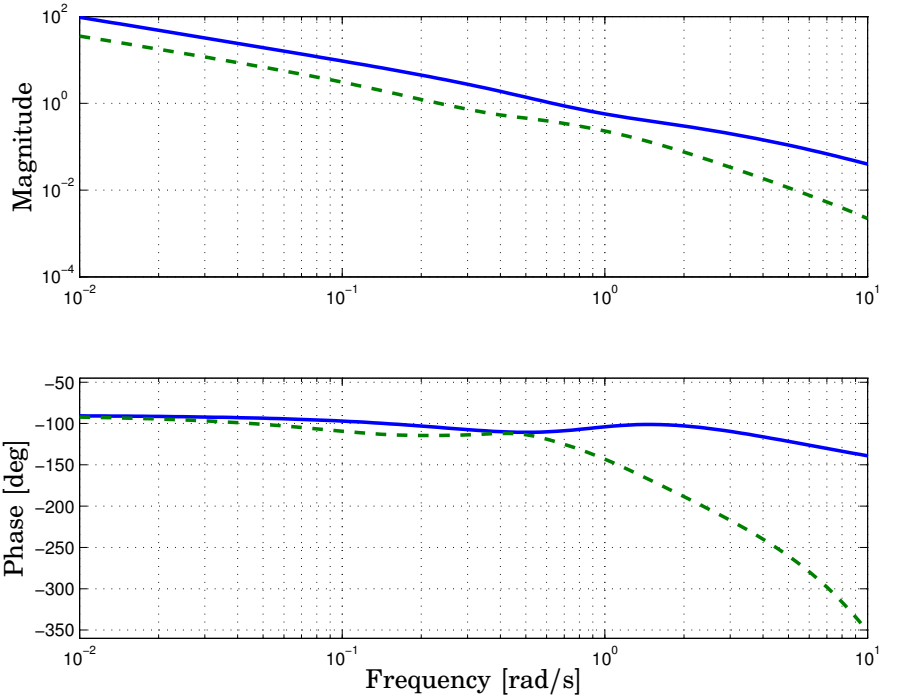

Figure 4.5 Bode plots of the compensated open loop system with $G_{11}(s)K_{11}(s)$ (solid line) and $G_{22}(s)K_{22}(s)$ (dashed line).

Simulations

The PID controllers are implemented as discrete-time controllers in Matlab/Simulink. The controllers are verified against the nonlinear model of the plate reactor developed in Section 3.1, including actuator models. The choice of sampling time is based on the cross-over frequency of the open loop compensated system in Figure 4.5, where $\omega_c \approx 0.2 - 0.6$ rad/s. A few guidelines on how to select sampling time are given in [Åström and Wittenmark, 1997], e.g. $T_s\omega_c \approx 0.15 - 0.50$. This results in a recommended sampling time of 0.2 – 0.8 seconds. A sampling time of $T_s = 0.10$ s is chosen to improve the disturbance rejection. The closed loop system is evaluated in simulations for different disturbance scenarios. The feedback controller should keep the temperatures T_1 and T_2 at the constant reference temperature 90°C, despite any disturbances.

Step disturbance A constant load disturbance is applied, to test the controller and excite possible cross-couplings. The first disturbance occurs

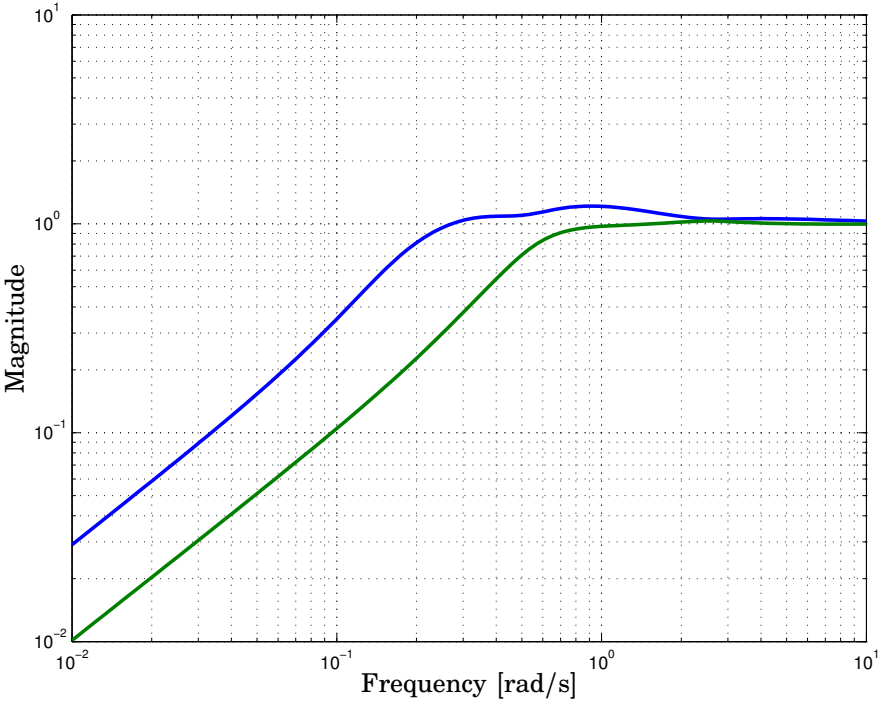

Figure 4.6 Magnitude plot of the sensitivity function **S** for the closed loop system showing the maximum and minimum singular values $\sigma_{\max}$ and $\sigma_{\min}$.

at the first injection point at $t = 70$ s, then later at the second injection point at $t = 160$ s. In the simulation model, the disturbances $\mathbf{d}(t)$ are implemented as a step function acting on the reactor temperature derivatives in the 1st and 16th control volume, that is, the control volumes in which reactant B is being injected, compare with (3.2),

$$\frac{dT_{r,1}}{dt} = f_1(T_r, T_w, c_A, c_B, u) + \frac{d_1}{\rho c_p V_r} \tag{4.16}$$

$$\frac{dT_{r,16}}{dt} = f_{16}(T_r, T_w, c_A, c_B, u) + \frac{d_2}{\rho c_p V_r} \tag{4.17}$$

$$d_1 = \begin{cases} 0 & t \leq 70 \text{ s}; \\ 100 \text{ J/s} & t > 70 \text{ s}; \end{cases} \qquad d_2 = \begin{cases} 0 & t \leq 160 \text{ s}; \\ 100 \text{ J/s} & t > 160 \text{ s}; \end{cases} \tag{4.18}$$

where ρ and c_p are the density and heat capacity of the reactor fluid and V_r is the volume of one reactor control volume. The load disturbances **d** can be viewed as a step increase of 100 J/s in the heat release. The load

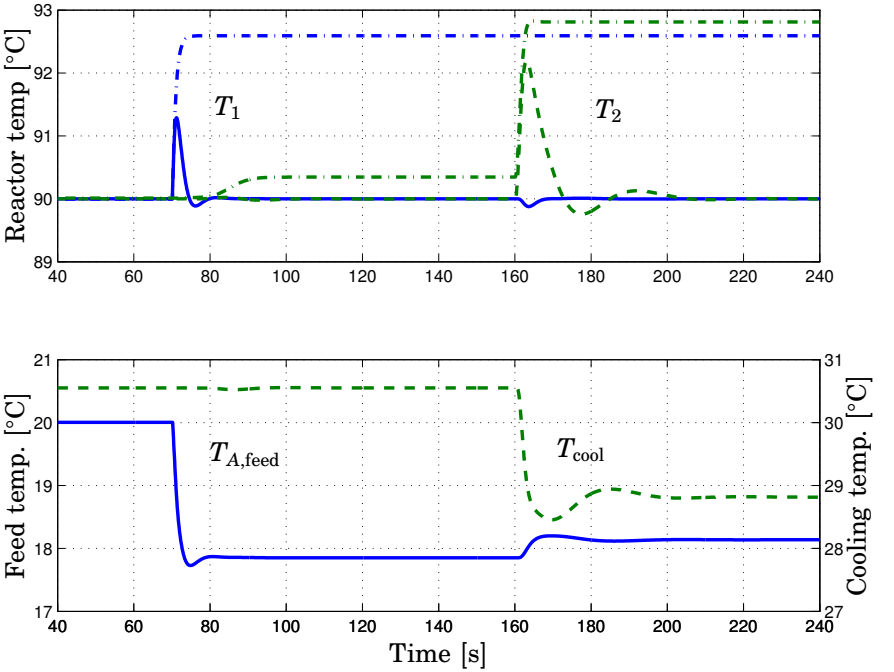

Figure 4.7 Simulated response for step disturbance steps. Upper plot: The first load disturbance affects T_1 (solid) at $t = 70$ s. The second load disturbance affects T_2 (dashed) at $t = 160$ s. The dash-dotted lines represent the uncontrolled response. There is almost no interaction between the two control loops. Lower plot: The control inputs $T_{A,\text{feed}}$ (solid) and T_{cool} (dashed).

disturbances would increase the reactor temperatures around 2.6°C if no feedback control is applied.

Figure 4.7 shows the closed loop response. The interconnection between the two independent control loops is negligible. The control error in the undisturbed control loop remains below 0.1°C during each step disturbance. The integral part of each PID controller guarantees zero error in steady-state. The AMIGO tuning gives the closed loop system fast and well-dampened responses. The disturbance at the second injection point is attenuated slightly slower, as the slower input dynamics and the longer time delay of the T_{cool} input require a more cautious tuning of the T_{cool}-controller than the $T_{A,\text{feed}}$-controller.

Ramp disturbance Figure 4.8 shows another disturbance scenario, where ramp disturbances in the feed concentrations $c_{A,\text{feed}}$ and $c_{B,\text{feed}}$ lead

to 5% more heat being released from the reaction. This results in higher temperatures at the injection points, where the main part of the reaction occurs. The disturbance is implemented as

$$c_{A,\text{feed}} = \begin{cases} c_{A,\text{feed}}^{\text{nom}} & t \leq 100 \text{ s}; \\ \left(1 + \frac{0.05(t-100)}{40}\right) c_{A,\text{feed}}^{\text{nom}} & 100 \leq t < 140 \text{ s}; \\ 1.05 c_{A,\text{feed}}^{\text{nom}} & t \geq 140 \text{ s}; \end{cases} \tag{4.19}$$

with similar equations for $c_{B,\text{feed}}$. The uncontrolled response gives reactor temperatures close to 96°. With decentralized control using $T_{A,\text{feed}}$ and T_{cool}, the temperatures remain below 91°. The increase in T_1 is quickly stopped and its control error remains constant during the ramp disturbance. T_2 has a larger control error during the ramp disturbance, due to warmer reactor fluid flowing down from T_1 at $t = 115$ s acting as an additional disturbance. When the ramp disturbances converge to their new constant value at $t = 140$ s, the reactor temperatures return to their set-points. The feed concentration disturbances do not excite any cross-couplings as the disturbances affect both control loops simultaneously.

Another input/output pairing The step disturbance scenario from Figure 4.7 is repeated for another input/output pairing, where T_1 is now controlled by the feed injection distribution u_B and T_2 is again controlled by the cooling temperature T_{cool}. The control design is repeated following the same steps described above. The purpose is to investigate how the performance of the decentralized controller change when the control inputs are more closely coupled.

Figure 4.9 shows the simulation results of the step disturbance. We can clearly see a one directional cross-coupling between the two control loops. When the step disturbance occurs at the first injection at $t = 70$ *s*, the feed injection of B has to be redistributed from the first to the second injection point, to keep the reactor temperature T_1 at the reference. The redistributed flow of reactant B will cause more heat being released at the second injection point, thus forcing the second controller to manipulate T_{cool} to control T_2. So this local disturbance effects both control loops through the cross-couplings of the inputs. During the second load disturbance the effect of the control action in cooling temperature T_{cool} has a very small effect on T_1, i.e., the interconnection in this direction is very weak. The process can therefore be approximated as almost triangular. To compensate for this triangular structure, a decoupler may be designed, which may improve the performance.

The drawback with this input/output pairing is that one of the control inputs, u_B simply redistributes the heat, whereas the second control input

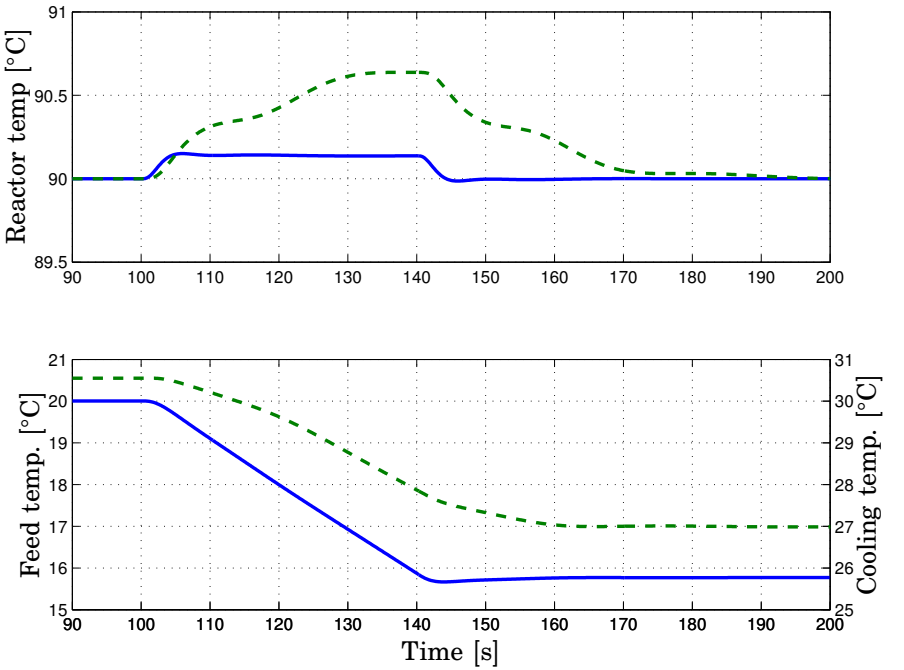

Figure 4.8 Ramp disturbance in $c_{A,\text{feed}}$ and $c_{B,\text{feed}}$, which leads to more heat being released at both injection points simultaneously. Upper plot: T_1 (solid), T_2 (dashed). Lower plot: $T_{A,\text{feed}}$ (solid), T_{cool} (dashed).

T_{cool} can actually increase the heat removal. Compare with the first input/output pairing, where both $T_{A,\text{feed}}$ and T_{cool} can independently control how much heat that may be absorbed or transferred away. This disadvantage may also be confirmed in the ramp disturbance scenario, where the $u_B - T_{\text{cool}}$ pairing has deteriorated performance.

Additional control inputs So far two of the three control inputs have been used at the same time. However, in some cases it would be beneficial to exploit all three inputs to control the reactor temperatures T_1 and T_2. It is non-trivial how to exploit this extra flexibility within the framework of a decentralized controller.

One example may be to start with the controller defined in (4.8), with $T_{A,\text{feed}}$ and T_{cool} as primary control inputs, and use the injection flow distribution u_B as an extra degree of freedom when either of these primary inputs are near saturation. For example, if $T_{A,\text{feed}}$ decreases below some threshold and approaches its limit, the feed of reactant B may be redistributed to the second injection point, thus reducing the risk of saturation.

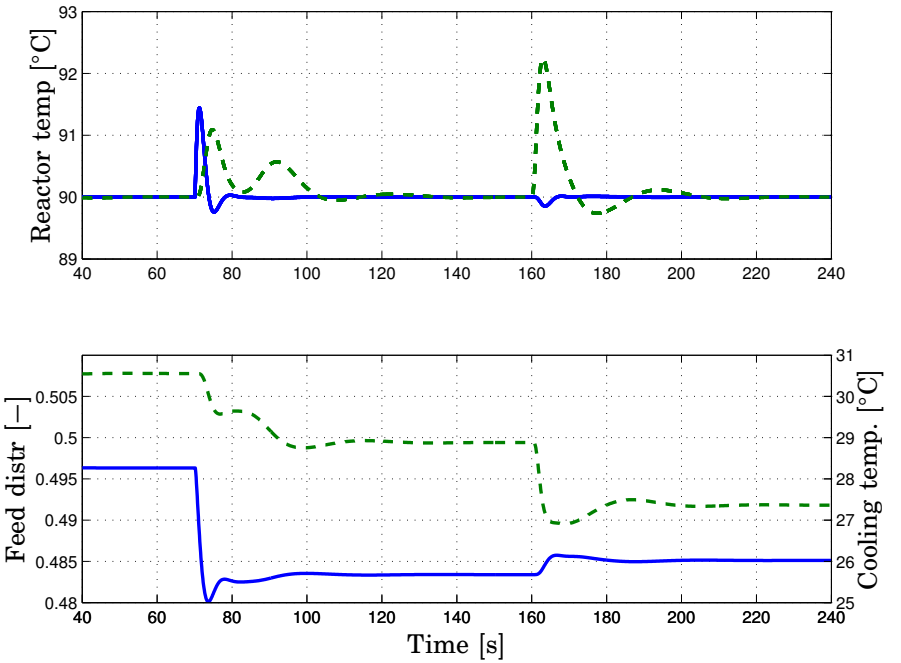

Figure 4.9 Simulated response for load disturbance steps using the u_B/T_{cool}-pairing. Here the two control loops have a significant one-way interconnection. Upper plot: T_1 (solid), T_2 (dashed). Lower plot: $T_{A,\text{feed}}$ (solid), T_{cool} (dashed).

Extensions of the Control Structure

The flexible configuration of the plate reactor allows multiple injection points and cooling zones. It is therefore necessary to discuss how the decentralized control structure may be adapted to fit various configurations, besides the previously presented with two injection points and one cooling zone. Furthermore, the decentralized control structure should be extendable to allow additional control inputs and measurements to be used.

Control structures for a general process configuration In Section 2.4, the flexible configuration of the plate reactor was presented. So far there have been two injection points and one cooling zone. Assume now that the plate reactor has five injection points and five cooling zones, see Figure 4.10. In this configuration, $T_1 \dots T_5$ denote the temperatures at the five injection points and $T_{\text{cool},1} \dots T_{\text{cool},5}$ denote the inlet temperatures of the cooling water for the five independent cooling zones. With additional injection points, it is possible to increase the throughput in steady-state with at least 25%, since the heat transfer capacity of the reactor is better

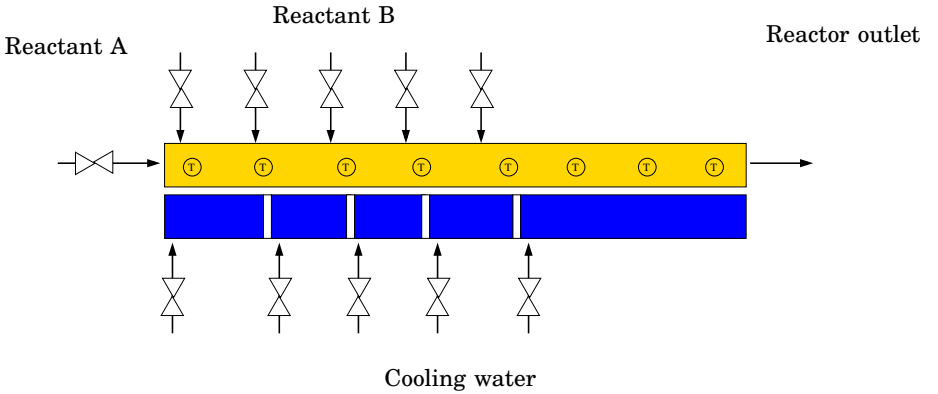

Figure 4.10 The plate reactor with five injection points and five independent cooling zones.

utilized. Subsequently, 25% more heat is being removed from the reaction. The question is now how to adapt the decentralized control scheme to this process configuration.

The heat from the reaction at each injection point will result in a reactor temperature profile with five local temperature maxima. The objective of the feedback control is to control these temperatures to a given reference temperature. A straight forward extension of the previous control scheme is to close the loop around each temperature maximum and design five decentralized control loops, see Figure 4.11. The first temperature maximum is controlled by the feed temperature $T_{A,\text{feed}}$. The remaining temperature maxima are controlled by the inlet temperatures of the individual cooling zones. The inlet temperature of the last cooling zone may be manipulated to control the outlet temperature of the reactor fluid, according to specifications from downstream processing. Each control loop will affect the other control loops downstream, but not the loops upstream, except for the weak cross-coupling between the feed temperature loop and the first cooling zone loop. The injection flow rate in the first injection point is determined to be 35% of the total feed of B, 17% in the second and third, 16% in the fourth and 15% of the total feed is added in the fifth injection point, that is, $[u_{B1}\ u_{B2}\ u_{B3}\ u_{B4}\ u_{B5}]^T = [0.35\ 0.17\ 0.17\ 0.16\ 0.15]^T$.

The control design is repeated following the same steps described above. It is worth noting that the gains from the five cooling temperatures to the designated reactor temperatures are roughly one-third of the gain in previous configuration, see (4.6) and (4.7), since each cooling zone here is smaller. In addition, the potential for interactions is larger, since the actuators are placed closer to each other, thus having a higher impact

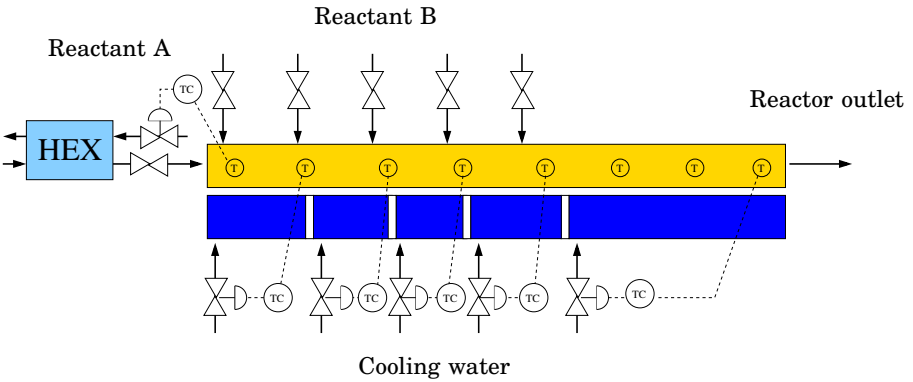

Figure 4.11 Closed loop control of the reactor temperatures. The controllers are indicated with the symbol TC (temperature control). The flow valve at each cooling zone is a symbolic representation of an arbitrary actuator type.

on its downstream neighbors. However, the dynamics between control input and controlled output is also faster, which allows for fast and accurate temperature control. The resulting six inputs six outputs closed loop system is analyzed as previous with the multivariable sensitivity function $\mathbf{S}$ defined in (4.15). The maximum gain for all input directions is around 1.40 at 0.3 rad/s, see Figure 4.12.

The load disturbance scenario is repeated, now with step disturbances of 100 J/s at the first and third injection point, see Figure 4.13. The lower plot shows the control actions of the feed temperature and the different cooling temperatures, where the subscript i in $T_{\text{cool},i}$ indicates the number of the cooling zone starting from left in Figure 4.11. The disturbance is quickly attenuated. The effect downstream of the disturbance is small at the third injection point (at $t = 160$ s) and even smaller at the first injection point (at $t = 60$ s).

The ramp disturbance scenario is also investigated, see Figure 4.14. The control error is at most 0.2°C, which is lower than for the original configuration. The faster input dynamics and less time delay allow more aggressive tuning with the AMIGO method, given a fixed robustness margin in terms of the sensitivity function. In addition, the effect of the ramp disturbance is smaller, since the feed disturbance is distributed among five injection points instead of two injection points.

Feed-forward control The control loops in Figure 4.11 use local measurements for feedback control. The configuration of the process allows easily feed forward connections, where the temperature sensor upstream of a control loop may provide information about incoming disturbances.

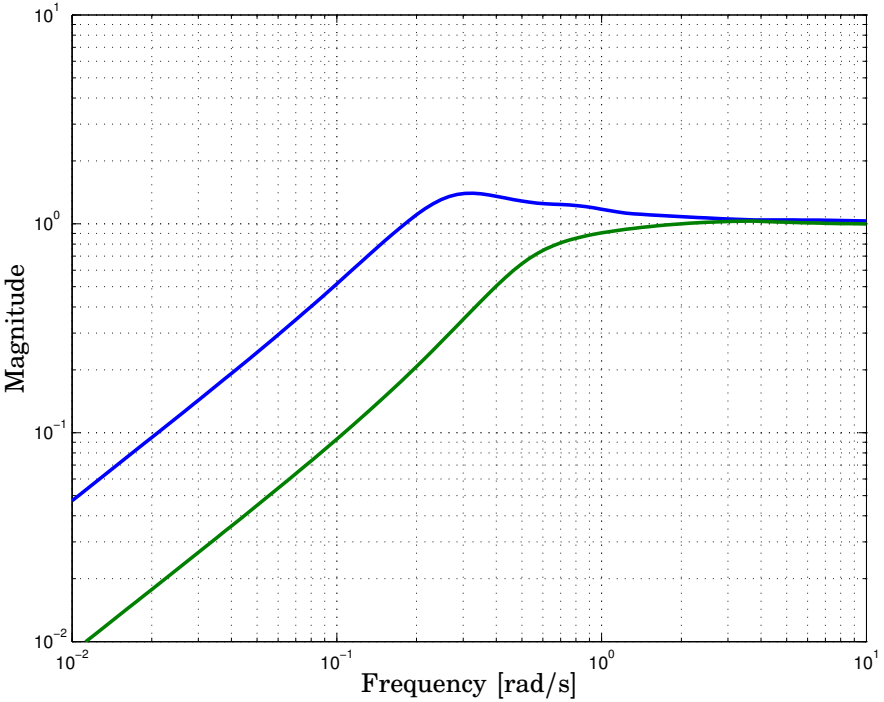

Figure 4.12 Magnitude plot of the sensitivity function S for the closed loop system with five injections and five cooling zones. The lines represent the maximum and minimum singular values, $\sigma_{\max}$ and $\sigma_{\min}$.

The flow time between each sensor is around 4-5 seconds, which offers plenty of time to compensate for disturbances using feed forward signals to improve performance. In this specific case for the plate reactor, standard feedback control is sufficient. In addition to the feed forward signal from the sensor, there is also a possibility of feed forward from the controller upstream. Eventually, the decentralized control structure using feed forward connections from both sensors and actuators have more resemblance with centralized multivariable control than the original decentralized control scheme. Adding more information to each control loop may increase the performance, but may also introduce increased sensitivity to model uncertainty.

Considering temperature constraints So far the controller has focused on tracking given reference temperatures. For some applications, there will be a safety constraint on the reactor temperature $T_r \leq T_{\max}$. The constraint can be derived from material limitations, possible by-product

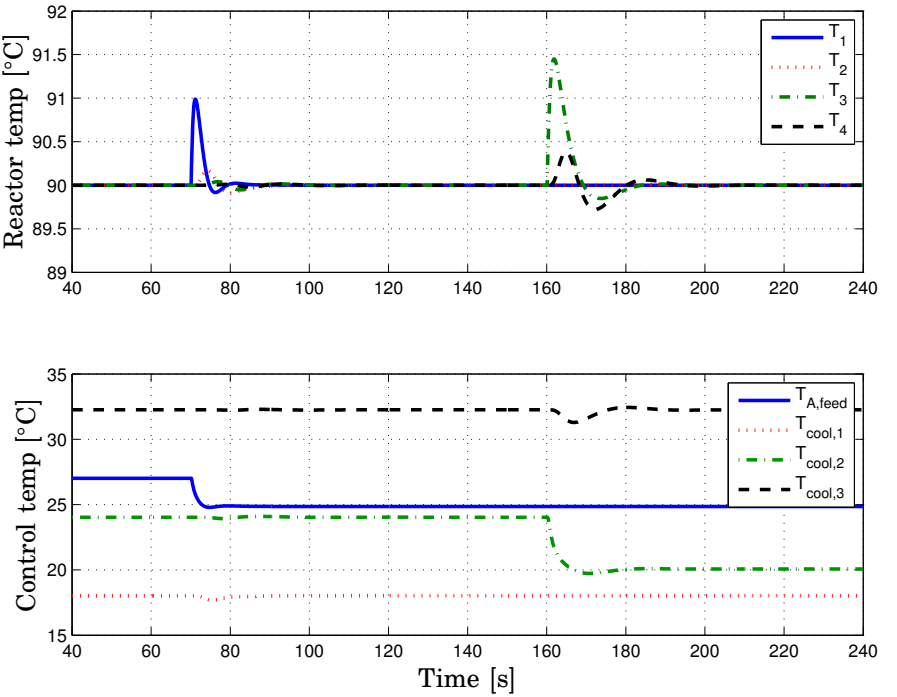

Figure 4.13 Simulated response for load disturbance steps with five injections and five cooling zones. The disturbances enter at the first (T_1) and the third (T_3) injection point, respectively.

formation or the boiling point for the given reactor pressure. Too high temperatures may lead to mechanical failures, reduced product quality or even a thermal runaway situation. Violations in the temperature constraints may provoke unnecessary and expensive emergency shutdowns.

It is non-trivial how to include temperature constraint in the decentralized control structure presented above. Constraint handling in decentralized control is often managed by choosing a nominal operating point that gives a large margin to the constraint, mainly because of the lack of reliable constraint handling. This may be very inefficient. One alternative is to have gain scheduling of the controller parameters, where the controller gain increases as the temperature approaches the constraint limit.

Another alternative is to extended the control structure with additional control inputs. In the plate reactor application, the reactor temperatures are normally controlled by the feed temperature and the cooling temperatures. However, when a reactor temperature increases and approaches the

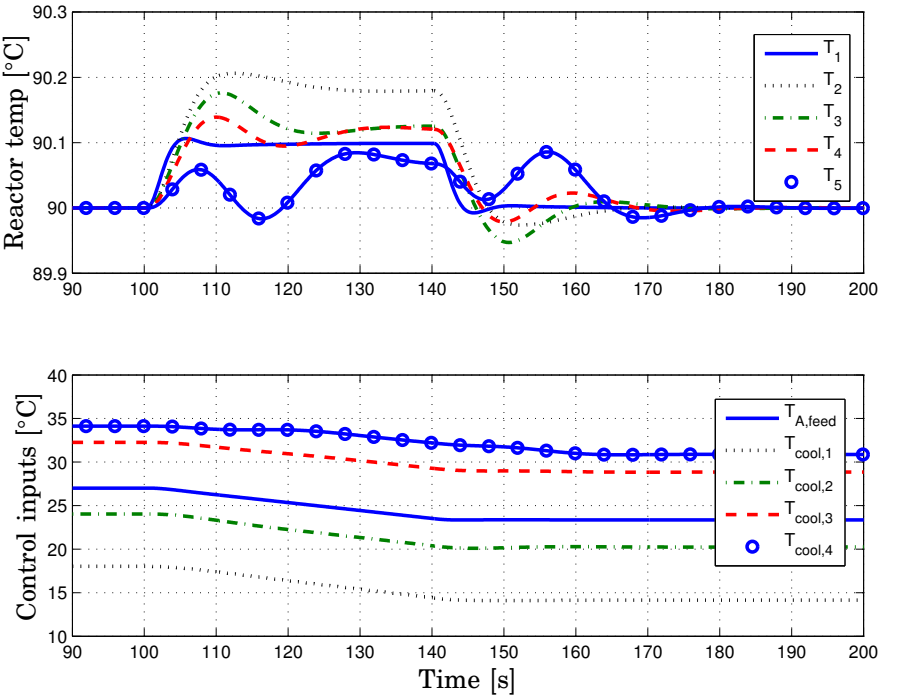

Figure 4.14 Simulated response for ramp disturbance steps with five injections and five cooling zones. The disturbance affect all five injection points simultaneously.

constraint, the control actions of $T_{A,\text{feed}}$ or $T_{\text{cool},i}$ are usually not sufficiently fast. Therefore, the corresponding injection flow rate may be decreased and that will very quickly reduce the heat release from the reaction and the reactor temperature to avoid violating the constraint.

An example: Assume the plate reactor has five injection points and five cooling zones. Six feedback loops are constructed as in Figure 4.11. The nominal temperature reference is $T^{\text{ref}} = 90°\text{C}$. The reactor temperature is limited to $T_{\max} = 92°\text{C}$. The objective is to control the reactor temperature at 90° and to stay below the limit at all times.

To improve the constraint handling in the plate reactor, the injection flow rates are also manipulated, but only when the temperature is close to the constraint. The idea is that when the temperature increases above a certain threshold and approaches the limit, the feed injection is quickly decreased. Meanwhile, the ordinary temperature controller using $T_{A,\text{feed}}$ or $T_{\text{cool,i}}$ also takes action to decrease the temperature. As soon as the temperature decreases below the threshold, the injection flow rate can

slowly return to its nominal value, to ensure stoichiometric conditions in steady-state. This behavior can be implemented with the following injection controller for u_{Bi} and T_i, where $i = 1 \ldots 5$ corresponds to the five injection points,

$$u_{Bi} = u_{Bi}^{\text{nom}} - u_{Bi}^{\text{nom}} \kappa \frac{\tau s + \tau + 1}{\tau s + 1} \cdot \max(0, T_i - T^{\text{threshold}}). \tag{4.20}$$

The injection controller is activated as soon as the reactor temperature $T_i > T^{\text{threshold}}$, where the threshold is set the 91°C, to have time to avoid crossing the limit at 92°C. The max-operator ensures that the injection flow remains bounded by its nominal value, $u_{Bi} \leq u_{Bi}^{\text{nom}}$. The gain κ defines the high-frequency gain and τ is the time constant with which the injection flow rate returns to its nominal value. In this example, $\kappa = 0.5$ and $\tau = 10$ s. The choice of τ should be correlated to the cross-over frequency of the temperature controller, which is $\omega_c \approx 0.20$ rad/s, see Figure 4.5.

Figure 4.15 shows the closed loop response of the combined temperature control and constraint handling together with the open loop response and the response using temperature control alone. A step disturbance of 200 J/s occurs at $t = 60$ s in the third injection point, i.e., the third injection flow rate will be manipulated to improve the constraint handling. The nominal flow rate $u_{B3}^{\text{nom}} = 0.17$, that is, 17% of the total feed of B is injected here. As soon as the temperature T_3 passes the threshold at 91°C, the injection flow rate u_{B3} is decreased. Meanwhile, the standard feedback loop manipulates $T_{\text{cool},2}$ to achieve temperature tracking at $T^{\text{ref}} = 90$°C. Due to these actions, the reactor temperature remains below the limit, $T_{\max} = 92$°C. The following undershoot and overshoot in temperature come from the combined actions of the two control inputs working independently in parallel. A feed forward signal from the injection controller to the temperature controller may decrease the under- and overshoot. The main drawback with this method is the lack of information sharing between the two control loops. Each loop does not know what the other loop is actuating. When operating closer to the constraints, centralized information becomes more and more essential. This leads us to the centralized controllers in the next section.

Summary and Conclusions

Decentralized control may successfully control the reactor temperature inside the plate reactor. Using system analysis and choosing the most suitable input/output pairing, for example through RGA, may give decentralized control loops with lower cross-couplings, which may improve the performance compared to other pairings. For the plate reactor, the injection flow rates are very good for temperature control, but may upset the stoichiometric balances. If stoichiometric constraints are enforced,

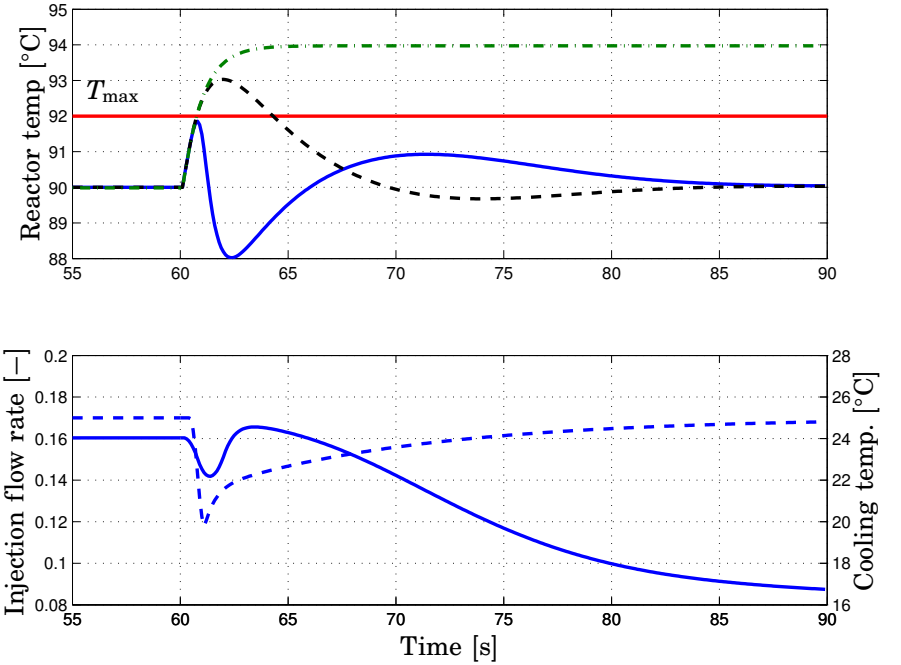

Figure 4.15 Constraint handling with decentralized control for a step disturbance at the third injection point. Upper plot: Reactor temperature T_3. The combination of feedback control and constraint handling (solid). For comparison, the uncontrolled response (dash-dot) and feedback control using only $T_{\text{cool},2}$ (dashed). Lower plot: Control inputs of $T_{\text{cool},2}$ (solid) and u_{B3} (dashed) for the combined feedback and constraint handling case.

the cross-couplings between the control inputs increase. The most suitable control inputs were the feed temperature and the cooling temperatures, which induce very little cross-coupling.

It is recommended to consider the implications of the process design on the control design already in an early development stage. It is important to build the process to facilitate the feedback control of the plate reactor at stationary operation.

It is difficult to handle temperature constraints in a decentralized control structure. When operating closer to the constraints, the control actions gets larger to avoid the constraints, which may excite cross-couplings and even lead to instability. When temperature constraints are of great importance, other control methods that can explicitly handle constraints may be considered, e.g. MPC. In this case, the combined temperature and con-

straint handling controller may be replaced by a two-input single-output MPC controller.

Finally, the decentralized control structure can be extended with additional inputs, outputs, feed forward connections, decouplers and special controllers handling state constraints. But then the controller has more resemblance with a centralized controller than its original decentralized nature. It may then be worthwhile to consider a centralized control approach to take advantage of the multivariable capabilities of e.g. a multi-input multi-output MPC controller.

4.6 Centralized Control

In the previous section, a decentralized controller was designed using PID controllers and evaluated in simulations. The result was good for processes with low cross-coupling. When the inputs of the process have more cross-coupling, the performance of the decentralized controller may decrease. Furthermore, it is non-trivial how to extend the control structure with additional control inputs or to handle state constraints.

The outline for this section is as follows. First, the model used for control design is presented. Then the state and disturbance observer is designed to achieve accurate estimation and integral action. Thereafter, the focus is on temperature control of the plate reactor using MPC. Finally, concentration measurements enable control of the stoichiometric conditions inside the reactor and it is demonstrated how the MPC controller can be designed to combine temperature and stoichiometric control objectives.

Introduction

In this section, an MPC controller will be designed to control the plate reactor around a nominal operating point. A few control methods were briefly reviewed in Section 4.2. The MPC approach is chosen, since it may take advantage of multiple inputs multiple outputs (MIMO) models, offers explicit handling of input and state constraints and is becoming well known in the process industry.

MPC relies on the receding horizon principle, see e.g. [Maciejowski, 2002]. The controller solves, at each sampling instant, a finite horizon optimal control problem. Only the first value of the optimal control variable solution is applied and the remaining solution is discarded. The same procedure is then repeated at each sampling instant, and the prediction horizon is shifted forward one step. Hence, the name receding horizon control.

The MPC algorithms used in this section come from the software package MPCtools, [Åkesson, 2006]. It is free software, based on the standard Matlab language, without any other additional toolboxes required and has been developed at the Department of Automatic Control, Lund University. For scenarios with temperature constraints, the controller has been implemented using the algorithms from the MPC toolbox in Matlab [Mathworks, 2007b], due to its improved soft constraint handling.

Models for Control Design

There are numerous approaches to apply the MPC concept on tubular reactors. The main difference is what model structure to use when approximating the PDEs defining the system, e.g. finite differences, the method of characteristics [Shang *et al.*, 2007], proper orthogonal decomposition or the SVD method [Hoo and Zheng, 2001]. In these papers, the low-order model approximates the PDE model and the controller is designed based on the low-order model.

A nonlinear model of the plate reactor and the reaction kinetics was derived from first principles in Chapter 3. At first, consider a plate reactor with two injection points and one cooling zone. A linear MPC controller is developed based on notations from [Maciejowski, 2002] and [Åkesson, 2003]. The nonlinear model is linearized around some nominal operating point $(\mathbf{x^0}, \mathbf{u^0})$. The linear system is sampled with $T_s = 0.5$ seconds to a discrete-time system. The choice of sampling time is based on the cross-over frequency of the open loop compensated system in Figure 4.5, where $\omega_c \approx 0.2 - 0.6$ rad/s. A few guidelines on how to select sampling time are given in [Åström and Wittenmark, 1997], e.g. $T_s\omega_c \approx 0.15 - 0.50$. This results in a recommended sampling time of 0.2 – 0.8 seconds. A short sampling time increases the performance to reject disturbances and follow setpoint changes. On the other hand, shorter sampling time gives less time for computations and it may require a longer prediction horizon, which increases the computational requirement of the MPC. This should be compared to the decentralized controller in the previous section, where the controller was sampled with $T_s = 0.1$ s, since there were no computational limitations.

The process model can be defined as

$$\mathbf{x}(k+1) = \mathbf{A}\mathbf{x}(k) + \mathbf{B}\mathbf{u}^{\text{sp}}(k) \tag{4.21}$$

$$\mathbf{y}(k) = \begin{bmatrix} \mathbf{y_z}(k) \\ \mathbf{y_a}(k) \end{bmatrix} = \begin{bmatrix} \mathbf{C_z} \\ \mathbf{C_a} \end{bmatrix} \mathbf{x}(k) = \mathbf{C_y}\mathbf{x}(k) \tag{4.22}$$

where $\mathbf{x}$ is the state vector and $\mathbf{u}^{\text{sp}}$ is the control input vector. The control inputs are used as set-points to the low-level feedback controllers, hence

the superscript 'sp'. In the rest of this section, the superscript is omitted for clarity, when the meaning is clear from the context. The measurement vector $\mathbf{y}$ is divided into $\mathbf{y_z}$, which is the measured controlled output vector and $\mathbf{y_a}$, which is the vector with additional measured, but not controlled, outputs.

As described in Section 3.1, the plate reactor model is discretized into $n = 30$ control volumes. There are five states in each control volume, the temperature in the reactor and in the cooling water and the concentrations of the two reactants and one of the products. In addition, there are extra states associated with the actuator dynamics for each control input. The state vector $\mathbf{x}$ can be written as

$$\mathbf{x} = \begin{bmatrix} \mathbf{T_r}^T & \mathbf{T_w}^T & \mathbf{c_A}^T & \mathbf{c_B}^T & \mathbf{c_C}^T & \mathbf{x}_{\text{act}}^T \end{bmatrix}^T, \tag{4.23}$$

where $\mathbf{T_r}, \mathbf{T_w}, \mathbf{c_A}, \mathbf{c_B}$ and $\mathbf{c_C}$ are all vectors of size N and $\mathbf{x}_{\text{act}}$ represents the actuator states. The actuator models for the feed temperature $T_{A,\text{feed}}$ and the feed injection flows u_{Bi} are each approximated with a first order system, whereas the actuator for the cooling water T_{cool} is approximated with a second order system. In total, the linear model has 155 states, including the actuator models. The reactant injections are described by injections into the 1st and 16th control volume.

State and Disturbance Estimation

In MPC, full state feedback is assumed and since the concentrations are not possible to measure, state estimation is required. In addition, there are process disturbances, measurement noises and model errors that need to be considered. Traditionally, the process model is augmented with a disturbance model that represents the lumped effect of plant-model mismatch and/or unmodeled disturbances. The disturbance models have often integrating states acting on the control inputs, the measured outputs, the states of the process or any mix of these. The choice of disturbance model is a very important part of the control design and tuning and will have a direct impact on the transient and steady-state behavior of the closed loop system.

In this thesis, we use the following nomenclature. When integrating disturbances are added to the control inputs, we have an *input disturbance* model. When integrating disturbances are added only to the measured outputs we have an *output disturbance* model and finally if integrating disturbances are added directly to the derivatives of the process states, we have a *state disturbance* model.

In [Pannocchia and Rawlings, 2003], necessary and sufficient conditions on the disturbance models to achieve offset-free model predictive

control are derived. It is for example not sufficient to add one integrating disturbance to each controlled output, when there are additional outputs measured. Instead, it is required to have a number of integrating disturbances equal to the number of measured variables. In [Pannocchia, 2003], different disturbance models for MPC are investigated to improve the robustness of the closed loop system. In [Åkesson and Hagander, 2003], a disturbance observer is developed for non-square processes to provide integral action when the number of measured outputs exceeds the number of control inputs. In addition to disturbance states on the control inputs, the method in [Åkesson and Hagander, 2003] suggests adding disturbance states acting on the measured – but not controlled – outputs.

The equations for the linear Kalman Filter with this disturbance model can then be written as

$$\begin{bmatrix} \dot{\hat{\mathbf{x}}} \\ \dot{\hat{\mathbf{d}}}_\mathbf{a} \\ \dot{\hat{\mathbf{d}}}_\mathbf{i} \end{bmatrix} = \underbrace{\begin{bmatrix} \mathbf{A} & 0 & \mathbf{B_d} \\ 0 & 0 & 0 \\ 0 & 0 & 0 \end{bmatrix}}_{A_e} \begin{bmatrix} \hat{\mathbf{x}} \\ \hat{\mathbf{d}}_\mathbf{a} \\ \hat{\mathbf{d}}_\mathbf{i} \end{bmatrix} + \underbrace{\begin{bmatrix} \mathbf{B} \\ 0 \\ 0 \end{bmatrix}}_{B_e} \mathbf{u} + \mathbf{K}(\mathbf{y} - \hat{\mathbf{y}}) \tag{4.24}$$

$$\begin{bmatrix} \hat{\mathbf{y}}_\mathbf{z} \\ \hat{\mathbf{y}}_\mathbf{a} \end{bmatrix} = \underbrace{\begin{bmatrix} \mathbf{C_z} & 0 & 0 \\ \mathbf{C_a} & \mathbf{I} & 0 \end{bmatrix}}_{C_e} \begin{bmatrix} \hat{\mathbf{x}} \\ \hat{\mathbf{d}}_\mathbf{a} \\ \hat{\mathbf{d}}_\mathbf{i} \end{bmatrix} \tag{4.25}$$

where $\hat{\mathbf{x}}$ is the estimated state vector, $\hat{\mathbf{d}}_\mathbf{a}$ is the estimated disturbance vector acting on the measured uncontrolled output and $\hat{\mathbf{d}}_\mathbf{i}$ is the estimated disturbance vector acting on the control inputs, compare with (4.21)-(4.22). The matrix $\mathbf{B_d}$ determines how the disturbance states affect the process states, which will be different depending on the chosen disturbance model. Here, we consider first the input disturbance model, hence $\mathbf{B_d} = \mathbf{B}$. The estimated measurements are divided into two vectors, the controlled outputs $\hat{\mathbf{y}}_\mathbf{z}$ and the uncontrolled outputs $\hat{\mathbf{y}}_\mathbf{a}$. The Kalman filter gain $\mathbf{K}$ is given as the solution of the following Riccati equation

$$\mathbf{K} = (\mathbf{A_e}\mathbf{P}\mathbf{C_e}^T)(\mathbf{C_e}\mathbf{P}\mathbf{C_e}^T + \mathbf{V})^{-1} \tag{4.26}$$

$$\mathbf{P} = \mathbf{A_e}\mathbf{P}\mathbf{A_e}^T + \mathbf{W} - (\mathbf{A_e}\mathbf{P}\mathbf{C_e}^T)(\mathbf{C_e}\mathbf{P}\mathbf{C_e}^T + \mathbf{V})^{-1}(\mathbf{A_e}\mathbf{P}\mathbf{C_e}^T), \tag{4.27}$$

where $\mathbf{W}$ represents the covariance of the noise on the process states and the extra disturbance states and $\mathbf{V}$ represents the covariance of the

measurement noise. Here, we choose

$$\mathbf{W} = \begin{bmatrix} 0.01 \cdot \mathbf{I}_1 & 0 \\ 0 & 100 \cdot \mathbf{I}_2 \end{bmatrix}, \quad \mathbf{V} = \mathbf{I}_3, \tag{4.28}$$

where $\mathbf{I}_1$ and $\mathbf{I}_2$ have sizes matching the process states and the disturbance states, respectively. $\mathbf{I}_3$ has the size of the number of measurements. The chosen weights on $\mathbf{W}$ and $\mathbf{V}$ emphasize that there is low noise on the process state, high noise on the disturbance states and medium noise on the measurements. The Kalman filter with the disturbance observer described above is included in the MPC formulations in the software package MPCtools [Åkesson, 2006].

Temperature Control

Similarly to the decentralized control, the temperatures after the two injection points T_1 and T_2 are to be controlled, tracking a given reference temperature. In addition, there are also measurements of the inlet and outlet temperature of the cooling water, here approximated with $T_{w,1}$ and $T_{w,30}$, where the index refers to the 1st and 30th control volume. The feed temperature $T_{A,\text{feed}}$ and the cooling temperature T_{cool} are chosen as control inputs. The flow scheme in Figure 4.16 shows the centralized control structure and the plate reactor. The inputs, outputs and disturbance states are defined as

$$\mathbf{r} = [T_1^{\text{ref}} \quad T_2^{\text{ref}}]^T, \quad \mathbf{y_z} = \mathbf{C_z x} = [T_1 \quad T_2]^T, \quad \mathbf{y_a} = \mathbf{C_a x} = [T_{w,1} \quad T_{w,30}]^T \tag{4.29}$$

$$\mathbf{u} = [T_{A,\text{feed}} \quad T_{\text{cool}}]^T, \quad \hat{\mathbf{d}}_a = [\hat{d}_{\text{Tw1}} \quad \hat{d}_{\text{Tw30}}]^T, \quad \hat{\mathbf{d}}_i = [\hat{d}_{\text{Tfeed}} \quad \hat{d}_{\text{Tcool}}]^T, \tag{4.30}$$

where the disturbing states $\hat{\mathbf{d}}_\mathbf{a}$ and $\hat{\mathbf{d}}_\mathbf{i}$ are added to the measured, but not controlled, outputs and the control inputs, respectively.

The cost function and controller parameters The cost function for the MPC formulation can be written as

$$V(k) = \sum_{i=1}^{H_p} \|\hat{\mathbf{y}}_\mathbf{z}(k+i|k) - \hat{\mathbf{r}}(k+i|k)\|_\mathbf{Q}^2 + \sum_{i=0}^{H_u-1} \|\Delta\hat{\mathbf{u}}(k+i|k)\|_\mathbf{R}^2, \tag{4.31}$$

where $\hat{\mathbf{y}}_\mathbf{z}$ is the vector of the predicted controlled outputs, $\hat{\mathbf{r}}$ is the vector of the predicted reference values and $\Delta\hat{\mathbf{u}}$ is the vector of the predicted control input changes. H_p is the prediction horizon, H_u is the control horizon, $\mathbf{Q}$

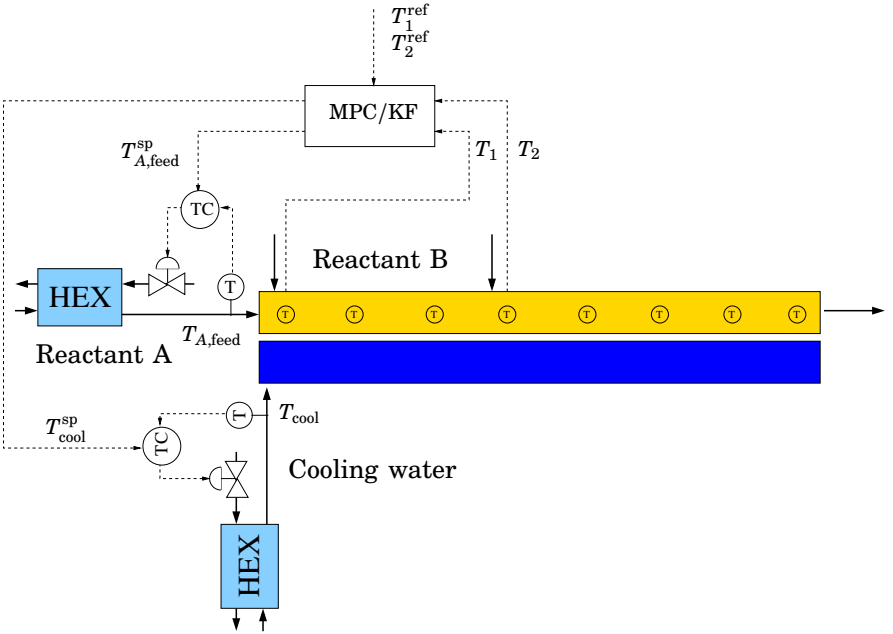

Figure 4.16 Flow scheme of the centralized control and estimation. The MPC controller send set-points to the local feedback controllers in a cascade loop. The centralized controller can easily take advantage of additional measurements. Compare with the decentralized control structure in Figure 4.4.

is the weighting matrix for the controlled variables and $\mathbf{R}$ is the weighting matrix for the control actions.

For the temperature control of the plate reactor, we can write the cost function as

$$\begin{aligned} V(k) \quad = \quad & \sum_{i=1}^{H_p} \left|\left| \begin{bmatrix} \hat{T}_1(k+i|k) \\ \hat{T}_2(k+i|k) \end{bmatrix} - \begin{bmatrix} \hat{T}_1^{\text{ref}}(k+i|k) \\ \hat{T}_2^{\text{ref}}(k+i|k) \end{bmatrix} \right|\right|_{\mathbf{Q}}^2 + \\ & \sum_{i=0}^{H_u-1} \left|\left| \begin{bmatrix} \Delta\hat{T}_{A,\text{feed}}(k+i|k) \\ \Delta\hat{T}_{\text{cool}}(k+i|k) \end{bmatrix} \right|\right|_{\mathbf{R}}^2 \end{aligned} \tag{4.32}$$

The prediction horizon is chosen as $H_p = 100$ and the control horizon $H_u = 30$. For a complex process like the plate reactor, it is necessary to choose a reasonably large prediction horizon H_p, so that all important process dynamics can be observed within the prediction window, thus allowing the optimization to "see" the best operating point within the prediction window. In this case the prediction window is the prod-

uct $H_p \cdot h = 100 \cdot 0.5 = 50$ seconds, which covers the thermal dynamics, the residence time and provides stability to the system. To reduce the computational complexity while maintaining the length of the prediction window, it is possible to use a longer sampling interval h. However for good disturbance rejection property a short sampling interval is desired.

The weighting matrices for the controlled variables and the control signals are chosen as $\mathbf{Q} = \mathbf{I}$ and $\mathbf{R} = \rho \cdot [r_1 \quad 0; \quad 0 \quad r_2]$. The value of $\mathbf{Q}$ corresponds to both controlled temperatures T_1 and T_2 being equally important. The two control inputs $T_{A,\text{feed}}$ and T_{cool} have the same units and may be used equally much, thus $r_1 = r_2 = 1$. The relation between the matrices Q and R, here $\rho = 10$, can be seen as a move suppression factor, defining the aggressiveness of the controller.

Constraints There are constraints on the control inputs $15°\text{C} \leq T_{A,\text{feed}} \leq 80°\text{C}$ and $15°\text{C} \leq T_{\text{cool}} \leq 80°\text{C}$. In the actuator systems for these inputs, there are additional limitations that may be approximated as rate limits on the control signal, $-2°\text{C/s} \leq \dot{T}_{A,\text{feed}} \leq 3°\text{C/s}$ and $-2°\text{C/s} \leq \dot{T}_{\text{cool}} \leq 1°\text{C/s}$.

Analysis of the closed loop system When no constraints are active, the MPC controller is a linear controller, which allows analysis of the closed loop system. Figure 4.17 shows the sensitivity function S for the closed loop system, compare with Figure 4.6 from the decentralized case. The integral action that removes constant offsets due to disturbances and uncertainties is clearly visible at low frequencies. All disturbances with a frequency up to 0.18 rad/s will be attenuated. The peak of the maximum singular value of the sensitivity function is around 1.9, which is higher than for the decentralized controller. A more elaborate tuning may reduce the sensitivity peak.

Simulations

Step disturbance The step disturbance scenario from (4.16-4.18) and Figure 4.7 is repeated, now using MPC instead of the PID-based decentralized controller. The MPC controller should keep the temperatures T_1 and T_2 at the constant reference temperature 90°C. A constant load disturbance d_1 is applied at the first injection point at $t = 70$ s, then a similar disturbance d_2 is applied at the second injection point at $t = 160$ s. The disturbances can be viewed as step increases of 100 J/s in the heat release from the reaction. The disturbances would increase the reactor temperatures with roughly 2.6°C if no feedback control is applied.

Figure 4.18 shows the step disturbances response. The sampling time of $h = 0.5$ s delays the control action compared to the faster sampling time $h = 0.1$ s of the decentralized controller. There is a clear cross-coupling

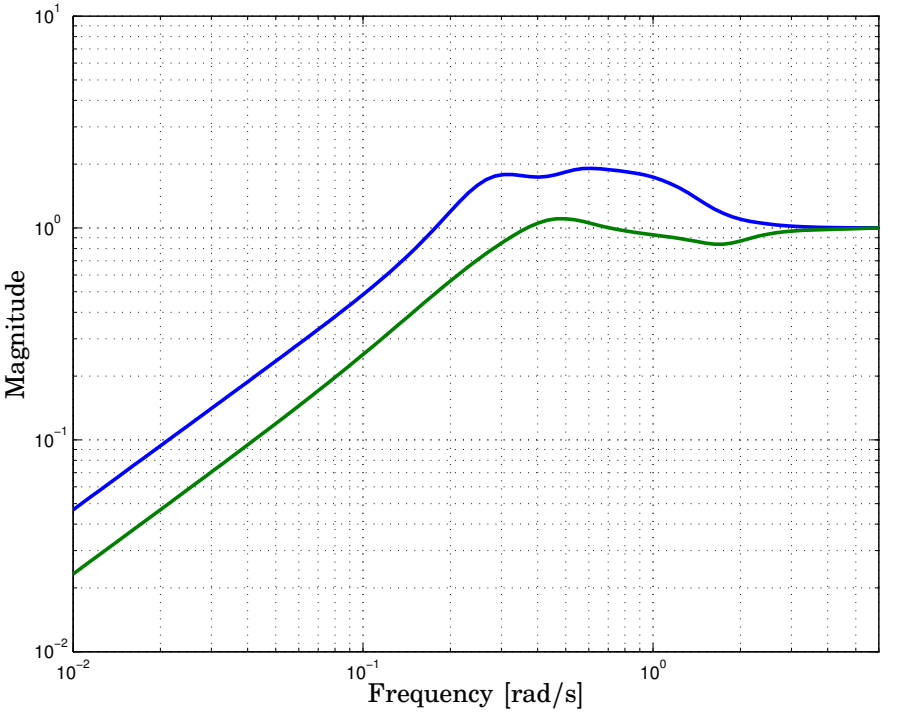

Figure 4.17 Magnitude plot of the sensitivity function S for the closed loop system using MPC. The maximum and minimum singular values $\sigma_{\max}$ and $\sigma_{\min}$ are plotted for all frequencies up to the Nyquist frequency of 6.28 rad/s.

between the two control inputs after each of the step disturbances. The cross-coupling is much larger than for the decentralized controller, which may seem counter-intuitive, considering the information advantage of the centralized controller. The main reason for the cross-coupling is the centralized disturbance estimation and a disturbance model that poorly describes the physical disturbance. The Kalman filter uses four disturbance states, each one representing an integrating disturbance on the two control inputs and the two measurements of the uncontrolled cooling water temperature, see (4.24-4.25). Let us focus on the two input disturbance states $\hat{\mathbf{d}}_{\mathbf{i}}$. The disturbance states on the cooling water $\hat{\mathbf{d}}_{\mathbf{a}}$ have very limited impact on the controlled outputs.

When a disturbance enters the system, the Kalman filter will find a disturbance estimate $\hat{\mathbf{d}}$ that minimizes the square of the estimation error $\mathbf{x}(k) - \hat{\mathbf{x}}(k|k-1)$. The transients of the disturbance estimation can be seen in Figure 4.19, where the step disturbance causes transients in both

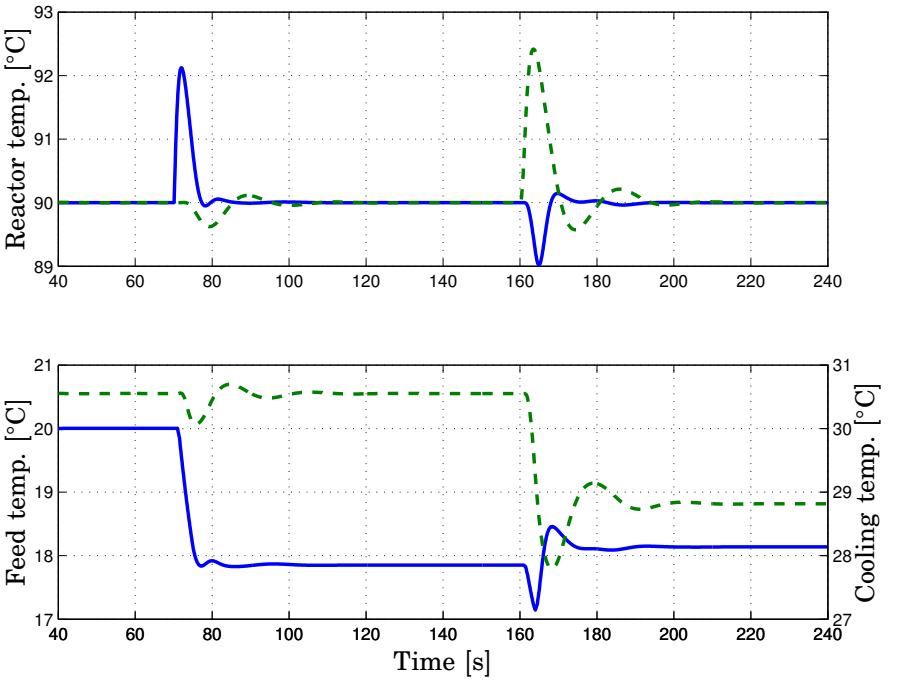

Figure 4.18 Simulated response for step disturbances using MPC. Upper plot: The first step disturbance affects T_1 (solid) at $t = 70$ s. The second step disturbance affects T_2 (dashed) at $t = 160$ s. Lower plot: The cross-coupling between the control inputs $T_{A,\text{feed}}$ (solid) and T_{cool} (dashed) arise from the centralized input disturbance estimation

disturbance estimates. In the Kalman filter, the disturbance at the first injection point can be represented as a disturbance in the feed temperature $T_{A,\text{feed}}$ and/or a disturbance in the cooling inlet temperature T_{cool}. Directly after the step disturbance, the optimal estimate is to use both disturbance states to represent the step disturbance, as the disturbances are modelled as integrated white noise. These transients cause the cross-couplings seen in the control inputs in the lower plot of Figure 4.18. Eventually, the measurements from the reactor lead to the more realistic estimate, where the disturbance state on $T_{A,\text{feed}}$ represents the step disturbance due to its higher steady-state gain.

Note that the disturbance model used here is derived to achieve integral action, without considering its transient response. We will now investigate another disturbance model to obtain more insight how the choice of disturbance model may influence the transient response of the closed loop system.

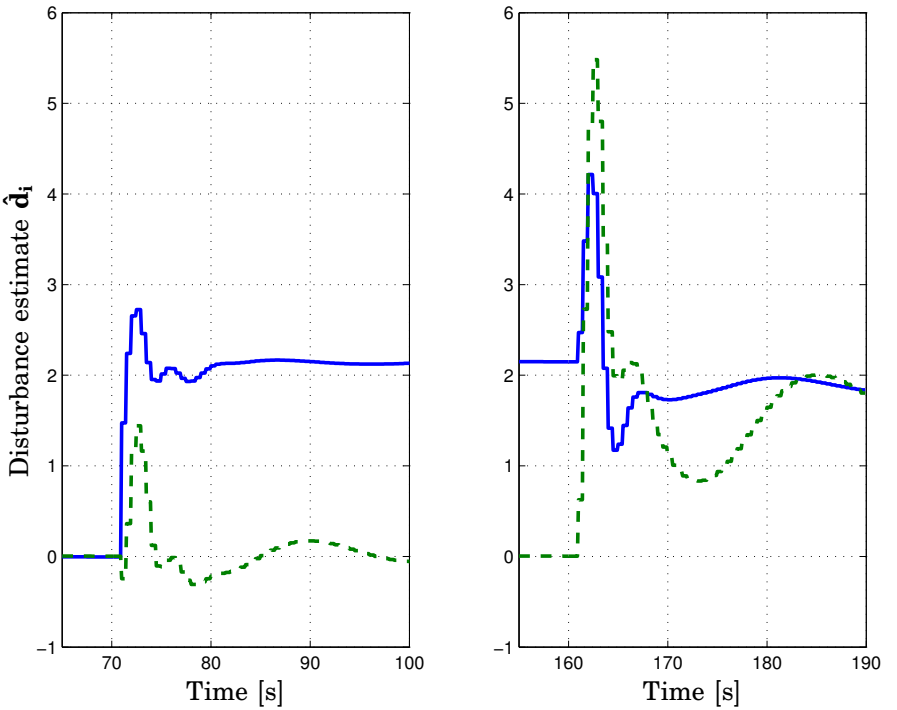

Figure 4.19 Disturbance estimation during step disturbances using input disturbance states on $T_{A,\text{feed}}$ (solid) and T_{cool} (dashed). Left plot: Step disturbance at first injection point at $t = 70$ s. Right plot: Step disturbance at second injection point at $t = 160$ s.

A state disturbance model Besides input disturbance models, a common choice is integrating disturbances on the measured outputs. However, for the plate reactor application, the temperature measurements are fairly reliable, instead, integrating disturbances are added to the derivatives of the reactor temperature states in the 1st and 17th control volume where the maximum temperatures occur. The Kalman filter equations from (4.24) – (4.25) are modified with the new disturbance model

$$\mathbf{B_d} = \mathbf{C_z}^T, \quad \hat{\mathbf{d}}_a = [\hat{d}_{\text{Tw1}} \quad \hat{d}_{\text{Tw30}}]^T, \quad \hat{\mathbf{d}}_i = [\hat{d}_{\text{T1}} \quad \hat{d}_{\text{T2}}]^T. \tag{4.33}$$

The integrating disturbances acting on T_1 and T_2 will give offset-free steady-state estimation on these two controlled outputs. To achieve integral action on the controlled outputs when additional measurements are used, integrating disturbances are added to the extra measured (uncontrolled) outputs as described in (4.24-4.25). A closed loop analysis with

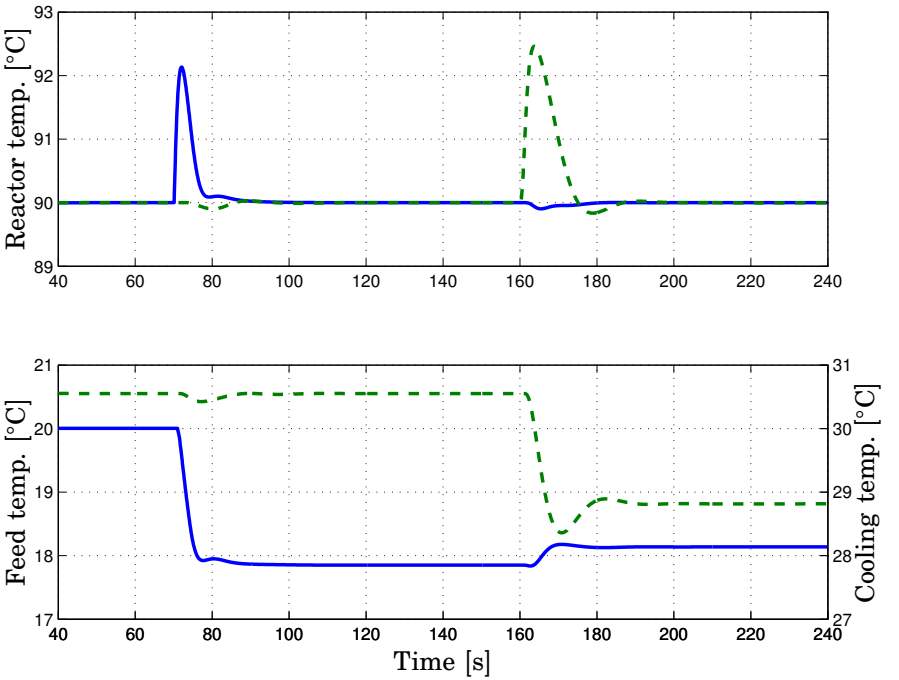

Figure 4.20 Simulated response for step disturbances using MPC and a state disturbance model. The first step disturbance affects T_1 (solid) at $t = 70$ s. The second step disturbance affects T_2 (dashed) at $t = 160$ s. The cross-coupling between the control inputs $T_{A,\text{feed}}$ (solid) and T_{cool} (dashed) are much lower with this type of disturbance model.

the new disturbance model gives a sensitivity function $\mathbf{S}$ with a $\sigma_{\max} = 1.6$ and a cross-over frequency of 0.15 rad/s, yielding a lower $\sigma_{\max}$ than with the input disturbance model.

The step disturbance scenario is repeated, see Figure 4.20. The cross-couplings between the control inputs are almost negligible. The control error in the undisturbed output is at most 0.1°C during the step disturbances, which is similar to the performance of the decentralized controller.

This state disturbance model is very similar to the actual disturbance applied to the process (4.16-4.18), so it should not be a surprise that this disturbance model will estimate the step disturbances more efficiently and with less cross-coupling. The simple truth is that the better the disturbance model can represent the actual disturbance, the better performance we will get. However, the disturbance model should represent the lumped effect of any plant-model mismatch and/or disturbance, so the open question is what disturbance model will be best for an arbitrary disturbance

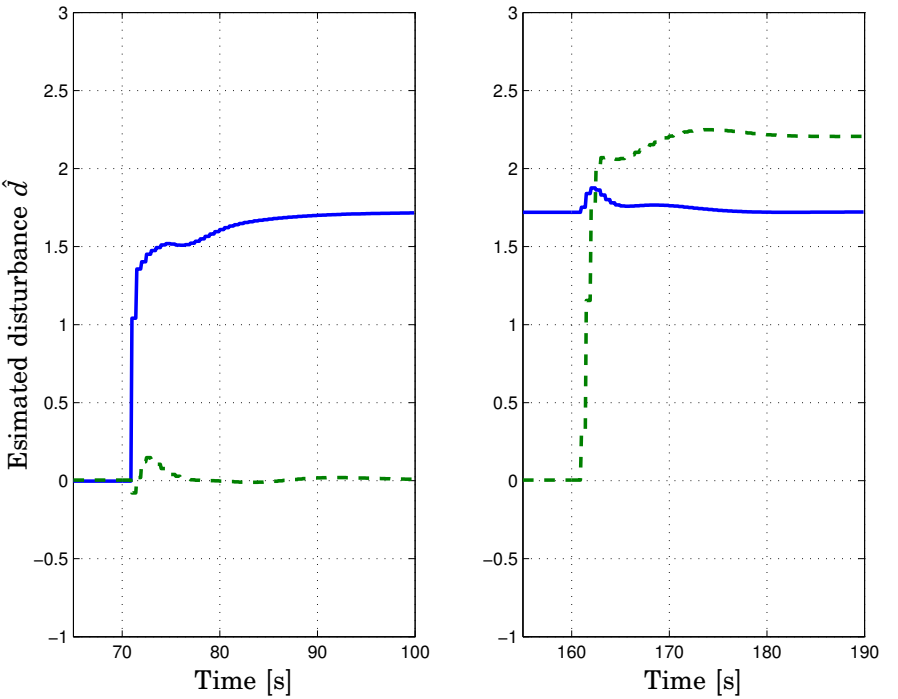

Figure 4.21 Disturbance estimation during step disturbance using a state disturbance model on T_1 (solid) and T_2 (dashed). Left plot: Step disturbance at the first injection point at $t = 70$ s. Right plot: Step disturbance at the second injection point at $t = 160$ s.

or plant-model mismatch.

The estimated disturbance states $\hat{\mathbf{d}}_\mathbf{i}$ are plotted in Figure 4.21. Since the disturbance model is very similar to the actual disturbance, the estimation shows almost no cross-coupling between the two disturbance states. This translates directly into an improved performance of the closed loop control.

Ramp disturbance The ramp disturbance scenario from (4.19) is repeated with the MPC controller, testing both the input disturbance model and the state disturbance model. The feed concentrations of $c_{A,\text{feed}}$ and $c_{B,\text{feed}}$ increase linearly along a ramp during 40 s, thus increasing the heat being released from the reaction.

For the ramp disturbance, the closed loop response with the input disturbance model is slightly better than with the state disturbance model, see Figure 4.22. The difference in T_1 is negligible and the actions of the

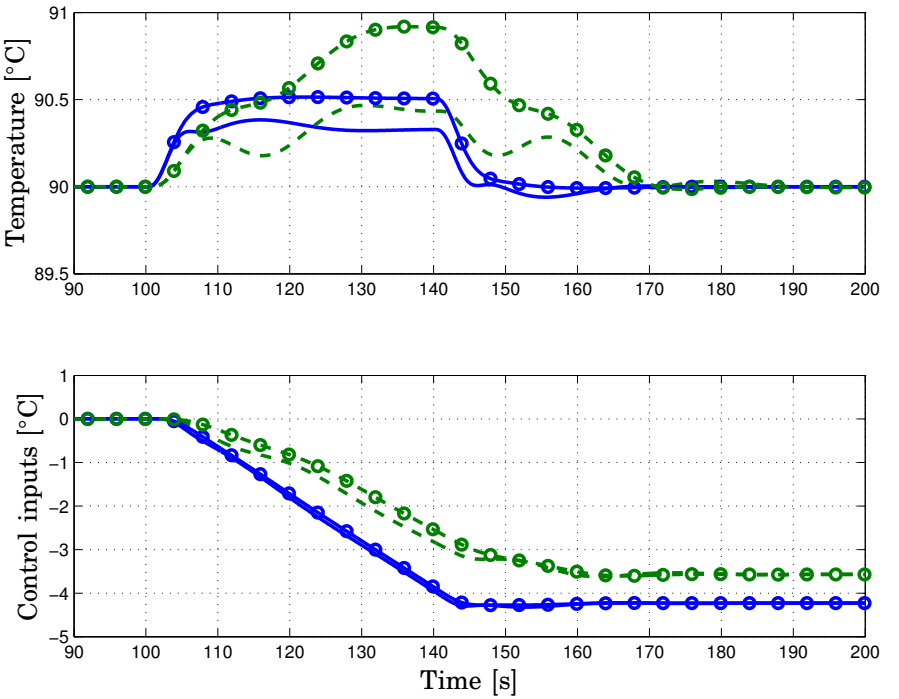

Figure 4.22 Ramp disturbance in feed concentrations using either input disturbance (no circles) or state disturbance (with circles) model. Upper plot: Reactor temperatures T_1 (solid) and T_2 (dashed). Lower plot: Control inputs $T_{A,\text{feed}}$ (solid) and T_{cool} (dashed).

control input $T_{A,\text{feed}}$ are almost identical. The only difference is in the disturbance estimation, where the input disturbance model yields a slightly faster response to the disturbance and the control error in T_2 remains smaller.

Alternative control inputs Now consider another pair of control inputs, u_B and T_{cool}, to compare with the decentralized controller from Figure 4.9. This choice of inputs yields larger cross-couplings between the control inputs, as the feed injection distribution u_B affects the feed injection both at the first and the second injection point, $u_{B1} = u_B$ and $u_{B2} = 1 - u_B$. The MPC controller is designed using the same steps as described above. The tuning matrix R is set to [10 0; 0 10], after that a scaling factor of 80 has been introduced on u_B to compensate for the different units and gains of the inputs.

The state disturbance model is used to achieve offset-free estimation

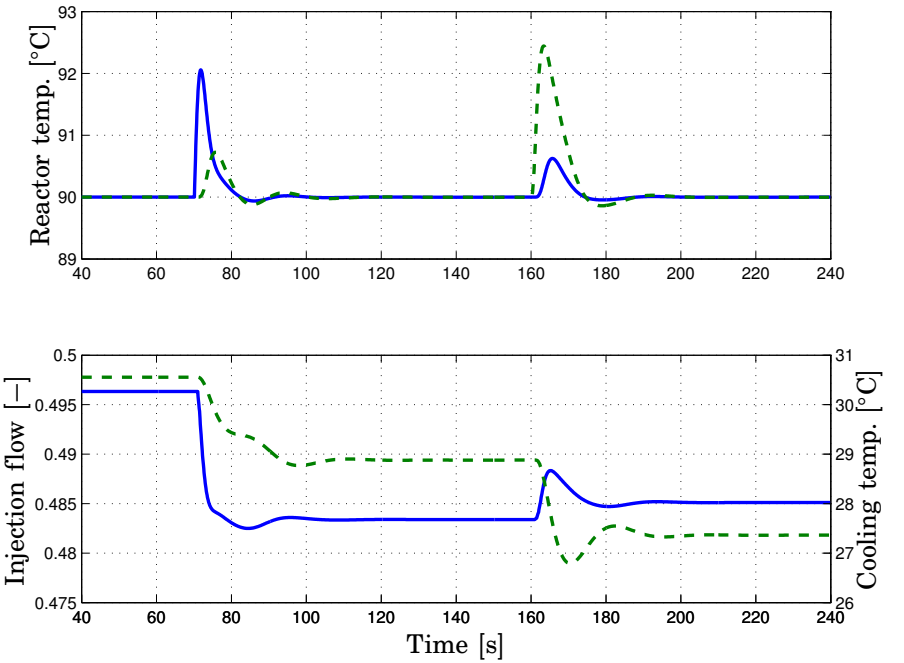

Figure 4.23 Simulated response for step disturbances using MPC. Upper plot: T_1 (solid) and T_2 (dashed). Lower plot: The feed injection distribution u_B (solid) and the cooling temperature T_{cool} (dashed). The disturbance at T_1 leads to a small redistribution of the injection flow, from the first to the second injection point.

and integral action in steady-state. The input disturbance model would, for these inputs, give poor performance as it will represent disturbances very inefficiently. For example, an increase in the heat release at T_1 may be represented as a disturbance on u_B, but that estimated disturbance will also affect T_2.

The closed loop response during the step disturbance is plotted in Figure 4.23. The cross-coupling between the inputs is clearly seen in the lower plot. The disturbance forces a decrease in u_B, that is, more reactant is being redistributed from the first to the second injection point. Subsequently, T_{cool} has to decrease to compensate for the increased heat release at the second injection point. The MPC controller can anticipate the effects of the control actions and there is for example no extra transient when the warmer reactor fluid flows down towards the second injection point, as for the decentralized controller in Figure 4.9.

Multiple injection points and cooling zones To increase the productivity of the plate reactor, additional injection points may be used, see e.g. Figure 4.10 where the reactor has five injection points and five cooling zones. In this configuration, $T_1 \dots T_5$ denote the temperatures at the five injection points and $T_{\text{cool},1} \dots T_{\text{cool},5}$ denote the inlet temperature of the cooling water for the five independent cooling zones. The additional cooling zones may improve the steady-state performance, but the main advantage is to allow a more flexible feedback control.

A MPC controller is designed with the feed temperature and the five cooling temperatures as control inputs. Integrating disturbances are added to the derivatives of the five controlled temperature states, i.e., a state disturbance model where $\mathbf{B_d} = \mathbf{C_z}^T$. Step disturbances are applied at the first and third injection point, similar to a 100 J/s increase in heat release from the reaction. The closed loop response is plotted in Figure 4.24. The disturbance at T_1 propagates down to T_2, but is heavily attenuated. The disturbance at T_3 can also be seen in the downstream temperature T_4, but it is also quickly dampened.

Improving the response using additional inputs The previous section showed that the temperatures in the plate reactor can be accurately controlled using the feed temperature $T_{A,\text{feed}}$ and the cooling temperatures $T_{\text{cool},1} \dots T_{\text{cool},5}$. This set of control inputs may be sufficient in most operating conditions. However, these control inputs have somewhat slow input dynamics and especially when temperature constraints are present, additional control means may be necessary. Here we will present a method how the feed flow rates can be used in feedback control, to improve the dynamic response.

The feed flow injections $u_{B1} \dots u_{B5}$ determines the amount of reactant B being injected at each feed point. The response from feed flow rate to the reactor temperature is fast, see the model analysis in Section 3.2. By including the feed flow injections in the MPC controller design, the controller is given additional inputs to improve the temperature control of the plate reactor. In decentralized control, it is non-trivial how to extend the control structure with additional inputs. The largest challenge there is to introduce constraint handling in such a way that the different control loops with different control objectives do not interact and cause oscillations or instability. With a multivariable process model, the MPC controller can anticipate the interactions between the different control inputs. The challenge here is to find a suitable cost function and weighting matrices, to achieve the desired closed loop behavior.

The stoichiometric relation between A and B requires that the feed flows of A and B maintain a constant ratio. Whenever the feed flow rate of B is changed in any injection point, this stoichiometric balance may be

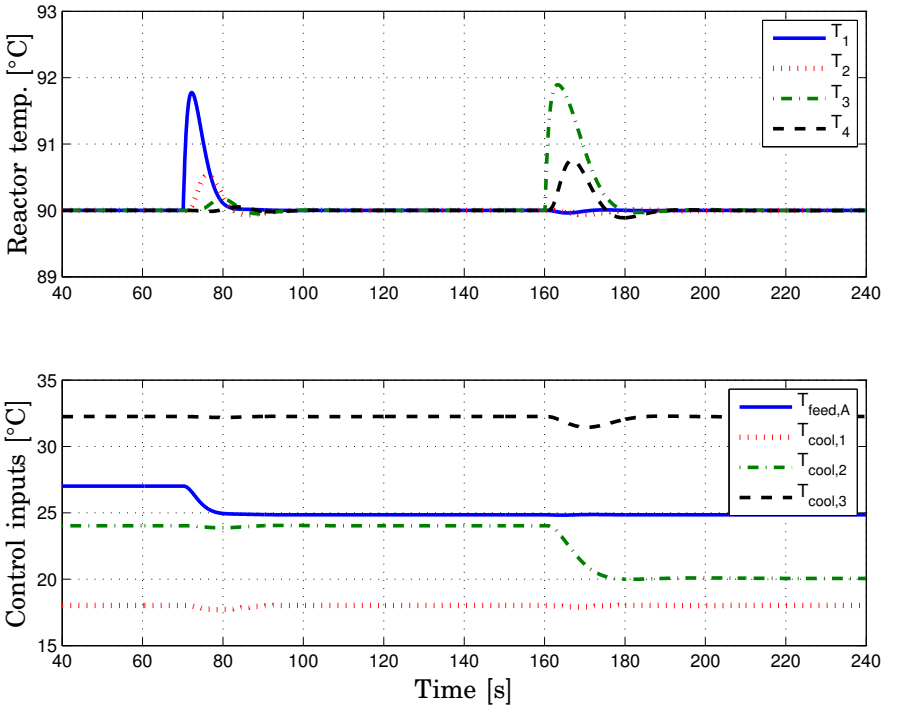

Figure 4.24 Simulated response for step disturbances using MPC with 5 injection points and 5 cooling zones. Upper plot: The disturbances affect T_1 and T_3 directly and propagates down to T_2 and T_4, respectively. Lower plot: The feed temperature and the cooling temperatures are changed to compensate for the step disturbances.

temporarily upset. Therefore, input targets to $u_{B1} \ldots u_{B5}$ are added to the MPC cost function (4.32), that is, we introduce the cost term $||\mathbf{u}^{\text{sp}}_{\mathbf{B,feeds}} - \mathbf{u}_{\mathbf{B,feeds}}||^2$, where the vector $\mathbf{u}^{\text{sp}}_{\mathbf{B,feeds}}$ are the nominal values of the five injection flows at the linearization point. This leads to the feed flow rates being at their nominal values in steady-state, but may during transients be used for feedback control. The cost function of the MPC controller may now be formulated as the following.

$$
\begin{aligned}
V(k) \;=\; & \sum_{i=1}^{H_p} \left|\left| \begin{bmatrix} \hat{\mathbf{T}}(k+i|k) \\ \hat{\mathbf{u}}_{\mathbf{B,feeds}}(k+i|k) \end{bmatrix} - \begin{bmatrix} \hat{\mathbf{T}}^{\text{ref}}(k+i|k) \\ \hat{\mathbf{u}}^{\text{sp}}_{\mathbf{B,feeds}}(k+i|k) \end{bmatrix} \right|\right|^2_{\mathbf{Q}} \\
& + \sum_{i=0}^{H_u-1} \left|\left| \begin{bmatrix} \Delta\hat{\mathbf{u}}_{\mathbf{temps}}(k+i|k) \\ \Delta\hat{\mathbf{u}}_{\mathbf{B,feeds}}(k+i|k) \end{bmatrix} \right|\right|^2_{\mathbf{R}},
\end{aligned}
\tag{4.34}
$$

where $\hat{\mathbf{T}}$ is a vector with the controlled temperatures and $\hat{\mathbf{T}}^{\text{ref}}$ is the corresponding reference vector. The vector $\hat{\mathbf{u}}_{\mathbf{temps}}$ represents the original inputs, the feed temperature and the five cooling temperatures, and the vector $\hat{\mathbf{u}}_{\mathbf{B,feeds}}$ represents the feed flow rates $u_{B1} \ldots u_{B5}$. A scaling factor of 80 has been introduced on $u_{B1} \ldots u_{B5}$ to compensate for the different units compared to the temperature inputs. The weighting matrices are defined as

$$\mathbf{Q} = \begin{bmatrix} \mathbf{Q_1} & 0 \\ 0 & \mathbf{Q_2} \end{bmatrix} = \begin{bmatrix} 1 \cdot \mathbf{I}_{5x5} & 0 \\ 0 & 0.1 \cdot \mathbf{I}_{5x5} \end{bmatrix} \tag{4.35}$$

$$\mathbf{R} = \begin{bmatrix} \mathbf{R_1} & 0 \\ 0 & \mathbf{R_2} \end{bmatrix} = \begin{bmatrix} 10 \cdot \mathbf{I}_{5x5} & 0 \\ 0 & 0.01 \cdot \mathbf{I}_{5x5} \end{bmatrix}. \tag{4.36}$$

With this choice of $\mathbf{Q}$ and $\mathbf{R}$, we emphasize the temperature tracking over the input targets of $\mathbf{u}_{\mathbf{B,feeds}}$. Furthermore, the feed flow rates are cheap to use transiently, as $\mathbf{R_2} < \mathbf{R_1}$, but in steady-state the feed flow rates return to their input targets.

Figure 4.25 shows the closed loop system during a step disturbance at the first injection point. The reactor temperature is here controlled by manipulating a combination of $T_{A,\text{feed}}$ and u_{B1}, where u_{B1} gives the fast effect and $T_{A,\text{feed}}$ deals with the slow and steady-state effect. The input targets for the feed flow rates will force u_{B1} to return to its nominal reference value and stoichiometric conditions in steady-state. The temperature response from Figure 4.24 is plotted for comparison, where only the feed temperature is used as control input. The temperature response is clearly faster using the feed flow rates as additional control inputs. The only drawback is that the change in feed flow rate causes a brief imbalance in the stoichiometric conditions. By varying the weighting matrices $\mathbf{R_2}$ and $\mathbf{Q_2}$, it is possible to adjust how much the controller should use the feed flow rates for the transient response. In addition, the weighting matrix $\mathbf{Q_2}$ determines how fast the feed flow rates should return to their set-points.

The control concept presented above can be viewed as mid-ranging control. In [Allison and Isaksson, 1998], different designs and applications of mid-ranging control are presented, for example, MPC implementations. More information on mid-ranging control is also given in Chapter 9.

Temperature constraints Let us now consider temperature constraints in the plate reactor. The scenario was introduced in Figure 4.15, where the decentralized controller was adapted to consider temperature constraints. A 200 J/s step disturbance is applied at the third injection point at $t = 60$ s. The MPC controller is designed as before with 11 inputs using the cost function in (4.34) and the weighting matrices in (4.35 - 4.36). The

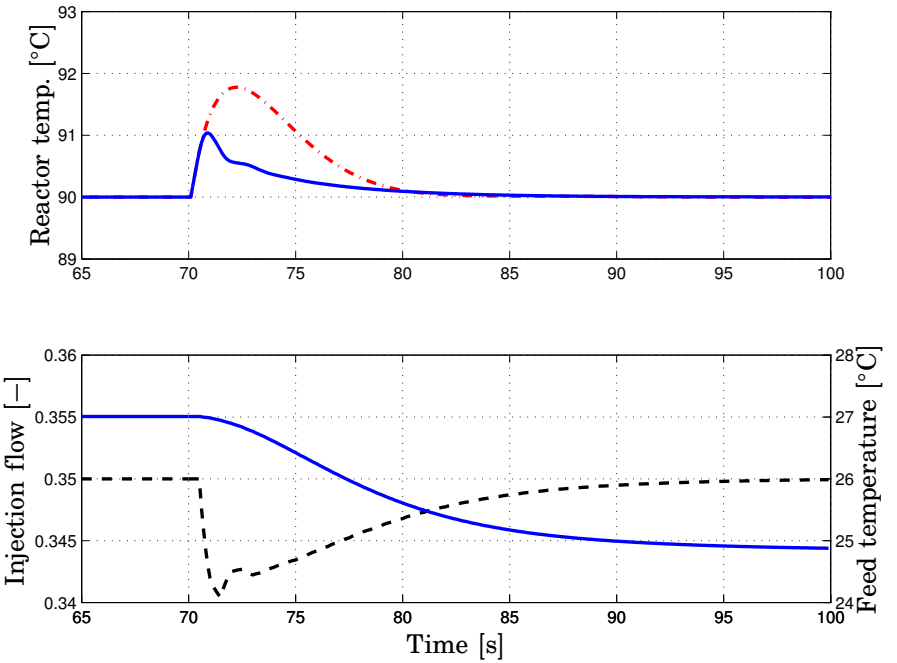

Figure 4.25 Simulated response for a step disturbance in T_1 (solid). Upper plot: By using the feed injection flow rates $u_{B1} \dots u_{B5}$ as additional inputs, the speed of the temperature control can be improved. The response in T_1 from Figure 4.24 (dash-dot) is plotted for comparison. Lower plot: The feed injection input u_{B1} (dashed) quickly decreases the reaction rate. Eventually, u_{B1} returns to its nominal value, while $T_{A,\text{feed}}$ (solid) compensates for the increased injection feed again.

objective is to stay below the maximum temperature limit of $T_{\max} = 92°\text{C}$. Similar to the decentralized case, the threshold for constraint handling is chosen with some margin, i.e., the reactor temperature is limited to 91°C in the MPC formulation. The closed loop response is plotted in Figure 4.26. When the disturbance pushes the process over the threshold, the controller implements very aggressive control actions, showing its non-linear behavior. The temperature response in T_3 experiences an undershoot, which is magnified by the nonlinear dynamics of the process. If the controller is tested on the linear process model, the undershoot is much smaller. After the undershoot, the controller dynamics are once again linear and the convergence to the desired temperature reference can be tuned by varying the weighting matrices $\mathbf{Q}$ and $\mathbf{R}$.

Summary and conclusions of the temperature control Temperature control of the plate reactor has been implemented with a centralized

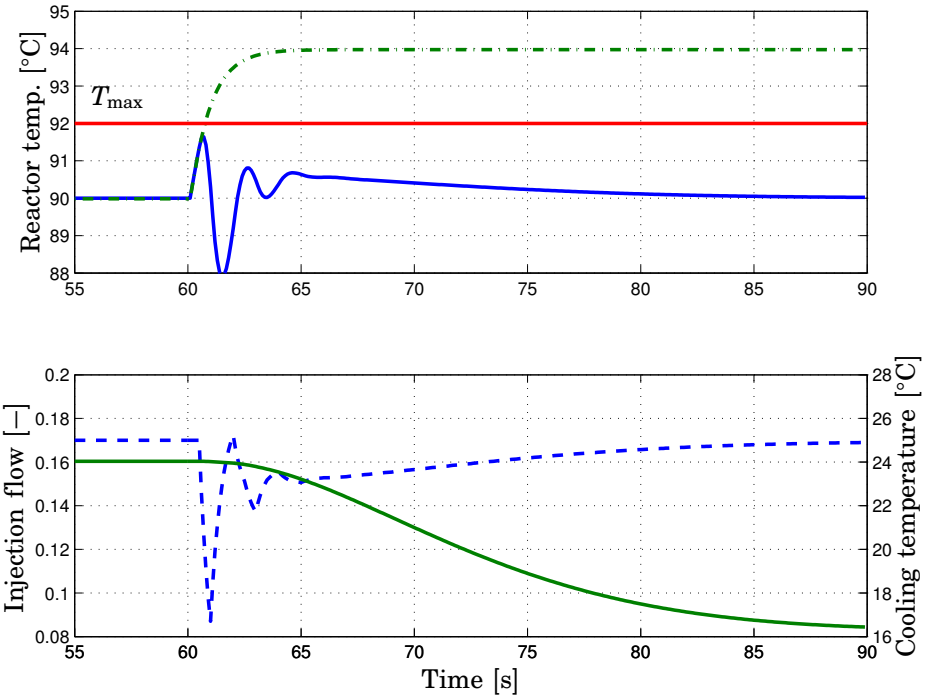

Figure 4.26 Simulated response for step disturbances in T_3 with temperature constraints. Upper plot: The reactor temperature T_3 (solid) and the uncontrolled response (dash-dot). The horizontal line indicates the temperature constraint. When the temperature passes the threshold of 91°C, it triggers the nonlinear action from the MPC controller. Lower plot: The feed injection input u_{B3} (dashed) quickly decreases the reaction rate and then slowly returns to its nominal value, while $T_{\text{cool},2}$ (solid) compensates for the increased injection feed again.

MPC controller. The centralized controller takes advantage of a multivariable process model to anticipate the cross-couplings of the process. However, it has been demonstrated that cross-couplings may appear through the disturbance estimation instead. The choice of disturbance model is important, since the transient of the disturbance estimates will affect the closed loop response.

The overall performance of the centralized controller is similar to the decentralized controller. The low computational effort of the decentralized controller allows fast sampling, which improves its response to disturbances. The main benefit with centralized control is its improved flexibility in the constraint handling. When the reactor temperature approaches

its limit, the quick response of the injection flow can easily be combined with the feed and cooling temperature inputs. When a control input is saturated, the centralized control structure allows other inputs to be used. The main drawbacks are the increased complexities in terms of implementation, reduced transparency to the operator and a more difficult tuning procedure.

Concentration Control

In this section, we will extend the control objective to also consider concentration control. More specifically, in addition to the temperature control previously presented, the aim is now to also control the stoichiometric conditions inside the plate reactor. The main motivation comes from disturbances in the feed concentrations or feed flow rates.

Consider a plate reactor system with two injection points and one cooling zone. There are four manipulated inputs, $u_{B1}, u_{B2}, T_{A,\text{feed}}$ and T_{cool}.

Estimation The temperature control of the plate reactor has been based on temperature measurements from sensors inside the reactor. A Kalman filter uses the measurement information to estimate the process states and disturbance states to achieve integral action in the temperature tracking.

When the stoichiometric conditions are considered, temperature measurements are no longer sufficient. To get consistent estimations for the concentration control, some measurements of the concentrations are required to achieve observability, see e.g. [Winkin *et al.*, 2000], where conditions for controllability and observability for tubular reactors are derived. In this case, we consider measurements of the outlet concentrations of reactants A and B, $c_{A,30}$ and $c_{B,30}$, where the index 30 indicates the concentration in the last control volume of the process model. In total, we have 14 measurement signals, ten temperature sensors in the reactor, two temperature sensors at the inlet and outlet of the cooling water, respectively, and finally the two outlet concentration sensors.

To achieve integral action, a state disturbance model is used, that is, disturbance states are added to each derivative of the 14 measured states, $\mathbf{B_d} = \mathbf{C_y}^T$, compare with Eqs. (4.22) and (4.24).

Cost function and controller tuning The cost function now has two separate objectives, temperature control and stoichiometric control. The former objective defines the nominal operating point at $T^{\text{ref}} = 90°\text{C}$, which ensures good conversion. The latter objective is defined as minimizing the difference between the outlet concentrations of the reactants A and B, $c_{A,30} - c_{B,30}$. When the concentration difference is zero, stoichiometric

conditions are achieved. The MPC cost function from (4.34) is modified to

$$V(k) = \sum_{i=1}^{H_p} \left|\left| \begin{bmatrix} \hat{\mathbf{T}}(k+i|k) \\ c_{A,30}(k+i|i) - c_{B,30}(k+i|i) \end{bmatrix} - \begin{bmatrix} \hat{\mathbf{T}}^{\text{ref}}(k+i|k) \\ 0 \end{bmatrix} \right|\right|_{\mathbf{Q}}^2 + \sum_{i=0}^{H_u-1} \left|\left| \begin{bmatrix} \Delta\hat{\mathbf{u}}_{\mathbf{temps}}(k+i|k) \\ \Delta\hat{\mathbf{u}}_{\mathbf{B,feeds}}(k+i|k) \end{bmatrix} \right|\right|_{\mathbf{R}}^2. \tag{4.37}$$

Note that the new control objective removes the necessity of the target set-points from (4.34) for the feed flow inputs.

The weighting matrices are defined as

$$\mathbf{Q} = \begin{bmatrix} \mathbf{Q_1} & 0 \\ 0 & \mathbf{Q_2} \end{bmatrix} = \begin{bmatrix} 1 \cdot \mathbf{I}_{2x2} & 0 \\ 0 & 1 \end{bmatrix} \tag{4.38}$$

$$\mathbf{R} = \begin{bmatrix} \mathbf{R_1} & 0 \\ 0 & \mathbf{R_2} \end{bmatrix} = \begin{bmatrix} 10 \cdot \mathbf{I}_{2x2} & 0 \\ 0 & 1.5 \cdot \mathbf{I}_{2x2} \end{bmatrix}. \tag{4.39}$$

With this choice of $\mathbf{Q}$, we have equal concern of temperature and stoichiometric deviations. A scaling factor of 80 has been introduced on u_{B1} and u_{B2} to compensate for the different units compared to the temperature inputs. The choice of $\mathbf{R}$ indicates that the feed flow inputs are cheaper to use than temperature inputs. However, the optimization problem is more complex than that. If the feed flow inputs are used to control the temperature, they may cause an imbalance in the stoichiometry, which introduces an additional cost. Therefore, the controller will mainly use the feed flow inputs to control the stoichiometry and the temperature inputs to control the reactor temperatures.

By adjusting the relationship between $\mathbf{Q_1}$ and $\mathbf{Q_2}$, we can arbitrarily shift the focus of the controller from temperature to stoichiometric control or vice versa.

Simulation The combined temperature and stoichiometric control is evaluated in closed loop simulations for ramp and step disturbances. The temperature references are as before $T_1^{\text{ref}} = T_2^{\text{ref}} = 90°\text{C}$. At $t = 20$ s, the ramp disturbance from (4.19) is repeated, but now the feed concentration of reactant A *decreases* with 5%, while $c_{B,\text{feed}}$ remains constant. This leads to a shortage of A and an excess of B. At $t = 150$ s, a temperature step disturbance from (4.17) is applied at the second injection point, corresponding to a sudden increase in the heat release of 100 J/s. In the open loop response, the feed concentration disturbance leads to a shortage of A at the second injection point and T_2 decreases to 83°C, due

to the decreased heat release from the reaction. The excess of B leads to a drop in conversion γ_B (2.5) to 94%, while the shortage of A increases γ_A to 99%. With the temperature control alone, the temperature effect of the feed disturbance can be quickly attenuated, but the differences in conversion will remain.

The closed loop response with temperature and stoichiometric control is plotted in Figures 4.27 – 4.30. When the feed concentration of A decreases at $t = 20$ s, the MPC controller quickly increases the feed temperature to compensate for the reduced heat release at the first injection point. Figure 4.30 shows the four most important estimated disturbance states, the disturbances acting on T_1, T_2, $c_{A,30}$ and $c_{B,30}$. The feed concentration disturbance at $t = 20$ s is estimated using all four disturbance states. The temperature effect of the disturbance is described as a temperature disturbance in T_1 and T_2 and the concentration effect of the disturbance is described as a concentration disturbance in $c_{A,30}$ and $c_{B,30}$. Note the different times when the disturbance states are affected, which are given by the flow delays in the reactor. For example, the disturbance states on $c_{A,30}$ and $c_{B,30}$ remain zero until 30 seconds after the actual disturbance enters the reactor.

When the feed disturbance reaches the second injection point, a shortage of A appears and the heat release is reduced much more than at the first injection point. The controller therefore raises the cooling temperature to 37°C. Meanwhile, the estimated disturbances on the outlet concentrations lead to a decrease in the feed flow rate u_{B2} at the second injection point to remove the excess of B and regain stoichiometric conditions, which are reached around $t = 120$ s when γ_A and γ_B both converge to 98.1%.

A step disturbance enters the system at $t = 150$ s, increasing the heat release at the second injection point with 100 J/s. The cooling temperature is quickly lowered, but as the disturbance has no effect on the stoichiometric conditions, the feed injections are unchanged. There is a small cross-coupling between the cooling and feed temperature after the step disturbance, however, note the different scales on the left and right y-axis of Figure 4.28.

There are some additional remarks on the stoichiometric control. The measurements of the outlet concentrations give a long dead-time, equal to the flow time, before the feed disturbance can be estimated. For this specific disturbance, it would be beneficial to have the concentration measurements directly in the feed flows or at the reactor inlet. That would significantly improve the transient response and the concentration measurements would then act as feed-forward signals. The outlet concentrations should still be measured to capture the effect of any other disturbance or uncertainty inside the reactor.

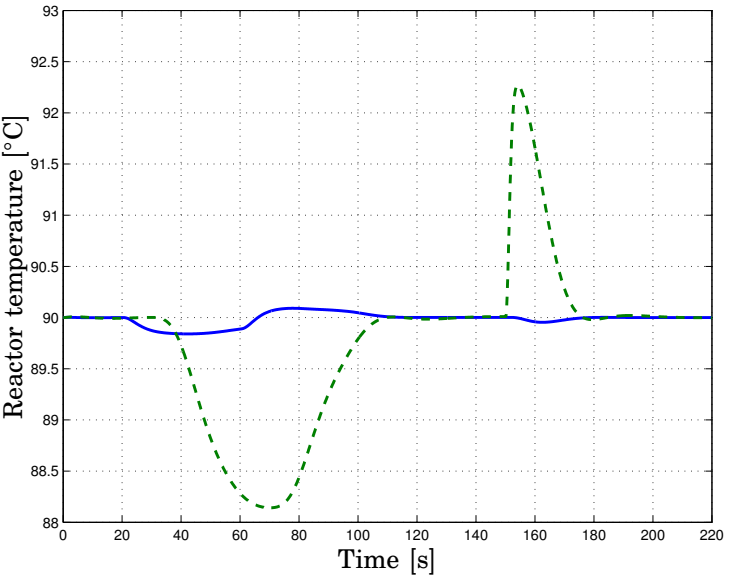

Figure 4.27 Combined temperature and stoichiometric control. The reactor temperature at the first (solid) and the second (dashed) injection point.

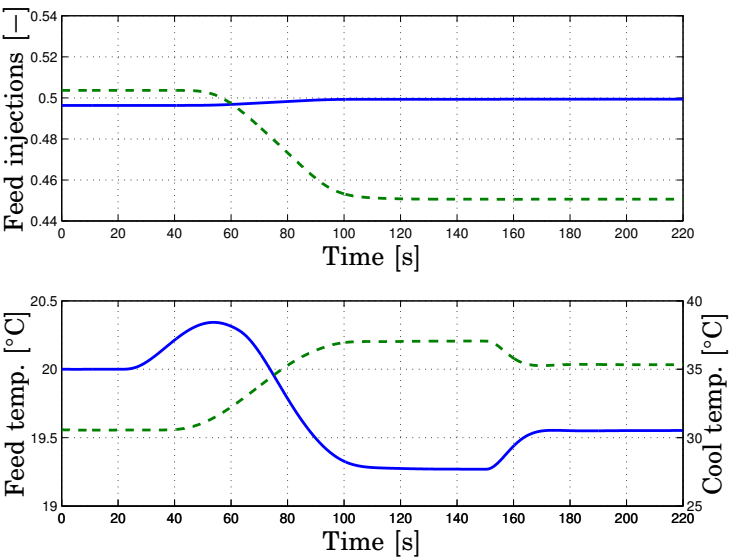

Figure 4.28 Combined temperature and stoichiometric control. Upper plot: Feed flow injections u_{B1} (solid) and u_{B2} (dashed) are manipulated to preserve stoichiometric conditions. Lower plot: Feed temperature $T_{A,\text{feed}}$ (left axis, solid) and cooling temperature T_{cool} (right axis, dashed) are focused on the temperature tracking. Note the different scales on the temperature inputs.

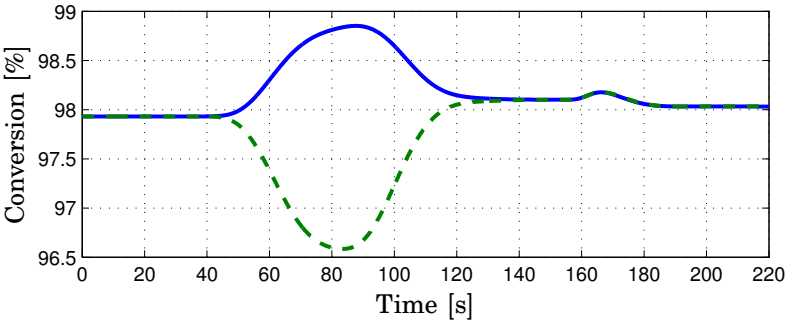

Figure 4.29 Combined temperature and stoichiometric control. Conversion of reactant A and B, γ_A (solid) and γ_B (dashed) at the reactor outlet. When the feed concentration $c_{A,\text{feed}}$ decreases at $t = 20$ s, the conversion drops after another 30 s, which corresponds to the flow time.

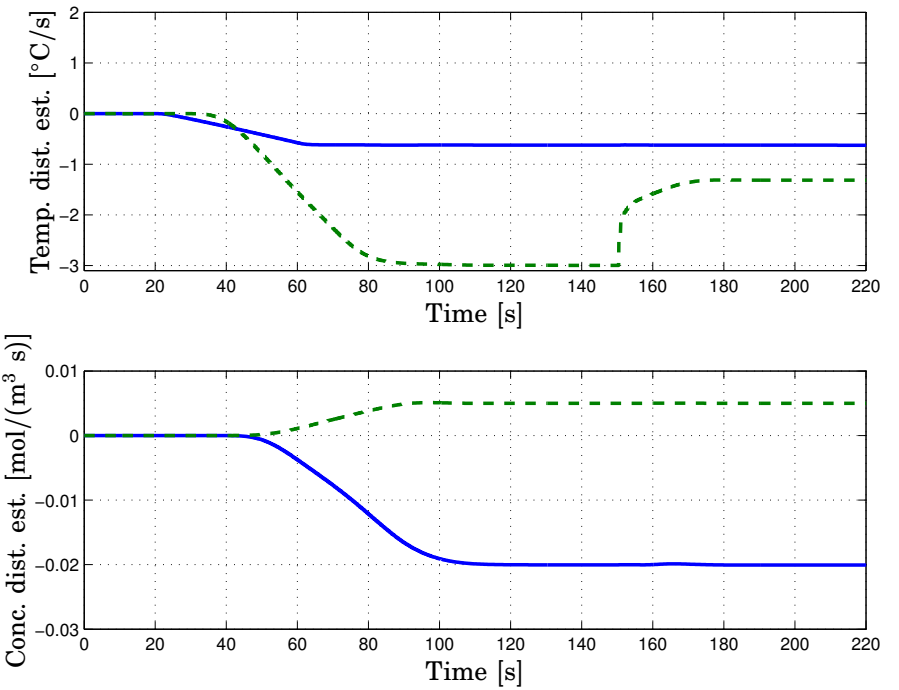

Figure 4.30 Disturbance state estimation in the combined temperature and stoichiometric control. Upper plot: Disturbance states acting on $\dot{T}_1$ (solid) and $\dot{T}_2$ (dashed). Lower plot: Disturbance states acting on $\dot{c}_{A,30}$ (dashed) and $\dot{c}_{B,30}$, normalized with $c_{A,\text{feed}}$ and $c_{B,\text{feed}}$, respectively.

Maximize Conversion

Another alternative control objective can be to focus entirely on the maximization of the reactant conversion, (2.5). This corresponds to minimizing the outlet concentrations of the reactants A and B. The MPC cost function may then be defined as

$$V(k) = \sum_{i=1}^{H_p} \left|\left| \begin{bmatrix} c_{A,\text{out}}(k+i|i) \\ c_{B,\text{out}}(k+i|i) \end{bmatrix} \right|\right|_{\mathbf{Q}}^2 + \sum_{i=0}^{H_u-1} \left|\left| \begin{bmatrix} \Delta\hat{\mathbf{u}}_{\mathbf{temps}}(k+i|k) \\ \Delta\hat{\mathbf{u}}_{\mathbf{B,feeds}}(k+i|k) \end{bmatrix} \right|\right|_{\mathbf{R}}^2 .$$

The references for the outlet concentrations are set to zero, as we wish all reactants to be converted into product. To achieve complete conversion of the sodium thiosulfate reaction, the reactor temperature is increased as high as possible, to the maximum allowed temperature $T_{\max}$. This means that the nominal operating point will have active temperature constraints and the temperature tracking problem will be changed to keeping the process at the maximum temperature. This control objective was presented in more detail in [Haugwitz *et al.*, 2007a].

4.7 Recommendations on the Process Design

With the flexible process configuration of the plate reactor, it is recommended to consider control design and possible loop interactions already on the process design phase. By designing the process to have a suitable number and location of actuators and sensors, it will be easier to find controllers that have inputs with low cross-coupling.

An example is shown in Figure 4.31, where the reactor has five injection points and one cooling zone. From Section 2.4, we know that the steady-state performance may be increased by using additional injection points. Furthermore, it is possible in steady-state optimizations to find an operating point where the five injection flow rates, the feed temperatures and the cooling temperature give a temperature profile with five local temperature maxima and very good steady-state performance, see Figure 2.11. However, it may be difficult to find decentralized feedback control loops that can achieve accurate temperature control and good disturbance rejection of all five temperature maxima. The feed temperature $T_{A,\text{feed}}$ and the cooling temperature T_{cool} are not sufficient to independently control the five temperature maxima. With these inputs only the two highest temperature maxima may be controlled, leaving the remaining three maxima uncontrolled. If the individual injection flow rates are used as manipulated inputs, the stoichiometric conditions will introduce cross-couplings,

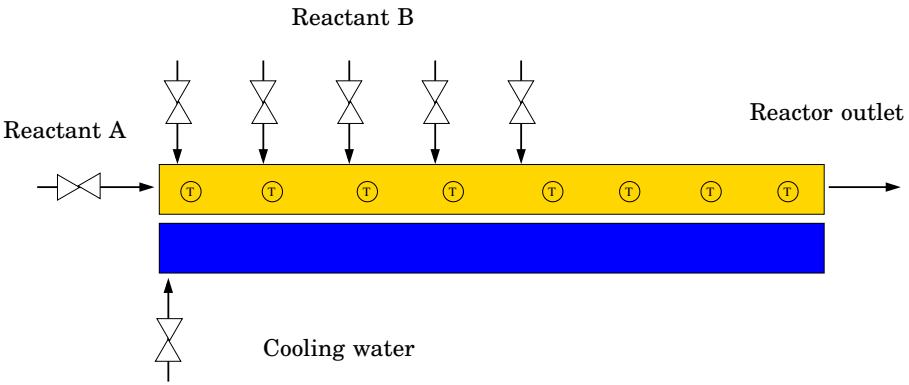

Figure 4.31 The plate reactor with five injection points and one cooling zone. The five temperature maxima may be controlled using any of the seven available inputs, but stoichiometric relations may introduce cross-couplings between some of the inputs.

remember the RGA analysis previously in this chapter. Centralized control is less sensitive, since the multivariable process model can describe and anticipate the cross-couplings introduced by this process design.

Regardless of decentralized or centralized control approach, it is recommended to consider the implications of the process design on the control design already in an early development stage. For example, with additional cooling zones as in Figure 4.10, an efficient decentralized control structure would be easier to find.

4.8 Summary, Comparisons and Conclusions

In this section, the methods presented in this chapter will be summarized. Specifically, the decentralized and centralized control approach will be compared on several layers, such as design, tuning, performance and flexibility.

Control design The decentralized controller is based on multi-loop PID controllers, where each PID-controller is designed independently of the other loops. The decentralized control structure is easy to understand, easy to implement and easy to tune. It is generally believed that a decentralized approach saves on the modeling effort, however, a thorough process knowledge is essential if the decentralized control should succeed, for example in the input/output pairing analysis. The feed and cooling temperatures are chosen as manipulated variables, as they are very loosely

coupled. The PID controllers are tuned using the novel AMIGO method, which is based on robust loopshaping and optimization of the integral gain.

The centralized controller uses Model Predictive Control, which can handle multivariable process models, input and state constraints and offers a flexible specification of the control objectives. A thorough process knowledge is essential also here, to design suitable disturbance models, prediction horizons and weighting matrices. It is rather straight forward to achieve an acceptable performance, but the increased complexity, when there are many inputs/outputs and multiple objectives in the cost function, means that the tuning to further improve the closed loop response is a very challenging task.

Control performance The performance of the temperature control is similar for the decentralized and centralized control. With correctly chosen control inputs, the process is largely decoupled, so the benefit with centralized control is negligible. In fact, the choice of disturbance model for the MPC may introduce virtual cross-couplings through the disturbance estimates. The response of the decentralized controller is slightly faster as it has a sampling time of $T_s = 0.10$ s compared to $T_s = 0.50$ s for the MPC controller. With suitable model reduction and improved algorithms, the MPC controller would also be capable of faster sampling times, thus improving the performance.

The advantage of the centralized controller becomes clearer when the chosen inputs have larger cross-coupling, e.g. feed flows and cooling temperatures, since the multivariable process model describes the interaction. This also allows the centralized controller to use additional control inputs or control objectives. A few examples of this has been demonstrated in this chapter. To improve the transient response of the temperature control, both feed flows and temperatures are used as control inputs. By varying the weight matrices, it is possible to gradually change what inputs to use and how much they should be used, without having to consider the cross-couplings between them. The controller can handle multiple objectives, such as temperature and stoichiometric control, where the temperature inputs deal with the temperature control and the feed inputs deal with the concentrations. The focus between temperature control and stoichiometric control can easily be shifted in the controller tuning.

Temperature constraints can be handled in the decentralized control structure by adding another control loop in parallel to the existing temperature controller. The challenge is to design the constraint handling controller so that the two controllers do not excite each other, leading to oscillations and potentially instability. This requires very good understanding of the process. The solution is to have a fast decrease in the feed

flow rate when the reactor temperature approaches the limit, and when the temperature drops, the feed flow is slowly returned to its nominal value. With the centralized controller, the closed loop response is similar, but the constraint handling is easier to implemented in the MPC framework.

Based on these results, decentralized control is sufficient for basic temperature control when input saturations or temperature constraints are non-existent or present but not always active. When choosing to operate closer to saturation limits or temperature constraints or focusing on the concentration control, a centralized MPC controller is recommended.

Process design It is important to consider the process design, choice of operating point and control design all together, to avoid process design that introduce cross-couplings in the process inputs. For example, when there are multiple injection points of reactant B, it may be beneficial to have the corresponding number of cooling zones, especially if the intention is to implement a decentralized control structure.

Sensor location is also an important part of the process design, where the sensors should be placed to give the best information about the process state. In many applications, the maximum reactor temperature should be controlled, however, it is non-trivial to place the sensors where the actual temperature maximum occurs. In decentralized control, this may lead to temperature violations if the measured temperature is lower than the highest actual temperature in the reactor. In the centralized controller, many temperature measurements are used and the full temperature profile is recreated based on the measurements. This reduces the sensitivity to wrongly placed sensors, but the estimates are subject to model uncertainty.

5

Start-up

5.1 Introduction

Start-up control of chemical reactors has been an area of research for many years. The main focus has been on batch and semi-batch reactors. Start-up of continuous reactors is similarly of great interest, since the risk of incidents are much higher during start-up than during steady state operation. At low temperature, almost no reaction occurs due to the temperature sensitive reaction rate. To start the reaction, heat must be provided into the reactor system, typically through the feed flows or the cooling water. At some reactor temperature, the reaction reaches the ignition point. The heat release from a strongly exothermic reaction leads to self-acceleration and the reactor temperature quickly increases to the nominal operating point, or, if care is not taken, above.

The transient from initial conditions to an optimal operating point and the temperature at which ignition occurs are highly nonlinear functions of the inputs and the states of the system. Therefore, the system is very sensitive to small changes in reactor inlet conditions or variations in physical parameters. Previous studies have been focusing on criteria to detect operating regions with parametrically sensitive behavior, see e.g. [Bauman *et al.*, 1990] or [Varma *et al.*, 1999]. However, the studies are often limited to finding non-sensitive operating points for steady-state and the impact of a feedback control system is often neglected. In [Zaldívar *et al.*, 2003], a general criterion to define runaway limits for tank reactors is presented, where the effect of feedback control on the runaway boundaries is briefly discussed. In general, feedback control can reduce the impact of model uncertainty, but due to actuator limitations present in industrial processes, the available bandwidth may not be sufficient to guarantee a safe start-up in regions with parametrically sensitive behavior.

In [Hahn *et al.*, 1971], open loop optimal start-up trajectories for a tubular reactor is computed, based on a distributed maximum principle for a given optimal steady state operating point. The reaction is exothermic and reversible. The reactor temperature and thus the yield are controlled by manipulating the reactor wall temperature with a constraint on the maximum reactor temperature. The optimal control trajectory is of bang-bang type with a singular arc to the steady-state. The study in [Hahn *et al.*, 1971], however, does not consider uncertainties or dynamic limitations in the actuator, and does not consider any closed loop feedback control.

In [Verwijs *et al.*, 1996], the start-up and safeguarding of an adiabatic tubular reactor system is considered. There, open loop trajectories of the manipulated variables are calculated by a generalized-reduced-gradient optimization. The safeguarding is realized through plant start-up rules e.g. minimizing the total amount of unreacted chemicals exiting the reactor during the start-up period. High levels of unreacted chemicals in the reactor outlet may lead to continued reaction and heat release in storage tanks. Without adequate cooling systems in these tanks, this temperature increase may start by-product formation and lead to a thermal runaway. During start-up, the safeguarding is implemented by monitoring the difference between the actual response of thermoelements and the optimal trajectories calculated in the model-based optimization. When the difference exceeds some limit, the reactor should be brought to shutdown to prevent the process from running into a hazardous situation state.

There are many interesting challenges associated with start-up control of temperature sensitive exothermic reactions; nonlinear dynamics, actuator limitations and process uncertainty. The nonlinear dynamics leads to multiple equilibrium profiles for a given set of control signals. One equilibrium profile corresponds to the situation when no reaction occurs due to too low reactor temperature. Another equilibrium profile occurs when almost all reactants have converted at high reactor temperature, which is the desired operating point. Finally, in between these points, there is an equilibrium profile, which is unstable, due to the exothermic reaction. See e.g. [Laabissi *et al.*, 2002] for an analysis of when there exist multiple equilibrium profiles.

There are two main approaches to handle process uncertainty, robust control and adaptive control. In robust control, the effects of the uncertainty is often taken into account by means of some min-max optimization, for example by using multiple models of the process and finding the best control input for the worst case, see e.g. [Wang and Rawlings, 2004]. In adaptive control, information from on-line measurements is used to reduce the amount of uncertainty. An early example is [Lenells, 1982], where adaptive start-up is investigated. A set of possible models is considered

at first and based on measurements during the start-up some models are rejected. The control input is computed based on the worst case of the remaining models. In [Tian and Hoo, 2003], a transition control framework is presented, to control a process from one steady state to another steady state. The nonlinear dynamics are approximated by switching between multiple fixed and adaptive models. H_∞ control design is employed to deal with disturbances and uncertainties. Reference trajectories for the transition are defined as ramp functions, where the time constant is set by the user.

In this chapter, start-up control of the plate reactor is considered. In contrast to the work in [Hahn *et al.*, 1971] and [Verwijs *et al.*, 1996], the plate reactor is equipped with a cooling system and multiple injection points for the reactants. Here, feedback control will be used to increase safety and robustness in the presence of uncertainty.

The aim of this chapter is to develop methods to achieve safe, robust and efficient start-up of an exothermic reaction. With actuator limitations, it is necessary to consider the interplay between open-loop optimal start-up trajectories and feedback control. By studying the parametric sensitivity, the start-up optimization problem can be formulated so that the optimal solutions have reduced sensitivity to uncertainty. This facilitates the task of the feedback controller to maintain safe operation despite its actuator limitations.

Dynamic optimization of large scale processes has received much attention both in theory and in industrial practice during the last two decades. The advent of faster computers has enabled application of computationally intensive algorithms also for process systems of realistic size. Application of dynamic optimization can be categorized into *on-line* and *off-line* methods. In the former category, model predictive control (MPC) has won wide-spread industrial use, see e.g. [Qin and Badgwell, 2003]. However, the size and complexity of the problem, in combination with fast dynamics, complicate on-line solution of the robust nonlinear optimal control problem in real-time.

Two methods to achieve robust start-up control are presented, a time-driven continuous approach and an event-driven hybrid approach. They both consider the sensitivity to uncertainties to achieve robustness by introducing constraints in the state-space for the optimal solutions. In both methods, optimal start-up trajectories are computed off-line and are then used as reference signals to a feedback control system. However, the optimization formulation, the problem structure and the implementation differ.

The time-driven continuous approach, see Chapter 6, utilizes off-line dynamic optimization on the full nonlinear model and the robustness of the optimal solutions may be achieved by introducing state constraints on

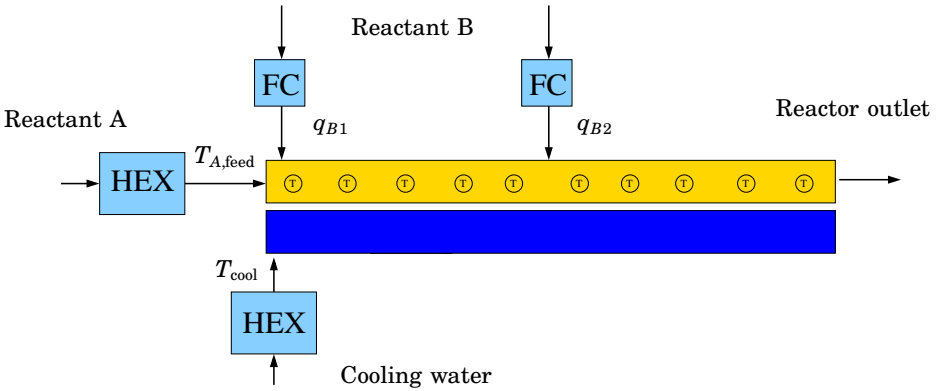

Figure 5.1 For the start-up control problem, we consider a reactor configuration with two injection points and one cooling zone. The feed temperature $T_{A,\text{feed}}$, the inlet cooling temperature T_{cool} and the feed injection flows q_{B1} and q_{B2} are used as manipulated variables.

the reactant B concentration. The resulting optimal solutions are then given as references to an online feedback control loop.

The event-driven hybrid approach, see Chapter 7, exploits the physical structure of the start-up control problem. The start-up sequence is divided into several modes, where each injection point along the reactor is started sequentially. Transition between these modes are only permitted if certain transition conditions are fulfilled. The conditions are here defined as points in the state-space, for example reactor temperature. The implementation is event-driven, as each mode transition corresponds to a state event when the transition condition turns true.

5.2 Dynamics and Problem Motivation

The process

For the Chapters 5 – 7, we consider a plate reactor with two injection points and one cooling zone, see Figure 5.1, and an exothermic reaction

$$A + B \rightarrow C + D. \tag{5.1}$$

Assume that the reaction has similar kinetics as the sodium thiosulfate reaction (2.2), but here the activation energy $E_a = 76000$ J/mol is 11% higher than for the sodium thiosulfate reaction studied in Chapters 2-4. The higher activation energy means that a higher reactor temperature is

Table 5.1 Nominal values and bounded uncertainties for the plate reactor for the start-up control problem in Chapters 5 – 7.

Variable/Parameter	Nominal value	uncertainty
Activation energy, E_a	76000 J/mol	2%
Pre-exponential factor, k_0	$2 \cdot 10^7$ m^3/(mol s)	5%
Heat of reaction, ΔH	$1.17 \cdot 10^6$ J/mol	5%
Heat transfer coefficient, h	3000 W/(m^2 K)	10%

needed for this reaction to achieve a similar reaction rate, compared to a reaction with a lower activation energy. This can also be interpreted as the reaction being more temperature sensitive. In addition, the feed concentrations $c_{A,\text{feed}}$ and $c_{B,\text{feed}}$ are assumed to be 70% higher than in Chapters 2-4.

The process model was defined in (3.2) in Chapter 3. All parameters[1] describing the reactor are the same as before.

Challenges

The main challenges during start-up control are severe process nonlinearities, limited actuator dynamics and uncertainties concerning the process model.

- The nonlinearities appear in particular in the reaction kinetics, where the reaction rate r is exponential in temperature. For example, the reaction rate at 30°C is 2.8 times larger than at 20°C and at 70°C it is almost 100 times larger than at 20°C. See also the nonlinear gain from feed injection rate u_{B1} to the temperature at the injection point T_1 in Figure 3.13.
- The actuator dynamics for the control inputs can in general be approximated by first or second order linear systems with time constants of a few seconds. These time constants of a few seconds should be compared to the reaction dynamics, where the reactor temperature can increase by more than 10°C/s. For large transitions, however, a nonlinear behavior appears for $T_{A,\text{feed}}$ and T_{cool}, which can be approximated as rate limits; $-2°\text{C/s} \leq \dot{T}_{A,\text{feed}} \leq 3°\text{C/s}$ and $-2°\text{C/s} \leq \dot{T}_{\text{cool}} \leq 1°\text{C/s}$.

[1]The heat transfer coefficient $h = 3000\text{W/(m}^2\text{ K)}$ is associated with a heat transfer area in the plate reactor of 0.0769 m^2. In some publications regarding the start-up problem, the geometry of a cylindrical tubular reactor was used that lead to $h = 1120\text{W/(m}^2\text{ K)}$, but h is then associated with a heat transfer area of 0.206 m^2. The product remains the same.

- The process model is subject to parametric uncertainty, see Table 5.1. The uncertainties associated with the model may lead to dramatic changes in the predicted heat release and the shape of the predicted temperature profiles compared to the real process. The process model can be reformulated as

$$\dot{x} = f(x, u, p), \quad p \in \mathcal{P}, \tag{5.2}$$

where x are the states, u are the control inputs, p are the uncertain parameters and $\mathcal{P}$ is the uncertainty set associated with the model parameters.

The main uncertainty is associated with the reaction kinetics. A reasonable model for the reaction kinetics is available, however, it is often only validated for the desired operating point. Therefore, especially during start-up, there may be considerable uncertainty concerning the reaction kinetics. In addition, as we will see in the motivating examples, the uncertainties are much more challenging during the start-up than in steady-state operation, as the effects of the uncertainty may change abruptly during the start-up transition. In steady-state operation, the effects of the uncertainties are often constant and has already been compensated for by the controller during the transition to the steady-state.

Problem formulation

The overall objective is to find control inputs that transfer the state of the process safely from an initial point, where the reactor is cold and no reactant B is fed, to an optimal operating point with maximum reactant conversion. The objectives can be formulated as

1. The main design objective is safety, which means that the temperature T_r throughout the reactor should at all times stay below a maximum limit, $T_{\max} = 160°\text{C}$.
2. Maximize the reactant conversions at the reactor outlet, γ_A and γ_B, defined as

$$\gamma_A = \frac{c_{C,\text{out}}}{c_{C,\text{out}} + c_{A,\text{out}}}, \qquad \gamma_B = \frac{c_{C,\text{out}}}{c_{C,\text{out}} + c_{B,\text{out}}}, \tag{5.3}$$

where the subscript 'out' denotes the concentrations at the reactor outlet. With the chemical reaction (2.1), this is equivalent to minimizing the amount of unreacted A and B in the reactor outflow.

3. The time to reach the optimal operating point should be as short as the primary objective permits.

Dynamic optimization can be used to generate feasible start-up trajectories in the presence of control limitations and nonlinear dynamics. However, the process uncertainty adds another dimension to the complexity of the start-up problem. Therefore, robustness is the key focus in this problem formulation. Robustness is often associated with the ability for a feedback controller to compensate for disturbances and uncertainties. Here, we consider the feedback controller as fixed. Instead, we focus on the robustness of the off-line computed optimal trajectories, that is, the sensitivity of the optimal solution to model uncertainty. As will be described in the next section, optimal start-up trajectories may be arbitrarily sensitive to uncertainty, if the issue of robustness is not addressed in the formulation of the optimization problem.

Solving the start-up problem for a process with uncertain parameters is a challenging problem. Clearly, control trajectories computed based on a nominal model is not likely to reproduce the predicted output profiles for all models within the uncertainty set. For the plate reactor start-up, open loop application of the control trajectories may lead to degraded performance, and more importantly, violation of the temperature constraint. Introduction of a feedback control system, which is designed to track the predicted temperature profiles, significantly decreases the effects of modeling errors. However, for large parameter variations, the limitations of the actuator systems and the non-linear characteristics of the process may lead to violation of the safety requirements also in the presence of a well-designed feedback system. However, the ability of the feedback system to enforce the safety requirements is strongly dependent on the properties of the pre-computed control profiles. Start-up trajectories that have large sensitivity to parameter variations can be expected to be more difficult for the control system, which has limited authority, than trajectories for which the parametric uncertainty is small.

To summarize, parametric uncertainty has profound consequences for the start-up problem. In particular, it is not sufficient to meet the three objectives listed above for a nominal parameter set. To meet the objectives for *all* parameters sets, a complimentary objective can be stated as:

Formulate the optimization problem so that the optimal control input $u(t)$ gives nominal state trajectories $x^{\mathrm{nom}}(t)$ that have low sensitivity to parameter uncertainty.

Motivating examples

In this section, a few motivating examples of open-loop controlled start-up sequences will be presented. The nonlinear dynamic model from Chapter 3 is used for the simulations. The initial conditions are the following

$$\mathbf{T_r} = 20°\text{C}, \quad \mathbf{T_w} = 20°\text{C}, \quad \mathbf{c_A} = c_A^0, \quad \mathbf{c_B} = 0, \quad \mathbf{c_C} = 0, \tag{5.4}$$

where the vectors $\mathbf{T_r}, \mathbf{T_w}, \mathbf{c_A}, \mathbf{c_B}$ and $\mathbf{c_C}$ represent the variables along the reactor, see the process model in (3.2). The initial conditions for the control inputs are

$$u_{B1} = 0, \quad u_{B2} = 0, \quad T_{A,\text{feed}} = 30°\text{C}, \quad T_{\text{cool}} = 20°\text{C}. \tag{5.5}$$

First, consider the naive approach of injecting the secondary reactant B at a reactor temperature around 20°C, see solid line in Figure 5.2. However, due to the low reaction rate at low temperatures, the reaction does not start despite nominal injection of u_{B1}. The feed temperature $T_{A,\text{feed}}$ is therefore increased to increase the reactor temperature, thus also the reaction rate. At $t = 100$ s the reactor temperature has increased so much that the reaction becomes self-accelerating, as the heat release from the reaction leads to a positive feedback loop. The temperature increases from 65°C to 180°C, which gives a rough estimate of the potential dynamics during the start-up. However, the simulation model is not developed to accurately represent this kind of high-frequency behavior, as that time-scale would require full CFD-simulations to account for more exact flow dynamics, mixing, turbulence and heat transfer.

Note that the nonlinear dynamics yield multiple stationary solutions as $u_{B1} = 0.5$ and $T_{A,\text{feed}} = 30°\text{C}$ may result in a reactor temperature of 32 or 155°C.

In industrial start-up procedures, it is common to specify a certain start temperature at which it is safe to begin the feed injections, see e.g. [Verwijs *et al.*, 1996]. The second case utilizes this approach, where the feed temperature $T_{A,\text{feed}}$ is increased to 70°C before any injection of B is allowed to start, dash-dotted line in Figure 5.2. At the resulting higher reactor temperature, the relation between u_{B1} and T_1 is nearly linear and the reaction starts almost immediately upon injection. The difference between the nonlinear dynamics in the first start-up and the nearly linear dynamics in the second case is very interesting.

Figure 5.3 plots the reactor temperature T_1 as function of the two primary control inputs, u_{B1} and $T_{A,\text{feed}}$. Two arrows indicate the common start and end point of the trajectories. With the 3-dimensional plot, the difference between the two approaches are seen as two distinct routes to the common end point. The solid trajectory passes through an area of

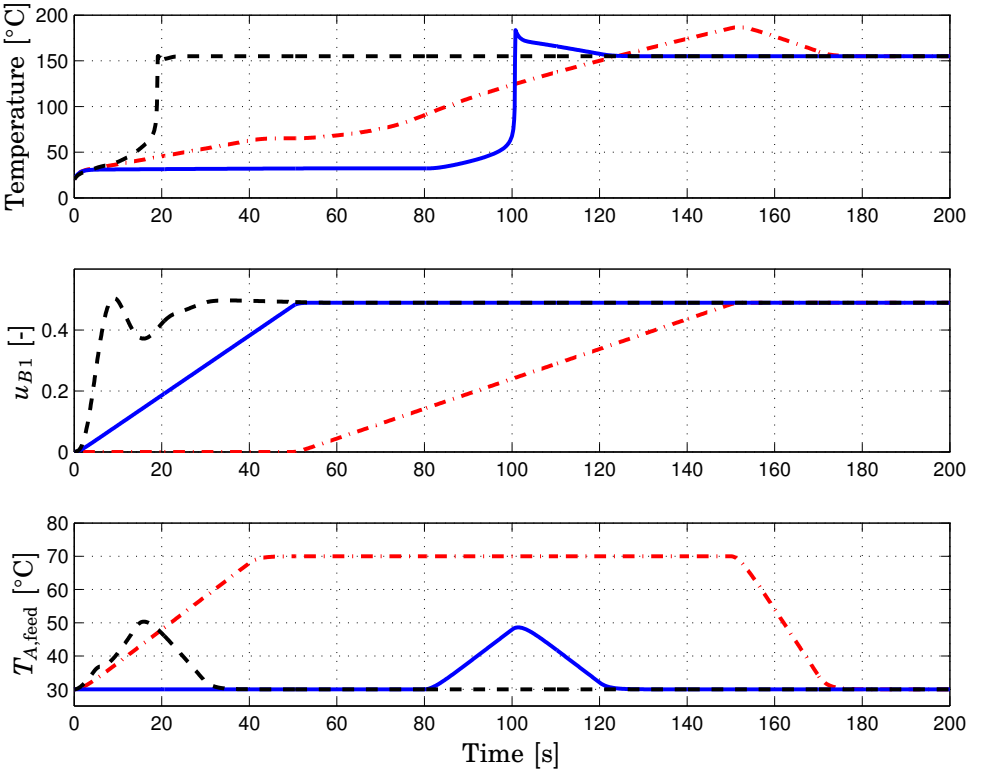

Figure 5.2 Simulations of various start-up attempts. The solid line represents the case when injection is begun before heating the reactant feed. The dash-dotted line represents the opposite case, when the feed is heated before injection begins. The dashed line represents the result of a dynamic start-up optimization without any robustness considerations.

the state-space where the nonlinear dynamics are significant, whereas the dash-dotted trajectory passes through areas with essentially linear dynamics.

Even though the process dynamics are sometimes highly nonlinear, dynamic optimization based on the nonlinear process model may give efficient and accurate start-up trajectories, see dashed line in Figures 5.2 and 5.3. The nominal operating point is reached within 20 seconds, by injecting the feed and increasing the feed temperature at the same time. However, this almost time-optimal solution considers only the nominal plant, which makes it extremely sensitive to any kind of plant/model mismatch or disturbance.

Assume now that there is a 2% plant/model mismatch in the activation

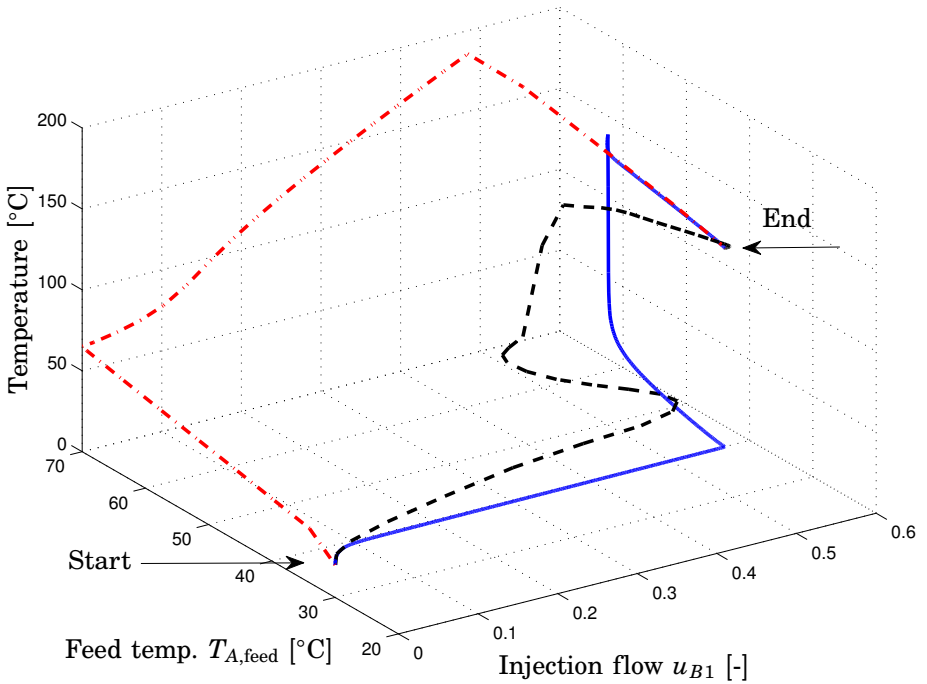

Figure 5.3 3D plot of the state-state trajectories during the start-up. For low temperatures and high injection flows, the process displays a higher degree of non-linearity. The solid line represents the case when injection is begun before heating the reactant feed. The dash-dotted line represents the opposite case, when the feed is heated before injection begins. The dashed line represents the result of a dynamic start-up optimization without any robustness considerations.

energy E_a, which is within the uncertainty set in Table 5.1. A 2% higher E_a reduces the reaction rate for a certain temperature. The open-loop controlled start-up is repeated with the trajectories from the dynamic optimization of the nominal model. The reduced reaction rate leads to the reaction occurring further downstream in the reactor and T_1 remains around 31°C. The temperature at the second injection point T_2 is plotted in Figure 5.4. The plant/model mismatch leads to T_2 being lower initially and then higher than the nominal trajectory, that is, the parameter error changes sign during the ignition process. The effects of the plant/model mismatch has the character of very fast transients, which may be very difficult for any feedback controller to compensate for.

The open-loop start-up trajectories may be analyzed before being im-

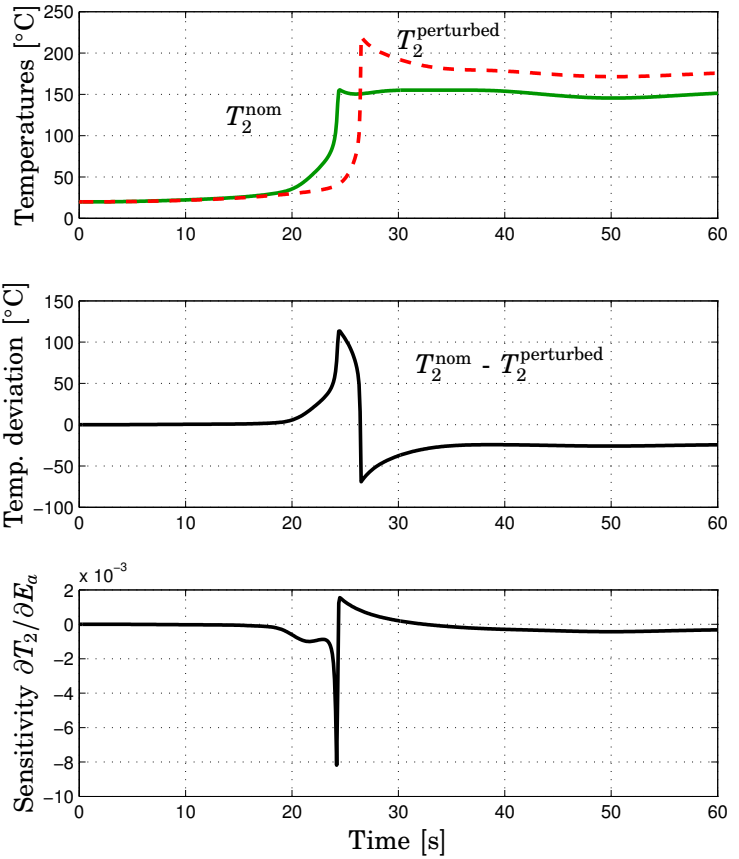

Figure 5.4 Upper plot: The optimal start-up from Figure 5.2 is very sensitive to uncertainties. In the perturbed case (dashed) the activation energy E_a is 2% higher than in the nominal model (solid). Middle plot: The model mismatch leads to first a lower temperature than predicted, but after the ignition of the reaction, the mismatch leads to higher temperatures. Lower plot: The temperature sensitivity to parameter variations in E_a.

plemented. The state sensitivity to parameter changes, $\partial x/\partial p$, gives an indication of how parametric uncertainty affects the behaviour of the process, see Figure 5.4. The higher sensitivity, the higher is the impact of the model mismatch. For small parameter changes Δ, the state trajectories are

given by

$$x = x^{\text{nom}} + \frac{\partial x}{\partial p}\Delta p^{\text{nom}}, \tag{5.6}$$

where

$$\Delta = \frac{p - p^{\text{nom}}}{p^{\text{nom}}} \tag{5.7}$$

is the dimensionless deviation factor of the parameter, here 0.02 for E_a. This linear approximation is only valid for very small parameter changes, due to the severe nonlinearities of the process.

Summary

The start-up control problem is challenging for three reasons, highly nonlinear dynamics of the process, slow input dynamics and rate limits for some control inputs, and finally, the uncertainty in terms of plant/model mismatch. Three motivating examples have been presented. The first two examples show that the start-up trajectories can lead through either very nonlinear dynamics or almost linear dynamics. The third example shows that dynamic optimization can lead to very efficient start-up trajectories, but it is not sufficient to only consider the nominal model for a safe and robust start-up.

In the next two chapters, the robust start-up control problem will be approached by using sensitivity analysis for two different control implementations.

6

Start-up: Dynamic Optimization

6.1 Introduction

We consider off-line dynamic optimization of the start-up trajectories. The optimal trajectories are used as feed forward and set-point terms in a local feedback system, see Figure 6.1, which should ensure that the optimal trajectories are tracked also in the presence of disturbances and modeling errors.

Dynamic optimization can easily give high performance solutions based on a nominal model. A greater challenge is to find solutions with robust performance, so that the solutions have reduced sensitivity to model uncertainty. In [Diehl *et al.*, 2006], an approximate technique is presented for robust nonlinear optimization, which utilizes a linearization of the uncertainty set. The main contribution of that paper is two methods to preserve sparsity to achieve efficient computation for large scale problems.

The robustness of the optimal solutions are considered in terms of parametric sensitivity. By introducing two key specifications in the optimization formulation, high-frequency penalties on the control inputs and state constraints on reactant B, the sensitivity of the optimal solutions can be significantly reduced, which increases the robustness of the closed loop start-up control problem. The robustness is introduced based on process insight and the extra specifications have only a small contribution to the computational complexity, compared to a min/max optimization problem formulation. The robustness of the proposed method is verified in Monte-Carlo simulations, where the values of the parametric uncertainties are randomly generated from a uniform distribution.

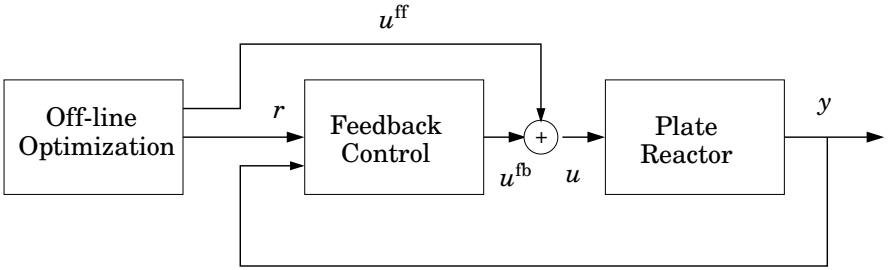

Figure 6.1 General block diagram for the start-up control with off-line optimization and online feed forward and feedback control.

6.2 Dynamic Optimization

Overview

Historically, there has been two main approaches to dynamic optimization, namely, dynamic programming and the maximum principle. Dynamic programming was proposed in [Bellman, 1957] as an elegant method to derive an optimal control policy as a function of the system states. The method has been successfully used to solve a large number of important problems in various fields, such as automatic control, inventory control and economics. The method is however difficult to apply to large scale problems due to the well-known curse of dimensionality. The maximum principle, [Pontryagin *et al.*, 1962], originating from the calculus of variations, defines the conditions for a function to be the optimal control profile. The optimality conditions form a two point boundary value problem. Solution of this problem includes integration of the system dynamics as well as the adjoint equations.

During the last two decades, a new family of methods has emerged, referred to as *direct* methods. Direct methods address the problem by transcription of the original infinite dimensional problem into a finite dimensional problem, which in turn is solved by means of algebraic nonlinear programming (NLP). The popularity of the direct methods is mainly due to their applicability to large scale problems, and in addition, the fact that some direct methods permit path constraints of states and controls to be enforced.

There are two main approaches to solving optimization problems using direct methods. In *single shooting*, see e.g. [Vassiliadis, 1993], the control variables are discretized, usually by introducing a piecewise polynomial parametrization. In each iteration, the dynamic equations are integrated in order to evaluate the cost function and the constraints. In order to ob-

tain first order gradient information, the sensitivity equations may also be integrated. The NLP for the parametrized control variables is usually of moderate size and can be solved by standard codes. In contrast, in *simultaneous methods*, see e.g. [Biegler *et al.*, 2002], both the control variables and the state variables are discretized. Since the dynamics must be discretized with sufficient accuracy, the resulting NLP is large but sparse. Recent advances in specialized algorithms have increased the applicability of the simultaneous methods, [Wächter and Biegler, 2006]. There are two main reasons for choosing a simultaneous method in this application. Firstly, the simultaneous methods have good numerical stability properties, which is important for the plate reactor system, since the system dynamics is unstable in some operating conditions. Secondly, one of the most important elements of the optimization problem is a temperature path constraint, which is straight forward to enforce using a simultaneous method.

Transcription Method

A key element of a simultaneous method is the scheme used to discretize the differential equation. Here, we use orthogonal collocation over finite elements with Radau points and Lagrange polynomials, for its numerical stability properties. The purpose of the transcription procedure is to translate the infinite dimensional dynamic constraint into a finite dimensional constraint, which can be incorporated into the final algebraic non-linear program.

The method will be briefly explained in this section. Consider the differential equation

$$\dot{x} = f(x,u), \quad x(0) = x_0, \tag{6.1}$$

where x are the state variables and u are the control variables. The optimization horizon is divided into N_e finite elements, and within each element, N_c collocation points, $\tau_j \in [0,1]$, are defined. Introducing the element lengths h_i, the time instants of the collocation points may be expressed $t_{ij} = t_i + h_i\tau_j$, where t_i denotes the start time of element i. Introduce the polynomial state variable approximations

$$x_{N_c+1}(t) = \sum_{k=0}^{N_c} x_{ik} l_k^{N_c+1}\left(\frac{t-t_{i-1}}{h_i}\right) \quad t \in [t_{i-1}, t_i], \tag{6.2}$$

where $l_k^{N_c+1}$ denotes Lagrange interpolation polynomials of order N_c+1 and x_{ij} are parameters. The control variables are discretized using the approximation

$$u_{N_c}(t) = \sum_{k=1}^{N_c} u_{ik} l_k^{N_c}\left(\frac{t-t_{i-1}}{h_i}\right) \quad t \in [t_{i-1}, t_i], \tag{6.3}$$

where the Lagrange polynomials, $l_k^{N_c}$, of order N_c has been introduced, and u_{ij} are parameters. The collocation equations may now be written

$$\sum_{k=0}^{N_c} x_{ik} \dot{l}_k^{N_c+1}(\tau_j) = h_i f(x_{ij}, u_{ij}) \tag{6.4}$$

for all $i = 1 \ldots N_e$ and $j = 1 \ldots N_c$. In order to enforce continuity of the state variables between elements, the constraints

$$x_{i-1,N_c} = x_{i,0} \tag{6.5}$$

must be enforced. The variables x and u and the original dynamic constraint (6.1) are now replaced by the parameters x_{ij} and u_{ij} and the equality constraints (6.4) and (6.5) in the final transcribed algebraic non-linear program.

It is interesting to note that this collocation scheme can be shown to be equivalent to a fully implicit Runge-Kutta method. Accordingly, the strong stability properties, see e.g. [Petzold, 1986], of this class of methods are still valid.

Tools

Formulation of a dynamic optimization problem is an iterative process, which requires careful tuning of the cost function, the constraints and the method used to transcribe the continuous dynamics. In addition, the properties of the numerical method used to solve the problem must be considered. The demanding task of *formulating* the problem is often complicated further by the details of how to *encode* the problem so that it fits the numerical algorithm. This encoding procedure is largely routine, but it is time consuming, error-prone and tends to distract the user from the key task of formulating the actual problem to be solved. Therefore, automatic computer software is important to bridge the gap between the requirements of the algorithms and the user's need of intuitive means to formulate the problem at hand. There is, however, a delicate balance between ease of use and restrictiveness when designing such software tools.

The plate reactor model is formulated in the modeling language Modelica, see [Modelica Association, 2005]. Modelica is an object oriented language which enables the user to state mathematical equations declaratively. In addition, Modelica offers abstractions useful for structuring of large models, such as class inheritance, components and connection of components. There is a large number of free and commercial Modelica libraries covering application areas such as electronics, mechanics, thermodynamics, fluid mechanics and vehicles.

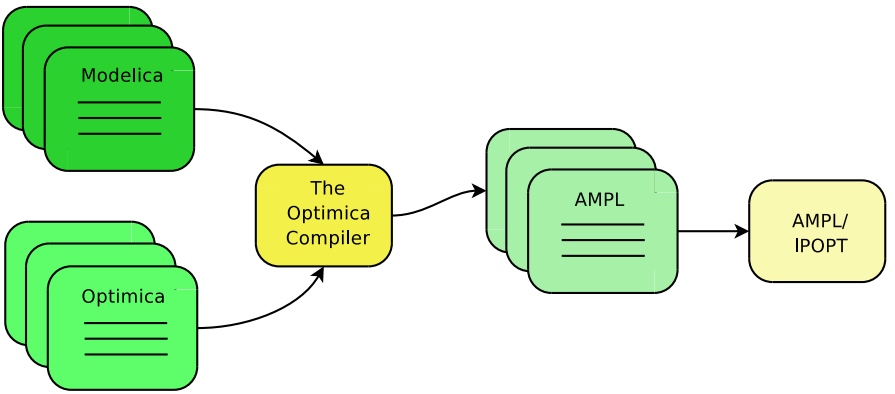

Figure 6.2 Flow sheet of the automatic code generation tool. The dynamic model and the optimization problem are formulated separately. The Optimica Compiler then automatically generates the nonlinear optimization problem in AMPL code. Finally, IPOPT is called to solve the resulting nonlinear problem.

In the optimization problem, the Modelica model represents the dynamic constraint. However, it is desirable to be able to express, formally, also the optimization quantities, such as cost and constraints. This sort of constructs are not part of the current version of the Modelica language specification. Therefore, a project, The JModelica Project, aiming at creating a flexible Modelica environment targeted at extensible compiler design has been initiated, see [Åkesson *et al.*, 2007; Åkesson and Årzén, 2007]. A primary target of the project is to formulate a language extension, entitled Optimica, of Modelica which offers high level descriptions of dynamic optimization problems. In addition, a prototype Modelica/Optimica compiler is under development. Using this compiler, a Modelica description of the process, and a complementing Optimica description for the optimal control problem can be automatically translated into AMPL, [Fourer *et al.*, 2003], which is a language for mathematical programming, see Figure 6.2. The resulting NLP was then solved using AMPL and IPOPT, which is an interior point optimization algorithm, [Wächter and Biegler, 2006].

All optimization results in this chapter were obtained using the Modelica/Optimica compiler, AMPL and IPOPT.

6.3 The Model

In this chapter, we consider a reactor configuration with two injection points for reactant B and one single cooling flow, that is, the same water cools the entire reactor. The two injection points are located at the reactor

inlet and mid section, respectively. The dynamic optimization is based on the nonlinear model from Chapter 3.

Four control variables are used as manipulated variables in the start-up optimization problem, $u_{B1}, u_{B2}, T_{A,\text{feed}}$ and T_{cool}. Note that the feed flow rates u_{B1} and u_{B2} may be used independently of each other. Stoichiometric conditions will be achieved in steady-state by proper formulation of the cost function. The absolute and rate limits on the control variables are

$$\begin{aligned} 0 \leq & u_{B1} \leq 0.8 \\ 0 \leq & u_{B2} \leq 0.8 \\ -2^\circ\text{C/s} \leq & \dot{T}_{A,\text{feed}} \leq 3^\circ\text{C/s} \\ 20^\circ\text{C} \leq & T_{A,\text{feed}} \leq 90^\circ\text{C} \\ -2^\circ\text{C/s} \leq & \dot{T}_{\text{cool}} \leq 1^\circ\text{C/s} \\ 15^\circ\text{C} \leq & T_{\text{cool}} \leq 90^\circ\text{C} \end{aligned} \tag{6.6}$$

and there are constraints on the reactor temperature

$$T_{r,i} \leq T_{\max} = 160^\circ\text{C for } i = 1 \ldots N \tag{6.7}$$

For each control input, there is an actuator system. Therefore, the output of the optimization will be the setpoints to these actuator systems, denoted by $u_{B1}^{\text{sp}}, u_{B2}^{\text{sp}}, T_{A,\text{feed}}^{\text{sp}}$ and $T_{\text{cool}}^{\text{sp}}$, hence the superscript 'sp'. For clarity, the superscript will be omitted when the meaning is clear from the context.

6.4 The Optimization Problem

Definition of a dynamic optimization problem is an iterative procedure. The problem specification given in this section is the result of such a procedure, where successive refinement of objectives and constraints have resulted in the final formulation.

Specifications

The state x of the reactor should be transferred from a cold stable equilibrium where no reaction takes place, to stable equilibrium at high reactor temperature, where almost all of the reactants A and B are converted to C. By minimizing the concentration of the reactants A and B at the outlet of the reactor, ignition of the reactor, and transfer of the state, can be achieved.

As discussed in the previous section, it is very important to consider the robustness properties of the optimal solution. The robustness properties of a particular solution may be analyzed by calculating the state sensitivity with respect to parametric uncertainty, $\partial x/\partial p$. It is clear that a bang-bang solution, resulting e.g. from solving a minimum time problem, would not be robust, since the success of such a strategy is based on *timing*. In the presence of model uncertainty, the timing of the bang-bang sequence might not match the actual state of the system, with degraded performance as a result.

We introduce two specifications that will improve the robustness of the optimal solution; *i*) a penalty on the high frequency use of the control inputs, *ii*) a constraint on the accumulated amount of reactant B at each injection point.

High frequency penalties on control signals High frequency penalties on the inputs are introduced in the optimization, since it is impossible to implement arbitrarily fast control trajectories. In addition, high frequency penalties improves the numerical solution of the optimization as the problem becomes less singular.

In the optimization problem, there exist rate limits on the feed temperature and cooling temperature $\dot{T}^{\text{sp}}_{A,\text{feed}}$ and $\dot{T}^{\text{sp}}_{\text{cool}}$. These derivatives are penalized in the cost function as one kind of high frequency penalty. However, penalties on the derivatives of the injection flow rates, u^{sp}_{B1} and u^{sp}_{B2}, were not sufficient. Instead a more general high-pass filter was introduced to increase the flexibility in the optimization formulation. By varying the cut-off frequency ω^f_c of the filter, it is possible to vary the frequency at which the HF-filter starts penalizing the control signal.

The high frequency penalties are important for the nominal solution, but they should also be considered in the context of the closed loop system. The optimal control profiles are implemented as feed forward signals in the closed loop feedback control system, see Figure 6.1. The feedback controller should be able to compensate for effects of the model mismatch. Clearly, the feedback system cannot be expected to suppress effects from model mismatch at frequencies higher than its bandwidth.

It is then convenient to design the high-pass filter cut-off frequency in terms of the frequency domain for the closed loop system. The frequency content of the off-line computed control variables should be such that high frequencies are not injected into the system. For the plate reactor, the bandwidth of the closed loop system is close to 0.5 rad/s at the final steady-state operating point, see also Figure 6.12. The limited bandwidth arises from actuator dynamics and limited control inputs. Accordingly, the bandwidth of the filter, ω^f_c was chosen to 0.5 rad/s. For comparison, the case of $\omega^f_c = 5$ rad/s was evaluated. The filter was implemented as a third

order Butterworth high-pass filter.

Accumulation of reactant B For safety reasons, it is undesirable to have large amounts of reactant B accumulated in the reactor during start-up. This may lead to sudden ignitions and thermal runaways. This can be formally analyzed by investigating the state sensitivity with respect to the parametric uncertainties, see Section 6.4. The analysis shows that high concentrations and high temperatures give extremely high sensitivity for the given uncertainties. Therefore, it is required that the concentration of B should not exceed a specified maximum level. The constraints are chosen based on the steady-state values at optimal operation for the nominal model. In this application the concentration constraints were set to 200 mol/m^3 at the first injection point and 400 mol/m^3 at the second injection point.

The constraints on c_B has also another interesting physical interpretation. By limiting the amount of reactant B inside the reactor, the reaction rate r is limited, see equation (2.3). As a consequence, the rate of the change of the temperature, $\dot{T}_r$, is also limited, see (3.2). This is a more natural way of constraining the temperature derivative than introducing explicit constraints on the derivative in the optimization problem.

Constraints on reactor temperature The reactor temperature, T_r, should not exceed the specified maximum temperature anywhere along the reactor length, in order not to damage the reactor. The maximum temperature should be chosen somewhat conservative, in order to allow for temperature fluctuations due to disturbances and parameter uncertainty. The maximum temperature allowed in the reactor is $T_{\max} = 160°\text{C}$, while the corresponding temperature bound in the optimization problem was set to 155°C.

Absolute and rate limitations of the control inputs There is a complicated interplay between the feed forward trajectories and the closed loop system, which must be considered in the presence of model uncertainty. Enough control authority must be allocated to the feedback control system to enable it to compensate for any model mismatch. This is done by enforcing more conservative constraints in the optimization procedure than is required by the physical plant, see (6.6)-(6.7). In the optimization formulation, more restrictive bounds were enforced (6.8).

The Optimal Control Problem

Given the specifications presented in the previous section, the optimization problem may now be formulated as

$$\min_u \int_0^{t_f} \alpha_A c_{A,N}^2 + \alpha_B c_{B,N}^2 + \alpha_{u_{B1}} (u_{B1,f}^{\text{sp}})^2 + \alpha_{u_{B2}} (u_{B2,f}^{\text{sp}})^2 + \alpha_{T_f} (\dot{T}_{A,\text{feed}}^{\text{sp}})^2 + \alpha_{T_c} (\dot{T}_{\text{cool}}^{\text{sp}})^2 \, dt$$

subject to

$$\begin{aligned} \dot{x} &= f(x,u) \\ T_{r,i} &\leq 155, \quad i = 1 \ldots N \quad c_{B,1} \leq 200, \quad c_{B,2} \leq 400 \\ 0 &\leq u_{B1}^{\text{sp}} \leq 0.7, \quad 0 \leq u_{B2}^{\text{sp}} \leq 0.7 \\ -1.5 &\leq \dot{T}_{A,\text{feed}}^{\text{sp}} \leq 2, \quad -1.5 \leq \dot{T}_{\text{cool}}^{\text{sp}} \leq 0.7 \\ 30 &\leq T_{A,\text{feed}}^{\text{sp}} \leq 80, \quad 20 \leq T_{\text{cool}}^{\text{sp}} \leq 80 \end{aligned} \tag{6.8}$$

where $c_{A,N}$ and $c_{B,N}$ are the concentrations of A and B at the reactor outlet. $u_{B1,f}^{\text{sp}}$ and $u_{B2,f}^{\text{sp}}$ are the high-pass filtered control variables corresponding to injection of reactant B. The weighting coefficients are denoted α_j. $T_{r,i}$ are the reactor temperatures in the N control volumes. The terms $c_{B,1}$ and $c_{B,2}$ are the concentrations at the first and the second injection point, respectively. Note that at time $t = 0$, the only term that is non-zero, is the first term in the cost function $c_{A,N}$, since reactant A flows through the reactor. The remaining five terms in the cost function are zero, as they all are directly or indirectly associated with actions of the control inputs. In steady-state, at the end of the optimization time t_f, all terms except the two concentrations are zero. Therefore, the values of α_A and α_B determine the steady-state optimal operating point. To achieve high conversion of both reactants, these weights are chosen so that stoichiometric relations are achieved, thus maximizing the conversion.

The problem was transcribed and solved as described in Section 6.2, using the automatic Modelica-based software. The input and state variables were discretized over a time horizon of 150 s using a grid of 450 points, which resulted in a large scale optimization problem with approximately 145 000 variables. The execution time for solving the optimization problem was 1-2 hours on a Intel Core Duo 2.13 GHz system.

Scaling and Initial Guess

Scaling proved to be important in order for the numerical algorithm to converge. Therefore, all states and controls were scaled to the same order

of magnitude. In addition, the automatic scaling facilities of IPOPT were utilized. Further, the convergence as well as the execution time of the optimization algorithm is dependent on the initial guess supplied to the NLP solver. Therefore, a square problem, with fixed inputs was solved initially, to generate initial guesses for all variables. Then the actual optimization problem could be solved with satisfying convergence rate.

Optimization Results

In this section the effects of the given specifications on the optimal solution are presented and analyzed.

Overview of the characteristics The optimization results are plotted in Figures 6.3 and 6.4. The main characteristic is the need for heating to achieve ignition. By increasing the feed temperature $T_{A,\text{feed}}$ the reactor temperature increases and after ignition the reaction becomes self-accelerating and $T_{A,\text{feed}}$ can return to its initial value. Similarly, the cooling temperature T_{cool} is increased to promote ignition at the second injection point. The maximum conversion occurs when the reactor temperatures around the two injection points are at the maximum limit of 155°C.

In the optimization formulation, the reactant B concentration around the two injection points is limited, see Figure 6.4. The constraints on c_B ensure that there is only a limited accumulation of unreacted chemicals in the reactor. The injection flow rates, u_{B1} and u_{B2}, are initially low to comply with the c_B-constraints. Before more B can be injected, the temperature at the injection points needs to be increased by $T_{A,\text{feed}}$ and T_{cool}. The higher reactor temperature increases the reaction rate, which leads to more of the injected B being consumed. It is then possible to increase the injection of B and still comply with the constraint in c_B. The constraints in c_B reduce the risk of uncontrolled ignition and increases the robustness of the optimal trajectories.

Results when varying the high frequency penalty on u_{B1} ***and*** u_{B2} Two cases have been considered, $\omega_c^f = 0.5$ and $\omega_c^f = 5.0$ rad/s. The optimal control profiles for both cases are shown in Figure 6.3. When $\omega_c^f = 5.0$, there is clearly more high frequency content of the injection control inputs. This allows the start-up to be somewhat faster as the control actions can be more aggressive, when the temperature reaches the maximum value, see Figure 6.4.

When $\omega_c^f = 0.5$, the optimization gives a slower transient to the maximum temperature value, since the injection control is penalized for lower frequencies than in the previous case. Notice that the temperature constraints are active for both cases at the optimal steady-state operation point.

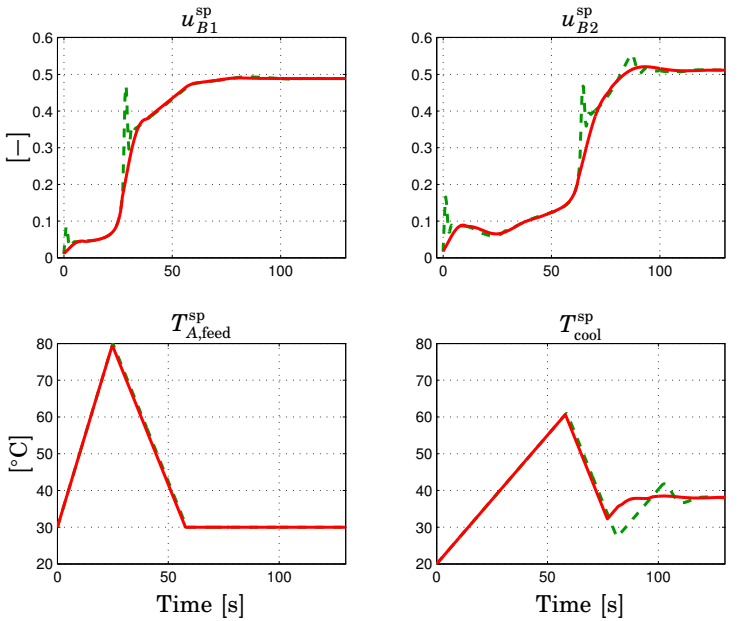

Figure 6.3 Optimal control profiles. The dashed curves correspond to the case $\omega_c^f = 5.0$ rad/s and the solid curves corresponds to $\omega_c^f = 0.5$ rad/s.

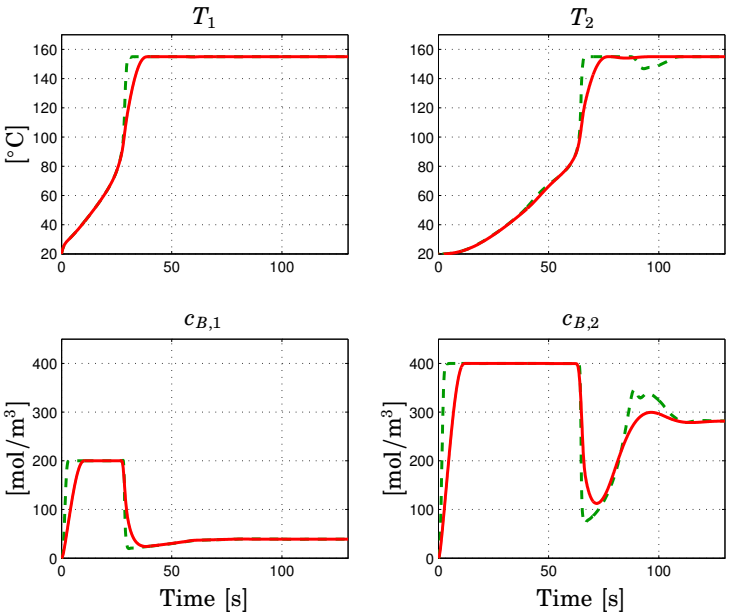

Figure 6.4 Optimal profiles profiles for reactor temperature and concentration of substance B. The left plots correspond to the first injection point, whereas the right plots correspond to the second injection point.

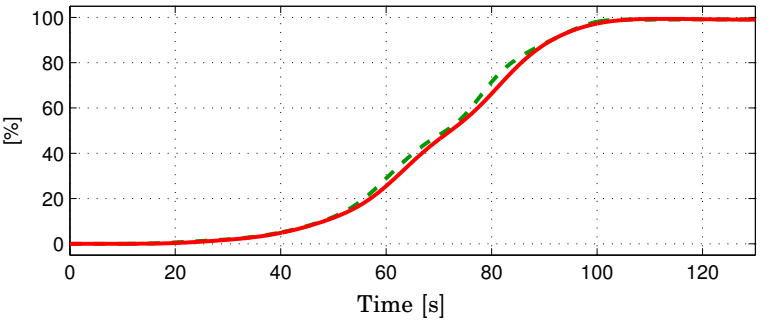

Figure 6.5 Conversion of reactant A at the outlet. The dashed curve correspond to the case $\omega_c^f = 5.0$ and the solid curve correspond to $\omega_c^f = 0.5$.

The high frequency content of the case when $\omega_c^f = 5.0$ leads to control input trajectories that require exact timing to satisfy the temperature constraints. This optimal solution will be much more sensitive to parametric uncertainty, as will be demonstrated in Section 6.7.

However, there is almost no difference in the settling time of the conversion, γ_A, see Figure 6.5. With time to reach maximum conversion being the primary performance measure, there seems to be almost no performance loss for increasing robustness of the optimal solution in this case.

Results for varying the bounds on c_B In Figures 6.6, 6.7 and 6.8 the optimal start-up trajectories are shown for three cases of different concentration bounds on reactant B. The high frequency penalty on the injection control inputs was fixed to $\omega_c^f = 0.5$ rad/s for all three cases.

With tighter constraints on c_B, the reactor temperature needs to be higher before more reactant can be injected. This is clearly shown in the lower plots of Figure 6.6, where $T_{A,\text{feed}}^{\text{sp}}$ and $T_{\text{cool}}^{\text{sp}}$ are increased to raise the reactor temperature before more injection can occur. Figure 6.8 shows the slower transient to the final operating point in terms of conversion, when tighter constraints are used. However, when higher concentrations are permitted, the start-up trajectories enter regions in the state-space where the state sensitivity for parametric uncertainty is very high, see Section 6.4.

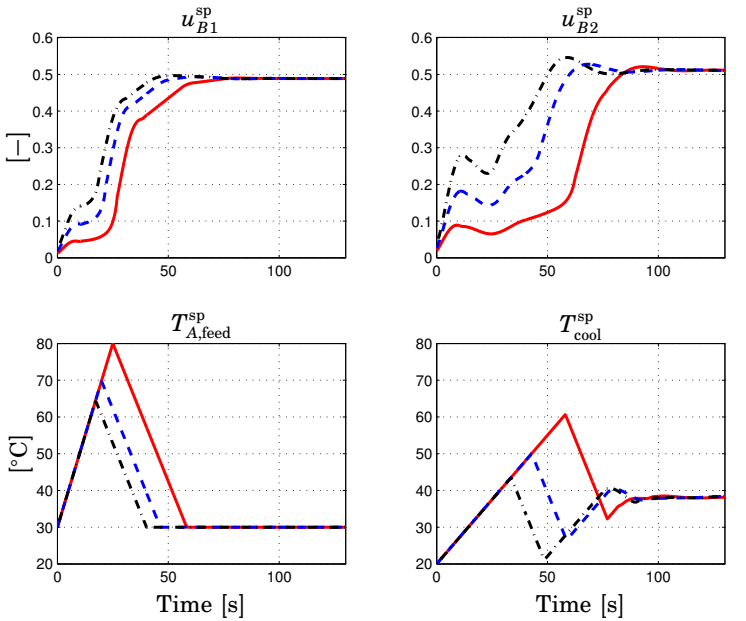

Figure 6.6 Control signals for optimal start-up for various c_B-constraints. $c_{B,1} \leq 200$, $c_{B,2} \leq 400$ (solid), $c_{B,1} \leq 400$, $c_{B,2} \leq 800$ (dashed), $c_{B,1} \leq 600$, $c_{B,2} \leq 1200$ (dash-dot)

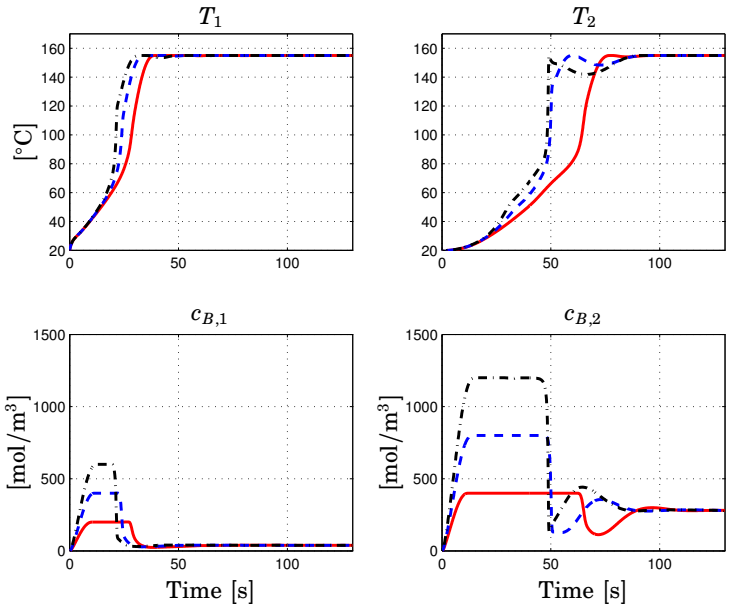

Figure 6.7 Temperatures and concentrations during optimal start-up for various c_B-constraints defined in Figure 6.6.

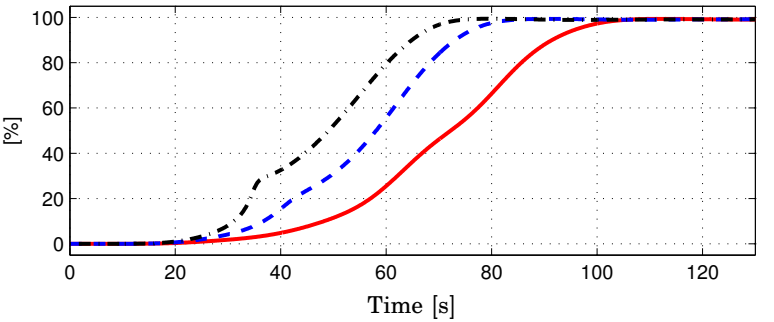

Figure 6.8 Conversion of reactant A at reactor outlet during optimal start-up for various c_B-constraints defined in Figure 6.6.

Sensitivity Analysis

In the presence of uncertainty, there will be deviations in the actual state trajectories from the off-line computed optimal trajectories. Sensitivity analysis is performed to quantify the impact of the optimization specifications on the parametric sensitivity of the optimal trajectories. In addition, we will study and compare the sensitivity of the open loop optimal trajectories for the uncertain parameters from Table 5.1.

The state sensitivity to parameter changes, $\partial x/\partial p$, gives an indication of how parametric uncertainty affects the behaviour of the process. The higher sensitivity, the higher is the impact of the model mismatch. For small parameter changes Δ, the state trajectories are given by

$$x = x^{\text{nom}} + \frac{\partial x}{\partial p}\Delta p^{\text{nom}}, \quad \text{where} \quad \Delta = \frac{p - p^{\text{nom}}}{p^{\text{nom}}} \tag{6.9}$$

is the dimensionless deviation factor of the parameter. In the start-up of the plate reactor, temperature is the most important safety concern. Therefore, the following analysis is focused on the sensitivity of the temperature at the second injection point T_2 to parameter variations. An analysis on T_1 would give similar results.

Table 6.1 summarizes the maximum temperature sensitivity during start-up time to parameter changes for various c_B-constraints and cut-off frequencies ω_c^f. The value in each entry of the table is the maximum temperature deviation due to a 0.1% increase in the specific parameter, for example

$$\max_{t\in[0,t_f]} (T_2(t) - T_2^{\text{nom}}(t)) = \max_{t\in[0,t_f]} \frac{\partial T_2(t)}{\partial E_a} 0.001 \cdot E_a^{\text{nom}} \tag{6.10}$$

Table 6.1 Maximum deviation in T_2 due to parametric sensitivity for different start-up specifications.

	$\omega_c^f = 0.5$ $c_{B,2} \leq 400$	$\omega_c^f = 0.5$ $c_{B,2} \leq 800$	$\omega_c^f = 0.5$ $c_{B,2} \leq 1200$	$\omega_c^f = 5$ $c_{B,2} \leq 400$
$\frac{\partial T_2}{\partial E_a} \cdot 0.001 E_a^{\text{nom}}$	-1.5 °C	-14.9 °C	-51.8 °C	-2.2 °C
$\frac{\partial T_2}{\partial k_0} \cdot 0.001 k_0^{\text{nom}}$	0.062 °C	0.71 °C	8.6 °C	0.091 °C
$\frac{\partial T_2}{\partial \Delta H} \cdot 0.001 \Delta H^{\text{nom}}$	0.24 °C	2.0 °C	15.8 °C	0.35 °C
$\frac{\partial T_2}{\partial h} \cdot 0.001 h^{\text{nom}}$	-0.14 °C	-1.4 °C	-15.4 °C	-0.18 °C

This linear approximation is only valid for very small parameter changes, due to the severe nonlinearities of the system. For the wider range of uncertainties described earlier in Table 5.1, the nonlinear effects have to be considered in order to analyze the state sensitivity, see the next section.

For tighter c_B-constraints, the effect of the model mismatch on the state trajectories is significantly smaller, up to an order of magnitude. The maximum sensitivity in each case occurs when the reaction ignites and the temperature increases very quickly. Start-up trajectories that have large sensitivity to parameter variations can be expected to be more difficult for the control system, which has limited authority, than trajectories for which the parametric uncertainty is small. However, the decreased sensitivity comes at the price of somewhat longer start-up time, see Figure 6.8.

The sensitivity of the optimal trajectories when $\omega_c^f = 5$ rad/s is roughly 50% higher than for $\omega_c^f = 0.5$ rad/s, but it is in turn much smaller than the sensitivity for higher constraints on c_B. The choice of cut-off frequency for the high-pass filter has a smaller, but still significant, impact compared to the c_B-constraints on the sensitivity of the optimal solutions. From Table 6.1 it can also be noted that the reactor temperature is most sensitive to changes in the activation energy E_a, this because the reaction rate r depends exponentially on E_a, but only linearly on for example k_0.

The sensitivities discussed in this section were computed using the numerical solver DASPK, see [Maly and Petzold, 1996]. This algorithm implements a BDF method for solving index-1 DAE systems, and can also integrate the sensitivity equations.

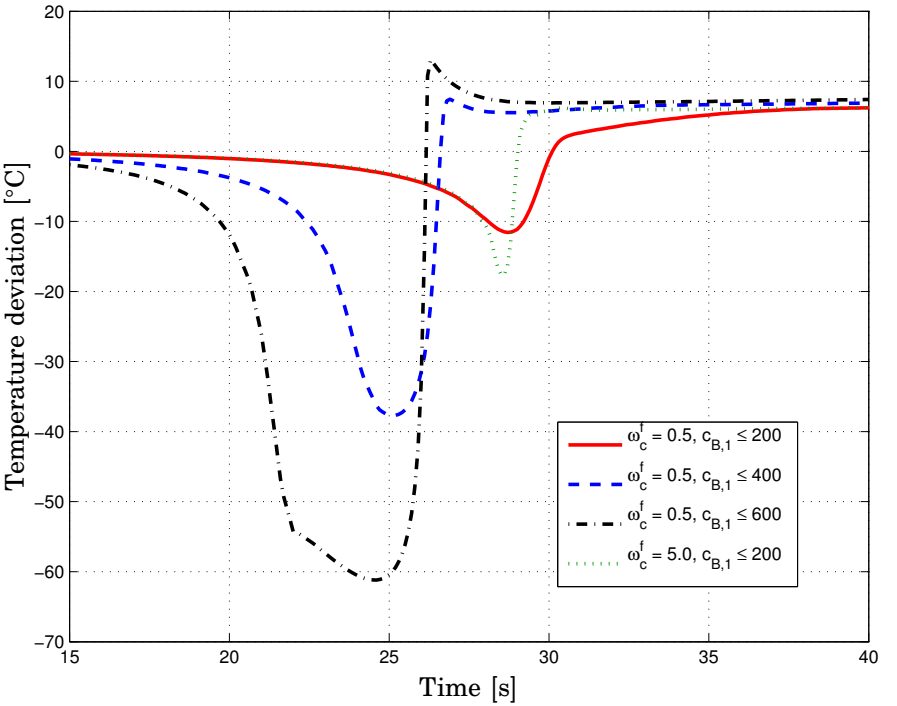

Figure 6.9 Difference in temperature at first injection point T_1 for the nominal trajectory and the actual trajectory caused by model mismatch for various c_B-constraints.

Effects of model mismatch

In the previous section, linear sensitivity analysis showed that tighter concentration constraints in the optimization formulation gave optimal trajectories that have significantly reduced sensitivity to parameter uncertainty. That analysis is limited to small parameter variations, so in this section we will use open loop simulations with the nonlinear model to include the nonlinear and multiparametric effects in the sensitivity analysis.

Up to now, optimal start-up trajectories have been presented for the nominal model. Here we will take a first look at the effect of model mismatch. The uncertainty of the model parameters were described in Table 5.1. One specific case of model mismatch is now studied to provide some insights. The parameter errors are the following; the heat transfer coefficient h 10% lower, the heat of reaction ΔH 5% higher, the pre-exponential coefficient k_0 5% lower and the activation energy E_a 2% higher than in

the nominal model. This model mismatch is selected, since it is one of the most difficult cases of model mismatch for the feedback controller to handle, according to the Monte Carlo simulations that will be presented in Section 6.7.

Figure 6.9 shows the difference $\Delta T = T_1 - T_1^{\text{nom}}$ between the actual temperature and the nominal temperature at the first injection. The higher value in E_a and lower value in k_0 will reduce the reaction rate and the subsequent heat release. Thus, the actual temperature will be lower than the nominal temperature before ignition occurs. After the ignition, the higher value in ΔH leads to more heat being released, thus the actual temperature will be higher than the nominal. A reduced heat transfer coefficient h will also lead to the actual temperature being higher than the nominal. The combination of these four parameter errors form a challenging model mismatch for a feedback controller to handle. First the mismatch leads to lower temperatures, but after ignition has occurred, the effect of the mismatch is the directly opposite.

Figure 6.9 shows that the effect of the model mismatch is significantly smaller when tighter concentration constraints in B are enforced or when lower cut-off frequency ω_c^f is used. This supports the results of Table 6.1 even when the nonlinear effects and uncertainty in multiple parameters are considered simultaneously. In the next sections, we will extend the robustness analysis to the closed loop system.

6.5 Feedback Control

The dynamic optimization algorithm calculates open loop trajectories for the four manipulated variables. Feedback control is necessary, however, due to process uncertainties and disturbances. Only temperature feedback is available. In the feedback control structure, the optimization results are used as reference and feed forward trajectories,

$$\begin{aligned} T_1^{\text{ref}} &= T_1^{\text{opt}}, \quad T_2^{\text{ref}} = T_2^{\text{opt}}, \\ T_{A,\text{feed}}^{\text{ff}} &= T_{A,\text{feed}}^{\text{sp,opt}}, \quad T_{\text{cool}}^{\text{ff}} = T_{\text{cool}}^{\text{sp,opt}}, \quad u_{B1}^{\text{ff}} = u_{B1}^{\text{sp,opt}}, \quad u_{B2}^{\text{ff}} = u_{B2}^{\text{sp,opt}}, \end{aligned} \tag{6.11}$$

where the superscript 'opt' denotes the optimal results from (6.8).

Figure 6.10 shows the Bode diagrams of four open loop transfer functions from the control inputs to the reactor temperatures T_1 and T_2. The transfer functions are linearizations of the process model at steady-state after the start-up. In the Bode diagram, we can see that the injection flow rates of reactant B, u_{B1}^{sp} and u_{B2}^{sp}, have larger process gain and faster impact on T_1 and T_2 than $T_{A,\text{feed}}^{\text{sp}}$ and $T_{\text{cool}}^{\text{sp}}$ have. However, there are several

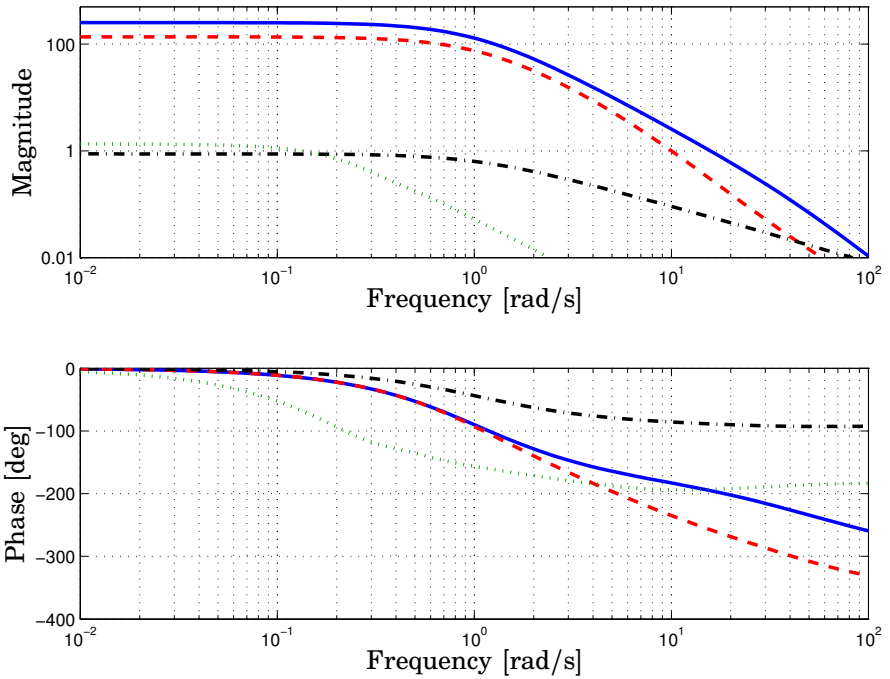

Figure 6.10 Bode diagrams; $u_{B1}^{\text{sp}} \rightarrow T_1$ (solid), $u_{B2}^{\text{sp}} \rightarrow T_2$ (dashed), $T_{A,\text{feed}}^{\text{sp}} \rightarrow T_1$ (dash-dot) and $T_{\text{cool}}^{\text{sp}} \rightarrow T_2$ (dotted). The large difference in gain comes from a lack of scaling.

nonlinear effects that should be considered when choosing control signals for feedback. For example, the injection flow rates may affect the stoichiometric balance and should thus be used with care in steady-state. Clearly, the variables $T_{A,\text{feed}}^{\text{sp}}$ and $T_{\text{cool}}^{\text{sp}}$ also affect the reactor temperatures, but their input dynamics and rate limits will prevent achieving a desirable bandwidth for the closed loop system using these two inputs only.

Therefore, a mid-ranging control structure, see e.g. [Åström and Hägglund, 2005], shown in Figure 6.11 is introduced. The idea of mid-ranging is to use control variables with fast impact, in this case, u_{B1}^{sp} and u_{B2}^{sp}, to account for high frequency variations. This is realized by the controllers C_1 and C_2 in Figure 6.11. Meanwhile, variables with slower impact, in this case, $T_{A,\text{feed}}^{\text{sp}}$ and $T_{\text{cool}}^{\text{sp}}$, are used to compensate for low frequency variations or effects of model mismatch, using controllers C_3 and C_4. The actions of $T_{A,\text{feed}}^{\text{sp}}$ and $T_{\text{cool}}^{\text{sp}}$ on the process, enable the two injection flow rates u_{B1}^{sp} and u_{B2}^{sp} to return to their optimal values, thus achieving the correct stoichiometric conditions between A and B in steady state. To reduce the

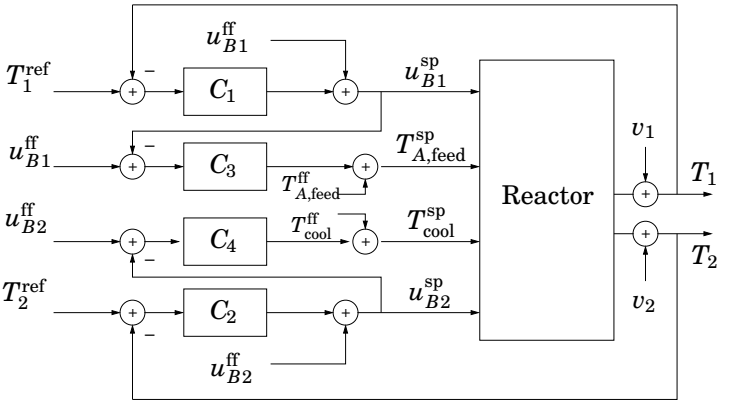

Figure 6.11 Block diagram for the mid-ranging feedback control system.

interaction between the fast and the slow control variables, the slow control loops are designed to have a closed loop bandwidth that is an order of magnitude smaller. For more details on mid-ranging control, see Chapter 9.

Each controller C_1, C_2, C_3 and C_4 in Figure 6.11 is implemented as a PID-controller. The tuning of the controller parameters is based on the AMIGO method, which involves robust loop-shaping and optimization of the integral gain, see [Åström and Hägglund, 2005].

Finally, to analyze the resulting closed loop system, the singular values of the sensitivity function S is plotted in Figure 6.12. S is the transfer function from the disturbance signals v_1 and v_2 to the temperature signals T_1 and T_2 and it is defined as

$$S = [I + PC]^{-1}, \tag{6.12}$$

where P is the linearization of the nominal reactor model at steady-state and C represents the mid-ranging control structure depicted in Figure 6.11. The closed loop system has good attenuation of constant and low frequency disturbances and model-mismatch effects. The maximum singular value for any frequency is 1.17 at 1.7 rad/s, which implies that the feedback control gives a good robustness. However, $\sigma_{\max} \geq 1$ for $\omega \geq 0.9$ rad/s. This indicates that the feedback controller will have difficulties in attenuating model-mismatch effects with higher frequencies.

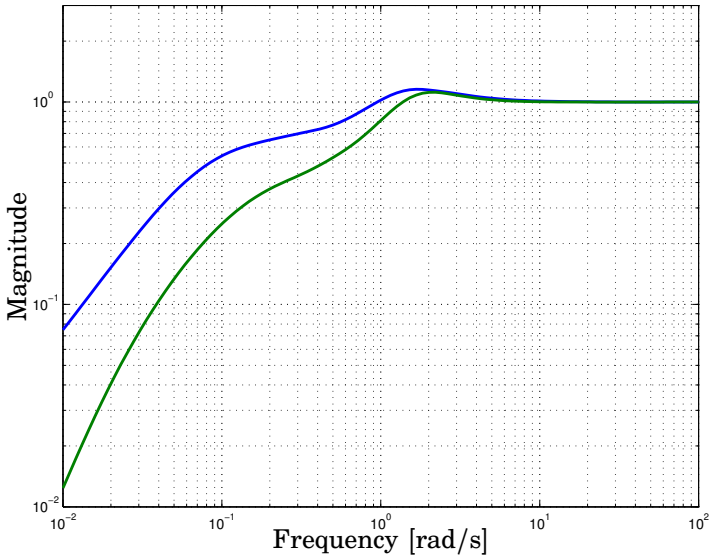

Figure 6.12 Plot of maximum and minimum singular values of the sensitivity function S

6.6 Simulation with Feedback Control

In this section, the closed loop system with feedback control is simulated and analyzed, see Figure 6.1. The result of the feedback is compared to the optimal solution given that the true values of the uncertain parameters had been known.

In Figures 6.13 and 6.14, the start-up trajectories for three cases are plotted; the optimal solution for the nominal plant, the feedback solution when there is model mismatch (as defined in Section 6.4) and finally the optimal solution knowing the exact model mismatch. The specifications in the optimization problem are $\omega_c^f = 0.5$ rad/s and $c_{B,1} \leq 200$ and $c_{B,2} \leq 400$ mol/m^3. The model mismatch and its effect was described in Section 6.4.

The feedback controller takes the temperature trajectories T_1^{ref} and T_2^{ref} from the optimal solution as references. The controller manipulates primarily u_{B1} and u_{B2} to achieve this reference tracking, despite tracking errors resulting from model mismatch. As described in Section 6.4, this model mismatch leads initially to lower temperatures than in the reference. Thus, the controller have to increase the injection flow rates of B to compensate. After the ignition, the model mismatch quickly gives higher temperatures than for the nominal model, see e.g. Figure 6.9. The

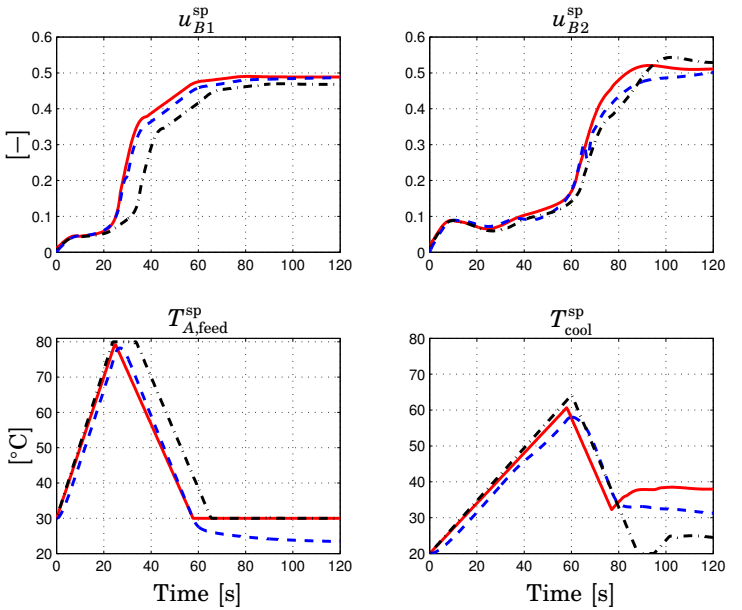

Figure 6.13 The control input set-points. Comparison of optimal solution with nominal model (solid), feedback control with model mismatch (dashed) and the optimal solution when the exact model mismatch is given (dash-dot).

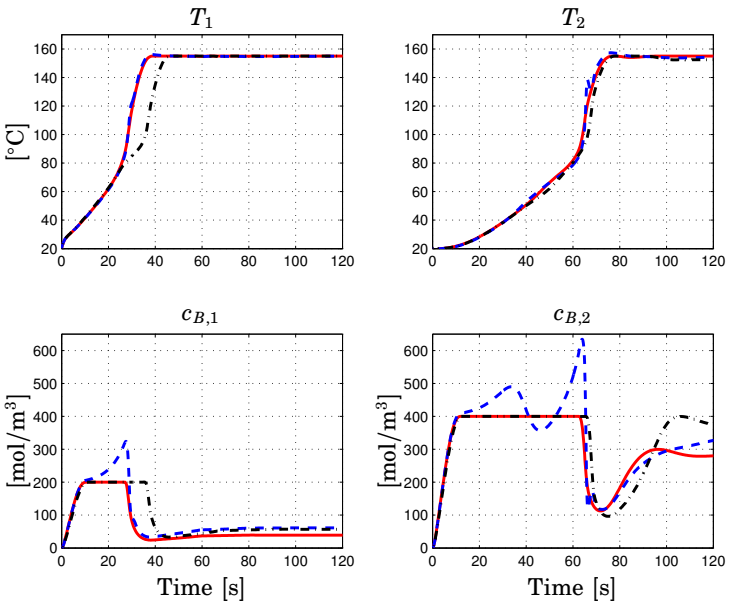

Figure 6.14 The state variables. Comparison of optimal solution with nominal model (solid), feedback control with model mismatch (dashed) and the optimal solution when the exact model mismatch is given (dash-dot).

controller quickly lower the flow rates again.

Meanwhile, to achieve stoichiometric conditions in steady-state, the mid-ranging control reduces the pre-heating $T_{A,\text{feed}}$ and cooling T_{cool}, to allow the injection flow rates u_{B1} and u_{B2} to return to their pre-defined optimal trajectories. In other words, during the transients the higher heat release is compensated for by u_{B1} and u_{B2}, but in stationarity by $T_{A,\text{feed}}$ and T_{cool}. In this way, mid-ranging allows each control input to be used at its best depending on its limitations, dynamics and available bandwidth. The control limitations for $T_{A,\text{feed}}$ and T_{cool} were more restrictive in the optimization formulation, to allocate some additional flexibility to the feedback controller. The feedback controller is bound by the original limitations defined in (6.6)-(6.7).

The feedback control tracks the optimal temperature trajectories and preserves the optimal injection flow rates with the mid-ranging control. However, these optimal trajectories are computed for the nominal model and may not be optimal due to model mismatch. It may then be interesting to see how the feedback solution compares with an optimal start-up if the exact model mismatch had been known, see the dash-dot lines in Figures 6.13 and 6.14. As the activation energy is higher, the reactor flow needs to be heated more, before injection can be increased further, thus avoiding excessive accumulation of B. The higher heat release leads to less reactant being injected at the first point, since $T^{\text{sp}}_{A,\text{feed}}$ is already at its lower limit of 30°C. Thus, the injection of B is slightly redistributed from the first to the second injection point. To adjust for the increased heat release, the cooling temperature $T^{\text{sp}}_{\text{cool}}$ is lowered in steady-state.

The feedback controller succeeds in tracking the temperature references, but the concentration of reactant B increases temporarily due to the model mismatch, see the lower plots in Figure 6.14. This may be avoided if concentration feedback is available. The resulting operating point will be different for the feedback solution and the optimal solution knowing the model mismatch. However, the conversion of reactant A is 98.8% for both operating points, thus the feedback control does not loose any efficiency for this particular model mismatch.

6.7 Monte Carlo Simulations

In this section, the effect of the off-line computed start-up trajectories on the robustness of the closed loop system is evaluated by means of Monte Carlo simulations. To reduce the state sensitivity of the optimal trajectories to parametric uncertainties, we have introduced two key specifications in the optimization problem; *i*) high frequency penalties on u^{sp}_{B1} and u^{sp}_{B2}

defined by a cut-off frequency ω_c^f and *ii*) constraints on c_B at the two injection points. The temperatures at the first and second injection points were evaluated and compared for five cases,

Case 1: Feedback control disabled, optimal trajectories computed for $\omega_c^f = 0.5$ rad/s, $c_{B,1} \leq 200$ mol/m^3 and $c_{B,2} \leq 400$ mol/m^3

Case 2: Closed loop control, optimal trajectories computed for $\omega_c^f = 0.5$ rad/s, $c_{B,1} \leq 600$ mol/m^3 and $c_{B,2} \leq 1200$ mol/m^3

Case 3: Closed loop control, optimal trajectories computed for $\omega_c^f = 0.5$ rad/s, $c_{B,1} \leq 400$ mol/m^3 and $c_{B,2} \leq 800$ mol/m^3

Case 4: Closed loop control, optimal trajectories computed for $\omega_c^f = 0.5$ rad/s, $c_{B,1} \leq 200$ mol/m^3 and $c_{B,2} \leq 400$ mol/m^3

Case 5: Closed loop control, optimal trajectories computed for $\omega_c^f = 5.0$ rad/s, $c_{B,1} \leq 200$ mol/m^3 and $c_{B,2} \leq 400$ mol/m^3

The first case is open loop control, the remaining four are closed loop control. Cases 2, 3 and 4 displays the effect of tighter c_B-constraints. Case 5 considers less high frequency penalties on the injection control inputs.

For each case, 5000 simulations were carried out. In each simulation, the values of the model parameters $E_a, \Delta H, k_0$ and h were randomly generated from a uniform distribution, based on the uncertainties in Table 5.1. The closed loop system is simulated and the reactor temperatures at the injection points are recorded. Then a new sample of the uncertain parameters is generated and the whole procedure is repeated.

To visualize the sensitivity of the five cases to the uncertainties, envelope curves were constructed, see Figure 6.15. They show the minimum and maximum temperature among the 5000 simulations for each sample time t. The horizontal dashed line indicates the safety limit of 160 °C. Any temperature above this may lead to safety shut-down to avoid damage to the reactor. A larger area between the minimum and maximum temperature indicates a higher variation in reactor temperature due to insufficient robustness to the model mismatch. The same feedback controller is used for all cases, since the focus is to investigate how the sensitivity of the different reference trajectories affect the robustness of the closed loop system.

In the first case, without feedback control, the reactor temperature at the first injection point spans an interval from 145 to 164°C at steady state. At the second injection point, there are some situations where the reaction does not even ignite directly after injection, but instead ignition occurs further downstream in the reactor. This gives an even larger temperature interval. The remaining cases include feedback control.

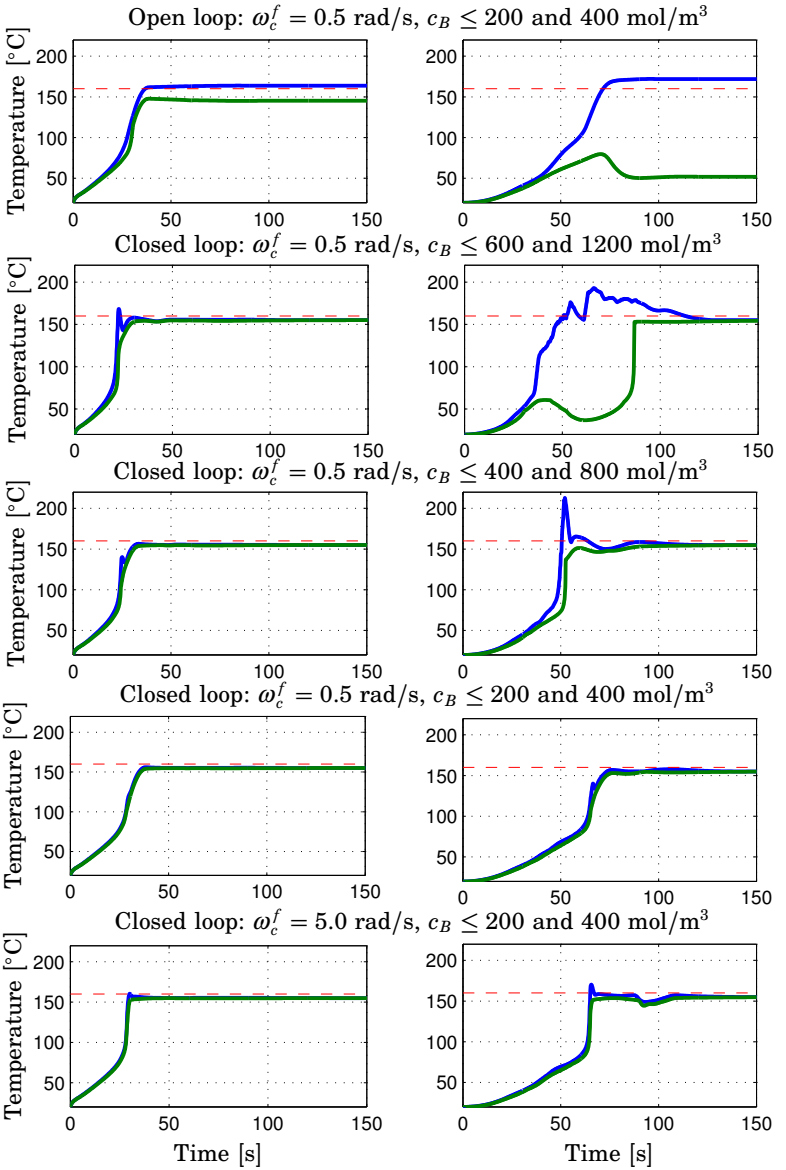

Figure 6.15 Maximum and minimum reactor temperature at the first (left column) injection point and the second injection point (right column) at each time instant out of 5000 sample simulations

The second case has the least restrictive c_B-constraints. The optimal solution based on the nominal model is then extremely sensitive for uncertainties, see Section 6.4. Therefore, the Monte Carlo simulations for this case show the widest range between the minimum and maximum reactor temperature. In fact, the time for ignition of the reaction at T_2 varies from 45 to 87 seconds, due to the effects of different model mismatch.

In the third case, the c_B-constraints are somewhat stricter than in the second case. The parameter uncertainty leads to model mismatch that the feedback controller can not handle fast enough. In fact, the feedback controller actually worsen the situation, since the transient results are even worse than without feedback. In steady-state, however, the temperatures are back to the nominal values, due to the integral action.

The most robust start-up is achieved in the fourth case, where tighter c_B-constraints and a low ω_c^f yield optimal solutions with very low sensitivity to uncertainty. Therefore, the effects of the model mismatch is small and the feedback controller succeeds in keeping the temperature below the safety limit.

In the fifth and final case, the same c_B-constraints are enforced, but there is less penalty on the high frequency components of the injection control inputs u_{B1} and u_{B2}. Due to the very fast transient, the maximum temperature limit for the nominal model, the optimal solution is sensitive to model mismatch. There are some parameter values within the uncertainty region, for which the feedback controller can not keep the reactor temperatures below the safety limit.

To summarize, the first case shows that feedback is necessary. However, due to limited bandwidth in the feedback controller, the optimal start-up trajectories can not be computed based on any arbitrary optimization specification. The feedback controller has large difficulties with handling the effect of the plant/model mismatch, especially when the effect of the mismatch changes sign at the ignition point. To avoid unsafe start-up, the optimal start-up trajectories need to have low sensitivity to parameter uncertainty. This is achieved by introducing high-frequency penalties on the control signals and enforcing concentration constraints on reactant B.

6.8 Summary and Conclusions

In this chapter, it has been shown how dynamic optimization can be used to generate trajectories for start-up of a plate reactor. The complex interplay between the formulation of the optimization problem and the implementation of its solution in a closed loop setting has been discussed. With model mismatch, an optimal solution may lead to transients that

the feedback controller can not handle due to limited bandwidth. Therefore the specifications of the optimization problem include concentration constraints on the injected reactant B and high frequency penalties on the control inputs. This results in an optimal solution with a significantly reduced sensitivity to uncertainties compared to solutions closer to the time-optimal. Temperature feedback control ensures that the optimal temperature trajectories are tracked. A mid-ranging control structure is used to take advantage of all four available control inputs. The proposed optimization specifications have been evaluated in Monte Carlo simulations, under the assumption of uncertain parameter values, with satisfying result.

The design procedure has been supported by automatic code generation tools, where the model description has been expressed in the Modelica language. The availability of automatic tools has enabled focus to be shifted from the details of *encoding* the problem towards *formulation* of the actual optimization problem. As a result, the iterative process of formulating a dynamic optimization problem is supported.

A natural extension of this work may be to include the sensitivity analysis in the optimization formulation, i.e., solving the optimization problem with a upper bound on the sensitivity or including the sensitivity in the cost function. With the latter approach, it is possible to choose a weighting coefficient corresponding to how much the model can be trusted. For large uncertainties, there may be a large penalty on the sensitivities and vice versa. It would also be interesting to consider the uncertainty by using multi-parametric optimization, where the uncertainty in the parameters are included in the optimization problem in the form of multiple models.

7

Start-up: A Hybrid Approach

7.1 Introduction

In [Verwijs *et al.*, 1994] and [Verwijs *et al.*, 1996], start-up of adiabatic tubular reactors are studied. The safeguarding of the start-up can be formulated as a few conditions that should be true before the feed of reactant is initiated. These conditions, defined in Section 7.3, and the experience from the dynamic optimization in Chapter 6 lead to the hybrid event-driven start-up method presented in this chapter. Even though the reactor has continuous dynamics, we will show that start-up control using hybrid modes may lead to increased safety and robustness of the start-up in the presence of control limitations and uncertainties. It also connects naturally to the practice of start-up in the industry.

7.2 The Model

In this chapter, we consider a reactor configuration with two injection points for reactant B and one single cooling flow, that is, the same water cools the entire reactor. The two injection points are located at the reactor inlet and mid section, respectively. The control design is based on the nonlinear model from Chapter 3.

Four control variables are used as manipulated variables in the start-up optimization problem, $u_{B1}, u_{B2}, T_{A,\text{feed}}$ and T_{cool}. The limitations on control inputs and temperatures were given in Eqs. (6.6) – (6.7).

For each control input, there is an actuator system. Therefore, the output of the hybrid controller will be the setpoints to these actuator

systems, denoted by $u_{B1}^{\text{sp}}, u_{B2}^{\text{sp}}, T_{A,\text{feed}}^{\text{sp}}$ and $T_{\text{cool}}^{\text{sp}}$. For clarity, the superscript 'sp' is dropped when the meaning is clear from the context.

7.3 Start-up Conditions

There are many interesting problems associated with start-up of temperature sensitive exothermic reactions. Inspired by [Verwijs *et al.*, 1996] and the experience from Chapter 6, we propose two start-up conditions that need to be satisfied in order to achieve a safe start-up. Each condition is illustrated with an example.

Start-up condition 1: Ignition
The reactor temperature at the injection point should be driven to a required initial temperature, that is, $T \geq T^{\text{start}}$ at which reactant B can be fed into the reactor safely, meaning that the reaction rates are high enough to sustain the reaction.

The required initial temperature T^{start} will be used as a transition point, to ensure safe operation.

Example: Consider here injections in the first injection point only. In Figure 7.1, several start-up trajectories are plotted. The two control variables u_{B1} and $T_{A,\text{feed}}$ are on the x-axis and y-axis, respectively. The reactor temperature at the first injection point T_1 is on the z-axis.

The solid line is open loop start-up, where initially u_{B1} is increased, but the reaction does not start due to low reaction rate. When $T_{A,\text{feed}}$ is subsequently increased, ignition occurs very sudden and the temperature increases extremely fast and exceeds the maximum temperature allowed, $T_{\max} = 160°\text{C}$. $T_{A,\text{feed}}$ is then decreased to its original steady-state value. The process dynamics along this path is extremely nonlinear and offers no chance for any feedback controller with limited actuator bandwidth to control the reactor temperature.

The dashed line is open loop start-up where the reactant A is pre-heated *before* injection of B is allowed. The dynamic response is much smoother and less nonlinear. However, the reactor temperature exceeds $T_{\max}$ also here, so it is not feasible to maintain constant pre-heating of reactant A while injecting B.

Finally, the dash-dotted line is start-up with closed loop feedback using the hybrid start-up control that will be presented in Section 7.6. Reactant A is pre-heated, to increase T_1 before injection is allowed to start. The feedback control ensures that the reactor temperature reaches steady-state without violating $T_{\max}$.

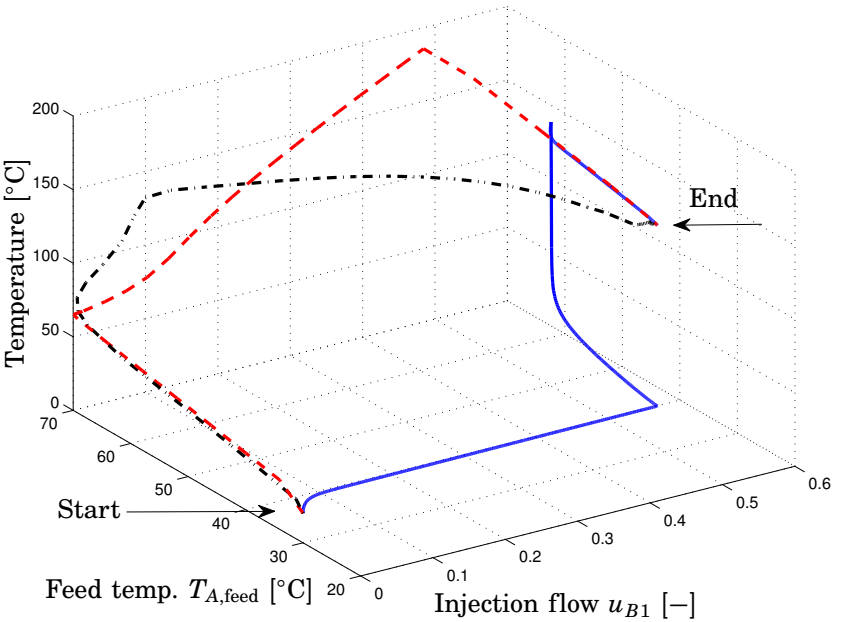

Figure 7.1 Start-up trajectories with open loop control injecting at low temperature (solid) and at high temperature (dashed), and finally closed loop response with the hybrid controller from Section 7.6 (dash-dot).

An advantage with increasing the reactor temperature before starting the injection is that it decreases the amounts of B flowing through the reactor unconsumed. This reduces the risk of further heat release in storage tanks downstream of the reactor, which may not be equipped with any cooling capacity.

In addition to the ignition condition, there is another condition for the subsequent injection points. Consider now *two* injection points.

Start-up condition 2: Conversion
Before the next downstream injection starts, it is necessary to check that almost all reactants injected upstream has converted, that is, $c_B < c_B^{\text{conv}}$ *after the upstream injection point.*

If there are large amounts of unreacted B in the reactor flow and even more B is added in the injection point, the heat release at the injection point may be much larger than anticipated.

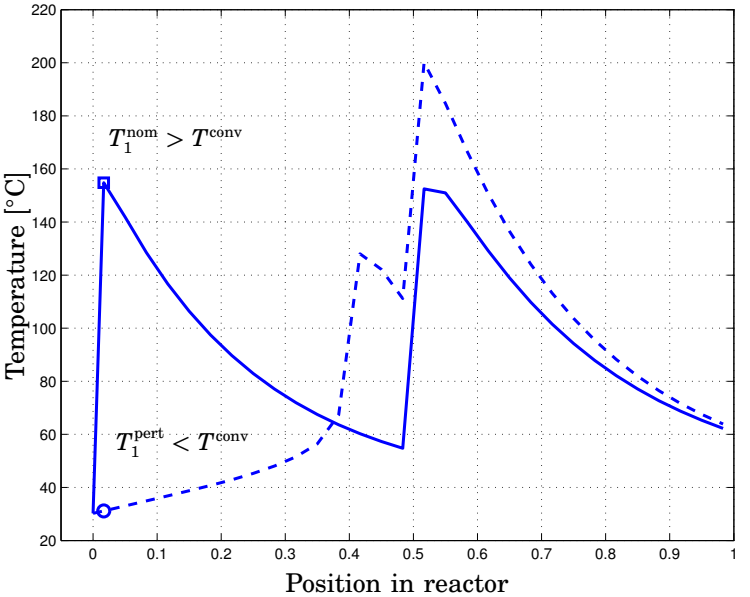

Figure 7.2 Temperature profiles along the uncontrolled reactor in steady state, nominal case (solid) and for small perturbations in the process parameters (dashed). Note that in the perturbed case, the temperature at the first injection point is much lower than the required $T^{\text{conv}} = 145°\text{C}$.

With a concentration measurement available, it is straight forward to check this condition, as the amount of injected reactant is known. With temperature measurements only, this condition is translated to a temperature condition on $T_1 \geq T^{\text{conv}}$ corresponding to the high temperature, resulting from the massive heat release from the reaction. For example, we may use $T^{\text{conv}} = 145°\text{C}$, which corresponds to a conversion of 98%. A very low T_1 is an indication on very low heat release, which corresponds to a very low conversion.

Example: In the nominal operating point, the steady-state temperature profile has two temperature maxima, see Figure 7.2. The temperature at the first injection point is around 155°C, which is a clear indication that most of the injected B is consumed in the exothermic reaction, so this fulfills the conversion condition. If the same control inputs that lead to the nominal operating point are applied in open loop to a process with some small plant/model mismatch[1], the resulting temperature profile will

[1]The mismatch is 5% lower ΔH and k_0, 2% lower E_a, and 10% larger h, see Table 5.1.

be completely different, see Figure 7.2. For this specific plant/model mismatch the reaction is more temperature sensitive, so most of the substance B fed into the first injection point remains unreacted. This is also seen in the reactor temperature at the first injection point, $T_1^{\text{pert}} << T_1^{\text{conv}}$, which is clearly not satisfying the conversion condition. Later in the reactor, the temperature increases due to heat release from the reaction and the reaction self-accelerates. The problem is that the reaction occurs too close to the second injection point and the cooling effect from the water is not sufficient to remove the heat before the next injection point. When more B is injected at the second injection point, the reactor temperature increases up to 200°C, which may damage the reactor, lead to unwanted by-product formation and initiate an emergency shutdown. This hazardous situation could have been avoided if the conversion start-up condition $T_1 \geq T_1^{\text{conv}}$ had been checked before the second feed was initiated.

7.4 Start-up Modes

In the previous section, we defined two conditions necessary for safe start-up:

- **Ignition**: The reactor temperature at the injection point $T \geq T^{\text{start}}$, to ensure high reaction rate so that the reaction is sustained.
- **Conversion**: The reactor temperature at the upstream injection point $T \geq T^{\text{conv}}$, to ensure that most of the reactant B being injected there has been consumed.

To satisfy these two conditions and based on experiences from the start-up optimization in Chapter 6, repeated here in Figure 7.3, the start-up sequence is divided into four modes, schematically outlined in Figure 7.4. The two required temperatures T^{start} and T^{conv} will be used as transition points in the start-up sequence. This means that the condition has to be fulfilled in order for the start-up sequence to proceed.

Identifying Start-up Modes

Figure 7.3 shows the optimization results from the start-up method in Chapter 6. Dynamic optimization is applied to the nonlinear model with the four control inputs $u_{B1}, u_{B2}, T_{A,\text{feed}}$ and T_{cool}. To reduce the sensitivity to uncertainties in model parameters, concentration constraints were enforced of reactant B at the two injection points and high frequency penalties on the inputs. At $t = 0$, the injection flows u_{B1} and u_{B2} start feeding reactant B into the reactor. After 10 seconds, the constraints in reactant B concentration have been reached at the two injection points.

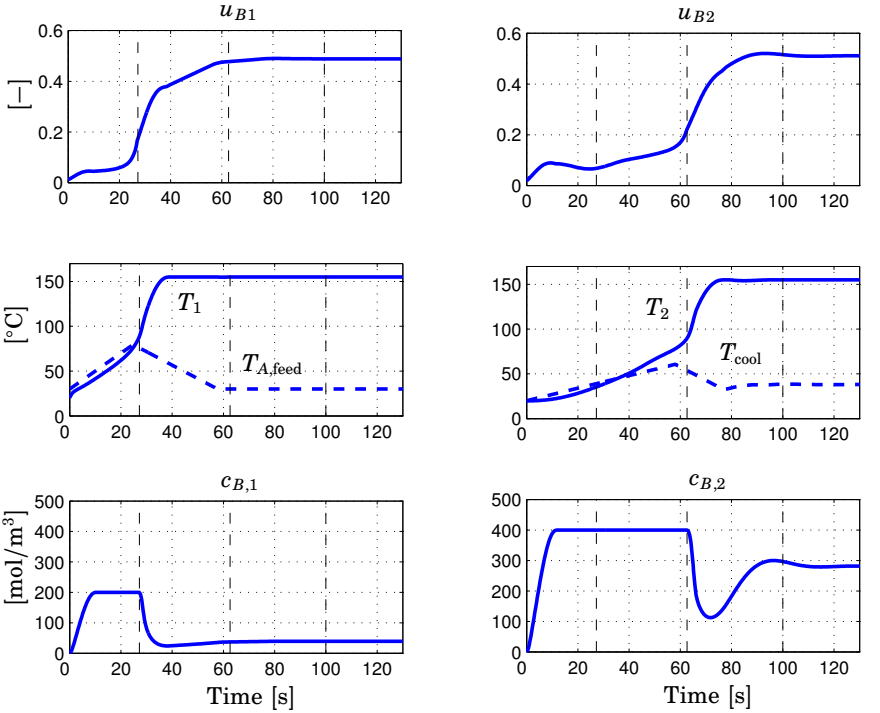

Figure 7.3 Optimization results from the start-up method in Chapter 6. The vertical dashed lines indicate the transition between different start-up modes.

This effectively halts any further increase in feeding. Meanwhile, the feed and cooling temperatures are slowly increased as fast as the actuator systems can manage. The increased reactor temperature leads to increased reaction rate and around $t = 25$ s the reactant consumption is sufficiently high, so that the feed injection flow u_{B1} can continue the transition to its steady-state value. During the first 25 seconds, pre-heating the feed is the most important task, the injected feed flows through the reactor largely unreacted due to the low reactor temperature. Therefore, it is quite natural to define the first start-up mode as a pre-heating mode where no injection is made, which lasts until the reactor temperature has reached a sufficient level to sustain the reaction.

At the second injection point, the constraint is also reached at $t = 10$ s. The cooling water can not heat the reactor, so the only heat comes from the reactor feed and the reaction heat at the first injection point. The reactor temperature T_2 increases therefore only slowly until around $t = 60$ s, when

the reactor temperature is sufficiently high to allow increased injection feed. This marks the end of the second start-up mode, where the first injection is increasing, but the second injection should wait for the reactor temperature to reach a certain limit.

Finally, at $t = 100$ s both injection feeds are at their steady-state values and the start-up is complete. This marks the end of the third start-up mode, where both injection feeds are operational.

Definition of Start-up Modes

The feedback in form of an event-driven start-up, where the injection start depends on the actual reactor temperature, leads to increased robustness, compared to a time-driven start-up sequence, where the injections start at pre-defined times from an off-line computed start-up scheme. With this feedback, it is easy to avoid dangerous situations as in Figure 7.2. Here is an example of the transition conditions for each mode, see Figure 7.4. The transition conditions given here are determined in the next section.

1. **Pre-heat:** To satisfy the first start-up condition in the first injection point, T_1 should be controlled with the inlet temperature $T_{A,\text{feed}}$ so that $T_1 > T_1^{\text{start}}$. No injection is allowed before this is fulfilled.
2. **First injection starts:** To satisfy the ignition condition for the second injection point, T_2 should be controlled with T_{cool} so that $T_2 > T_2^{\text{start}}$. To satisfy the conversion condition T_1 should be controlled so that $T_1 > T_1^{\text{conv}}$.
3. **Second injection starts:** To satisfy the conversion condition for the second injection point, control T_2 so that $T_2 > T_2^{\text{conv}}$. Then the start-up can be defined as completed.
4. **Final state:** This state can represent operation at steady-state or use of an optimizing controller with other objectives than the start-up controller.

7.5 The Hybrid Controller

The main components in the hybrid controller are the transition points - deciding when to switch mode - and the control variable trajectories u for each mode, bringing the process from the previous transition point to the next transition point. In Figure 7.5, the hybrid controller is schematically represented by the “Mode estimation”-block and the “Offline hybrid optimization”-block. Note how the feedback from the reactor P to the hybrid controller enables an event-driven start-up instead of a time-driven start-up, see Figure 7.6.

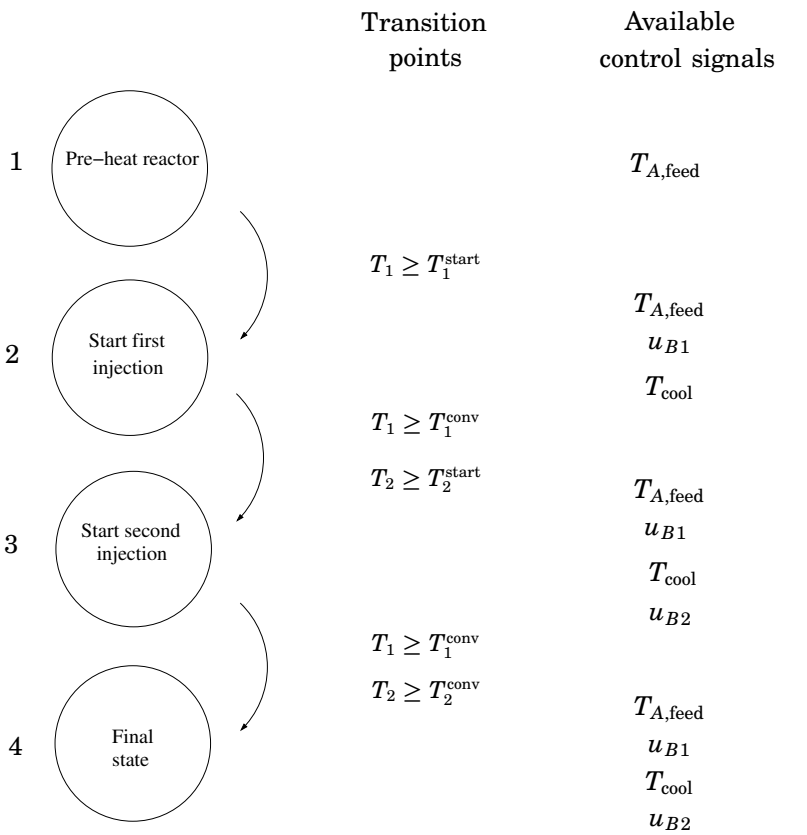

Figure 7.4 State machine to illustrate the different steps during start-up and the guards corresponding to each transition. Note that the transitions are one-directional and that not all control variables are available in each mode.

Choosing Transition Points

How should the transition points be computed? The aim is to choose transition points that promote start-up trajectories where the dynamics are less nonlinear and the sensitivity to uncertainties is small. This will facilitate the task of the feedback controller to achieve safe start-up despite uncertainties. For example, the transition point T_1^{start} represents the desired reactor temperature at which reactant B can be injected *safely*. We know from the nonlinear process model and Figure 7.1 that the process will react very differently depending on whether we inject B at $T_1 = 20°\text{C}$ or $65°\text{C}$.

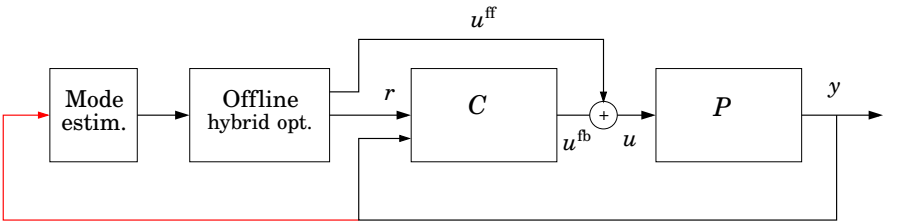

Figure 7.5 Event driven start-up, where the mode estimator and the hybrid controller yield reference $r(t, \text{mode})$ and control trajectories $u^{\mathrm{ff}}(t, \text{mode})$ depending on the current state.

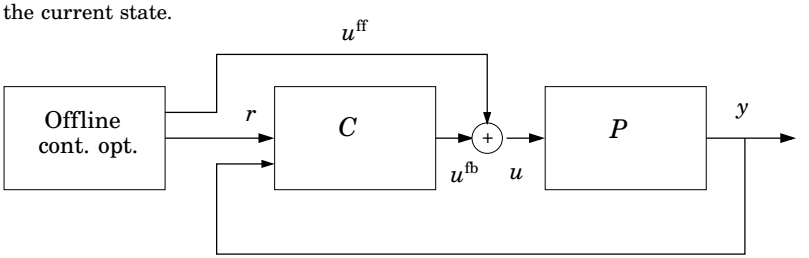

Figure 7.6 Block diagram of time-driven start-up from Chapter 6.

A sensitivity analysis using DASPK [Maly and Petzold, 1996] is performed to gain insights how to choose transition points that will ensure safe and robust start-up. Consider the temperature sensitivity with respect to the uncertain process parameter E_a, the activation energy, for various transition conditions, each defining a separate start-up trajectory.

$$T_1 = T_1^{\mathrm{nom}} + \frac{\partial T_1}{\partial E_a} \Delta E_a \tag{7.1}$$

The objective is to find transition points, T^{start}, leading to start-up trajectories, which have reduced sensitivity to parameter uncertainties.

Figure 7.7 shows the parametric sensitivity of the reactor temperature T_1 with respect to the activation energy E_a for the open loop system. For each transition condition, the optimal start-up trajectory has been computed as described in Chapter 6. It is clear that transition conditions forcing the reactor temperature to be higher before injection may start, significantly reduces the sensitivity, but also leads to a slightly longer start-up time. Similar analysis can be performed for the second injection point.

The sensitivity analysis gives quantitative measures of how the choice of transition points influence the situation for feedback control. Start-up trajectories that have large parametric sensitivity will lead to large deviations from the nominal trajectory, thus demanding large actions from the

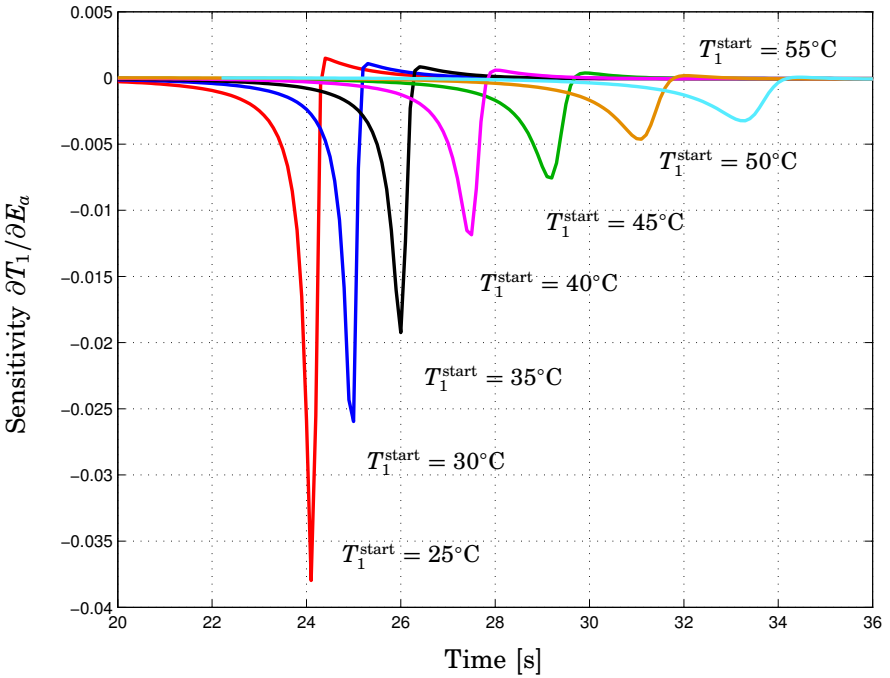

Figure 7.7 Parametric sensitivity of start-up trajectories for different transition conditions $T_1 \geq T^{\text{start}}$. The time of the sensitivity peaks reflects the somewhat longer start-up time that follows from higher T^{start}.

feedback controller. This may lead to actuator saturation and hazardous transients.

Based on Figure 7.7, two different sets of transition conditions are investigated in this chapter. This will provide us with a deeper insight how the choice of transition points affects the sensitivity of the start-up trajectories and in the long run also the robustness of the closed-loop system. The first set of transition conditions, here denoted as *lower* transition conditions are

$$\text{Lower t.c.} : T_1^{\text{start}} = 35°\text{C},\ T_2^{\text{start}} = 45°\text{C}. \tag{7.2}$$

The second set of transition conditions requires higher reactor temperatures before feed injections are allowed to start, thus denoted as *higher* transition conditions.

$$\text{Higher t.c.} : T_1^{\text{start}} = 55°\text{C},\ T_2^{\text{start}} = 65°\text{C} \tag{7.3}$$

According to Figure 7.7, the higher transition conditions should give trajectories with low sensitivity to uncertainty and the lower transition conditions may result in trajectories with higher sensitivity. The transition condition for the second injection point is 10°C higher, because c_A is lower at the second injection point compared to the first injection point, which leads to a lower reaction rate. Both sets of conditions use the same conversion condition, $T_1^{\text{conv}} = 145°\text{C}$, $T_2^{\text{conv}} = 145°\text{C}$, which corresponds to a conversion of 98% of reactant B to product C.

Reference trajectories

Given the transition points, the next step is to calculate suitable control trajectories that will bring the process from one transition point to the next. Without state constraints as in Chapter 6, start-up trajectories can easily be obtained by defining reference temperatures in terms of first order filters or ramps. However, it may require very fast changes in the control inputs to successfully track these references, as these references do not consider the dynamics of the process. Instead, the trajectories are here calculated offline with dynamic optimization based on the nonlinear process model using the same method as in Chapter 6. The cost function includes the reactant concentrations of A and B and the control inputs weighted by high-frequency filters. Remember, there is no hybrid structure within each mode. The dynamic optimization uses the nonlinear process model from Chapter 3, but as shown in the start-up scheme in Figure 7.4, not all control variables are available at all times. The process model and the optimization variables are therefore changed according to the current mode

- **Mode 1:** $\dot{x} = f_1(x,u,p)$, where $u = \{T_{A,\text{feed}}, T_{\text{cool}}\}$
- **Mode 2:** $\dot{x} = f_2(x,u,p)$, where $u = \{u_{B1}, T_{A,\text{feed}}, T_{\text{cool}}\}$
- **Mode 3:** $\dot{x} = f_3(x,u,p)$, where $u = \{u_{B1}, u_{B2}, T_{A,\text{feed}}, T_{\text{cool}}\}$
- **Mode 4:** $\dot{x} = f_4(x,u,p)$, where $u = \{u_{B1}, u_{B2}, T_{A,\text{feed}}, T_{\text{cool}}\}$

and the mode switches are given by transition points in terms of the temperatures T^{start} or T^{conv}, respectively.

The optimal trajectories for the two sets of transition points, (7.2) and (7.3), are plotted in Figures 7.8 and 7.9. The dashed lines represent the start-up with lower transition conditions and the solid lines represent the start-up with higher transition conditions. It is clear that the lower transition conditions allow the feed injections of B to begin earlier than if the transition conditions are set to higher temperatures, $t = 6.7$ s and 18 s, respectively. However, the injections at low temperature do not lead to a sustainable reaction, instead most of the injected B flows unreacted

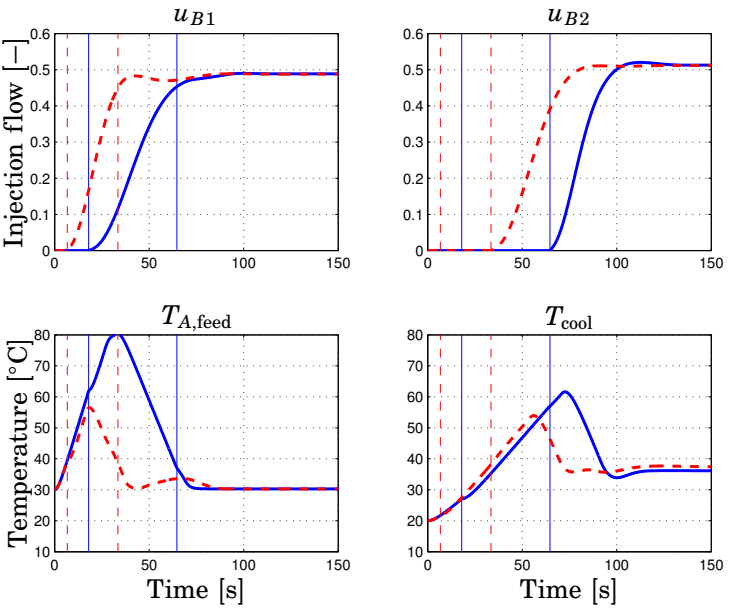

Figure 7.8 Optimal start-up trajectories for the four control inputs. Solid line represents the case when $T_1^{\text{start}} = 55°\text{C}$ and the dashed line represents the case when $T_1^{\text{start}} = 35°\text{C}$. The vertical lines indicate the first two mode changes.

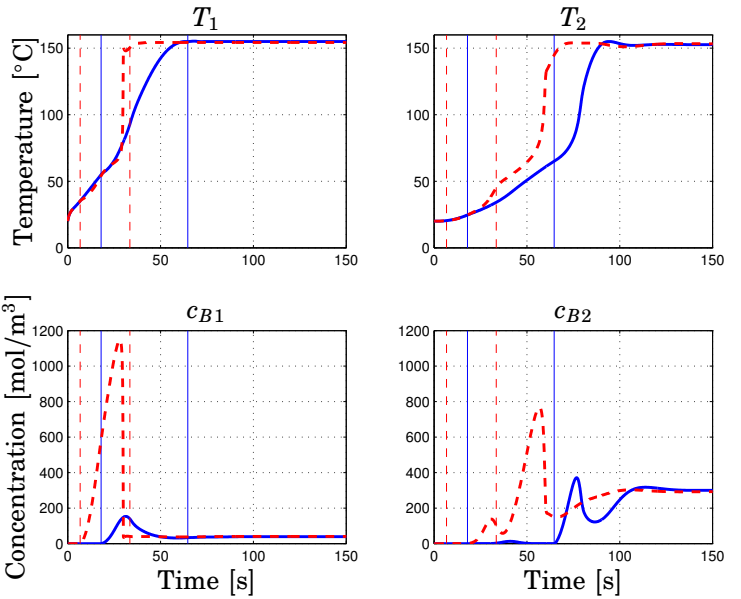

Figure 7.9 Optimal start-up trajectories for some process states. Solid line represents the case when $T_1^{\text{start}} = 55°\text{C}$ and the dashed line represents the case when $T_1^{\text{start}} = 35°\text{C}$. The vertical lines indicate the first two mode changes.

through the reactor and the concentration of B increases. Eventually, the reaction ignites and the temperature increases very quickly to the maximum value at 155°C and almost all B that is being injected is now consumed, thus decreasing c_B. As indicated in Figure 7.7, this start-up trajectory will be very sensitive to model uncertainty.

If the transition conditions are higher, the feed temperature needs to be further increased to fulfill the condition. When the temperature T_1 passes 55°C, the feed of B begins and almost all of the B being injected is also consumed directly after injection. The concentration levels remain very low. This leads to a smoother temperature response. The only disadvantage with the higher transition conditions is the somewhat longer time start-up time[2], 117 seconds compared to 102 seconds when using lower transition conditions.

Figures 7.8 and 7.9 show the optimal start-up trajectories for the nominal process model. In Section 7.7, we will investigate the robustness of the closed loop system for the different start-up trajectories in the presence of plant/model mismatch.

7.6 Feedback Control of the Reactor Temperature

Even though the trajectories of the hybrid controller are computed to ensure that the *ignition* condition and the *conversion* condition are satisfied, feedback control of the reactor temperature is necessary to satisfy the temperature constraints in presence of uncertainty. In addition, the integral action of the temperature feedback controllers ensures that the transition points defined in the hybrid controller are reached, to enable the switch to next mode.

Figure 7.5 shows the block diagram of the hybrid start-up controller. For a given mode, the off-line computed temperature references r are sent to the feedback controller C. The off-line computed control inputs u^{ff} are added as feed forward terms to the feedback control input u^{fb}. The sum of the feedback part and the feed forward part is sent to each actuator subsystem, to achieve the desired feed injection flow, feed temperature or cooling temperature. The superscript 'sp' in Figures 7.10-7.12 denotes the set-point value for the actuator subsystem.

During mode 1, there is no feed of reactant B. Figure 7.10 shows the straight forward temperature feedback implementation, where $T_{A,\text{feed}}$ is manipulated to track T_1^{ref} and T_{cool} is manipulated to track T_2^{ref}. The feed inputs u_{B1} and u_{B2} are fixed to zero.

[2]The start-up time is here defined as the time to reach a conversion of reactant A of 98% at the reactor outlet.

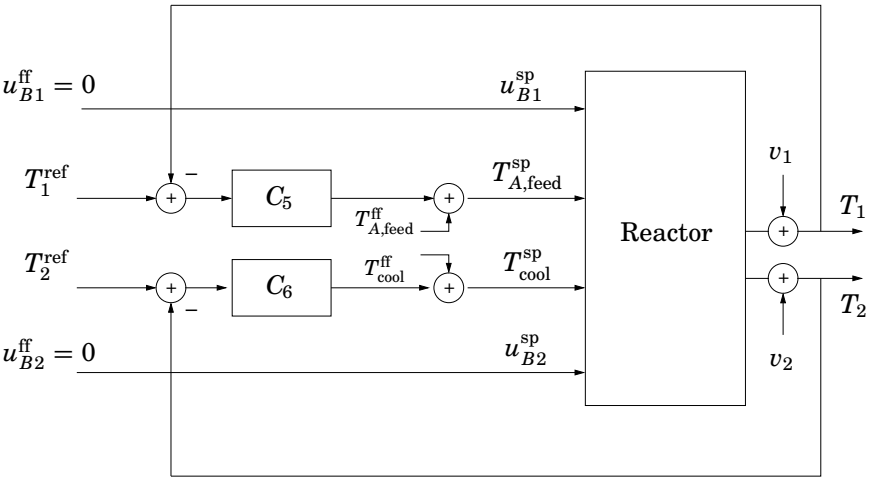

Figure 7.10 Block diagram for the feedback control during mode 1. The reactor temperatures T_1 and T_2 are controlled by manipulating the feed temperature $T_{A,\text{feed}}$ and the cooling temperature T_{cool}. No injections are allowed in this mode, hence $u_{B1}^{\text{ff}} = u_{B2}^{\text{ff}} = 0$.

During mode 2, reactant B is fed at the first injection point and the feedback control structure is changed to Figure 7.11. Similarly to the feedback control structure in Chapter 6, u_{B1} is manipulated to track T_1^{ref}, since u_{B1} has faster input dynamics and larger gain to T_1 than $T_{A,\text{feed}}$. In addition, a mid-ranging control loop manipulates $T_{A,\text{feed}}$ so that u_{B1} can converge to u_{B1}^{ff} in steady state, thus achieving stoichiometric conditions, see also Section 6.5. For more details on mid-ranging control, see Chapter 9. There is still no feed of B into the second injection point in mode 2, thus the reactor temperature remains controlled by the cooling temperature T_{cool}.

During mode 3 and 4, reactant B is being fed at both injection points and the feedback control structure is switched to Figure 7.12, which is identical to the one in Section 6.5.

The tuning of the parameters for the PID-controllers are based on the AMIGO method, which involves robust loop-shaping and maximization of the integral gain [Åström and Hägglund, 2005]. The models used in the control design are linearizations of the nonlinear model at the transition point at the end of each mode. For example, for the u_{B1}-controller in mode 2, the process is linearized at the end of mode 2 when $T_1 \approx 145°\text{C}$. From the start of mode 2 to end of mode 2, the steady-state gain from u_{B1} to T_1 varies from 44 to 262, due to the nonlinear reaction rate. To reduce the interaction between the fast (here C_1 and C_2) and the slow (here C_3

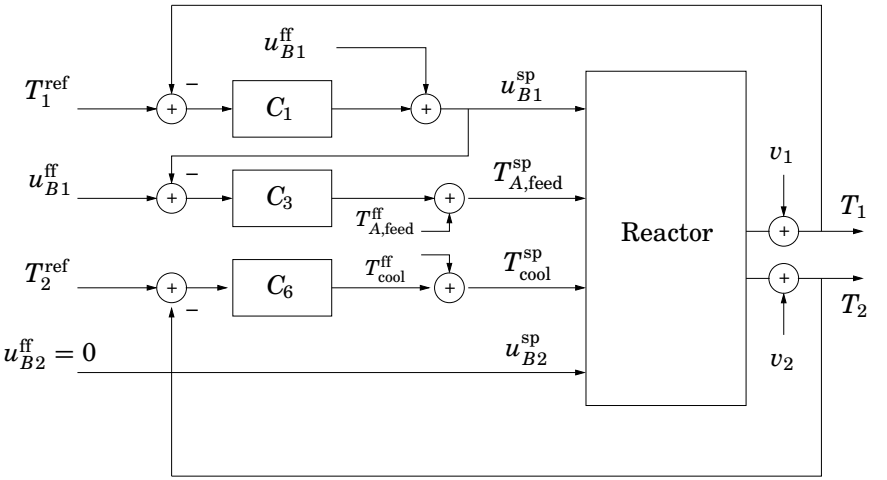

Figure 7.11 Block diagram for the feedback control during mode 2. The feed of B into the first injection point has begun. T_1 is controlled by manipulating the injection feed and T_2 is still controlled by the cooling temperature.

and C_4) control variables in the mid-ranging control structure, the slow control loops are designed to have a closed loop bandwidth that is an order of magnitude smaller.

7.7 Simulation of Hybrid Start-up

Simulation with Model Mismatch

To illustrate the robustness of the start-up controller, a simulation is performed with some plant/model mismatch, E_a 2% higher, ΔH 5% higher, k_0 5% lower and h 10% lower than in the nominal model, see Table 5.1. The set of higher transition conditions (7.3) is used, i.e., $T_1^{\text{start}} = 55°\text{C}$, $T_2^{\text{start}} = 65°\text{C}$, $T_1^{\text{conv}} = 145°\text{C}$ and $T_2^{\text{conv}} = 145°\text{C}$.

Figures 7.13 and 7.14 show the start-up sequence. The reactor temperature starts at 20°C. During the first mode, the aim is to pre-heat the feed flow so that $T_1 \geq T_1^{\text{start}} = 55°\text{C}$, see the transition conditions in Figure 7.4. The vertical lines indicate the mode changes. When the second mode becomes active, injection of reactant B starts in the first injection point and the reactor temperature quickly increases. When $T_1 \geq T_1^{\text{conv}} = 145°\text{C}$ and $T_2 \geq T_2^{\text{start}} = 65°\text{C}$, the two transition conditions are satisfied and the hybrid controller switches to mode 3. Reactant B flows into the sec-

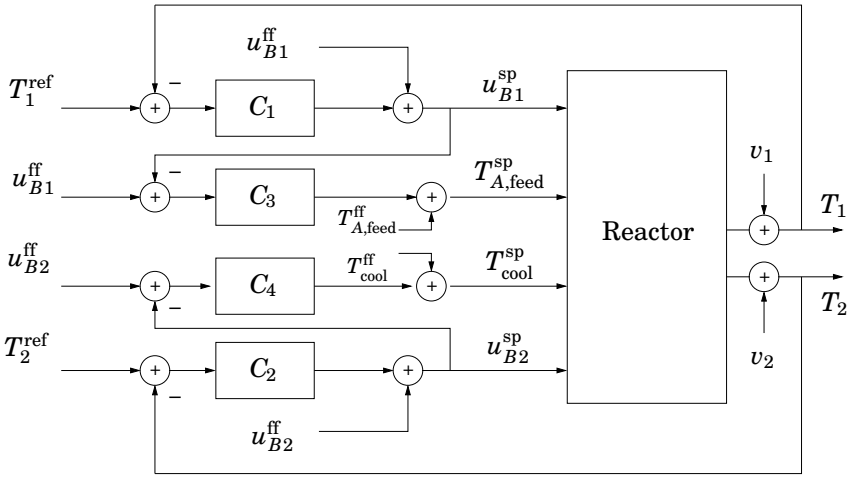

Figure 7.12 Block diagram for the mid-ranging feedback control system during mode 3 and 4. Reactant B is now being fed into the second injection point as well. The reactor temperatures are controlled by the injection flows.

ond injection point, increasing T_2. When T_1 and T_2 passes 145°C, mode 4 begins.

The uncertainties in E_a and k_0 lead to higher temperature required for the reaction to start, but when the reaction is ignited, the higher ΔH leads to more energy being released, thus leading to higher temperatures than in the nominal model. Before the reaction ignites in mode 2, the reactor temperature is slightly lower than the reference, thus the feedback controller increases the injection flow. After the ignition, the model mismatch gives higher heat release, which forces the controller to quickly reduce the injection flow. A similar pattern is seen in mode 3, when the reaction ignites at the second injection point. The mid-ranging effect is clearly seen during mode 4, when $T_{A,\text{feed}}$ and T_{cool} are slowly manipulated so that the injection flows u_{B1} and u_{B2} can converge to their feed forward signals, thus ensuring stoichiometric conditions.

The transition points can be viewed as constraints in the state space to avoid areas where the process nonlinearities are very large. This will also lead to a reduced sensitivity of the trajectories to uncertainties. It is therefore easier for the PID controllers to successfully track the given reference temperatures from the hybrid controller despite uncertainties. The next step is to verify the robustness of the closed loop system for any arbitrary plant/model mismatch within the uncertainty set.

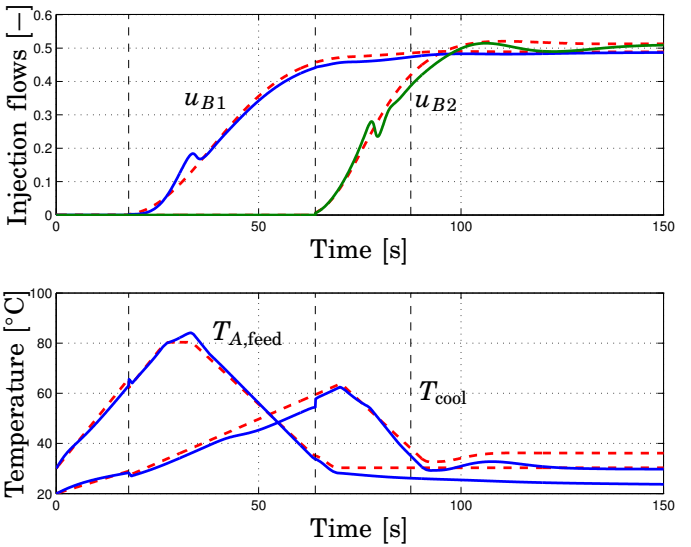

Figure 7.13 Setpoint signals (solid) from the feedback controller to the actuator systems during start-up. The dashed trajectories represent the feed forward signals from the hybrid controller. The vertical lines indicate the mode changes. Note the mid-ranging effect, where $T_{A,\text{feed}}$ and T_{cool} are manipulated so that the injection flows can converge to their feed forward signals.

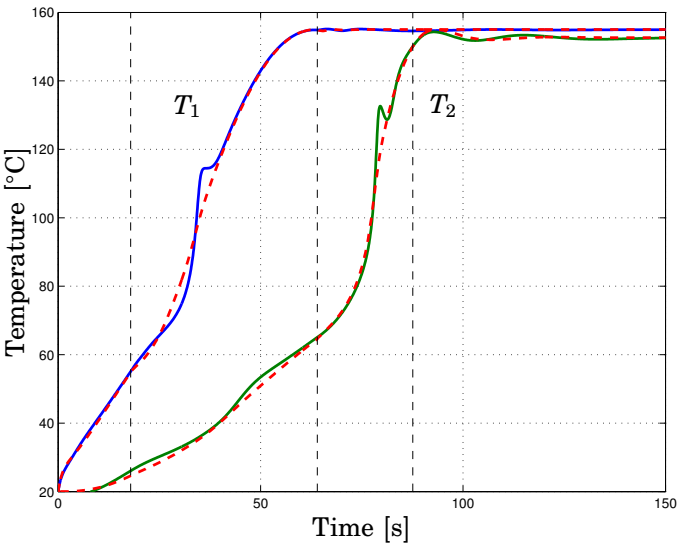

Figure 7.14 Reactor temperatures (solid) during start-up with perturbed model parameters. The dashed curves represent the offline optimized reference temperatures to the PID controllers. The vertical lines indicate the mode changes.

Monte-Carlo Simulations

The simulation in the previous section, showed the closed loop response for a particular set of model mismatch. In this section, the robustness of the closed loop system is further evaluated by means of Monte Carlo simulations. Three different cases are investigated.

Case 1: Feedback control disabled, optimal trajectories computed for the higher transition conditions, $T_1^{\text{start}} = 55°\text{C}$, $T_2^{\text{start}} = 65°\text{C}$.

Case 2: Closed loop control, optimal trajectories computed for the higher transition conditions, $T_1^{\text{start}} = 55°\text{C}$, $T_2^{\text{start}} = 65°\text{C}$.

Case 3: Closed loop control, optimal trajectories computed for the lower transition conditions, $T_1^{\text{start}} = 35°\text{C}$, $T_2^{\text{start}} = 45°\text{C}$.

For each case, 5000 simulations were carried out and in each simulation the values of the model parameters $E_a, \Delta H, k_0$ and h were randomly generated from a uniform distribution, based on the uncertainties in Table 5.1. The closed loop system was simulated and the reactor temperatures at the injection points are recorded. Then a new sample of the uncertain parameters is generated and the whole procedure is repeated. The same controller parameters are used for the two closed loop simulations.

To visualize the sensitivity of the start-up trajectories to the uncertainties, envelope curves were constructed, see Figure 7.15. They show the minimum and maximum temperature at the two injection points among the 5000 simulations for each sample time t. The horizontal line indicates the safety limit of 160 °C. Any temperature above this may lead to safety shut-down to avoid damage to the reactor. A larger area between the minimum and maximum temperature indicates a higher variation in reactor temperature due to insufficient robustness to the model mismatch.

The top plots show the open loop response, when the off-line computed control inputs are directly applied to the process. T_1 will vary between 145 and 165°C. The uncertainties have even larger impact on T_2, where the trajectories vary from 49 to 171°C. This means that for some parameter sets, the reaction never reaches ignition and the intended operating point, while for some parameter sets the temperature violates the constraint. There is a clear need for feedback control to handle the effects of the uncertainties.

The middle plots show the closed loop response when higher transition conditions are enforced. The envelope curves show that the maximum and minimum temperature of T_1 almost coincide, that is, the variation of the temperature due to the model mismatch is very small. At the second injection point, the variation is larger, but still within a narrow bound. The higher transition points leads to optimal start-up trajectories with reduced

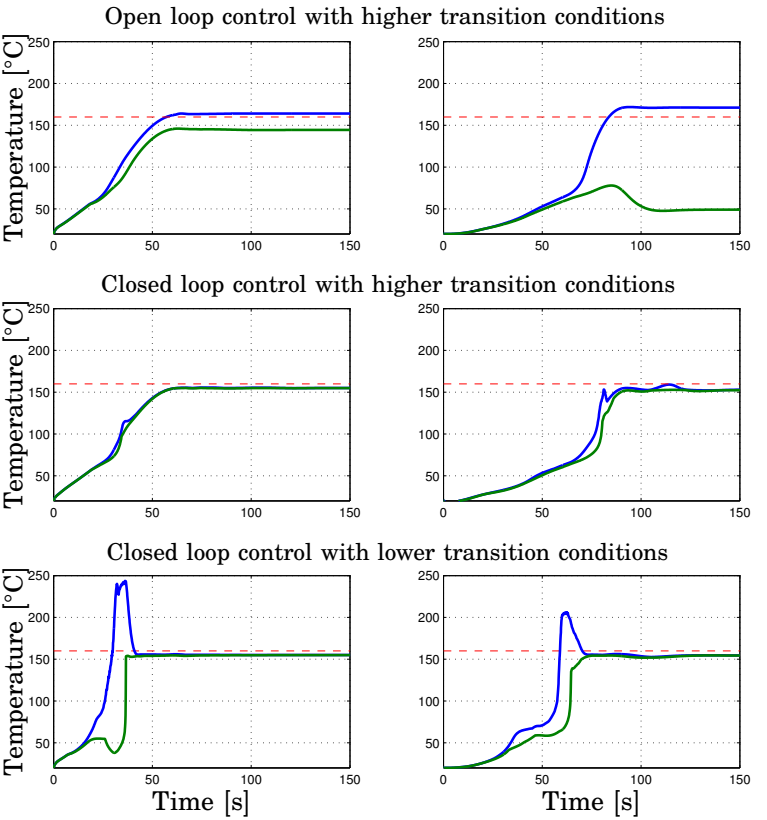

Figure 7.15 Maximum and minimum reactor temperatures at the reactor temperatures T_1 (left plots) and T_2 (right plots) for the 5000 Monte Carlo simulations.

sensitivity. This allows the feedback controller to successfully keep the reactor temperature below 160°C, despite the uncertainties.

The bottom plots show the closed loop response when the lower transition conditions are enforced. In this case, the feed injections are started earlier and the start-up trajectories are much more sensitive to the model mismatch. The feedback controller can not track the given reference temperatures due to its limited bandwidth. In fact, the situation is worse with feedback compared to the open loop case, since the feedback controller has large difficulties when the effect of the model mismatch changes sign after the reaction ignition. For some plant/model mismatch, the reactor temperatures increase above the safety limit, which may lead to an emergency shutdown.

To summarize, feedback control is necessary due to the model mismatch. Feedback control can in general handle effects of uncertainty and disturbances, but when the uncertainties are combined with large nonlinearities and limited control inputs, the feedback can actually lead to degraded performance. Therefore, it is necessary to consider the sensitivity of the start-up trajectory to model-mismatch when computing the hybrid controller. It is clear that transition points that require higher reactor temperatures before feed injections are allowed, lead to more robust trajectories, thus improving the robustness of the closed loop system.

7.8 Summary and Conclusions

In this chapter, the objective has been to improve the robustness of the closed loop system, by computing reference trajectories bringing the process to the nomial operating point through specified transition points. The transition points should be chosen so that the resulting start-up trajectory has low sensitivity to uncertainties. The simulations in this and the previous chapter have been carried out with standard PID controllers. It is possible to replace the PID controllers with any kind of controller from robust control theory, however, the focus here has been on deriving methods to generate start-up trajectories that will simplify the task of the feedback controller.

To achieve safe and robust start-up, the start-up sequence is divided into several steps and each step is associated with a transition condition that needs to be satisfied to allow the start-up to continue. This event-driven start-up improves the robustness to uncertainties and disturbances as it forces the process to be in a certain state-space area before the next start-up step is initiated. For example, no injections should be allowed before the reactor temperature is high enough to allow safe ignition. The choice of transition points has a significant influence on the sensitivity of the start-up trajectory. Monte-Carlo simulations confirm that higher transition conditions lead to less sensitive solutions. Closing the loop and use of PID control during start-up increases the robustness, but closing the loop for the reference trajectories as in Figure 7.5 improves the robustness even further.

7.9 Comparison between Start-up Methods

This section will compare the hybrid start-up approach developed in this chapter with the start-up method developed in Chapter 6, where the entire

start-up trajectory was optimized in one step, hereafter referred to as the continuous approach.

Design

As stated before, the start-up control problem is challenging for three reasons, process uncertainty, highly nonlinear dynamics and input saturations. The dynamics and the saturations can be described with a process model. The uncertainty is considered by analyzing the sensitivity of the off-line computed start-up trajectories. The sensitivity of the start-up trajectories was reduced in both methods by enforcing some kind of path constraints in the state-space and introducing penalties on the use of the control variables. The Monte Carlo simulations, see Figures 6.15 and 7.15, indicate that the reduced sensitivity of the trajectories decreases the effect of the plant/model mismatch and the feedback controller can much easier stabilize the system along the intended start-up trajectories.

In the continuous approach, the constraints were defined as upper bounds on the reactant B concentration. In the hybrid approach, the start-up trajectory has to pass through certain transition points, here defined in terms of reactor temperatures.

Figure 7.16 shows the start-up trajectories plotted in the state-space plane of reactor temperature T_2 and concentration c_{B2} at the second injection point. The trajectories start at lower left at $T_2 = 20°\text{C}$ and end at $T_2 = 155°\text{C}$. In the continuous approach, the injection of B is initiated at $t = 0$. Due to the very low reactor temperature and reaction rate, the injected B is not consumed and the concentration increases until it hits the concentration constraint imposed by the optimization. Three different constraint levels are plotted, $c_{B2} \leq 400, 800$ and $1200\ \text{mol/m}^3$, respectively. The reactor temperature is increased by warmer feed, less cooling and heat from the reaction flowing downstream from the first injection point. Eventually, the temperature, thus also the reaction rate, is so large that the concentration of B decreases and leaves the constraint.

In the hybrid approach, no injections are allowed until the reactor temperature has reached the transition point, $T_2^{\text{start}} = 65°\text{C}$ and $T_2^{\text{start}} = 45°\text{C}$, respectively. By postponing the feed injection until the temperature is higher, the reactant B can be fed into the reactor more safely, meaning that the reaction rates are high enough to sustain the reaction. This avoids accumulating large concentrations of B, which otherwise would increase the sensitivity to uncertainties. The small transients in the two hybrid start-up trajectories before the transition points are passed depends on unconsumed B flowing downstream from the first injection point. For the lower transition conditions, a larger amount of unreacted B passes the second injection point compared to the trajectory with the higher transition conditions.

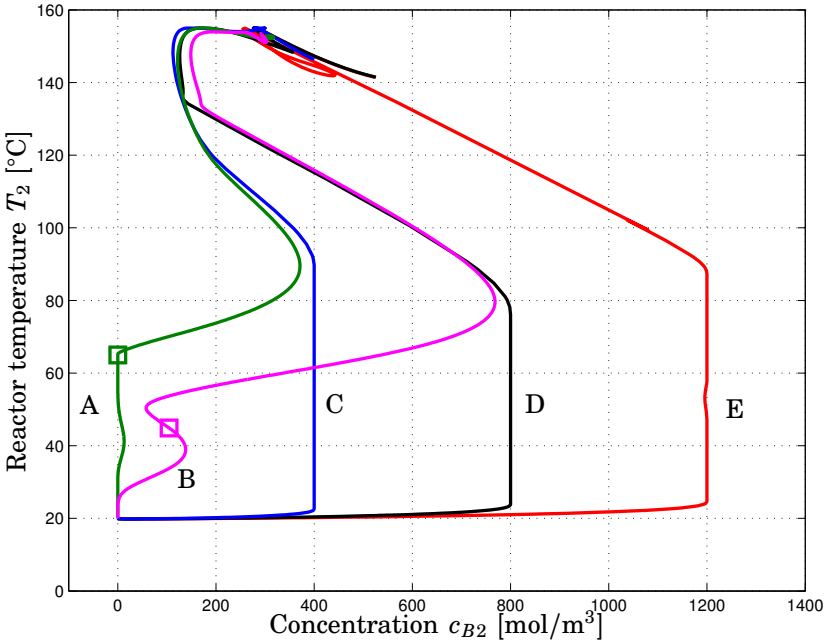

Figure 7.16 A state trajectory plot of the concentration of B and the temperature at the second injection point during start-up. From left to right, the trajectories are with hybrid start-up $T_2^{\text{start}} = 65°\text{C}$ (line A), hybrid start-up $T_2^{\text{start}} = 45°\text{C}$ (line B), continuous approach with the constraint $c_{B2} \leq 400$ mol/m^3 (line C), $c_{B2} \leq 800$ mol/m^3 (line D) and at the far right the trajectory when $c_{B2} \leq 1200$ mol/m^3 (line E) is plotted. Note the squares at $[c_{B2}, T_2] = [0,\ 65]$ and $[c_{B2}, T_2] = [105,\ 45]$, which represent the transition points $T_2^{\text{start}} = 65°\text{C}$ and $T_2^{\text{start}} = 45°\text{C}$, respectively.

In addition to the path constraints, the sensitivity of the start-up trajectories was reduced by introducing standard penalties on the control inputs in the cost function of the optimization. This was particularly important to achieve a well-behaved response when the reactor temperatures approach the limit at 155°C.

Implementation

With the continuous approach, the off-line computed trajectories are sent to a feedback controller to be used as references and feed forward signals, see Figure 7.6. The trajectories are time-driven and the solution relies on the feedback controller to keep the temperatures close to the references.

With the hybrid approach, the trajectories for each mode are functions

of time, but the transition between each mode is associated with a transition condition, here defined in temperature. This yields an event-driven start-up, see Figure 7.5. It may of course be possible to implement the off-line computed trajectories of the hybrid approach as functions of time as in Figure 7.6, but that would remove the valuable feedback from the event-based transition points.

Conclusions

To summarize, there are advantages for both approaches.

Advantages for the continuous approach

- Slightly faster start-up time, as injections may begin at $t = 0$.
- The implementation is simpler with the same feedback control structure during the entire start-up.
- The setup of the optimization problem is easier, using the same model and control inputs during the entire start-up.
- The concentration constraint is a more efficient way to introduce path constraints in the optimization problem, to avoid areas in the state-space with large sensitivity.

Advantages for the hybrid approach

- Transparent strategy, start one injection at a time, easier to get operator acceptance.
- The event-driven implementation avoids injection before safe ignition temperature has been reached.
- It may be easier to define the path constraints in terms of temperature conditions than defining concentration constraints.
- When the reactor is pre-heated before any injection may start, less unreacted chemicals exit the reactor. This reduces the risk of unexpected heat release from the reaction in storage tanks downstream.

In the comparison, it is worth noting that the transition condition defines the temperature at which injection may begin, whereas the concentration constraint gives a very natural limit to how fast the injection may increase. The best option may then be to combine them, that is, using the hybrid approach, but including concentration constraints in the optimization formulations.

8

The Utility System: Design, Control and Experiments

In this chapter, the utility system for the plate reactor will be presented and controlled. The utility system is a general purpose hydraulic and thermodynamic system that can deliver water to the cooling plates of the plate reactor, thus enabling accurate temperature control. Within the work of this thesis, it has been used as a cooling system and is therefore referred to as either cooling system or utility system.

In Section 8.1, the process design phase is presented. In Section 8.2 the mid-ranging control structure is presented. The control design and tuning is discussed in Section 8.3. The experimental set-up at Alfa Laval AB in Lund is presented in Section 8.4. In Section 8.5 the controller hardware equipment is briefly presented. Disturbances during the experiments are discussed in Section 8.6. The experimental results are shown in Section 8.7 and some concluding remarks on the utility system are summarized in Section 8.8.

8.1 Hydraulic and Thermodynamic Design

To get the desired flow rate and temperature of the cooling water into the cooling plates of the plate reactor, a utility system has been designed and tested. The hydraulic and thermodynamic design was done by Rolf Christensen at Alfa Laval AB in Lund. Three different flow configurations have been tested. Common for all three is that an external heat exchanger is used. The main reason is that the cooling water, entering from the left in Figure 8.1, may be polluted and lead to fouling inside the plate reactor. The external heat exchanger allows a closed hydraulic system for the cooling water of the reactor and the heat exchanger can easily be disconnected and removed for cleaning.

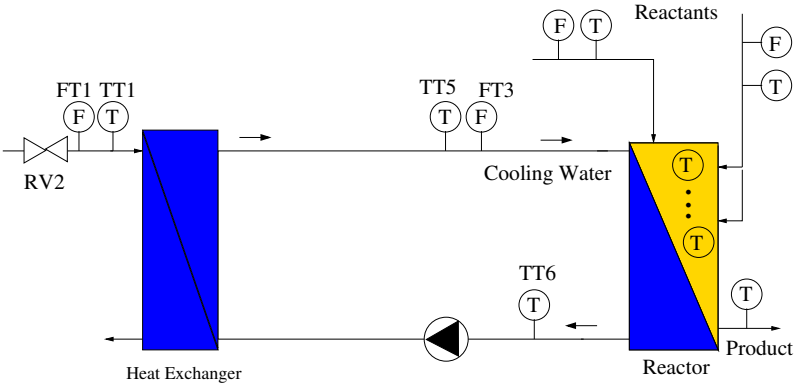

Figure 8.1 Flow configuration 1 with an external heat exchanger to prevent polluted water entering the plate reactor and cause fouling.

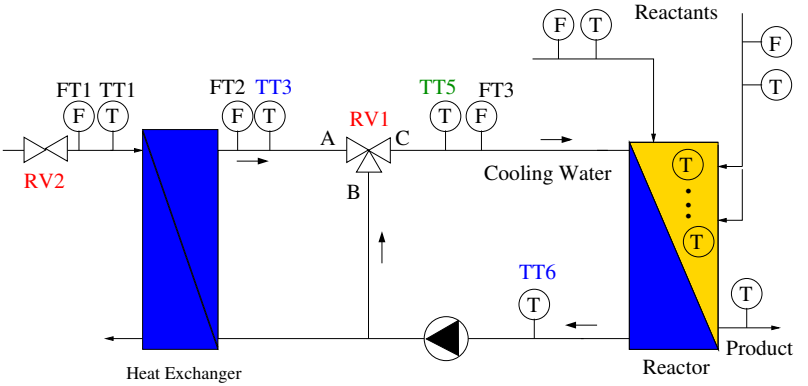

Figure 8.2 Flow configuration 2 with a three-way control valve

The first and simplest version is a single flow loop with an external heat exchanger HEX, where the cooling inlet temperature $TT5$ is controlled by varying the flow rate $FT1$ on the left side of HEX, see Figure 8.1. There are several disadvantages with this design. First, there is rarely a need to cool the entire water flow due to the limited heat generation in the plate reactor compared to needs in an emergency, for which the heat exchanger has to be designed. Secondly, there is some thermal inertia inside the heat exchanger, which increases the dynamics between input and output.

The second alternative is a system with variable recycle of the cooling flow from the outlet of the plate reactor, directly to port B of the control valve RV1, see Figure 8.2. With a three-way control valve, the appropriate

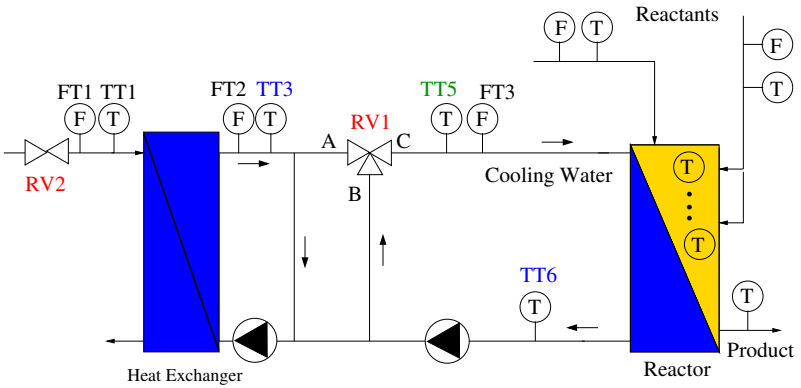

Figure 8.3 Flow configuration of the cooling system with recycle loops around the heat exchanger (HEX) and the plate reactor. Note that the control signals v_1 and v_2 corresponds to the positions of control valves RV1 and RV2. The cooling water temperature $TT5$ is the controlled output.

cooling temperature $TT5$ can be reached by mixing water with the two temperatures $TT6$ and $TT3$. One part of the flow will go to the control valve RV1 directly, the other part will pass through the heat exchanger HEX and then to the control valve. The response of this configuration is faster than for the first alternative, thus facilitating the temperature control. The flow through the heat exchanger will be varying, entirely depending on the valve position RV1 and will always be lower than $FT3$. The varying flow rate will increase the nonlinearity of the system and the low flow rate of $FT2$ will increase the sensitivity of $TT3$ to disturbances in $FT1$.

The third alternative is seen in Figure 8.3, where another recycle loop is introduced around the heat exchanger HEX. Two pumps are needed compared to one pump in the two first alternatives, but with this set-up, the flow rates through the heat exchanger and the cooling plates are almost constant, regardless of valve position. Here, the possible flow rate through the heat exchanger is more flexible, so the heat exchanger can be used more adequately. With a higher flow rate of $FT2$ the heat exchanger is also less sensitive to disturbances in $FT1$.

This flow configuration is common in for example heating systems for houses and in pasteurization units for food applications, [Petitjean, 1994]. The recycles give a fast and less sensitive system, but one should be careful when introducing recycle in the process, since it can lead to large changes in the process dynamics, [Morud and Skogestad, 1996]

Modeling of the Utility System

To better understand how the cooling system works, an energy balance is derived around the control valve RV1.

$$(q_{AC} + q_{BC})c_p\rho TT5 = q_{AC}c_p\rho TT3 + q_{BC}c_p\rho TT6 \tag{8.1}$$

$$TT5 = \frac{q_{AC}}{q_{AC} + q_{BC}}TT3 + \frac{q_{BC}}{q_{AC} + q_{BC}}TT6 \tag{8.2}$$

where q_{AC} is the flow rate through valve port A and q_{BC} through port B, see Figure 8.3. Note that this is a simple mixing process with two flows of different temperatures.

Now define the flow ratio as the amount of flow through the control valve port A divided by the flow through port C, which is the sum of the flows through port A and B.

$$\beta = \frac{q_{AC}}{q_{AC} + q_{BC}} \tag{8.3}$$

β can take values from 0 to 1, where 0 corresponds to port A being fully closed and 1 to port B being closed.

The temperature TT5 that should be controlled is then given by

$$TT5 = (TT3 - TT6)\beta + TT6 \tag{8.4}$$

where β can be seen as the manipulated variable. From Eq. 8.4 we see that the process gain is varying depending on the temperatures in the utility system and that the gain is negative, since $TT6 > TT3$ (if the utility side is cooling the reactor). Remember that we have here neglected the very fast valve dynamics and the short transport delay from valve to sensor.

Apart from the feedback signal from $TT5$, the controller could use measurements from $TT6$ and $TT3$ in a feed forward term to improve its response to disturbances. So far experiments have shown that feedback alone can deal with variations in $TT6$ and $TT3$ very well, see Figure 8.13.

Before the construction of the experimental unit, a more systematic model of the utility system was derived to learn more about the system, what the limitations were and the dynamics of the system. The thermodynamic and hydraulic equations were derived for each component such as pumps, control valves, adjustment valves and a simple heat exchanger model. The model was implemented in Modelica and simulated in Dymola, see [Modelica Association, 2005] and [Dynasim, 2001]. The utility system

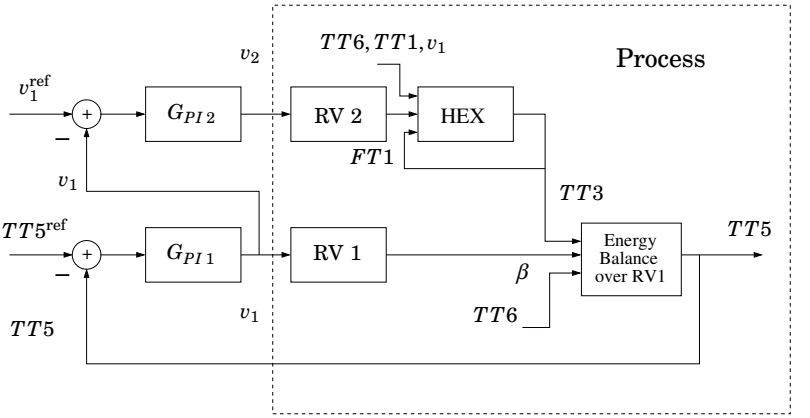

Figure 8.4 Mid-ranging control structure of the utility system. PI-controller G_{PI1} controls the cooling inlet temperature $TT5$ and G_{PI2} acts so that v_1 may operate around a desirable working point specified by v_1^{ref}.

model was then connected to the plate reactor model from Chapter 3 in order to simulate the combined system. After the experiments had been carried out, the model was verified and re-tuned with the experimental data, in terms of time constants of the valves and the thermal inertia.

8.2 Mid-ranging Control Structure

The cooling temperature $TT5$ should follow the reference temperature $TT5^{\text{ref}}$. The main control signal v_1 of the temperature controller is the desired position of the control valve RV1. The valve opening gives the flow ratio β, i.e. how much of the flow that goes through port A divided by the total flow through port C, see Figure 8.3. The second control signal v_2 is the position of control valve RV2, which indirectly controls the temperature $TT3$. By combining the two control signals in a mid-ranging control structure, see Figure 8.4, the cooling temperature $TT5$ can be controlled, and the extra degree of freedom is used to have the control valve RV1 work around some desired operating point, e.g. 50%, to avoid valve saturation.

The term mid-ranging refers to control problems where there are two control inputs and only one output to control, see e.g. [Allison and Ogawa, 2003] and [Allison and Isaksson, 1998]. Often the inputs differ significantly in their dynamic effect on the output, and the faster input is in some way more costly to use or closer to saturation than the slow one. In this case, the fast input is v_1, affecting $TT5$ with the fast dynamics of control valve RV1, while the second control valve RV2 has the same

valve dynamics, but the control action also passes the dynamics of the heat exchanger HEX and some transport delays, which makes v_2 a slower input than v_1.

The mid-ranging idea is to have the fast input v_1 controlling the process output, and to use the effect of the slower input v_2 to gradually reset or mid-range v_1 to its desired value v_1^{ref}. Thus v_2 indirectly acts to prevent saturation in v_1 and also to control the process mainly using the "cheaper" v_2 in stationarity. With the use of the second control input v_2, the operating range of the process is often considerably increased. The desired value of v_1^{ref} may be in the middle of its working range, 50%, to have margin for all kinds of disturbances, hence the name mid-ranging.

There are several advantages with the mid-ranging structure compared to the case when only RV1 is the manipulated input and RV2 has a constant value, giving a constant cooling flow rate $FT1$. First, the operating range of the utility system is largely increased and valve saturation can be avoided. Second, the performance can be increased for large set-point changes. Third, the utility system will be less sensitive to external disturbances. The disadvantage is that effect of v_2 may be seen as a slow load disturbance to v_1, which may delay the convergence to steady-state. This can be avoided by introducing a feed forward signal from v_2 to v_1, see [Åström and Hägglund, 2005].

Another way to see mid-ranging control is how to combine two control inputs with different frequency contents. RV1 gives faster response in $TT5$, but have a small steady-state gain, which gives a small operating range. Whereas RV2 is slower, but with a much greater steady-state gain, giving larger operating range. In Figure 8.5, the Relative Gain Array (RGA) is shown for the two inputs and one output system. RGA may be used as an interaction measure to find suitable input/output pairings for multivariable systems. It may be computed for varying frequencies and different pairings may be preferred depending on the closed loop bandwidth. In Figure 8.5 we see that RV2 (dashed) dominates for low frequencies due to its large steady-state gain. For medium and high frequencies, which is the region where the closed loop bandwidth is, RV1 clearly dominates. However, instead of choosing either of these valves for control, the mid-ranging control technique coordinates *both* control valves to improve performance.

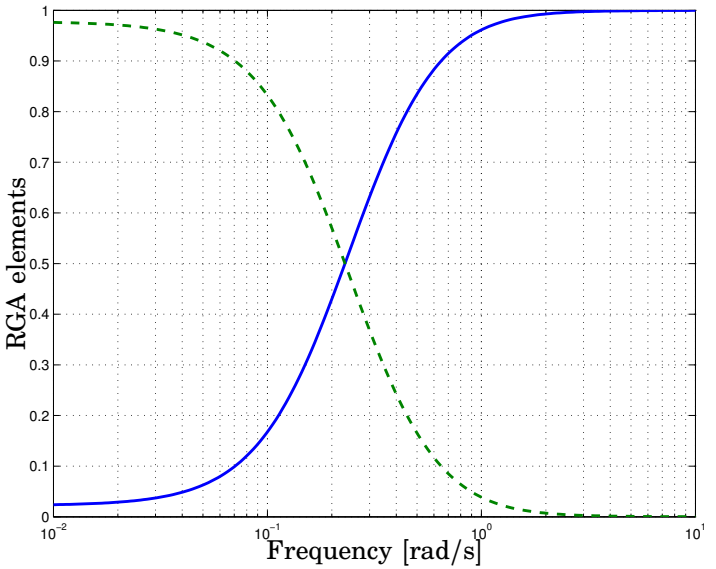

Figure 8.5 Relative Gain Array for the utility system when controlling the cooling temperature $TT5$ with valves RV1 and RV2. The control valve RV1 (solid) dominates for high frequencies, but for low frequencies RV2 (dashed) has greater impact on the cooling temperature.

8.3 Control Design and Tuning

Control Design

The nonlinear model of the utility system described in Section 8.1 and seen in Figure 8.4 is linearized and the corresponding block diagram can be seen in Figure 8.6. The cooling inlet temperature TT5 can for example be expressed as

$$TT5 = G_3 \begin{bmatrix} G_1 & G_2 \end{bmatrix} \begin{bmatrix} v_1 & v_2 \end{bmatrix}^T \tag{8.5}$$

where v_1 and v_2 are the two valve positions. G_1 represents the valve dynamics of RV1, G_2 represents the valve and heat exchanger dynamics and G_3 represents the mixing of the two water flows and the transport delay between valve and temperature sensor. Bode diagrams of the transfer functions from v_1 and v_2 to the cooling temperature $TT5$ can be seen in Figure 8.7. Note the distinctive differences in cross-over frequency and steady-state gain, which makes the system suitable for mid-ranging. The

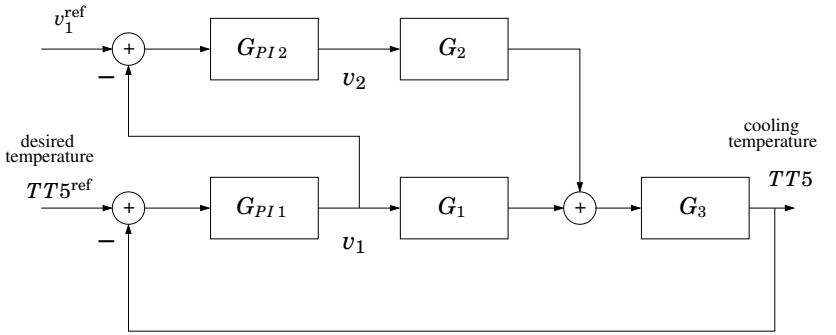

Figure 8.6 Mid-ranging control structure with transfer functions G_1 and G_2, derived from linearization of the utility model after experimental verification.

controllers G_{PI1} and G_{PI2} in Figure 8.6 are two PI-controllers with nonlinear gain to compensate for the nonlinear valve characteristics, see Figure 8.8.

First the nominal controller G_{PI1} is tuned to give good set-point tracking and load disturbance rejection performance. The controlled variable is the temperature of the cooling water $TT5$. We want $TT5$ to track a given reference value $TT5^{\text{ref}}$. It is controlled by manipulating the position of the control valve RV1. Mid-ranging control is then achieved by tuning G_{PI2}, so that v_1 can work around its reference value v_1^{ref}. G_{PI2} should be tuned to a slower response than G_{PI1} to avoid exciting cross-coupling effects.

Control Tuning

We start with a basic feedback PI-controller, see e.g. [Åström and Hägglund, 2005] and the control law

$$v^{\text{ref}} = K(TT5^{\text{ref}} - TT5) + \frac{K}{T_i}\int_0^t (TT5^{\text{ref}} - TT5)d\tau \qquad (8.6)$$

The controller sends a valve position reference, v^{ref}, to the control valve, which has an internal P-controller with a constant offset to reduce the steady-state error. The valve characteristics, that is, the flow ratio as a function of valve position $\beta = f(v)$, is a nonlinear function and should be compensated for. For constant pump speeds, the nonlinear relation has been experimentally measured, see Figure 8.8.

The valve process gains at the end positions are up to 10 times larger than the gain at the middle of the valve range. A controller with constant

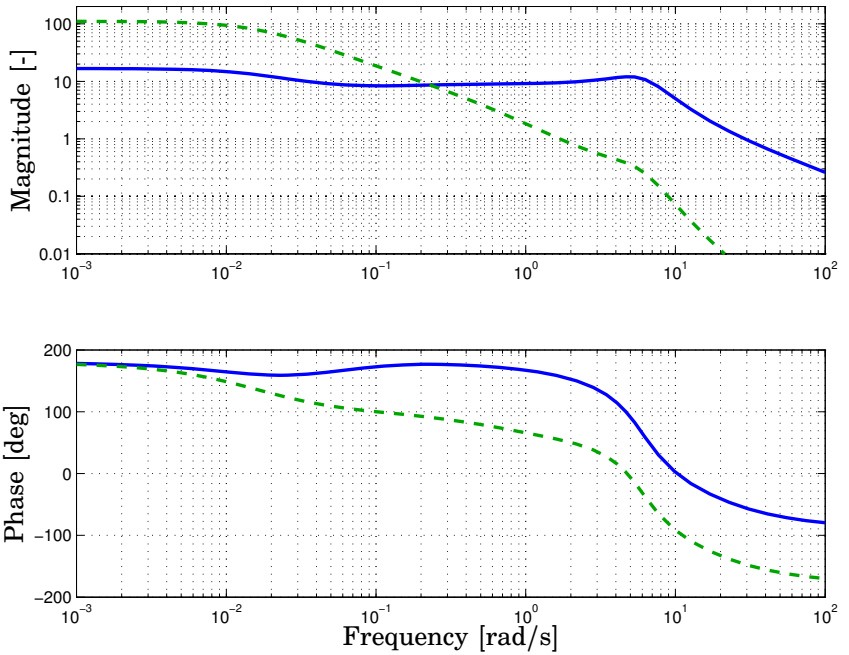

Figure 8.7 Bode diagrams of the transfer functions from v_1 (solid) and v_2 (dashed) to the cooling temperature $TT5$.

gain K would need to be tuned extremely conservative to be robust towards these large gain variations. With mid-ranging control, the effects of the nonlinear valve characteristics may be reduced, since the mid-ranging allows the control valve RV1 to operate around its linear range at 50%. We can also use the estimated valve characteristics from Figure 8.8 and include its inverse in the controller. The desired flow ratio β^{ref} is sent through the inverse of the valve characteristics to get the desired valve position v^{ref}. The inverse of the characteristics can be seen as a basic form of gain scheduling. The function from β to TT5 is now linearized, when we cancel the nonlinear effects from the valve with the known inverse. The control law becomes

$$\beta^{\text{ref}} = K(TT5^{\text{ref}} - TT5) + \frac{K}{T_i}\int_0^t (TT5^{\text{ref}} - TT5)d\tau \tag{8.7}$$

$$v^{\text{ref}} = f^{-1}(\beta^{\text{ref}}) \tag{8.8}$$

The PI-controllers can for instance be tuned using the λ-method, described in [Åström and Hägglund, 2005].

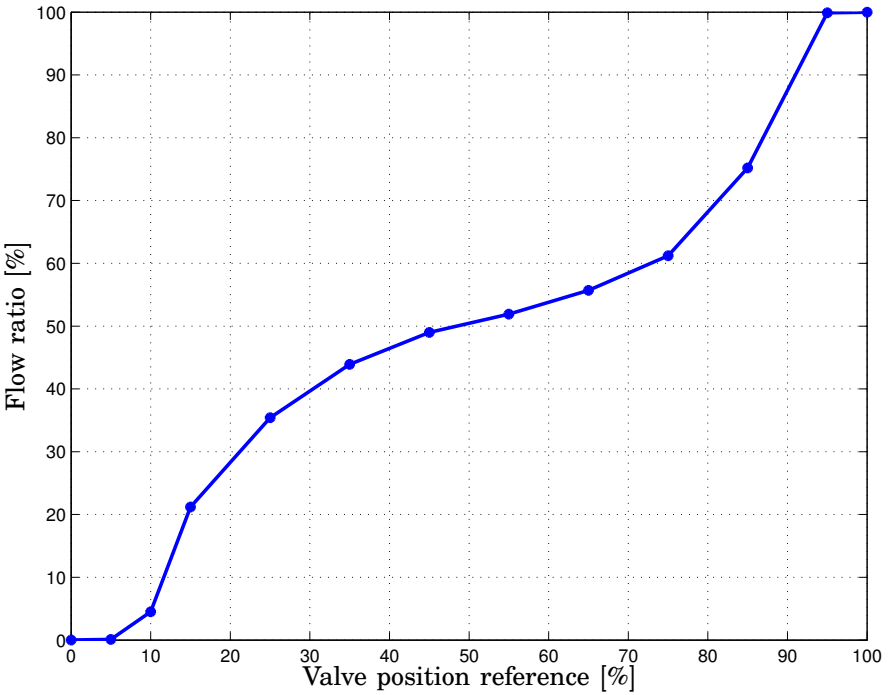

Figure 8.8 Valve characteristics, flow ratio as function of valve position

8.4 Experiments on the Utility System

Objectives with the Experiments

There were several objectives with the experiments. First, to verify the hydraulic and thermodynamic design of the utility system. Second, to analyze the coupling between the plate reactor and the utility system, including the sensitivity to disturbances. Third, to design a control system for the utility system and verify the performance.

The Experimental Set-up

An experimental set-up was constructed at the test lab of Alfa Laval AB in Lund. Rolf Christensen at Alfa Laval AB performed the hydraulic and thermodynamic design of the test unit, see Figure 8.9. Anders Håkansson at Adesign made the mechanical design. The test unit, see Figure 8.10, was assembled at Alfa Laval AB in Lund by local personnel. The electrical system was designed and installed by Pakon AB.

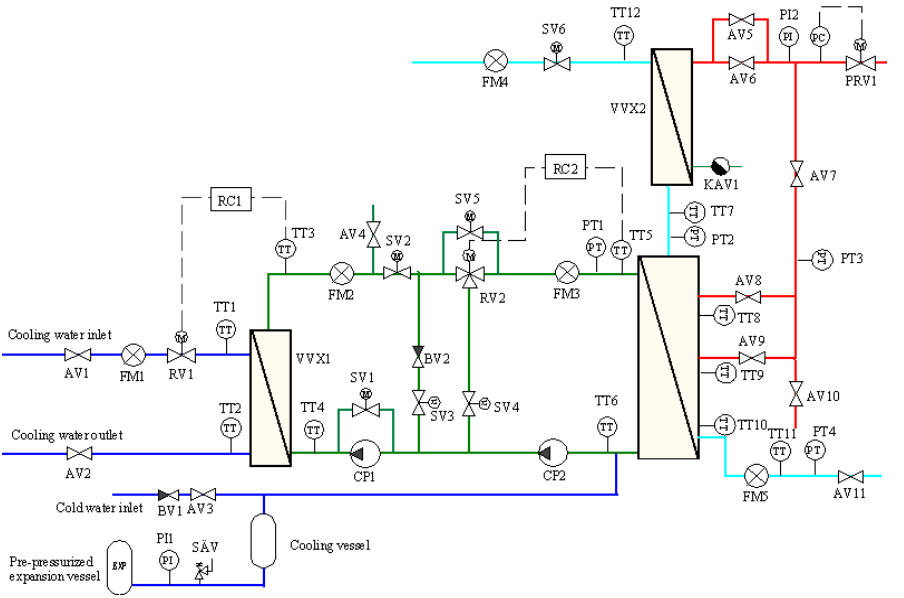

Figure 8.9 Experimental flow scheme. VVX1 is the external heat exchanger for the cooling water. VVX2 is an external heat exchanger to pre-heat the primary reactant.

The plate reactor was assembled with one reactor plate and two cooling plates, one on each side of the reactor plate. For the tests of the cooling system, it was sufficient to have a similar heat generation inside the plate reactor as from exothermic reactions. For simplification, instead of using chemical reactants giving exothermic reactions, water was used as reactant A and super-heated steam was used as reactant B. The steam is injected along the side of the plate reactor.

Methodology

The experiments were carried out in the test lab of Alfa Laval AB in Lund, Sweden. The test rig was extensively instrumented in order to monitor all important variables and properties of the system. The experiments were carried out in a specific order to ensure that all components had full functionality before the main tests were done. Every component was checked individually and every sub system was tested before it was used in the complete process. All experiments were carefully planned, in order to have full reproducibility of the experimental results. However, the manually operated steam system prevented exact and full reproducibility for some experiments. The steam injections have therefore been used mainly to get

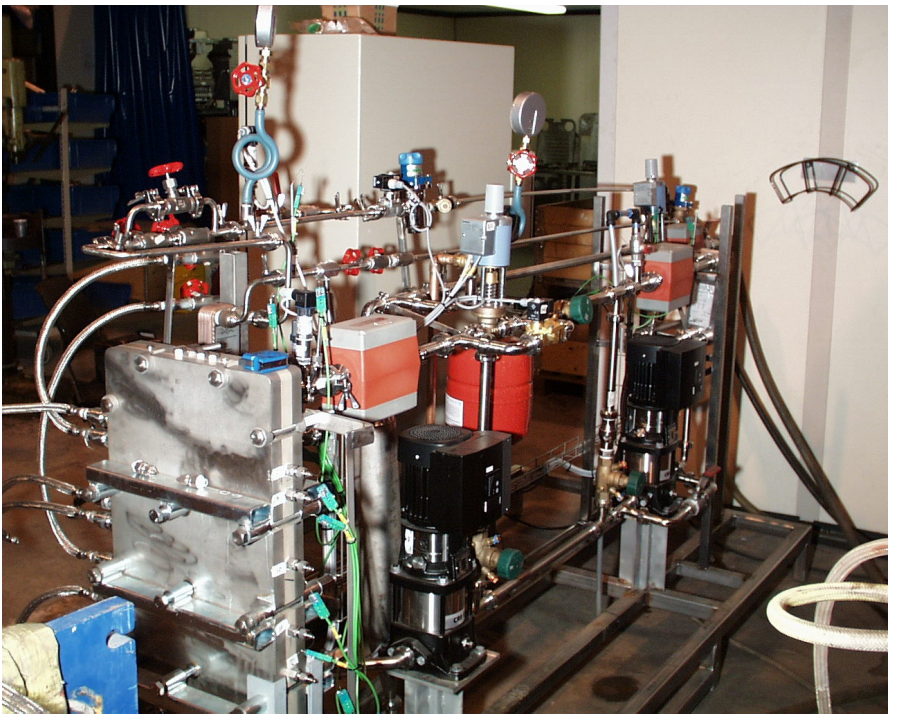

Figure 8.10 The experimental setup at Alfa Laval laboratory in Lund. The plate reactor is seen to the left and the utility system to the right. Note the injection pipes on the left side of the plate reactor and the thermocouples along the right hand side of the plate reactor.

a desired heat load inside the reactor to test the utility system and its control system. A full survey of existing disturbances was carried out, if possible to eliminate them and if not to be aware of them and take them into consideration during the experiments, see Section 8.11.

8.5 Control System Hardware

To have a large flexibility in performing the experiments, the test unit has two parallel independent control systems. With a simple switch the user can choose which control system to use for an experiment. The signals from each sensor are duplicated and sent to each of the control systems. The control systems then computes the appropriate actions, but only the output signals from the selected control system are sent to the control

valves and the pumps. The control systems will also have a process supervision task, which is connected to an automatic safety system.

The first control system is implemented by components from National Instruments and centered on their software package LabVIEW, [National Instruments, 2005]. The software enables easy configuration with their hardware components, such as data acquisition cards and analog output cards. The actual control algorithms and all process monitoring are done entirely in the LabVIEW software, thus giving high flexibility for testing new features without having to change any hardware.

The second control system is centered around an ECA controller from ABB with two PID control loops available, [ABB, 2000]. The system is hardware-oriented and functions and features are done with specific hardware components instead of programming it in software as in the LabVIEW system. This ABB-controller is a standard component in many industrial control systems, whereas the LabVIEW system is mostly found in laboratories or test stations.

All measurements are sent to a TopMessage logger from Delphin. The logger samples the 30 measurements with a sampling frequency of around 5 Hz. The logger sends the data to a PC through an OPC-server to the data acquisition program EasyView5 [Intab AB, 2005] from Intab AB.

8.6 Disturbances and Process Variations

Before the experiments were started, a rough analysis of potential disturbances was made. The plate reactor system has several input signals, all vulnerable to disturbances from the surroundings. The test rig was placed in the test lab of Alfa Laval in Lund, where many other experiments were carried out at the same time. All experiments take water from the central water system, which transfers possible disturbances from one experiment to another.

When a large pump is started anywhere in the lab, the pressure in the water system decreases for a very short moment. The process flow rate to the plate reactor, $FT4$, and the flow rate to the heat exchanger, $FT1$, are therefore also decreased for a short period of time. When the pump stops, the pattern is repeated but in opposite direction. When the pump actions are periodic, we get periodic disturbances in these signals, see Figure 8.11.

Another disturbance appears in the flow rate $FT4$ when high-pressured steam is injected into the reactor. The injected steam increases the pressure inside the reactor and decrease the flow rate $FT4$ as expected. However, the steam injection causes bubble formation and varying pressure inside the reactor, thus causing a disturbance and measurement noise in

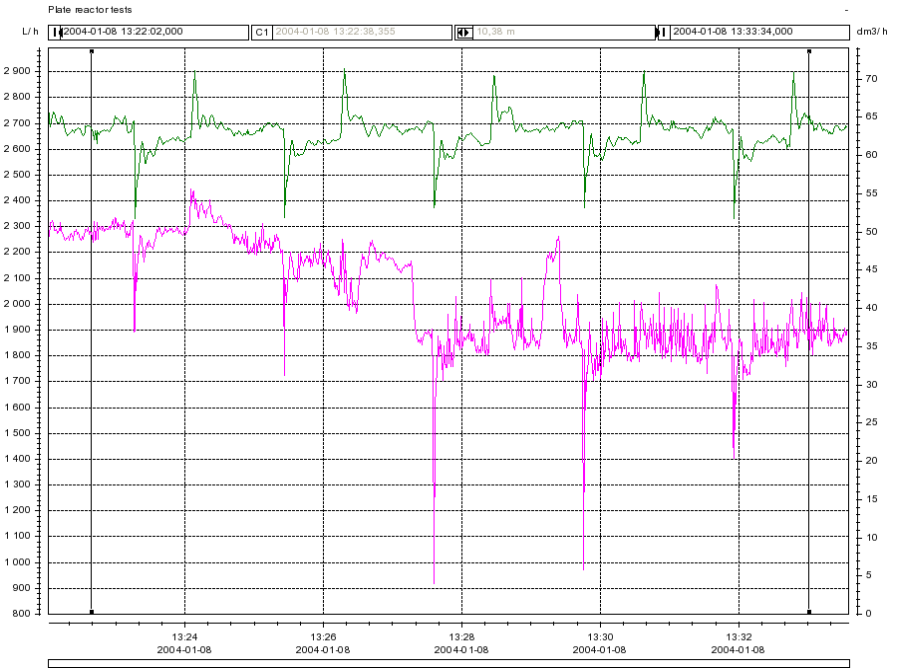

Figure 8.11 Measurement of process disturbances in the two flows $FT1$ (upper) and $FT4$ (lower), during utility system experiments. The disturbances enter the main water system roughly every two minutes.

the flow rates to and from the reactor $FT4$ and $FT5$, see Figure 8.11 from time $t = 13.28$. The variation in $FT1$ does not cause any significant variation in $TT3$, due to the low pass filter effect of the heat exchanger VVX1. The effect from the $FT4$-variations on the reactor temperature is larger, since the process flow is pre-heated in the small heat exchanger VVX2 with a constant steam flow. If the process flow is varying, the process inlet temperature will also vary. In a real production unit there would not be any of these variations, there would for example be individual pumps for each reactant. The disturbances are however interesting, since they give us information about the dynamics and sensitivities of the system that we otherwise would not get.

The chain of measurement equipment "thermocouples - transmitters - resistors" were calibrated at five different temperatures with a Pt-100 sensor as reference. The differences between individual measurements were large, at most 3°C. However, the largest cause for the differences was not the thermocouples, but the transmitters and the resistors. Some thermocouples have during the experiments given inaccurate measurements from

time to time and likely causes can for example be steam bubbles inside the reactor or glitches. Especially the thermocouples inside the reactor have given noisy data when the steam injection causes bubble formations.

8.7 Experimental Results

In Figure 8.12 we can see step responses in $TT5$ for the controller from (8.8) without and then with the nonlinear gain compensation for the nonlinear valve characteristics. For notations, see Figure 8.3. The PI-controller was auto-tuned with relay experiments around the 40 % operating point with $K = 3.0$ and $T_i = 1.0$ s. The step in $TT5^{\text{ref}}$ is from 25.4°C to 29.4°C. When the control valve is near its end position, RV1 = 5 %, the process gain from valve position to flow ratio is considerably larger than in the middle of the valve range, which was seen in Figure 8.8. Due to the increased process gain at this operating point the closed loop system becomes unstable, as seen around $t = 20$ s in Figure 8.12. The nonlinear gain compensation of the valve characteristics is enabled at $t = 35$ s and the system returns to the new set-point. The step response is repeated at time $t = 75$ s using the nonlinear gain compensation from start and the step response of the closed loop system is then stable and well-damped.

The next experiment is to keep the cooling water inlet temperature $TT5$ constant despite load disturbances inside the reactor. For notations, see Figure 8.3. The amount of injected steam is suddenly increased, thus increasing the heat release inside the reactor by 50%. The additional heat causes the outlet temperature $TT6$ of the cooling water to increase quickly, see upper plot in Figure 8.13. Due to the recycle loops, the inlet temperature $TT5$ of the cooling water will be quickly affected, unless necessary control actions are made. In this experiment, the mid-ranging control is disabled to more clearly see the dynamics of the closed loop. In Figure 8.13 it can be seen that the controller manages to keep the cooling temperature $TT5$ almost constant, despite the large change in heat release and outlet temperature $TT6$ of the cooling water. The control error is not larger than 0.3°C during the disturbance. The closed loop dynamics of $TT5$ are quite fast, but the recycle flows introduce very slow thermal modes, which can be seen in the control signal v_1 in the lower plot in Figure 8.13. At $t = 2384$ s, the heat release is returned to the initial level. The control valve is quickly adjusted to the new conditions.

The mid-ranging control structure is also experimentally verified, see Figure 8.14. The two left plots show a step decrease in the cooling temperature reference and the right plots show the step response after a step increase. The results from the experiment with the mid-ranging is plotted in solid lines, whereas the results without mid-ranging (v_2 is then

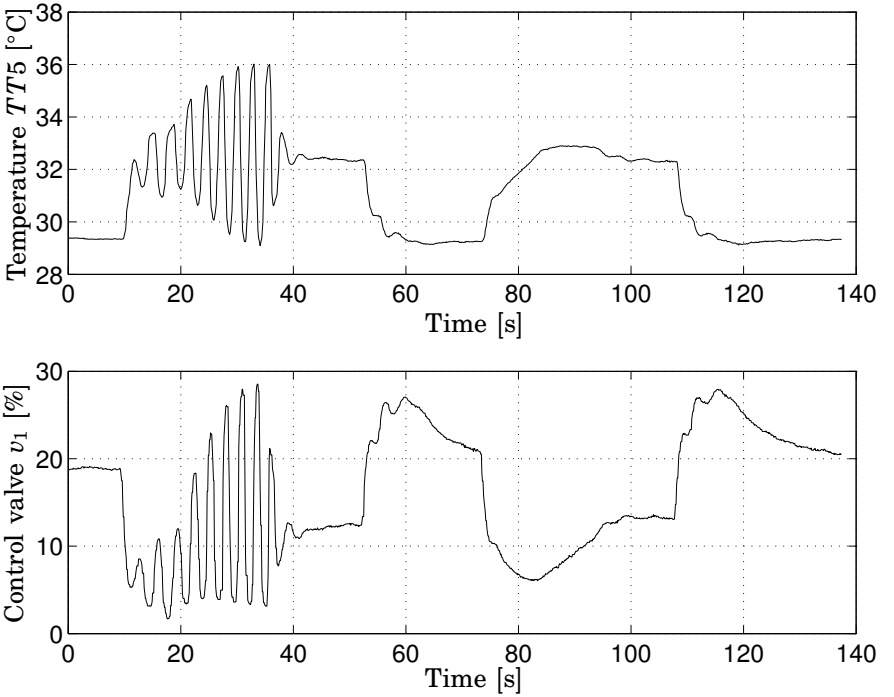

Figure 8.12 Step response first without and then with the inverse valve characteristics as nonlinear gain compensation.

held constant) have dashed lines. The control parameters for v_1, the first PI-controller, are the same for both experiments.

In the left plots, when $TT5^{\text{ref}}$ decreases from 29.5°C to 27.5°C, the cooling temperature follows the reference slightly better with mid-ranging than without, since here both valves v_1 and v_2 cooperate. However, the main advantage of the mid-ranging is that v_2 resets v_1 back to its nominal position, here 25%. The process is then better prepared for additional disturbances or reference changes. v_1 is here reset to 25% to achieve similar initial conditions for the two experimental cases. In general the fast control variable is reset to 50% to have good margin for disturbances in both directions.

In the plots on the right hand side of Figure 8.14, the temperature reference increases from 29.5°C to 32.5°C. The cooling temperature follows the reference very well in both cases. Without mid-ranging control (dashed), the position of the control valve v_1 has to be adjusted from 50%

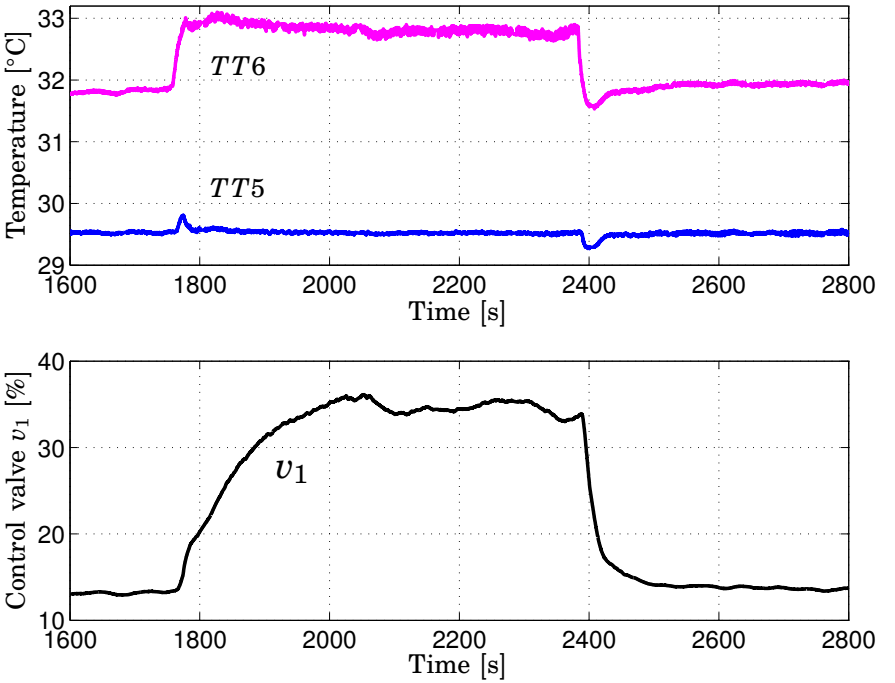

Figure 8.13 Load disturbance experiment with varying heat release inside the reactor. Upper plot: The heat release is suddenly increased, which directly affects the temperature $TT6$ of the cooling water coming out from the reactor. The controlled variable $TT5$, the inlet temperature of the cooling water, remains almost constant. Lower plot: The position v_1 of the three-way control valve.

to 20%, to track the reference. With mid-ranging (solid) v_1 is reset to 50%, which leaves it better prepared for additional changes in disturbances or references. The controller for v_1 is manually tuned to give as fast response as possible, with an overshoot of at most 25%. A smaller overshoot would require a much slower response.

The resulting closed loop dynamics can be locally approximated with linear dynamics using two poles and a zero,

$$G_{\text{cool}}(s) = \frac{0.21(s + 0.11)}{(s^2 + 0.21s + 0.024)}, \tag{8.9}$$

with a cross-over frequency $\omega_c = 0.2$ rad/s and a rise time[1] of roughly 6

[1]Here defined as the time from 10% to 90% of the steady-state value of a step response.

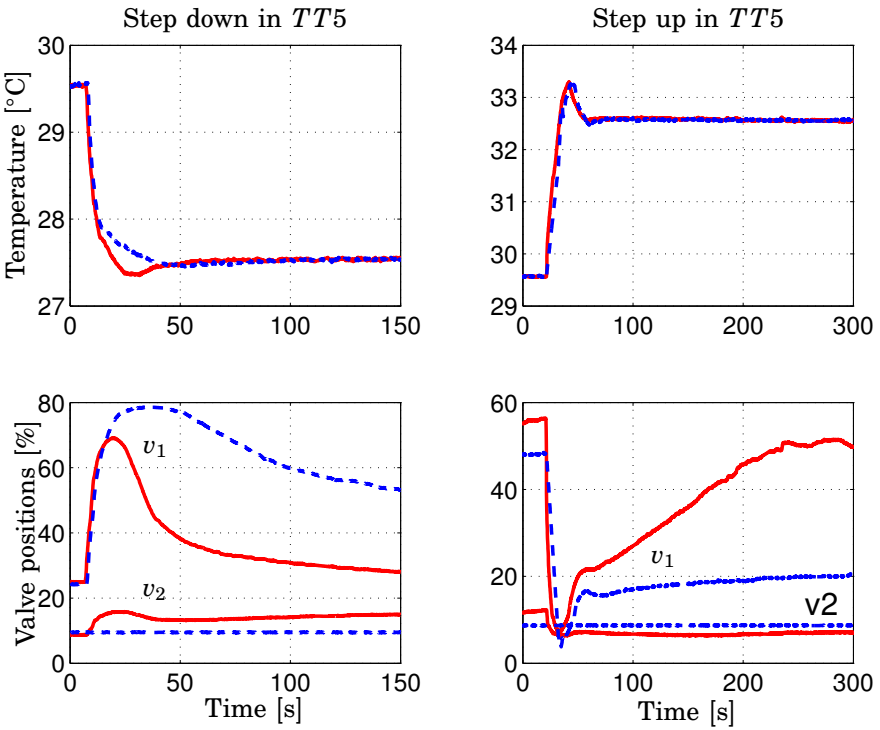

Figure 8.14 Step response experiments with mid-ranging (solid) and without (dashed). Left plots: Step down in cooling temperature. Right plots: Step up in cooling temperature. Lower plots: The control valve positions v_1 and v_2. Note that v_1 is reset to 25% in the left case and to 50% in the right case to get similar initial conditions as the case without mid-ranging.

seconds. For large setpoint changes, the valve v_1 saturates and a nonlinear behavior appears, which can be described with a rate limit function. The mid-ranging control will manipulate v_2 to allow v_1 to return to its nominal operating point. Experimental results for large setpoint changes for the cooling system are reported in chapter 9.

8.8 Summary

The utility system is a multi-purpose heating/cooling system. In this project, the utility system is designed to remove the heat from an exothermic reaction inside the plate reactor and allow fast, accurate and flexible temperature control.

To reduce fouling inside the cooling plates of the plate reactor, a closed flow circuit of water is used, where an external heat exchanger transfers heat from the cooling water to some cooling reservoir, for example a river or cooling towers. Recycle loops are introduced to improve the speed of the response of the system and to reduce the sensitivity to external disturbances.

A mid-ranging controller is designed, which uses two control valves to control the cooling temperature and reduces the risk of valve saturation. The mid-ranging control technique improves drastically the flexibility of the utility system and increases its operating range with existing equipment.

The utility system and its control system are verified in a series of experiments. The controller offers very good set-point tracking and disturbance rejection.

9

Constraint handling in Mid-ranging Control

9.1 Introduction

In the process industry most control loops are single-input single-output (SISO). The use of additional inputs of the process for control purposes is often considered to increase control authority, performance or flexibility. When a process has more control inputs than outputs, the question arises how to use the additional degrees of freedom. The general control problem for this type of processes is sometimes referred to as control allocation, i.e., how should the control actions be distributed among the available control signals to control the process output, see e.g. [Durham, 1993].

A specific example of control allocation is mid-ranging, see e.g. [Allison and Isaksson, 1998]. As stated in [Allison and Ogawa, 2003], mid-ranging refers to control problems where there are two control inputs and only one output to control. Often the inputs differ significantly in their dynamic effect on the output, and the faster input is sometimes more costly to use than the slow one. In general, the faster input, here denoted u_1, is also closer to saturation than the slower input, here denoted u_2. The mid-ranging idea, see block-diagram in Figure 9.1, is to have the fast input u_1 controlling the process output, and to use the effect of the slower input u_2 on y, to gradually reset or mid-range u_1 to its desired set-point value u_1^{sp}. Thus u_2 indirectly acts to prevent saturation in u_1.

The mid-ranging idea has been around for many years under different names, for example valve position control [Shinskey, 1996] or input resetting [Skogestad and Postlethwaite, 2005]. It is commonly used in the process industry, but is also used in other areas, e.g. in position control of the pickup-head in a CD-player.

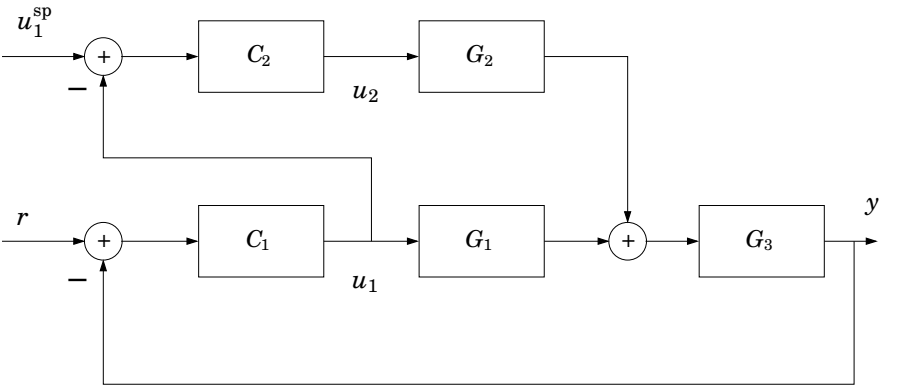

Figure 9.1 Mid-ranging control structure, for a process where G_3 represents common dynamics for u_1 and u_2. In the bio-reactor example $G_1 = 1$, which will be used in the sequel.

The controller method used in C_1 and C_2 in Figure 9.1 depends on the process. Traditionally, PID-controllers are used, but all SISO controllers are possible. For processes with more complex dynamics, time delays or input constraints, the desired mid-ranging effect may be achieved using multi-variable control design, such as Internal Model Control, Linear Quadratic Gaussian control or Model Predictive Control. When input constraints are present, a centralized controller in the form of MPC can give improved performance compared to decentralized controllers, see [Allison and Isaksson, 1998]. In MPC, the mid-ranging concept can be achieved by introducing target set-points to the fast control inputs. However, as stated in [Allison and Ogawa, 2003], there are numerous applications where an MPC-type solution might be considered overkill and where the decentralized control structure in Figure 9.1 offers a natural balance between complexity and performance.

Papers such as [Allison and Ogawa, 2003; Allison and Isaksson, 1998; Karlsson *et al.*, 2005] present tuning guidelines and applications of mid-ranging control, but there has so far been no discussion on constraint handling and anti-windup for this type of control structure. The main topic of this chapter is how to implement anti-windup in PID-based mid-ranging control, and it will be demonstrated that standard anti-windup schemes may lead to unnecessary performance degradation during saturation.

Problem Statement

Processes with two input signals and one output signal can in general be represented with the block diagram in Figure 9.1. In some situations like paper drying with steam and infrared light [Allison and Isaksson, 1998],

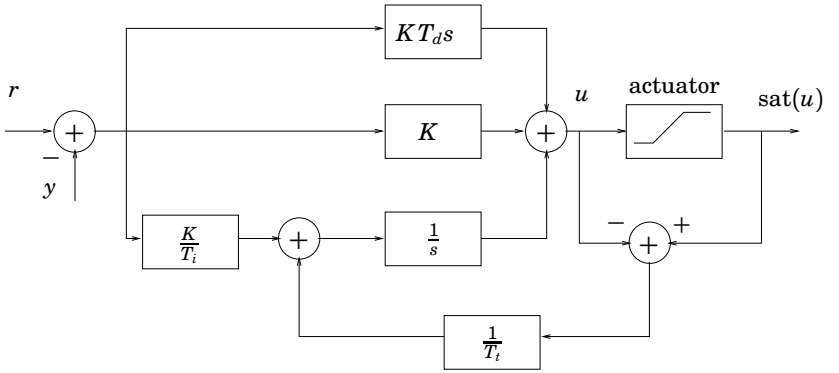

Figure 9.2 Basic scheme for anti-windup in a PID-controller. K is the proportional gain, T_i is the integral time and T_d is the derivative time.

it may be reasonable to use the approximation $G_3 = 1$, while for other processes, like the bio-reactor described in Section 9.2, it may be more natural to use $G_1 = 1$.

In standard applications of mid-ranging control, the dynamics in G_1 is significantly faster than that of G_2. As a rule of thumb, the controllers C_1 and C_2 should therefore be tuned to keep the dynamics from y to u_1 an order of magnitude faster than the dynamics from y to u_2 to avoid exciting cross-couplings. The controllers C_1 and C_2 can be tuned according to guidelines in e.g. [Allison and Ogawa, 2003].

Consider standard mid-ranging control for a general process with saturation of u_1. When u_1 saturates, i.e., $u_1 = u_1^{\max}$, due to a large change in the reference y or due to a large process disturbance, the feedback path from y to u_1 is broken. The second control input u_2 is manipulated to achieve $u_1 = u_1^{\text{sp}}$, so u_2 will by its influence on y bring u_1 out of its saturation. The key question now is what influence the anti-windup scheme of C_1 has on the performance of the closed loop system. Another question is whether the bandwidth of u_2 should be increased while u_1 is saturated, to more quickly affect y so much that u_1 does not have to be saturated.

Most controllers with integral action have some kind of anti-windup. The reason is to prevent the integrator state from becoming too large when the control input saturates and the control error $e = r - y$ does not go to zero. In this chapter, we consider PID-controllers as they are very frequent in the process industry. When implemented, they often have some kind of anti-windup scheme, one example is shown in Figure 9.2, see e.g. [Åström and Hägglund, 2005]. More general anti-windup methods can be found in e.g. [Kapoor *et al.*, 1998]. The time constant T_t in Figure 9.2 determines the speed at which the integral term is reset. There are very

few guidelines how to choose an appropriate T_t. A rule of thumb from [Åström and Hägglund, 2005] states that T_t should be larger than T_d, but smaller than T_i, for example $T_t = \sqrt{T_i T_d}$. A low T_t will give fast integrator reset and a high T_t will give slow integrator reset.

The rest of this chapter will demonstrate how applying this standard choice of T_t for C_1 can lead to unnecessary performance degradation when u_1 saturates. Guidelines will be derived for design of anti-windup schemes for mid-ranging control structures based on the analysis of the frequency response from y to u_2.

The chapter is organized as follows. In Section 9.2, a bio-reactor application of mid-ranging control is presented. In Section 9.3, the disadvantage of using $T_t \leq T_i$ is demonstrated in simulations of the bio-reactor application. Guidelines will be derived for how to choose a suitable time constant T_t, which gives u_2 the same bandwidth in the saturated case as in the unsaturated case. Section 9.4 presents a modification in the control structure that increases the bandwidth of u_2 to improve the performance in saturation. In Section 9.5, the guidelines are applied to a general purpose cooling/heating system. The aim is to show how the derived guidelines and modified control laws can be used for a process quite different from the bio-reactor. Finally, stability and performance for the proposed tuning are verified using theory for piecewise linear systems in Section 9.6.

9.2 Mid-ranging Control of a Bio-reactor

An example of a process where mid-ranging control can be applied is control of oxygen concentration in a stirred-tank bio-reactor used for cultivations of bacteria. Control of the bio-reactor is described in [Velut *et al.*, 2004] and [Karlsson, 2005]. To ensure sufficient oxygen transfer to the cultivation medium, a mechanical stirrer is used with feedback from the dissolved oxygen concentration to the stirrer speed. Bacterial growth leads to an exponentially increasing demand for oxygen, which causes the stirrer speed to saturate. The resulting decrease in dissolved oxygen concentration causes unnecessary stress on the bacteria, and also disables schemes for substrate feeding and monitoring of the cultivation that depend upon a constant dissolved oxygen concentration. The undesired effects may be avoided by mid-ranging the stirrer speed to a desired value by decreasing the reactor temperature. A lower temperature leads to decreased activity and reproduction of bacteria, thus reducing the oxygen demand. However, caution must be taken using the temperature control, since the model is only valid within a limited temperature range, and a too low temperature may significantly inhibit growth.

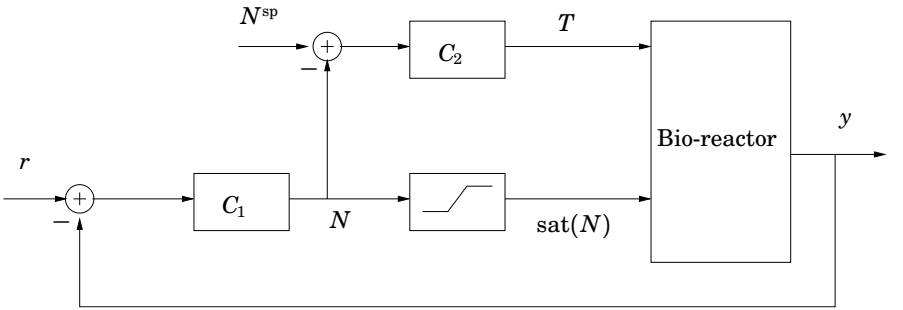

Figure 9.3 Block diagram for the bio-reactor

Figure 9.3 shows the block diagram of the bioreactor with the mid-ranging control structure. The stirrer speed N is the fast control input and the reference temperature T is the slower control input. A linearized second-order model of the oxygen and temperature dynamics can be described by

$$\dot{x}(t) = Ax(t) + B_1u_1(t) + B_2u_2(t) \tag{9.1}$$

$$y(t) = Cx(t) \tag{9.2}$$

where the first state x_1 denotes the dissolved oxygen concentration which is also the process output y, and the second state x_2 denotes the reactor temperature. The two control signals u_1 and u_2 represent the stirrer speed N and the reference temperature T, respectively. The effect of the stirrer speed on y is much faster than that of the reference temperature. Numerical values for the system matrices used in simulations are given by

$$A = \begin{bmatrix} -2400 & -5200 \\ 0 & -15 \end{bmatrix}$$

$$\begin{bmatrix} B_1 & B_2 \end{bmatrix} = \begin{bmatrix} 210 & 0 \\ 0 & 15 \end{bmatrix} \quad C = \begin{bmatrix} 1 & 0 \end{bmatrix}$$

For efficient use of the bio-reactor, it is essential to choose the set-point value u_1^{sp} for the stirrer speed close to the maximum value u_1^{max}. This narrow margin limits the control authority of u_1 around its set-point value.

PI-controllers are used for both C_1 and C_2. The nominal control parameters in the following simulations are $K_1 = 10$, $T_{i1} = 1/120$ hours, $K_2 = 0.02$, $T_{i2} = 10/120$ hours, $u_1^{max} = 1200$ rpm and $u_1^{sp} = 0.98u_1^{max} = 1176$ rpm. Four different cases will be investigated, the unsaturated

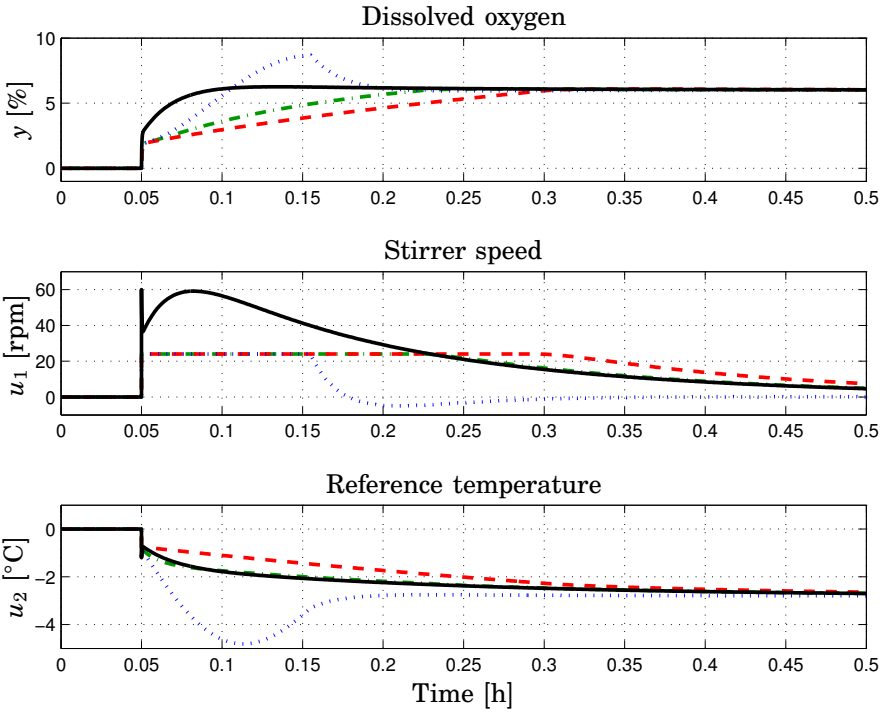

Figure 9.4 Step response for bio-reactor example. Fast anti-windup $T_t = T_{i1}/3$ (dashed), no anti-windup (dotted), nominal unsaturated system (solid), and $T_t = 1.2T_{i1}$ (dash-dotted), which is chosen to achieve the same bandwidth in u_2 for the saturated case as in the unsaturated case.

response, the saturated response with fast anti-windup $T_t = T_{i1}/3$, no anti-windup $T_t = \infty$ and finally T_t chosen according to the guidelines presented later in this section.

The closed loop responses for a step increase in the dissolved oxygen reference are plotted in Figure 9.4 for varying degrees of anti-windup. The fastest response is of course if the stirrer speed can not be saturated, but the stirrer speed is saturated at 1200 rpm, which corresponds to 24 rpm above the nominal operating point. If no anti-windup is used, the response is quick, but it experiences a large overshoot. Unless the controllers C_1 and C_2 are well separated in bandwidth, disturbances may actually cause instabilities if no anti-windup is used. When there is fast anti-windup, the response is very slow. The details behind these responses will be analyzed in the next section.

9.3 Analysis of Standard Anti-windup

In this section, we will now explain the responses in Figure 9.4, first by simple reasoning and then based on the frequency response from y to u_2.

During control design of C_1 and C_2, the controllers are tuned for the nominal, i.e., the unsaturated, case. The purpose of C_2 is to influence the process so that u_1 is mid-ranged to its set-point value u_1^{sp}. Remember that to avoid exciting cross-couplings in this decentralized control structure, the dynamic response of C_2 is tuned slower than the response of C_1. Furthermore, we assume that the signal sent from C_1 to C_2 is the *unsaturated* signal u_1.

When u_1 saturates at its maximum value $u_1^{\max}$, the feedback loop of u_1 is broken, and instead all feedback has to go through u_2. With fast anti-windup, the integrator is quickly reset and $u_1 \approx u_1^{\max}$, which gives $u_2 \approx C_2(u_1^{\text{sp}} - u_1^{\max}) = C_2 e_2$, where we define e_2 as the control error sent to C_2. When the operating point is chosen such that u_1^{sp} is close to $u_1^{\max}$, the control error e_2 that C_2 acts on is very small, which makes the changes in u_2 very small. The effect from u_2 to y, which may help end the saturation of u_1 is then very limited.

In contrast, if no or very slow anti-windup is used, the integrator state will quickly grow and the unsaturated control input u_1 will increase to large values. This will give a very large control error $e_2 = u_1^{\text{sp}} - u_1$, thus leading to a large control action in u_2, which will have a large impact on y, thus also bringing u_1 out of saturation.

It is apparent that C_2 in the saturated case receives a smaller control error e_2 compared to the unsaturated case, and this reduces significantly the effect that u_2 has on the closed loop performance, see the lowest plot in Figure 9.4. With fast anti-windup, u_2 adjusts very slowly resulting in a longer period of saturation of u_1. This standard choice of $T_t \leq T_i$ has consequently negative effects in the mid-ranging control setting.

Frequency response analysis

To support the simple reasoning above, the frequency response from r to u_2 is examined for the nominal, i.e., unsaturated case and the saturated case.

Given the block diagram in Figure 9.1 with $G_1 = 1$, the transfer function from r to u_2 in the nominal case can be derived as

$$u_2 = -\frac{C_1 C_2}{1 + C_1 G_3 - C_1 G_3 G_2 C_2} r \stackrel{\text{def}}{=} G_{\text{nom}}\, r. \tag{9.3}$$

The saturated case is less straight forward. The controllers and the process are governed by

$$\begin{aligned} y &= G_3 \text{sat}(u_1) + G_3 G_2 u_2, \\ u_1 &= C_1(r - y) + \frac{1}{sT_t}(\text{sat}(u_1) - u_1), \\ u_2 &= C_2(u_1^{\text{sp}} - u_1). \end{aligned}$$

In saturation[1], $\text{sat}(u_1) = u_1^{\max}$, which leads to

$$\begin{aligned} y &= G_3 u_1^{\max} + G_3 G_2 u_2, \\ u_1 &= C_1(r - y) + \frac{1}{sT_t}(-u_1) + \frac{1}{sT_t}(u_1^{\max}) \\ &= \frac{sT_t}{(sT_t + 1)} C_1(r - y) + \frac{1}{(sT_t + 1)} u_1^{\max}, \\ u_2 &= C_2(u_1^{\text{sp}} - u_1), \end{aligned}$$

where we define $C_{aw} = sT_t/(sT_t + 1)$ from the anti-windup scheme. The set-point for u_1 is assumed to be zero, $u_1^{\text{sp}} = 0$. The broken feedback loop reduces the transfer function from r to u_2 as follows,

$$\begin{aligned} u_2 &= -C_2 u_1 = -C_2 \left(C_{aw} C_1 (r - G_3 G_2 u_2) \right) \\ &= -\frac{C_2 C_{aw} C_1}{(1 - C_2 C_{aw} C_1 G_3 G_2)} r \stackrel{\text{def}}{=} G_{\text{sat}}\, r. \end{aligned} \tag{9.4}$$

Note that the transfer function G_{sat} is parameterized in the anti-windup time constant T_t.

The frequency responses for the different anti-windup cases are plotted in Bode diagrams in Figure 9.5. Consider first the frequency response for the unsaturated case. The low and high frequency responses can be approximated with

$$G_{\text{nom}} \approx \frac{-C_2}{G_3(1 - G_2 C_2)} \qquad \forall \quad \omega \leq 0.1 \text{ rad/s} \tag{9.5}$$

$$G_{\text{nom}} \approx -C_1 C_2 \qquad \forall \quad \omega \geq 100 \text{ rad/s} \tag{9.6}$$

In the saturated case, the choice of anti-windup time constant T_t affects mainly the gain and phase in the medium frequency range. No anti-windup gives a very large increase in the gain at $\omega = 25$ rad/h. Fast anti-windup decreases the gain considerably compared to the unsaturated

[1] Without loss of generality, we consider only the upper limit on u_1.

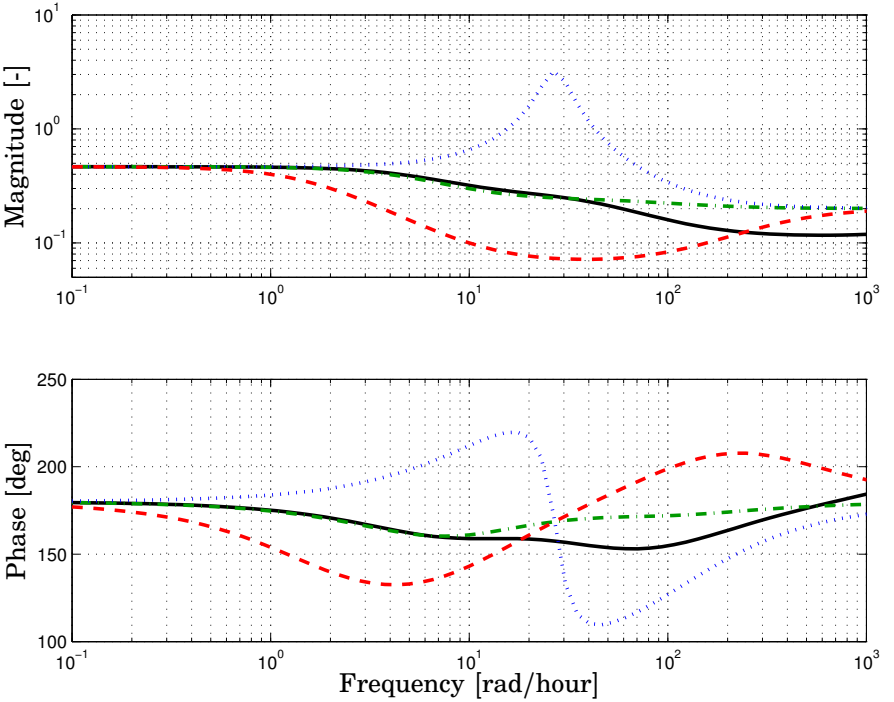

Figure 9.5 Bode diagrams of the transfer function from r to u_2 for the bio-reactor example. Unsaturated case (solid), no anti-windup (dotted), fast anti-windup $T_t = T_{i1}/3$ (dashed) and $T_t = 1.2T_{i1}$ (dashed-dotted) that gives similar bandwidth in the saturated case as in the unsaturated case.

case. This supports the initial reasoning above, that fast anti-windup leads to performance degradation in a mid-ranging control structure.

It is now possible to choose a T_t that gives better performance than the fast anti-windup, but avoids the overshoot from having no anti-windup. A natural choice is then to choose T_t, so that the frequency response from r to u_2 has a *similar* bandwidth as in the unsaturated case. It may be tempting to increase the bandwidth even further, above the bandwidth of the unsaturated case. This aggressive use of u_2 may introduce difficulties in the presence of input saturation of u_2, cross-couplings or unmodeled dynamics. Therefore, this choice of T_t seems as an appropriate trade-off between performance and robustness. As an alternative, this idea of similar bandwidths can also be implemented by choosing a fast anti-windup, but shifting the controller parameters in C_2 as soon as u_1 saturates, i.e., a form of gain scheduling.

In the bio-reactor example, a value of $T_t = 1.2T_{i1}$ is chosen. The re-

sponse in Figure 9.4 shows that the closed loop performance is better than with fast anti-windup. Note that by choosing T_t to achieve similar bandwidths, the control trajectories of u_2 coincide for the saturated case and the unsaturated case, and after u_1 leaves saturation, the trajectories of u_1 also coincide.

To summarize, by choosing a value of T_t that gives similar bandwidth in the saturated case as in the unsaturated case, the performance is improved and the control actions in u_1 and u_2 resemble the unsaturated case. Note that the suggested method for choosing T_t uses information of the nominal process and controllers. It is independent of the choice of set-point value u_1^{sp} and is not limited to a particular disturbance model or to particular reference trajectories. The idea can also be implemented by gain scheduling of C_2.

9.4 Modified Anti-windup Scheme

So far the main criterion for choosing the anti-windup time constant T_t has been to obtain the same bandwidth from r to u_2 in the saturated case as in the unsaturated case. The main objective has been to improve the performance, but with the limitation that u_2 should not be used more than in the unsaturated case.

Assume now that there is good process knowledge in G_2 and G_3 and the constraints on u_1 and u_2 are well known. It is then possible to use u_2 more aggressively while u_1 is saturated, to improve the performance and bring u_1 out of saturation as fast as possible. The more aggressive use of u_2 should be used with caution when there are nonlinearities associated with the input dynamics or there is model uncertainty.

In this section, a simple modification of the anti-windup scheme will be presented that increases the bandwidth of the frequency response, i.e., improves the performance during saturation. By manipulating the input signal to C_2 during saturation, the use of u_2 can be increased without having to change the control parameters in C_2. The modified anti-windup scheme can be seen in Figure 9.6.

$$\tilde{u}_1 = u_1 + K_s(u_1 - \text{sat}(u_1)) \tag{9.7}$$

$$u_2 = C_2(u_1^{\text{sp}} - \tilde{u}_1) = C_2\left(u_1^{\text{sp}} - u_1 - K_s\left(u_1 - \text{sat}(u_1)\right)\right) \tag{9.8}$$

In the unsaturated case, the last term is zero. When u_1 saturates, $\text{sat}(u_1) = u_1^{\max}$ and $u_1 - u_1^{\max} > 0$. The signal to C_2 is increased by the positive term $K_s(u_1 - u_1^{\max})$. The modification allows for a standard anti-windup scheme

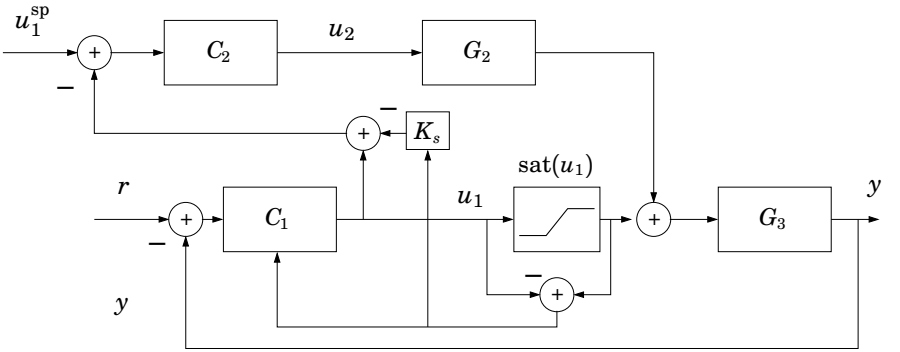

Figure 9.6 Mid-ranging control structure with modified anti-windup scheme. The gain K_s increases the input signal to C_2, thus generating higher control action in u_2 to improve performance when u_1 saturates.

with a small $T_t \leq T_i$ for fast integral reset, eliminating the risk of integrator windup and a possible overshoot. The difference $u_1 - u_1^{\max}$ is small using fast anti-windup, but with a suitable choice of K_s, performance can be improved. Note that the additional input to C_2, $u_1 - \text{sat}(u_1)$, is the same signal that is used for standard anti-windup of C_1.

With the modification, the response from r to u_2 will be

$$u_2 = -\frac{C_2(K_s+1)C_{aw}C_1}{(1-C_2(K_s+1)C_{aw}C_1G_2)}r \stackrel{\text{def}}{=} G_{K_s}r \tag{9.9}$$

With this modification, the bandwidth of the transfer function from r to u_2 is increased, see Figure 9.7. Caution should be used to avoid increasing the bandwidth into high frequency regions where there might be process uncertainties or risk of violating input constraints in u_2. Note that the low frequency response is not affected by K_s.

To find a suitable value of K_s a standard integral squared error cost function is used as performance criterion,

$$J = \int_0^{t_f} \left((r-y)^2 + \rho u_2^2 \right) dt \tag{9.10}$$

where ρ is a weight to compensate for scaling, or to suppress large use of u_2. The objective is to find K_s that minimizes the cost function J, for example by numerical search or simulations. In the bio-reactor application, the minimum cost was achieved with $K_s = 3$, with $\rho = 0.34$.

The modified anti-windup scheme is evaluated in step response in dissolved oxygen reference, see Figure 9.8. The performance with $K_s = 3$ is almost as good as the unsaturated case, since u_2 is being used more

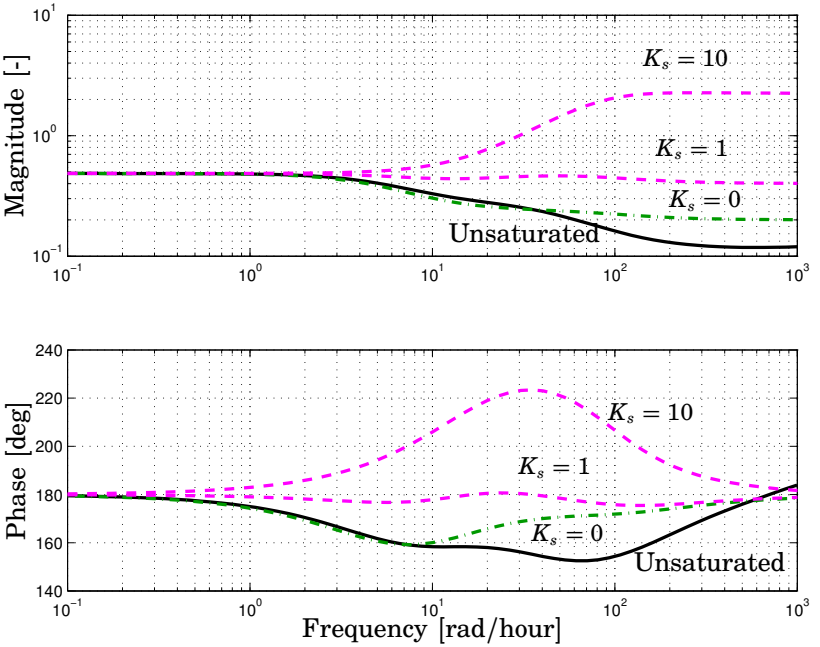

Figure 9.7 Bode diagram for transfer function from r to u_2 for bio-reactor with modified anti-windup scheme and different values of K_s. $T_t = T_{i1}$ has been used in all cases.

aggressively. If less control action in u_2 is desired, ρ should be increased. A larger reference step r will give larger control error $(r - y)$, thus favoring a higher K_s. For a faster C_2, a lower K_s is needed for the same performance. The value of K_s will also vary depending on the choice of T_t, which should be small $(T_t \leq T_i)$ to allow fast anti-windup. Dead-beat anti-windup should however be avoided, since it gives $u_1 = u_1^{\max}$, which renders the modification ineffective.

As an alternative to PID controllers, the mid-ranging control concept can also be achieved by Model Predictive Control. In MPC, a similar cost function to (9.10) is evaluated on-line for a specified prediction horizon. Performance of the closed-loop system may be further improved using MPC, but at the cost of developing a reliable process model and the computational effort involved in on-line optimization.

The main advantages with the proposed simple modification of standard PID-control are that it is only active as long as u_1 saturates, and that the calculation is very simple and it can be implemented in most commer-

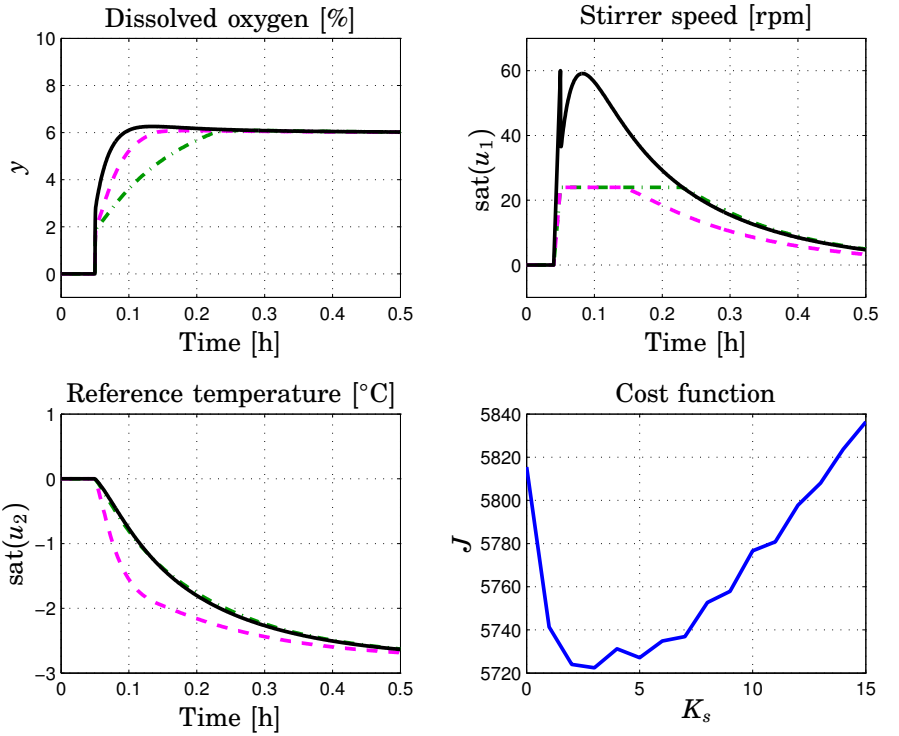

Figure 9.8 Step response with modified anti-windup scheme for bio-reactor. Nominal case (solid), standard anti-windup with $T_t = 1.2T_{i1}$ (dash-dotted), modified anti-windup with $T_t = T_{i1}$ and $K_s = 3$ (dashed). Lower right: cost function (9.10) evaluated for different values of K_s using $\rho = 0.34$.

cial PID packages. There is no need to change to a different set of control parameters in C_2 during saturation. A downside with the aggressive use of u_2 is the risk of exciting unmodeled dynamics or violating constraints in u_2. It is therefore essential to use a value of ρ that reflects the given process and its constraints. The modified closed-loop system should also be evaluated in simulations to verify performance.

9.5 Mid-ranging Control of a Cooling System

In this section, the previously derived guidelines are used on another process to show that the results are generally applicable. Consider the standard cooling system seen in Figure 9.9. The flow configuration can be used for general cooling/heating purposes, and is described in more detail

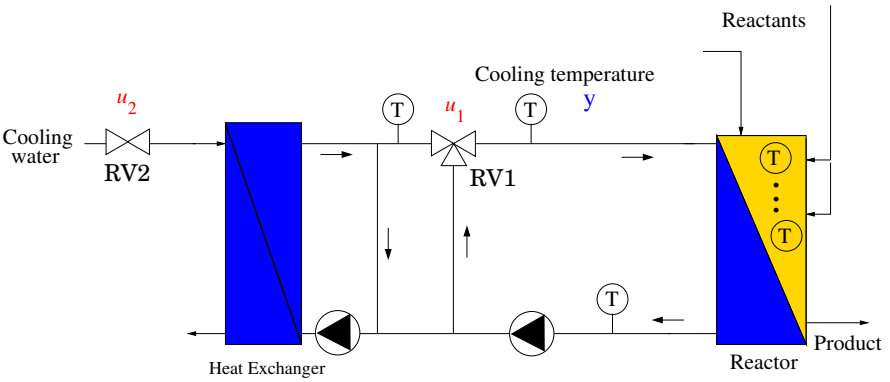

Figure 9.9 Flow configuration of the cooling system with recycle loops around the heat exchanger (HEX) and the reactor. Note that the control signals u_1 and u_2 corresponds to the desired positions of the control valves RV1 and RV2.

in Chapter 8. The system is a closed hydraulic system that transfers heat from the plate reactor on the right to cold water from a reservoir on the left via a heat exchanger. With recycle of the water coming out from the reactor directly back to the control valve RV1, the speed of the temperature control can be significantly improved. The second recycle, around the heat exchanger to the left, is implemented to keep the flow rate through the heat exchanger constant regardless of the current valve position of RV1.

A simple nonlinear model of the cooling system based on first principles has been derived, see Chapter 8. The control variables u_1 and u_2 are the desired positions of the two control valves and the output y is the inlet temperature of the cooling water for the reactor, see Figure 9.9. Linearization gives a model with three water temperature states x_p and two actuator states x_v for each control valve RV1 and RV2. The three water temperatures are the temperatures of the left (cold) side and the right (warm) side of the heat exchanger, and finally the left (cold) side of the reactor. The pressure dynamics and the thermal inertia are neglected. Constant heat is assumed to be conducted from the exothermic reaction to the cooling side of the reactor. The dynamic system can be described as

$$\begin{aligned}
\dot{x}_{v1}(t) &= A_v x_{v1}(t) + B_v u_1(t) \\
v_1(t) &= C_v x_{v1}(t) \\
\dot{x}_{v2}(t) &= A_v x_{v2}(t) + B_v u_2(t) \\
v_1(t) &= C_v x_{v1}(t) \\
\dot{x}_p(t) &= A_p x(t) + B_{p1} v_1(t) + B_{p2} v_2(t) \\
y(t) &= C_p x(t)
\end{aligned} \tag{9.11}$$

and when expressed together, we get

$$\begin{bmatrix} \dot{x}_{v1} \\ \dot{x}_{v2} \\ \dot{x}_p \end{bmatrix} = \underbrace{\begin{bmatrix} A_v & 0 & 0 \\ 0 & A_v & 0 \\ B_{p1}C_v & B_{p2}C_v & A_p \end{bmatrix}}_{A} \begin{bmatrix} x_{v1} \\ x_{v2} \\ x_p \end{bmatrix} + \underbrace{\begin{bmatrix} B_v & 0 \\ 0 & B_v \\ 0 & 0 \end{bmatrix}}_{B} \begin{bmatrix} u_1 \\ u_2 \end{bmatrix}$$

$$y = \underbrace{\begin{bmatrix} 0 & 0 & C_p \end{bmatrix}}_{C} \begin{bmatrix} x_{v1} \\ x_{v2} \\ x_p \end{bmatrix}. \tag{9.12}$$

Numerical values for the system matrices used in simulations are

$$A_v = \begin{bmatrix} -5.404 & -36.39 \\ 1 & 0 \end{bmatrix} \quad B_v = \begin{bmatrix} 1.1 \\ 0 \end{bmatrix} \quad C_v = \begin{bmatrix} -3.001 & 38.06 \end{bmatrix}$$

$$A_p = \begin{bmatrix} -0.085 & 0 & 0.085 \\ 0 & -1.1 & 0.60 \\ 0.072 & 0.075 & -0.15 \end{bmatrix} \quad \begin{bmatrix} B_{p1} & B_{p2} = \end{bmatrix} = \begin{bmatrix} -1.22 & 0 \\ 0.44 & -20.9 \\ 0.98 & -2.0 \end{bmatrix}$$

$$C_p = \begin{bmatrix} 0.416 & 0 & 0.584 \end{bmatrix}.$$

The two control valves are identical and the valve dynamics were determined by system identification from experimental data. The valve dynamics have a fast unstable zero, approximating higher order dynamics. The structure of the system matrix A reveals tight cross-couplings between the different temperature states and control valve positions due to the recycle loops.

The reference temperature for the cooling water is calculated by a controller for the plate reactor using multi-loop PID controllers or MPC, see Chapter 4. The purpose of the mid-ranging control is to track the given reference temperature as well as possible. The cooling temperature is mainly influenced by u_1 and control valve RV1. However, large reference changes or disturbances may cause saturation of u_1. To improve performance and increase the operating region of the hydraulic equipment, u_2 is manipulated to mid-range u_1 to a desired value. To have a suitable margin to the saturation limits, $u_1^{\text{sp}} = 0$, which corresponds to an actual valve position of RV1 of 50%. The constraints in u_1 are ± 0.5.

PI-controllers are used for both C_1 and C_2. The nominal control parameters in the following discussions are $K_1 = -0.03, T_{i1} = 1.0$ seconds, $K_2 = -0.05, T_{i2} = 30$ seconds.

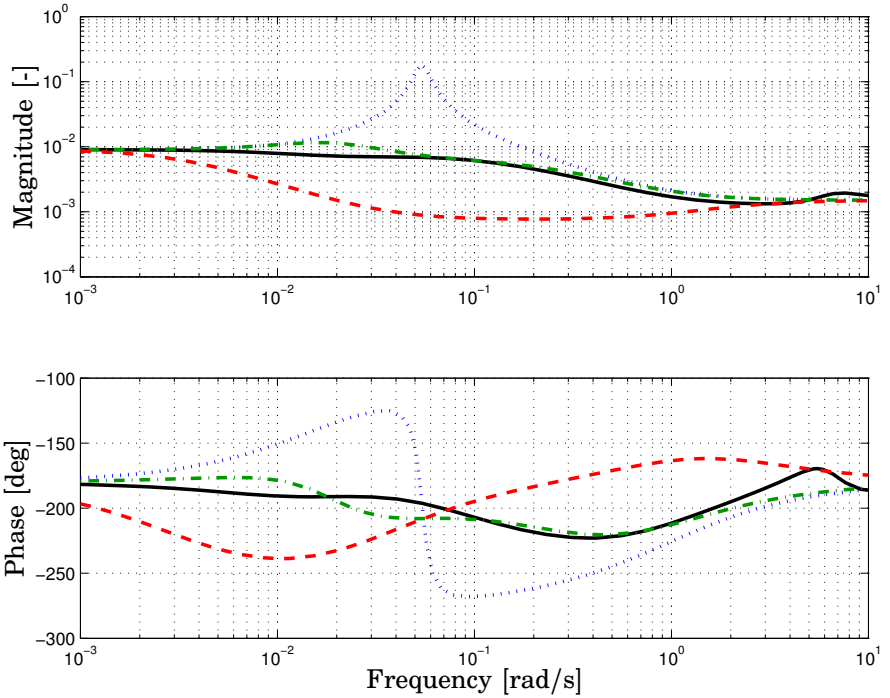

Figure 9.10 Bode plots of the transfer function from r to u_2 for the unsaturated case (solid), the saturated cases when $T_t = 4T_{i1}$ (dash-dot), $T_t = 0.5T_{i1}$ (dashed) and $T_t = 50T_{i1}$ (dotted).

Anti-windup for the Cooling system

Similar to the bio-reactor example, a fast time constant T_t of the anti-windup scheme may not always be beneficial for the cooling system.

The transfer functions from r to u_2 for the unsaturated and the saturated cases were defined in (9.3) and (9.4). Bode plots for different values of T_t are evaluated. By visual inspection, $T_t = 4T_{i1}$ gives the saturated system a similar bandwidth of the frequency response as for the unsaturated system, see Figure 9.10. As predicted, fast anti-windup gives lower gain, whereas slow anti-windup gives higher gain than the unsaturated case.

Experiments The proposed method was verified in experiments at the Alfa Laval laboratory in Tumba[2], Sweden. The equipment and the experimental set-up was presented in Section 8.4.

[2]The equipment was moved from Lund to Tumba after the experiments in Chapter 8.

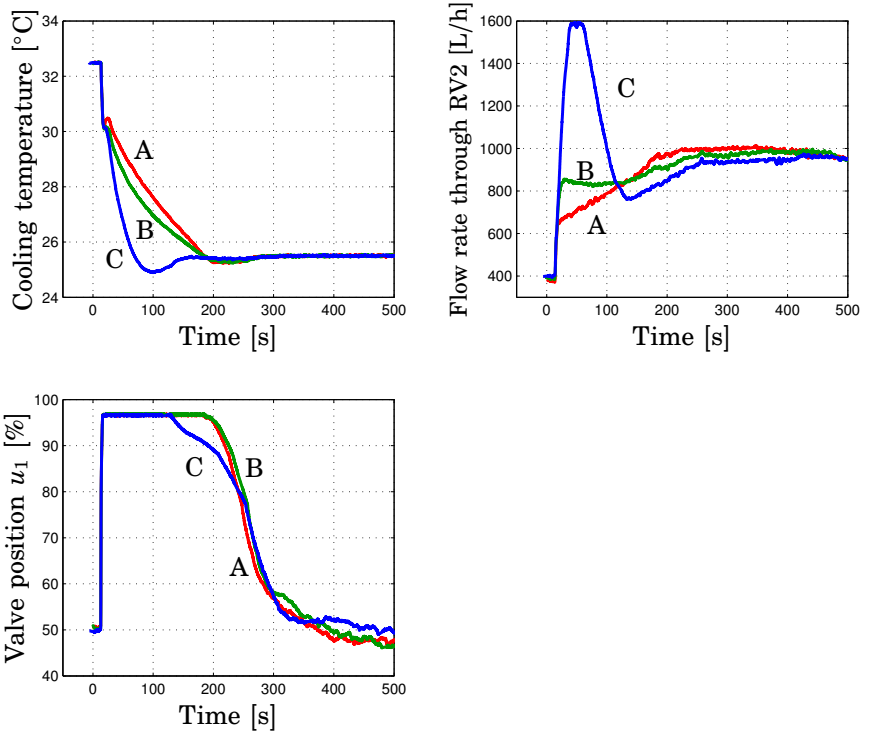

Figure 9.11 Experimental data: Closed-loop response for a step decrease of 7° C for the saturated cases when $T_t = 0.5T_{i1}$ (line A), $T_t = 4T_{i1}$ (line B) and $T_t = 50T_{i1}$ (line C). Instead of plotting the valve position u_2, the flow rate through the valve RV2 is plotted.

Experimental results are shown in Figure 9.11, where the closed-loop response is plotted for a step decrease in the temperature reference with 7°C. From practical limitations, there is no unsaturated case as in the previous simulations. The control input u_1 is quickly saturated, i.e., all water is circulated to the external heat exchanger to decrease the cooling water temperature to the reactor. With very slow anti-windup the integrator state in the controller increases well above 140%, thus increasing the input sent to the second controller. With a large controller error being sent to C_2, C_2 increases u_2 to allow u_1 to return to its nominal operating point. In Figure 9.11, the flow rate through RV2 is plotted instead of the valve position u_2, since the valve characteristics of RV2 are highly nonlinear. The slow anti-windup leads to more action in u_2, higher flow rate

through the heat exchanger, thus improving the transient response. However, the slow anti-windup causes a small overshoot in the temperature response. The overshoot is larger in simulations, but nonlinear effects in the real process dampen the effect.

With the fast anti-windup, the control input is also saturated, but the anti-windup resets the integrator so that the control error to C_2 is very small. The second control input u_2 increases therefore very slowly, leading to an overall very slow response. By manipulating the time constant of the anti-windup scheme, the response may move between these two extreme cases. The Bode plots indicated that $T_t = 4T_{i1}$ gave similar frequency response as the unsaturated case. On the real process, this value of T_t improved the closed loop performance compared to the fast anti-windup case.

We can clearly see the effect of the increased gain at medium frequencies from Figure 9.10 on the closed loop performance in Figure 9.11. Choosing a very slow anti-windup may be tempting, due to increased performance for this specific test, but is not recommended. In other operating points the windup phenomena may become larger and decrease the performance. In addition, the extra use of u_2 may excite unmodeled dynamics or violate input constraints not included in the study.

Modified Anti-windup Scheme for the Cooling System

To increase performance of the cooling system when u_1 saturates, the modified anti-windup scheme presented in Section 9.4 can be used. It is important to use caution when increasing the control action in u_2, since higher controller bandwidth might excite unmodeled dynamics or cause u_2 to saturate.

The cost function (9.10) is used. Based on available control authority in u_2, a reasonable choice of ρ is 150. If less control action in u_2 is desired, ρ should be increased. From simulations, the cost function is evaluated for varying K_s, see Figure 9.12. Standard fast anti-windup is used, $T_t = 0.5T_{i1}$. There is a clear minimum for $K_s = 60$ given this choice of T_t.

The choice of T_t and K_s can also be based on loop-shaping of the frequency response, see Figures 9.7 and 9.10. For example, a larger T_t and a smaller K_s would increase the gain at medium frequencies and reduce the gain at high frequencies.

Experiments The modified anti-windup scheme was also verified in simulations. The closed loop response when $K_s = 60$ and $T_t = 0.5$ is plotted in Figure 9.12 together with the previous cases from Figure 9.11. The modified scheme has higher gain at high frequencies from r to u_2, which is clearly seen in the top right plot. The temperature response is

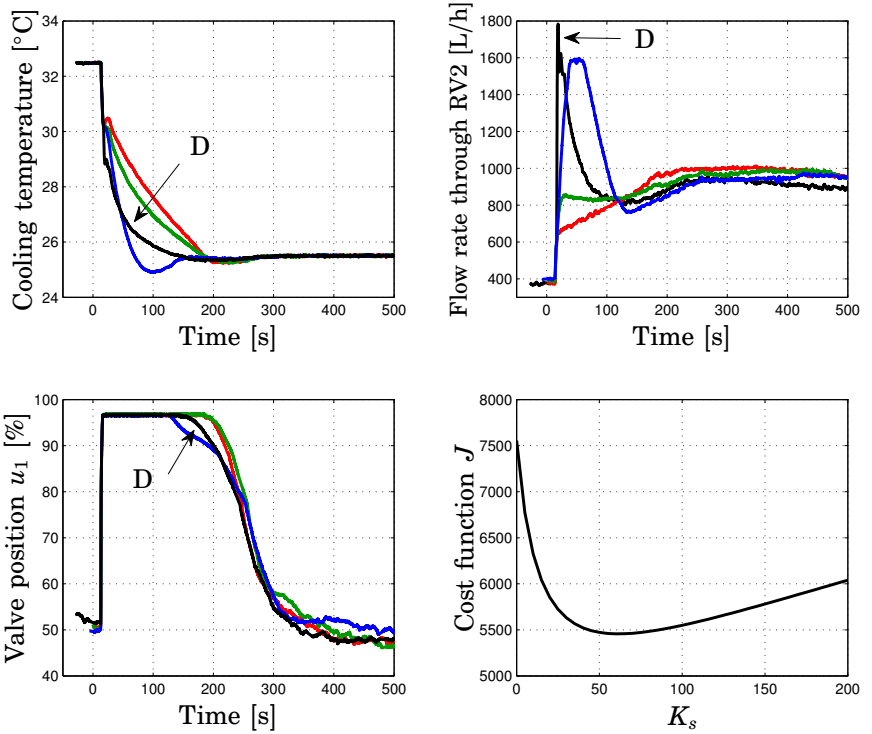

Figure 9.12 Experimental data: Closed-loop response for a step decrease of 7°C for the saturated cases from Figure 9.11 ($T_t = 4T_{i1}$, $T_t = 0.5T_{i1}$, and $T_t = 50T_{i1}$) and the final case when $T_t = 0.5T_{i1}$ with $K_s = 60$ (line D). On the lower right is the evaluated cost function for different values of K_s when $T_t = 0.5T_{i1}$. Instead of plotting the valve position u_2, the flow rate through the valve RV2 is plotted.

as quick as the case with very slow anti-windup, but it has almost no overshoot due to the fast anti-windup time constant.

9.6 Stability and Performance Analysis

Input-output stability for the bio-reactor using the proposed method for choice of T_t has been ensured using the circle criterion in [Karlsson, 2005]. We can also use the fact that the closed-loop system is piecewise linear for both the conventional anti-windup scheme and the modified scheme in Section 9.4. Various tools are available for stability and performance analysis of such systems, see for example [Hedlund and Johansson, 1999]

and [Rantzer and Johansson, 2000].

The proposed choice of T_t is based on frequency response analysis and improves the performance compared to the case with a standard choice of $T_t \leq T_i$. To provide a more thorough analysis of the combined unsaturated and saturated system, the cooling system from Section 9.5 is studied using algorithms from the PWL toolbox, [Hedlund and Johansson, 1999].

For the unsaturated case, the closed loop system matrix for the cooling system with controllers, see Eq 9.12, can be written as

$$A_1 = \begin{bmatrix} A - B_1K_1C + B_2K_2K_1C & B_1 - B_2K_2 & B_2 \\ -K_1C/T_{i1} & 0 & 0 \\ K_1K_2C/T_{i2} & -K_2/T_{i2} & 0 \end{bmatrix}. \tag{9.13}$$

where the first row corresponds to the seven process states, the second row is for the controller state of u_1 and the third row is for the controller state of u_2. The system matrix for the closed loop system in the saturated case can be written as

$$A_2 = \begin{bmatrix} A + B_2K_2K_1C & -B_2K_2 & B_2 \\ -K_1C/T_{i1} + K_1C/T_t & -1/T_t & 0 \\ K_1K_2C/T_{i2} & -K_2/T_{i2} & 0 \end{bmatrix} \tag{9.14}$$

Stability is then verified by finding a quadratic Lyapunov function $V(x) = x^TPx$ that gives negative rate both for the unsaturated and saturated case. This is easily computed using the PWL toolbox.

$$\dot{V} = x^T(A_1^TP + PA_1)x \leq 0 \tag{9.15}$$

$$\dot{V} = x^T(A_2^TP + PA_2)x \leq 0 \tag{9.16}$$

The performance is verified by calculating with the PWL toolbox an upper bound of the L_2-gain from a disturbance d acting on the control signal u_1 to y for various values of T_t, see Figure 9.13. We see that the extreme cases with fast or slow anti-windup have a significantly larger L_2-gain from d to y. Note also that the standard choice $T_t \leq T_i$ also gives unnecessarily low performance. These results confirm the previous analysis, indicating that $T_t = 4T_{i1}$ improves the performance when u_1 saturates.

9.7 Summary

This chapter has presented two rather different applications of mid-ranging control, a bio-reactor and a cooling system. The effects of anti-windup has

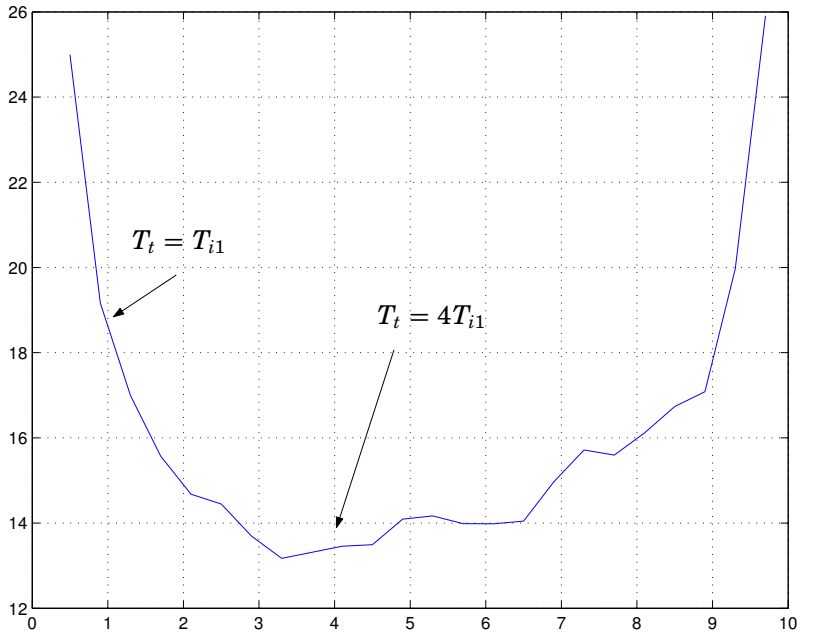

Figure 9.13 An upper bound on the L_2-gain from disturbance d to output y for varying anti-windup scheme time constant T_t for the cooling system.

been examined for the case when the fast control input u_1 is subject to saturation. It has been shown that default choices of anti-windup constant T_t are not extendable to the mid-ranging control structure, since they may decrease the control performance. However, removing the anti-windup mechanism leads to the characteristic windup phenomenon and potentially even to instability.

We have suggested a method, where the anti-windup parameter T_t is chosen to achieve similar bandwidths of the frequency response of the unsaturated and the saturated case. The method improves the performance for both studied processes when u_1 saturates, compared to using either no anti-windup or fast anti-windup. It preserves the closed loop bandwidth of u_2, to avoid excitation of unmodeled process dynamics and cross-couplings between the control variables.

If the knowledge of the process allows for increased bandwidth of the slow controller C_2 when u_1 saturates, we suggest a modified anti-windup structure that does not change the nominal controller design, but gives an increased control error to C_2 when u_1 saturates. This structure is parame-

terized in a constant K_s, which is found through numerical optimization of the integral square cost function (9.10). With this modification, u_2 is more aggressively used and the performance is significantly improved during saturation, without altering the nominal design. The ideas can also be implemented using gain-scheduling of the second controller C_2.

The stability and performance of the system with saturation can be analysed using theory of piecewise linear systems. The result from the piecewise linear analysis supports the previous analysis on how to choose a suitable anti-windup scheme.

10

Conclusion

10.1 Summary

The focus of this thesis has been to investigate the dynamics of the plate reactor and to develop control methods to exploit the increased potential of the new reactor concept. Some of the results are specific for the plate reactor, but many parts may be generalized to other applications of process control, for example the decentralized and centralized control design, the start-up/transition control design and use of mid-ranging control to handle two-input one-output systems.

The process The plate reactor combines the high-heat-transfer capabilities of plate heat exchangers with the efficient mixing and reaction control typical of microreactors, thus enabling intensified production. The flexible construction with multiple injection points and cooling zones improves the steady-state and dynamic performance and improves the possibilities for feedback control, but to take advantage of these benefits may require more complex control designs.

A nonlinear model of the reactor has been derived based on first principles, which allowed a detailed investigation on the process dynamics and the potential control inputs. The best control inputs for temperature control were the feed and cooling water temperatures, as they give low amount of cross-coupling. The feed injection flow rates of reactant B may also be useful for feedback control, especially to improve the transient response when experience large disturbances or operating close to the constraints. However, any change in the feed flows may affect the stoichiometric conditions, so there is a trade-off between improved response and transients in the conversion at the outlet.

It is important to consider the process design, choice of operating point and control design all together, to avoid process design that introduce

cross-couplings in the process inputs. For example, when there are multiple injection points of reactant B, it may be beneficial to have the corresponding number of cooling zones, especially if the intention is to implement a decentralized control structure.

The control at nominal operation The control of the plate reactor has been divided into two parts, control at nominal operation and start-up control. The control of the reactor at the nominal steady-state operating point is designed using either decentralized or centralized control. The multi-loop PID controllers proved to be sufficient to give good performance to various load disturbance scenarios. The decentralized control structure is easy to understand, easy to implement and easy to tune. Temperature constraints can be handled by introducing additional temperature controllers using the feed flow injections. These controllers operate in parallel with the original temperature controllers and are only activated when the reactor temperature crosses a specified threshold.

The centralized control design is based on Model Predictive Control, which can handle multivariable process models, input and state constraints and offers a flexible specification of the control objectives. By varying the cost function, the MPC controller can shift its focus from temperature control, to control the stoichiometric relation or to find control inputs that maximize the reactant conversion, all within the same framework. The MPC approach is especially advantageous when disturbances lead to input saturations or state constraint violations, as the multivariable process model allows all control actions to be calculated based on all available information.

When using additional control inputs in the decentralized control, the general approach is to separate the different control loops in the frequency domain, where one loop is fast and the other loop is slower, to avoid introducing interactions between the loops. In centralized control, additional inputs are added by extending the cost function and the multivariable process model describes the cross-couplings so there is no need for the inputs to be separated in the frequency domain. Additional inputs and control objectives increase the complexity of the tuning problem. It may be straight forward to obtain an acceptable performance, but to achieve the full potential of the MPC controller is a very challenging task.

The temperature control performance of the MPC controller is similar to the performance of the decentralized controller. The choice of disturbance model may influence the transient response of the MPC controller and should be considered as one of the many tuning parameters in the MPC design. The real strength of the MPC framework is demonstrated when adding more inputs, considering temperature constraints or extending the objectives to control both temperature and concentrations. The

decentralized controller may also be designed to address these issues, but it will lead to very complex control structures with possibly large interconnections between the control loops.

Based on the experiences from this thesis, decentralized control is sufficient for basic temperature control when input saturations or temperature constraints are non-existent or present but not always active. When choosing to operate closer to saturation limits or temperature constraints or focusing on the concentration control, a centralized MPC controller is recommended.

The start-up control The start-up control problem is challenging due to process uncertainty, highly nonlinear dynamics and input and temperature constraints. The dynamics and the constraint are easily captured by the process model described in the optimization problem. The open question is how to address the process uncertainty. A sensitivity analysis shows that trajectories where the accumulated reactant concentration and the reactor temperature are both high, are highly sensitive to parametric uncertainty. This will result in large plant/model mismatch and lead to large difficulties for the feedback controller.

In this thesis, robustness to uncertainty is achieved by introducing state-space constraints in the optimization formulation, to avoid optimal solutions that have large sensitivity. In the continuous approach, the concentration of the injected reactant B is constrained to avoid operation in highly sensitive regions. In the hybrid approach, the injection of reactant B is conditionally coupled to a reactor temperature, so that feed injections are only allowed when the temperature is sufficiently high to sustain the reaction. This can be viewed as having the concentration of B constrained to zero until the reactor temperature increases above a certain threshold. The robustness of the closed loop system is verified in Monte Carlo simulations for both approaches. The variations of the start-up trajectories due to the uncertainty decrease significantly for the solutions with low sensitivity.

The utility system and mid-ranging control Temperature control of the plate reactor is easier using the inlet temperature of the cooling water than the cooling flow rate. A utility system was designed and experimentally verified, which allows the inlet temperature of the cooling water to be accurately controlled. The temperature of the cooling water is controlled by manipulating a three-way control valve, mixing hot water from the reactor and colder water from an external heat exchanger. A mid-ranging control structure is implemented, where the external cooling flow rate is manipulated so that the three-way control valve may operate around some desired value, for example in the middle of its operating

range. Mid-ranging control is a very simple and efficient way to handle situations when the process has two inputs and one output.

The performance of a decentralized mid-ranging control structure was investigated when the fast control input saturates. The anti-windup scheme may be modified to improve the performance compared to very fast anti-windup or very slow anti-windup.

10.2 Suggestions for Future Work

When the Alfa Laval Plate Reactor project reaches the stage of full-scale tests, the decentralized and centralized control structures should be tested and verified in real experiments. Before these experiments can be carried out, further work is needed to validate the dynamic response of the model and to consider the location of the sensors.

To reduce the computational complexity of the MPC controller, the process model used for control design may be approximated using any of the techniques discussed in the beginning of Section 4.6.

After the design of linear MPC, it is a natural extension to consider control of the plate reactor using nonlinear MPC. This will allow model predictive control of the plate reactor from start-up to nominal operation using the same controller. It may also be used in production rate changes or other kinds of grade changes. The experiences from the start-up control in this thesis can be directly applied in the design of a nonlinear MPC controlled start-up.

The start-up optimization can be extended to include the sensitivity analysis in the optimization formulation, i.e., solving the optimization problem with a upper bound on the sensitivity or including the sensitivity in the cost function. With the latter approach, it is possible to choose a weighting coefficient corresponding to how much the model can be trusted. For large uncertainties, there may be a large penalty on the sensitivities and vice versa. It would also be interesting to consider the uncertainty by using multi-parametric optimization, where the uncertainty in the parameters are included in the optimization problem in the form of multiple models.

References

ABB (2000): *ECA-600 Processregulatorer*. `www.abb.se`.

Åkesson, J. (2003): "Operator interaction and optimization in control systems." Licentiate Thesis ISRN LUTFD2/TFRT--3234--SE. Department of Automatic Control, Lund University, Sweden.

Åkesson, J. (2006): "MPCtools 1.0—Reference Manual." Technical Report ISRN LUTFD2/TFRT--7613--SE. Department of Automatic Control, Lund Institute of Technology, Sweden.

Åkesson, J. and K.-E. Årzén (2007): "Tools and languages for modeling and optimization of large-scale dynamical systems." In *23rd IFIP TC 7 Conference on System Modelling and Optimization*. Krakow, Poland.

Åkesson, J., T. Ekman, and G. Hedin (2007): "Development of a Modelica compiler using JastAdd." In *Seventh Workshop on Language Descriptions, Tools and Applications*. Braga, Portugal.

Åkesson, J. and P. Hagander (2003): "Integral action – A disturbance observer approach." In *Proceedings of European Control Conference*. Cambridge, UK.

Alfa Laval AB (2006): "Alfa Laval Reactor Technology." `http://www.alfalaval.com`.

Alfa Laval patent (2001): "Patent: FR 0105578, Improved device for exchange and/or reaction between fluids, PCT WO 02/085511."

Alfa Laval patent (2002): "Patent: SE 0203395.9, Flow directing insert for a reactor chamber and a reactor, PCT WO 20/04045761."

Allison, B. J. and A. J. Isaksson (1998): "Design and performance of mid-ranging controllers." *Journal of Process Control*, **8**, pp. 469–474.

Allison, B. J. and S. Ogawa (2003): "Design and tuning of valve position controllers with industrial applications." *Transactions of the Institute of Measurement and Control*, **25**, pp. 3–16.

Andersson, R., B. Andersson, F. Chopard, and T. Norén (2004): "Development of a multi-scale simulation method for design of novel multiphase reactors." *Chemical Engineering Science*, **59**, pp. 4911–4917.

Åström, K. J. and T. Hägglund (2005): *Advanced PID Control*. ISA - The Instrumentation, Systems, and Automation Society, Research Triangle Park, NC 27709.

Åström, K. J. and B. Wittenmark (1997): *Computer-Controlled Systems*. Prentice Hall.

Bauman, E., A. Varma, J. Lorusso, M. Dente, and M. Morbidelli (1990): "Parametric sensitivity in tubular reactors with co-current external cooling." *Chemical Engineering Science*, **45**, pp. 1301–1307.

Bellman, R. (1957): *Dynamic Programming*. Princeton University Press, Princeton, N.J.

Bequette, B. (1991): "Nonlinear control of chemical processes: A review." *Industrial & Engineering Chemistry Research*, **30**, pp. 1391–1413.

Biegler, L., A. Cervantes, and A. Wächter (2002): "Advances in simultaneous strategies for dynamic optimization." *Chemical Engineering Science*, **57**, pp. 575–593.

Bouaifi, M., M. Mortensen, R. Andersson, W. Orciuch, B. Andersson, F. Chopard, and T. Norén (2004): "Experimental and numerical cfd investigations of a jet mixing in a multifunctional channel reactor : Passive and reactive systems." *Chemical Engineering Research and Design Journal*, **82**, pp. 274–283.

Bošković, D. and M. Krstić (2002): "Backstepping control of chemical tubular reactors." *Computers and Chemical Engineering*, **26**, pp. 1077–1085.

Bristol, E. (1966): "On a new measure of interaction for multivariable process control." *IEEE Transactions on automatic control*, **11**, pp. 133–134.

Christofides, P. (2001): *Nonlinear and robust control of PDE systems. Systems and control: Foundations and applications.* Birkhäuser.

Cougnon, P., D. Dochain, M. Guay, and M. Perrier (2006): "Real-time optimization of a tubular reactor with distributed feed." *AIChE Journal*, **52**, pp. 2120–2128.

Denbigh, K. and J. Turner (1971): *Chemical Reactor Theory*. Cambridge University Press.

Diehl, M., H. Bock, and E. Kostina (2006): "An approximation technique for robust nonlinear optimization." *Mathematical Programming*, **107**, pp. 213–230.

Dubljevic, S., N. El-Farra, P. Mhaskar, and P. Christofides (2006): "Predictive control of parabolic pdes with state and control constraints." *Int. Journal of Robust and Nonlinear Control*, **16**, pp. 749–772.

Durham, W. (1993): "Constrained control allocation." *Journal of Guidance, Control and Dynamics*, **16:4**, pp. 717–725.

Dynasim (2001): *Dymola, Dynamic Modeling Laboratory - User's Manual*. Dynasim AB.

Edgar, T. and D. Himmelblau (1989): *Optimization of chemical processes*. McGraw-Hill.

Fogler, S. (1992): *Elements of chemical reaction engineering*. Prentice Hall.

Fourer, R., D. Gay, and B. Kernighan (2003): *AMPL – A Modeling Language for Mathematical Programming*. Brooks/Cole — Thomson Learning.

Froment, G. and K. Bischoff (1990): *Chemical reactor analysis and design*. Wiley.

Green, A., B. Johnson, and A. John (1999): "Process intensification magnifies profits." *Chemical Engineering*, **106**, p. 66.

Hahn, D., L. Fan, and C. Hwang (1971): "Optimal startup control of a jacketed tubular reactor." *AIChE Journal*, **17**, pp. 1394–1401.

Hang, C. and K. J. Åström (2002): "Relay feedback auto-tuning of process controllers – a tutorial review." *Journal of Process Control*, **12**, January, pp. 143–162.

Hangos, K. and I. Cameron (2001): *Process Modelling and Model Analysis*. Academic Press.

Harris, T., J. Macgregor, and J. Wright (1980): "Optimal sensor location with an application to a packed bed tubular reactor." *AIChE Journal*, **26**, pp. 910–916.

Haugwitz, S. (2005): "Modeling and Control of the Open Plate Reactor." Licentiate Thesis ISRN LUTFD2/TFRT--3237--SE. Department of Automatic Control, Lund University, Sweden.

Haugwitz, S., J. Åkesson, and P. Hagander (2007a): "Dynamic optimization of a plate reactor start-up supported by Modelica-based code generation software." In *Proceedings of 8th International Symposium on Dynamics and Control of Process Systems*. Cancun, Mexico.

Haugwitz, S., J. Åkesson, and P. Hagander (2007b): "Dynamic start-up optimization of a plate reactor with uncertainties." *Submitted to Journal of Process Control*.

Haugwitz, S. and P. Hagander (2004a): "Mid-ranging control of the cooling temperature for an Open Plate Reactor." In *Proceedings of the 12th Nordic Process Control Workshop*. Gothenburg, Sweden.

Haugwitz, S. and P. Hagander (2004b): "Temperature control of a utility system for an Open Plate Reactor." In *Proceedings of Reglermöte*. Gothenburg, Sweden.

Haugwitz, S. and P. Hagander (2005): "Process control of an Open Plate Reactor." In *Proceedings of the 16th IFAC World Congress*. Prague, Czech Republic.

Haugwitz, S. and P. Hagander (2006): "Challenges in start-up control of a heat exchange reactor with exothermic reactions; a hybrid Approach." In *Proceedings of the 2nd IFAC Conference on Analysis and Design of Hybrid Systems*. Alghero, Italy.

Haugwitz, S. and P. Hagander (2007): "Analysis and design of startup control of a chemical plate reactor with uncertainties; a hybrid approach." In *Proceedings of the 16th IEEE Conference on Control Applications (CCA)*. Singapore.

Haugwitz, S., P. Hagander, and T. Norén (2006): "Process and control design for a novel chemical heat exchange reactor." In *Proceedings of Reglermötet*. Stockholm, Sweden.

Haugwitz, S., P. Hagander, and T. Norén (2007): "Modeling and control of a novel heat exchange reactor, the open plate reactor." *Control Engineering Practice*, **15:7**, pp. 779–792.

Haugwitz, S., M. Karlsson, S. Velut, and P. Hagander (2005): "Anti-windup in mid-ranging control." In *Proceedings of the 44th IEEE Conference on Decision and Control and European Control Conference ECC 2005*. Seville, Spain.

Hedlund, S. and M. Johansson (1999): "PWLTool, a Matlab toolbox for piecewise linear system." Technical Report ISRN LUTFD2/TFRT--7582--SE. Department of Automatic Control, Lund Institute of Technology, Sweden.

Hoo, K. and D. Zheng (2001): "Low-order control-relevant models for a class of distributed parameter systems." *Chemical Engineering Science*, **56**, pp. 6683–6710.

Hudon, N., M. Perrier, M. Guay, and D. Dochain (2005): "Adaptive extremum seeking control of a non-isothermal tubular reactor with unknown kinetics." *Computers and Chemical Engineering*, pp. 839–849.

Intab AB (2005): *Easyview 5.5, Efficient and complete software for graphing data*. `www.intab.se`.

Kapoor, N., A. Teel, and P. Daoutidis (1998): "An anti-windup design for linear systems with input saturation." *AUTOMATICA*, **34:5**, pp. 559–574.

Karafyllis, I. and P. Daoutidis (2002): "Control of hot spots in plug flow reactors." *Computers & Chemical Engineering*, **26**, pp. 1087–1094.

Karlsson, M. (2005): "Control of bacillus Subtilis culivations—Feeding strategies and the role of anti-windup in mid-ranging control." Master's Thesis ISRN LUTFD2/TFRT--5745--SE. Department of Automatic Control, Lund University, Sweden.

Karlsson, M., O. Slätteke, B. Wittenmark, and S. Stenström (2005): "Reducing moisture transients in the paper-machine drying section with the mid-ranging control technique." *Nordic Pulp and Paper Research Journal*, **20:2**, pp. 150–156.

Kookos, I. and J. Perkins (2001): "An algorithm for simultaneous process design and control." *Industrial & Engineering Chemistry Research*, **40**, pp. 4079–4088.

Laabissi, M., M. Achhab, J. Winkin, and D. Dochain (2002): "Equilibrium profiles of tubular reactor nonlinear models." *In Proceedings of 15th Int. Symposium on Mathematical Theory of Networks and Systems*.

Laabissi, M., M. Achhab, J. Winkin, and D. Dochain (2004): "Multiple equilibrium profiles for nonisothermal tubular reactor nonlinear models." *Dynamics of Continuous, Discrete and Impulsive Systems*, **11**, pp. 339–352.

Lenells, M. (1982): *Adaptive Start-up Control*. PhD thesis TFRT-1023, Department of Automatic Control, Lund University, Sweden.

Levenspiel, O. (1999): *Chemical Reaction Engineering*. Wiley.

Logist, F., I. Smets, and J. V. Impe (2005a): "Optimal control of dispersive tubular chemical reactors: Part I." *Proceedings of IFAC World Congress*.

Logist, F., I. Smets, and J. V. Impe (2005b): "Optimal control of dispersive tubular chemical reactors: Part II." *Proceedings of IFAC World Congress*.

Logist, F., I. Smets, and J. V. Impe (2007): "Derivation of generic optimal reference temperature profiles for steady-state exothermic jacketed tubular reactors." *Journal of Process Control,* In press, available online doi:10.1016/j.jprocont.2007.05.001.

Luyben, W. (2001): "Effect of design and kinetic parameters on the control of cooled tubular reactor systems." *Industrial & Engineering Chemistry Research*, **40**, pp. 3623–3633.

Maciejowski, J. M. (2002): *Predictive Control with Constraints*. Pearson Education Limited.

Maly, T. and L. R. Petzold (1996): "Numerical methods and software for sensitivity analysis of differential-algebraic systems." *Applied Numerical Mathematics*, **20:1-2**, pp. 57–82.

Mathworks (2007a): *Matlab - The Language of Technical Computing*. `www.mathworks.com`.

Mathworks (2007b): *Model Predictive Control Toolbox*. `www.mathworks.com`.

Modelica Association (2005): "Modelica – a unified object-oriented language for physical systems modeling, language specification." Technical Report. Modelica Association.

Morud, J. and S. Skogestad (1996): "Dynamic behaviour of integrated plants." *Journal of Process Control*, **6**, pp. 145–156.

National Instruments (2005): *LabVIEW 7.1, Graphical programming for engineers and scientists*. `www.ni.com`.

Nilsson, J. and F. Sveider (2000): "Characterising mixing in a hex reactor using a model chemical reaction." `http://www.chemeng.lth.se/exjobb/002.pdf`.

Pannocchia, G. (2003): "Robust disturbance modeling for model predictive control with application to multivariable ill-conditioned processes." *Journal of Process Control*, **13**, pp. 693–701.

Pannocchia, G., N. Laachi, and J. Rawlings (2005): "A candidate to replace pid control: Siso-constrained lq control." *AIChE Journal*, **51**, pp. 1178–1189.

Pannocchia, G. and J. Rawlings (2003): "Disturbance models for offset-free model predictive control." *AIChE Journal*, **49**, pp. 426–437.

Petitjean, R. (1994): *Total hydronic balancing*. Tour and Andersson AB.

Petzold, L. (1986): "Order results for implicit runge-kutta methods applied to defferential/algebraic systems." *SIAM Journal on Numerical Analysis*, **23:4**, pp. 837–852.

Phillips, C., G. Lausche, and H. Peerhossaini (1997): "Intensification of batch chemical process by using integrated chemical reactor heat exchangers." *Applied Thermal Engineering*, **17**, pp. 809–824.

Pontryagin, L. S., V. G. Boltyanskii, R. V. Gamkrelidze, and E. F. Mishchenko (1962): *The Mathematical Theory of Optimal Processes*. John Wiley & Sons, Inc.

Prat, L., A. Devatine, P. Cognet, M. Cabassud, C. Gourdon, S. Elgue, and F. Chopard (2005): "Performance evaluation of a novel concept "open plate reactor" applied to highly exothermic reactions." *Chemical Engineering Technology*, **28**, pp. 1028–1034.

Qin, S. J. and T. A. Badgwell (2003): "A survey of industrial model predictive control technology." *Control Engineering Practice*, **11**, pp. 733–764.

Ramshaw, C. (1995): "The incentive for process intensification." *In Proceedings 1st Intl. Conf. of Process Intensification for Chem. Ind.*, **18**.

Rantzer, A. and M. Johansson (2000): "Piecewise linear quadratic optimal control." *IEEE Transactions on Automatic Control*, **45:4**, pp. 629–37.

Schiesser, W. (1991): *The Numerical Method of Lines: Integration of Partial Differential Equations*. Academic Press.

Seferlis, P. and M. Georgiadis, Eds. (2004): *The integration of process design and control*. Elsevier.

Shang, H., J. Forbes, and M. Guay (2004): "Model predictive control for quasilinear hyperbolic distributed parameter systems." *Industrial & Engineering Chemistry Research*, pp. 2140–2149.

Shang, H., J. Forbes, and M. Guay (2007): "Computationally efficient model predictive control for convection dominated parabolic systems." *Journal of Process Control*, pp. 379–386.

Shinskey, F. (1996): *Process Control Systems*. McGraw-Hill.

Skogestad, S. and I. Postlethwaite (2005): *Multivariable Feedback Control: Analysis and Design*. Wiley.

Smets, I., D. Dochain, and J. V. Impe (2002): "Optimal temperature control of a steady-state exothermic plug-flow reactor." *AIChE Journal*, **48**, pp. 279–286.

Stankiewicz, A. and J. Moulin (2000): "Process intensification: Transforming chemical engineering." *Chemical Engineering Progress*, **96**, pp. 22–34.

Stein, G. (2003): "Respect the unstable." *IEEE Control Systems Magazine*, **23**.

Tian, Z. and K. Hoo (2003): "Transition control using a state-shared model approach." *Computers and Chemical Engieering*, **27**, pp. 1641–1656.

van de Wal, M. and B. de Jager (2001): "A review of methods for input/output selection." *Automatica*, **37**, pp. 487–510.

Varma, A., M. Morbidelli, and H. Wu (1999): *Parametric sensitivity in chemical systems*. Cambridge University Press.

Vassiliadis, V. (1993): *Computational solution of dynamic optimization problem with general differnetial-algebraic constraints*. PhD thesis, Imerial Collage, London, UK.

Vecchio, D. D. and N. Petit (2005): "Boundary control for an industrial under-actuated tubular chemical reactor." *Journal of Process Control*, **15**, pp. 771–784.

Velut, S., L. de Maré, and P. Hagander (2004): "A modified probing feeding strategy: control aspects." In *Reglermöte 2004*.

Verwijs, J., H. van den Berg, and K. Westerterp (1994): "Start-ip and safeguarding of an industrial adiabatic tubular reactor." *Chemical Engineering Science*, **49**, pp. 5519–5532.

Verwijs, J., H. van den Berg, and K. Westerterp (1996): "Startup strategy design and safeguarding of industrial adiabatic tubular reactor systems." *AIChE Journal*, **42**, pp. 503–515.

Wächter, A. and L. T. Biegler (2006): "On the implementation of an interior-point filter line-search algorithm for large-scale nonlinear programming." *Mathematical Programming*, **106:1**, pp. 25–58.

Wallén, A. (2000): *Tools for Autonomous Process Control*. PhD thesis ISRN LUTFD2/TFRT--1058--SE, Department of Automatic Control, Lund Institute of Technology, Sweden.

Wang, Y. and J. Rawlings (2004): "A new robust model predictive control method I: theory and computation." *Journal of Process Control*, **14**, pp. 231–247.

Winkin, J., D. Dochain, and P. Ligarius (2000): "Dynamical analysis of distributed tubular reactors." *Automatica*, **36**, pp. 349–361.

Zaldívar, J., J. Cano, M. Alós, J. Sempere, R. Nomen, D. Lister, G. Maschio, T. Obertopp, E. Gilles, J. Bosch, and F. Strozzi (2003): "A general criterion to define runaway limits in chemical reactors." *Journal of Loss Prevention in the Process Industries*, **16**, pp. 187–200.

Zheng, D. and K. Hoo (2004): "System identification and model-based control of distributed parameter systems." *Computers and Chemical Engineering*, **28**, pp. 1361–1375.

Appendix

List of Symbols

Table 10.1 State variables inside the plate reactor

Symbol	Unit	Description
c_A	$\mathrm{mol/m^3}$	Concentration of reactant A
c_B	$\mathrm{mol/m^3}$	Concentration of reactant B
c_C	$\mathrm{mol/m^3}$	Concentration of reactant C
T_r	°C	Reactor temperature
T_w	°C	Cooling water temperature

Table 10.2 Input variables to the plate reactor

Symbol	Value/Range	Description
$q_{A,\mathrm{feed}}$	$1.11 \cdot 10^{-5}$ $\mathrm{m^3/s}$	Feed flow of reactant A into the reactor
$q_{B,\mathrm{feed}}$	$2.78 \cdot 10^{-6}$ $\mathrm{m^3/s}$	Feed flow of reactant B into the reactor
u_{B1}	$0-1$	Scaled feed flow of B at injection point 1
u_{B2}	$0-1$	Scaled feed flow of B at injection point 2
q_{cool}	$1.00 \cdot 10^{-3}$ $\mathrm{m^3/s}$	The cooling water flow rate
$T_{A,\mathrm{feed}}$	$15-80$°C	The feed temperature of reactant A
$T_{B,\mathrm{feed}}$	20°C	The feed temperature of reactant B
T_{cool}	$15-80$°C	The inlet temperature of the cooling water
$c_{A,\mathrm{feed}}$	1470 $\mathrm{mol/m^3}$	The feed concentration of reactant A
$c_{B,\mathrm{feed}}$	11256 $\mathrm{mol/m^3}$	The feed concentration of reactant B

Table 10.3 Parameters and variables inside the plate reactor

Symbol	Value/Unit	Description
$A_{\text{heat}}^{\text{tot}}$	0.2061 m^2	Total heat transfer area
c_p	4180 J/(kg K)	Specific heat capacity of reactor fluid
d_r	0.0081 m	diameter of approx. tubular reactor
d_w	0.0129 m	diameter of approx. cooling jacket
$\mathcal{D}_e$	0.0371 m^2/s	Energy dispersion coefficient
$\mathcal{D}_m$	0.0371 m^2/s	Mass dispersion coefficient
E_a	68200 J/mol	Activation energy
h	3000 $\text{W}/(\text{m}^2\ \text{K})$	Heat transfer coefficient
ΔH	$1.172 \cdot 10^6$ J/mol	Heat of reaction per mole $Na_2S_3O_6$
k_0	$2.0 \cdot 10^7$ $\text{m}^3/(\text{mol s})$	Pre-exponential factor in reaction rate
L	8.1 m	Length of reactor channel
R	8.31434 J/(mol K)	Ideal gas constant
ρ_r	1000 kg/m^3	Density of reactor fluid
ρ_w	1000 kg/m^3	Density of cooling water
v_r	0.27 m/s	flow velocity of reactor fluid
v_w	14.0 m/s	flow velocity of cooling water
V_r^{tot}	$4.17 \cdot 10^{-4}$ m^3	Total reactor volume
V_w^{tot}	$5.8 \cdot 10^{-4}$ m^3	Total cooling water volume

The kinetic parameters and the values of the feed concentrations are given for the sodium thiosulfate reaction.